Mixture Forming Processes in Dredge Cutter Heads

Mixture Forming Processes in Dredge Cutter Heads

Proefschrift

ter verkrijging van de graad van doctor
aan de Technische Universiteit Delft,
op gezag van de Rector Magnificus prof. dr. ir. J.T. Fokkema,
voorzitter van het College van Promoties,
in het openbaar te verdedigen op dinsdag 3 juni 2003 om 13:30 uur

door
Marco DEN BURGER
werktuigkundig ingenieur
geboren te Rotterdam

Dit proefschrift is goedgekeurd door de promotor:
Prof. ir. W.J. Vlasblom

Samenstelling Promotiecommissie:

Rector Magnificus	voorzitter
Prof. ir. W.J. Vlasblom	Technische Universiteit Delft, promotor
Prof. dr. ir. G. Ooms	Technische Universiteit Delft
Prof. ir. J. de Koning†	Technische Universiteit Delft
Prof. ir. J. Meek	Technische Universiteit Delft
Prof. dr. A. Sellgren	Luleå University of Technology (Sweden)
Dr. ir. A.M. Talmon	WL|Delft Hydraulics
Dr. ir. N.P. Kruyt	Universiteit Twente

This study has been financed by the Vereniging van Waterbouwers in Bagger-, Kust- en Oeverwerken (VBKO).

Printed by printpartners Ipskamp.

Summary

This research was initiated by the need of the dredging industry to have a better understanding of the occurrence of spillage when using a cutter suction dredge. Spillage is defined as the soil that is cut during the dredging process, but is not sucked up by the suction pipe. This reduces the productivity of the cutter suction dredge and therefore needs to be minimized. Secondly, accurate predictions of the spillage are very important for a dredging company, as it enables a more accurate production estimate and will reduce the risks involved in obtaining dredging work. Spillage rates can be up to 50% when relatively hard formations are cut, resulting in only half of the material that is cut actually being sucked up. The cutter head is the device that is responsible for the actual excavation of the soil. The aim of this study is first of all to identify and describe the processes taking place inside the cutter head that are associated with spillage rather than to reduce the spillage. Furthermore, it focuses on the spillage-related processes while cutting relatively hard formations.

As the available literature on spillage processes is limited, especially for the cutting of rock, the execution of model tests is an essential part of this study. Therefore, a first requirement is identifying of appropriate scale laws. It appears that the flow inside the cutter head is scaled according to the Euler number and the particle dimension is scaled according to the Froude number.

As a first approach, the model(s) developed in his thesis mainly focused on the behavior of single particles inside the cutter head. This means that the behavior of a single particle is assumed to be representative for a large number of particles, neglecting particle-particle interactions and the disturbance of the flow due to the presence of the particles.

The first series of tests performed focused on the residence times of (single) particles inside the cutter head. The residence time is defined as the time span between injection of the particle into the cutter head and the time it is sucked up by the suction pipe. The aim was to determine the influence of the operational parameters (rotational velocity of the cutter head and suction flow) on the residence time of the particles. A short residence time is believed to

represent a high production percentage in practice. It appears that increasing the suction flow always resulted in a decrease in residence time. The influence of the rotational velocity was not that unambiguous, but it could have a significant influence on the residence time. Generally the measured residence times were so large that they are not representative for the situation in practice.

A model has been set up in order to simulate the particle trajectories inside the cutter head. The flow inside the cutter head was represented by a forced vortex and a sink. The forces acting on the particle that are taken into account are: gravitational force, drag force, added mass force and pressure gradient force. Simulations showed that the particles were hardly sucked up as the flow model is too simplistic. The absence of the pump effect of the cutter head in the flow model has a significant influence on the simulation results. Furthermore, the actual presence of the cutter head (i.e. the volume of steel) has not been taken into account. In future models the presence of the cutter head and the (layers) of cut material on the blades should be taken into account, as this will increase the fluid velocities inside the cutter head.

Cutting tests on a model scale have been performed in cemented banks of gravel with a crown cutter head. The tests have been performed to determine the influence of a concentration of particles inside the cutter head and to find the limitations of single-particle models. In addition, the tests results showed the influence of the rotational velocity of the cutter head and the suction flow on the production percentage. In the so-called ‘under-cut’ situation it appears that for every suction flow there is an optimum rotational velocity. The decrease in production for rotational velocities beyond the optimum resulted from the large centrifugal forces acting on the particles by which the particles were thrown out of the cutter head. Increasing the suction flow always resulted in an increase in production percentage. Furthermore, in the so-called ‘over-cut’ situation the production percentage was a factor 2 to 4 lower than in the under-cut situation. The tests results (and video-recordings) showed that the filling degree of the cutter head does have an influence on the production percentage. For determining production percentages the single particle model will therefore not suffice. Tests also showed that a decrease in ladder inclination angle resulted in a significant increase in production.

An additional series of tests has been performed to investigate the increase in production with increasing rotational velocity. In these tests the cutter head was not actually cutting but the gravel particles were brought in the cutter head by means of a silo and tube system. A cylindrical cutter head with straight adjustable blades and the crown cutter head were tested. Adjusting the blades of the cylindrical cutter head to increase the amount and intensity of the particle collisions with the blade did not result in an increase in production percentage. Furthermore, video-recording did not show evidence of particle collisions with the blades. Tests with the crown cutter head did show the increase in production percentage with

increasing rotational velocity. Therefore it is believed that the increase in production is the result of the increasing centrifugal force acting on the particle and the guiding action of the cutter blades. For a particle in contact with the blade, the centrifugal force has a component along the blade directed towards the cutter ring. This component of the centrifugal force can bring the particle closer to the suction mouth and increase the probability that it is sucked up. The optimum rotational velocity in these tests was identical to the optimum in the actual cutting tests. Moreover, the optimum rotational velocity has a value for which an outward flow exists near the cutter ring (due to the pump effect of the cutter head). This indicates that an outward flow does not necessarily have a negative influence on the production percentage when relatively large particles are considered. The increase in axial water velocities due to the pump effect and/or the increase of the component of the centrifugal force acting along the cutter blade could improve the transport of particles towards the suction pipe.

A mathematical model set up to simulate the particle trajectories along a cutter blade verified that the component of the centrifugal force along the blade can direct the particles towards the cutter ring. The external forces taken into account in the model are: gravitational force, drag force, added mass force, pressure gradient force, the normal force (perpendicular to the blade's surface) and the friction force between particle and blade. The normal force and friction force are reaction forces resulting from the contact between particles and the cutter blades. The flow inside the cutter head was, for reasons of simplicity, again represented by a forced vortex and a sink. The influence of the cutter head on the flow was not taken into account. The simulations showed that the fluid flow has a significant influence on the particle trajectories. For lower rotational velocities the gravitational force is clearly dominant, while for the larger rotational velocities the centrifugal acceleration is dominant. However, the dominant force never exceeds the other forces by more than a factor three to four. The velocity difference between water and the blade (slip) in combination with the drag coefficient was strongly determinative for the particle trajectories. Particles were only thrown out of the cutter head if an outward flow was imposed.

This research has provided substantial information on the processes taking place inside the cutter head for the cutting of relatively hard formations. It has indicated the difference in processes in relation to the cutting of (fine) sand resulting from larger gravitational and inertial forces acting on the particles. The importance of cutter head geometry and the blade geometry in specific is emphasized.

The simulation model for the particle trajectories shows the basic trends regarding the influence of the rotational velocity of the cutter head and the suction flow. More research on the flow inside the cutter head is needed to improve the model for the particle trajectories (especially along the blades). In future research, the influence of particle-particle interactions and the influence of the particles (or particle layers) on the flow should be taken into account

in the model; especially when production estimations are intended. The use of a continuum model instead of a single particle model needs to be investigated.

Samenvatting

Dit onderzoek is geïnitieerd vanuit de baggerindustrie vanwege de behoefte om het optreden van mors bij een snijkopzuiger beter te begrijpen. Mors is gedefinieerd als de grond die wel is losgesneden tijdens het baggerproces, maar niet wordt opgezogen door de zuigbuis. Dit vermindert de productiviteit van de snijkopzuiger en dient daarvoor geminimaliseerd te worden. Bovendien is een nauwkeurige schatting van de mors gewenst voor een baggermaatschappij, omdat het een nauwkeuriger productiebegroting mogelijk maakt en de risico's, die gepaard gaan met het aannemen van een werk, vermindert. Morspercentages kunnen in harde grondsoorten oplopen tot 50%, hetgeen betekent dat maar de helft van wat losgesneden wordt daadwerkelijk ook wordt opgezogen. De snijkop is het instrument dat feitelijk verantwoordelijk is voor de ontgraving. Het doel van deze studie is eerder het herkennen en beschrijven van de processen die plaatsvinden in de snijkop en gerelateerd zijn aan mors dan het verminderen van de mors. Bovendien concentreert het onderzoek zich op de aan mors gerelateerde processen voor het snijden van relatief harde grondsoorten zoals rots.

Vanwege de beperkte aanwezigheid van gerelateerde literatuur, met name voor het snijden van rots, vormt de uitvoering van schaalproeven een essentieel onderdeel van het onderzoek. Daardoor is een eerste vereiste het opstellen van de juiste schaalregels. Het blijkt dat de stroming wordt geschaald volgens het Euler getal en de afmeting van de losgesneden deeltjes volgens het Froude getal.

De ontwikkelde modellen in deze dissertatie zijn in eerste instantie gericht op het gedrag van enkele deeltjes in de snijkop. Dit betekent dat het gedrag van een enkel deeltje wordt verondersteld representatief te zijn voor het gedrag van een groot aantal deeltjes. De interactie tussen de deeltjes wordt dus verwaarloosd, evenals de verstoring van de stroming door de aanwezigheid van de deeltjes.

In de eerste reeks proeven is ingezoomd op de verblijftijden van de enkele deeltjes in de snijkop. Deze verblijftijd is gedefinieerd als de tijd tussen het injecteren van een deeltje in de

snijkop en de tijd van opzuigen door de zuigbuis. Het doel van de proeven was het vaststellen van de invloed van de operationele parameters (het toerental van de snijkop en het zuigdebiet) op de verblijftijd van een deeltje. Een korte verblijftijd komt in de praktijk overeen met een hoog productiepercentage. Het blijkt dat het verhogen van het zuigdebiet altijd resulteert in een afname van de verblijftijd. De invloed van het toerental is niet eenduidig, maar het toerental kan zeker een grote invloed op de verblijftijd hebben. In het algemeen zijn de gemeten verblijftijden zo hoog dat zij niet representatief kunnen zijn voor de situatie in de praktijk, omdat ze duiden op een onrealistisch hoge vullinggraad van de snijkop.

Een mathematisch model is opgesteld om de banen van de enkele deeltjes in de snijkop te simuleren. Hierbij is de stroming in de snijkop samengesteld uit een opgelegde wervel en een putstroming. Er is rekening gehouden met de volgende krachten, werkend op de deeltjes: de zwaartekracht, de sleepkracht, de weerstandskracht van de stroming op het deeltje, de kracht ten gevolge van de toegevoegde (of schijnbare) massa en de krachten ten gevolge van de drukgradiënten in de stroming.

De simulaties hebben aangetoond dat de deeltjes nauwelijks worden opgezogen vanwege de vereenvoudigingen in het stroommodel. De afwezigheid van de pompwerking van de snijkop in het stroommodel heeft een belangrijke invloed op de resultaten van de simulaties. Bovendien zou de aanwezigheid van de snijkop in rekening gebracht moeten worden in het stroommodel (vanwege de ruimte die het inneemt) alsmede de lagen van gesneden materiaal die zich op de bladen van de snijkop bevinden. Het innemen van de ruimte door de cutter en lagen van gesneden materiaal zal de stroomsnelheden in de snijkop verhogen.

Om de invloed van een hogere concentratie aan deeltjes in de snijkop te bepalen zijn snijproeven in bressen van gecementeerd grind uitgevoerd met een kroonsnijkop op modelschaal. Door middel van deze proeven kunnen ook de beperkingen van een model met enkele deeltjes worden vastgelegd. Een bijkomend doel van de proeven is het bepalen van de invloed van het toerental van de snijkop en het zuigdebiet (c.q. mengselsnelheid) op het productiepercentage.

In de zogeheten ondersnijdende situatie blijkt dat voor elke mengselsnelheid er een optimum toerental van de snijkop is. Het dalen van de productie boven het optimum toerental is het gevolg van de hoge centrifugaalkrachten die werken op de deeltjes, waardoor de deeltjes uit de snijkop worden geslingerd. Het verhogen van de mengselsnelheid daarentegen resulteert consequent in een verhoging van het productiepercentage. In de zogeheten bovensijdende situatie is de productie een factor 2 tot 4 lager dan in de ondersnijdende situatie. De invloed van het toerental van de snijkop is minder eenduidig dan in de ondersnijdende situatie.

De resultaten uit de metingen en bestudering van de video-opnamen hebben aangetoond dat de vullinggraad van de snijkop een grote invloed heeft op het productiepercentage. Voor het bepalen/voorspellen van productiepercentages zal het model met enkele deeltjes dus niet volstaan. De modelproeven hebben ook aangetoond dat het verlagen van de ladderhoek resulteert in een behoorlijke verhoging van het productiepercentage.

De aanvankelijke stijging van het productiepercentage met toenemend toerental van de snijkop is verder onderzocht door middel van een nieuwe serie proeven. Tijdens deze serie proeven is er niet gesneden door de snijkop, maar werd grind middels een silo en een buizensysteem in de snijkop gebracht. Een cilindrische snijkop met rechte, verstelbare bladen en de eerder gebruikte kroonsnijkop zijn met elkaar vergeleken.

Verwacht werd dat het verstellen van de bladen bij de cilindrische snijkop de hoeveelheid en de intensiteit van de botsingen zou beïnvloeden, waaruit de productiestijging verklaard zou kunnen worden. De productiestijging bleek echter niet op te treden bij de proeven met de cilindrische snijkop en bovendien hebben de videobeelden niet aangetoond dat er botsingen plaats vinden tussen de balden en het grind. De proeven met de kroonsnijkop toonden wel weer een productiestijging met toenemend toerental van de snijkop. Er wordt daarom aangenomen dat deze stijging in productie direct verband houdt met de vorm van de snijkop. Door de toename in centrifugaalkrachten op de deeltjes met toenemend toerental en de component van deze centrifugaalkrachten langs het blad worden de deeltjes richting de ring van snijkop getransporteerd. Doordat ze dichter bij de zuigopening komen wordt de kans verhoogd dat ze worden opgezogen.

Bovendien bleek uit de proeven met de kroonsnijkop dat het optimum toerental identiek was aan het optimum tijdens de werkelijke snijproeven. Dit optimum ligt rond een waarde waarvoor er een uittredende stroming bij de snijkopring bestaat vanwege de pompwerking van de snijkop. Dit toont aan dat een uittredende stroming niet per definitie een negatieve invloed heeft op het productiepercentage (althans wanneer relatief grote deeltjes worden beschouwd). De toename in axiale snelheid van het water in de snijkop door de pompwerking zou het transport van deeltjes richting de opening van de zuigbuis kunnen bevorderen.

Naar aanleiding van de proeven met de silo is een nieuw mathematische model opgesteld dat zich richt op de banen van deeltjes langs een blad van een snijkop. De krachten op de deeltjes die in rekening zijn gebracht in dit model zijn: de zwaartekracht, de sleepkracht, de weerstandskracht van de stroming op het deeltje, de kracht ten gevolge van de toegevoegde (of schijnbare) massa, de krachten ten gevolge van de drukgradiënten in de stroming, de normaalkracht en de wrijvingkracht tussen deeltje en blad. Uitkomsten van dit model hebben bevestigd dat de combinatie van toenemende centrifugaalkrachten op de deeltjes en de vorm

van het blad verantwoordelijk kan zijn voor het transport van deeltjes in de richting van de snijkopring.

De stroming in de snijkop was gemakshalve samengesteld uit een opgelegde wervel en een putstroming, waarbij de invloed van de snijkop zelf buiten beschouwing is gelaten. De simulaties hebben aangetoond dat de vloeistofstroming een grote invloed heeft op de banen van de deeltjes. Voor lagere toerentallen was de zwaartekracht duidelijk dominant, terwijl voor hoge toerentallen de centrifugaalkrachten dominant waren. Echter, de dominante kracht is nooit meer dan een factor 3 tot 4 groter dan de andere krachten. Het verschil in snelheid tussen water en blad (slip) gecombineerd met de weerstandscoëfficiënt (C_d waarde) is sterk bepalend voor de baan van een deeltje. Bovendien is uit de simulaties gebleken dat het uitslingeren van deeltjes, hetgeen tijdens de snijproeven en de proeven met de silo veelvuldig voorkwam, alleen gebeurde als er een uittredende stroming werd opgelegd in het simulatiemodel.

Dit onderzoek heeft bruikbare informatie opgeleverd omtrent de processen die zich afspelen in een snijkop voor het snijden van relatief harde formaties. Het verschil tussen het snijden van grof materiaal ten opzichte van relatief fijn materiaal is naar voren gekomen en de rol van de zwaartekracht en traagheidskrachten in deze is toegelicht. De rol van de snijkop geometrie in zijn geheel en de geometrie van de bladen in het bijzonder is benadrukt.

De simulatiemodellen voor de banen van de deeltjes in de snijkop als mede langs het blad, geven de basis trends wat betreft de invloed van het toerental van de snijkop en het zuigdebiet. Meer onderzoek naar de stroming in de snijkop (pompwerking) is noodzakelijk om de modellen voor de deeltjesbanen te verbeteren (met name langs de bladen). In toekomstig onderzoek moet de invloed van de onderlinge interacties tussen deeltjes en het beïnvloeden van de stroming door deze deeltjes (lagen van deeltjes op de bladen) in rekening gebracht worden. Dit is zeker van toepassing als productiebepalingen beoogd worden. Het verdient aanbeveling het gebruik van een continuümmodel te onderzoeken als vervanging van het model voor enkele deeltjes.

Table of Contents

Chapter 1
Introduction

The aim of this study is to identify and describe the processes associated with spillage for cutting relatively hard formations. The research was initiated by the need of the dredging industry to have a better understanding of the occurrence of spillage when using a cutter suction dredge. Spillage is defined as the soil that is cut during the dredging process, but is not sucked up by the suction pipe. This reduces the productivity of the cutter suction dredge and therefore needs to be minimized. Secondly, accurate predictions of spillage are very important for a dredging company, as it enables a more accurate production estimate and will reduce the risks involved in obtaining dredging work. Spillage rates can be up to 50% when relatively hard formations are cut, resulting in only half of the material that is cut actually being sucked up. The aim of this study was first of all to identify and describe the processes associated with spillage for cutting of relatively hard formations rather than to reduce the spillage.

1.1 The cutter suction dredge and the cutter head

Although the international dredging contracting market is dominated by the trailing suction hopper dredge, the cutter suction dredge is still widely used. Its ability to cut a wide range of soil types and its precision are the main advantages compared to other types of dredges. Therefore, it is both used for dredging of harbors and fairways as for land fill projects. Compared to other types of dredges, its dredging depth is limited. The largest cutter suction dredge reaches depths of up to 30 m, while the largest trailing suction hopper dredge can reach depths of up to 120 m. Figure 1.1 gives an example of a cutter suction dredge.

The cutter head is responsible for the actual excavation of the soil. It usually has six blades although there are also cutter heads with a different number of blades. The cutter head and the

cutter drive are mounted on a ladder. This ladder also provides the weight on the cutter head to ensure that the teeth on the cutter head can penetrate the soil.

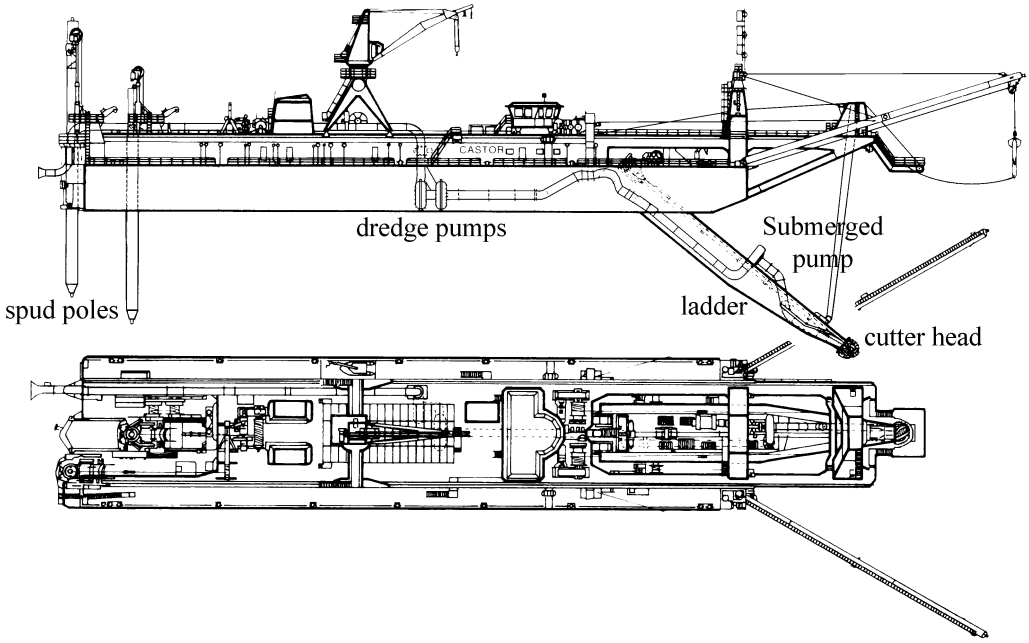

Figure 1.1: Cutter suction dredge Castor (Ballast Ham Dredging) and indication of relevant parts

The ladder can be lowered in order to cut at different depths. In practice, the maximum angle between the ladder and the horizontal is about 45 degrees. Larger angles lead to unacceptably high spillage rates. The left plot in Figure 1.2 shows a picture of a cutter head mounted on the ladder.

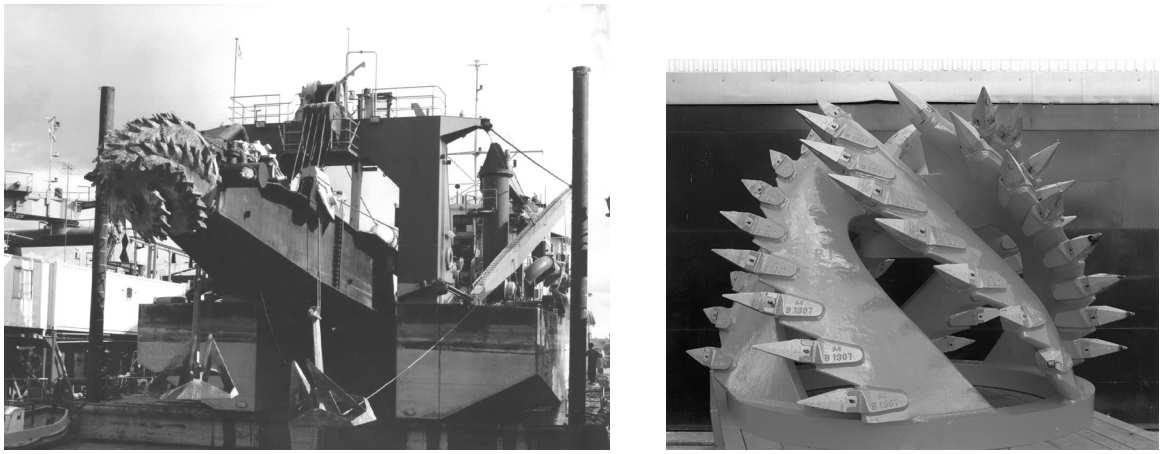

Figure 1.2: Cutter suction dredge HAM 219 and an example of a rock cutter head

Depending on the type of soil to be cut, either teeth or chisels are mounted on the blades. The teeth are connected to the blade by means of an adapter system. This adapter system enables a fast replacement of the teeth when they are worn-out. Furthermore, it ensures that the teeth are always positioned in the right way. The right plot in Figure 1.2 gives an example of a cutter head typically used in relatively hard formations. It has a compact geometry and thick blades which is necessary to withstand the high cutting forces. The adapters, the connections between the teeth and the blade, are clearly visible.

The cutter head drive shaft and the hub are connected by means of a screw joint. A cross-section of the cutter head when it is positioned in the breach/bank is shown in Figure 1.3.

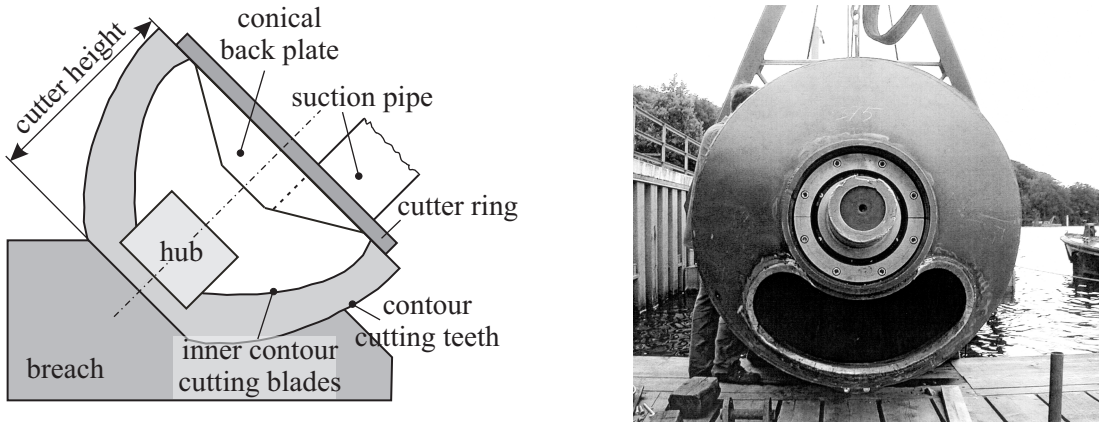

Figure 1.3: Cross-section of the cutter head when placed in a breach and front view of the back plate and suction mouth

Note that approximately half the cutter head is placed in the breach and not the entire cutter head. This is typical for the cutting of hard formations where the cutting forces are relatively high. The available cutter output limits the number of teeth that can be in the formation at the same time and thus the way the cutter head is positioned in the breach. For softer formations and lower cutting forces, the cutter head can be placed deeper in the formation.

The cut material is transported to the surface by means of a suction pipe that is also mounted on the ladder. It sticks through a back plate that closes the surface at the ring of the cutter head. This back plate is usually conical but it can also be flat. The advantage of a conical back plate as opposed to a flat back plate is that the distance between the breach and the opening of the suction pipe (i.e. the suction mouth) becomes smaller. This is beneficial for the production. The right plot in Figure 1.3 shows a front view of a conical back plate and the suction mouth.

A cutter head has two main functions. First of all, mechanically cutting of the soil and secondly, creating a water/soil mixture suitable for hydraulic transportation by the suction pipe. These two processes may set contradictory demands to the design and operational use of

a cutter head. From a cutting point of view, the cutter head needs to be designed in such a manner that an optimum between required power and wear is reached. From a production point of view, a minimum of spillage is required. A great deal of research is done on the cutting process of a cutter head and wear of the cutting teeth while cutting rock (Roxborough, 1975, Deketh 1995, Verhoef, 1997). However, little is known about the mixture forming process and the spillage phenomena (see paragraph 1.3).

1.2 Working method of a cutter suction dredge

The cutter suction dredge is basically a stationary type of dredge. It swings about a spud pole by means of side winches that are fastened by cables to side anchors. By slackening the starboard anchor cable and pulling in the port side anchor cable (or vice versa), the cutter suction dredge makes a circular movement about the spud pole. The angle of rotation of the cutter dredge depends on the position of the side anchors, but typical values are 30 degrees port to 30 degrees starboard side. The spud pole about which the cutter head swings (also called working spud) is mounted on a movable carriage, the spud carriage. As this working spud is fixed to the bottom, the cutter suction dredge can move forward by pressing the cylinder towards the stern (see Figure 1.4).

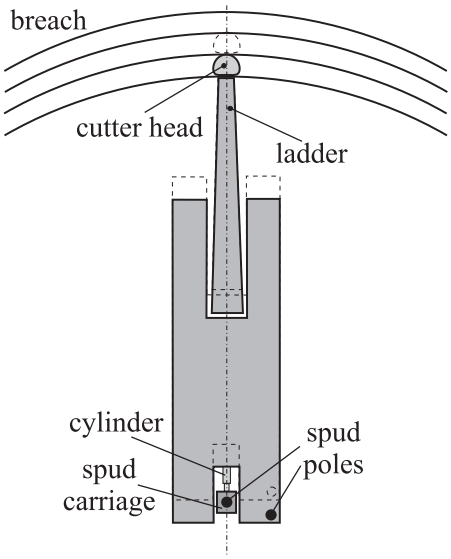

Figure 1.4: Swing and step pattern of a cutter suction dredge and its main parts

The second spud pole, shown in the figure on the starboard side at the stern of the cutter suction dredge, is the auxiliary spud. When the cylinder has reached the end of its stroke this auxiliary spud is lowered and the working spud is raised. The spud carriage is moved towards its initial position, the work spud is lowered and the auxiliary spud is raised again. The dredging procedure now continues.

The cutter head itself always rotates in the same direction, determined by the orientation of the teeth. Thus, depending on the direction in which the cutter suction dredge swings, there are two types of cutting: over-cut and under-cut. In the over-cut situation the teeth of the cutter head start to cut at the top of the breach/ bank working their way down. This means that the cutter blades move in the same direction as the cut particles that are moving towards the suction mouth. In the undercut situation the cutting teeth start to cut at the bottom of the breach working their way up (see Figure 1.5). Thus, in this case, the cutter blades move in opposite direction of the particles that move towards the suction mouth.

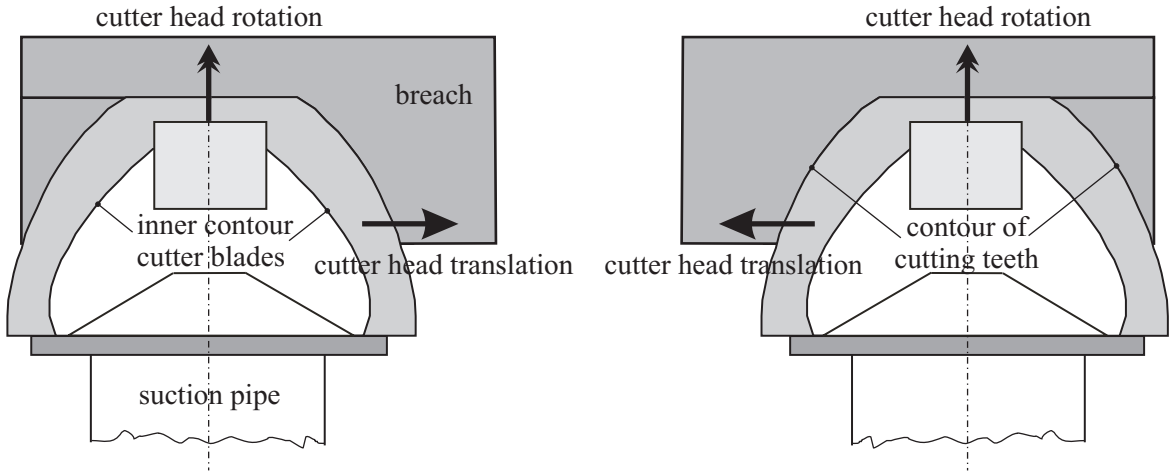

Figure 1.5: Two cutting situations: over-cut (left) and under-cut (right)

As the cutter suction dredge swings from starboard to port side and vice versa, both the under-cut and over-cut situation occur during the dredging operation. From practice it is know that, when cutting rock, in the under-cut situation the production is about two to three times higher than in over-cut situation.

Another disadvantage of spillage that has not been mentioned yet is the necessity of dredging a certain ‘over-depth’. When a certain depth is required the cutter head actually cuts at a larger depth than the required depth. This over depth is needed to take into account the spillage layer that is left on the bottom. Dredging of this over depth results in extra wear on the cutting teeth, more energy consumption and a more time consuming dredging operation. This results in a more costly dredging operation. So reducing the spillage leads, directly and indirectly, to a more efficient dredging process.

The table below shows a list of large cutter suction dredges owned by the Dutch dredging contractors.

Company	Boskalis		Ballast Ham Dredging	Van Oord ACZ
Name	Taurus	Ursa	Castor	Discovery Bay
Maximum dredging depth [m]	30	25	25	20
Suction pipe [mm]	Ø 850	Ø 950	Ø 850	Ø 800
Discharge pipe [mm]	Ø 850	Ø 900	Ø 850	Ø 750
Total power installed [KW]	15,618	15,830	13,957	8,277
Cutter output [KW]	3,680	3,300	3,680	-
Cutter head RPM	32	30	30	30
Suction flow [m^3/s]	3.4	3.0	3.4	3.0

The values for the rotational velocity of the cutter head and the suction flow are nominal values.

1.3 Process description and problem definition

As stated before, spillage can be defined as the soil that is cut during the dredging process but is not sucked up by the suction pipe. This definition implies two types of spillage:

- spillage resulting from the cutting process
- spillage resulting from the mixture forming process

The first type of spillage occurs because of the violent way in which the teeth penetrate the formation. Particles (chips) break out and are thrown away immediately. These particles have never really entered the cutter head. The second type of spillage is associated with the mixture forming process. In this case, the particles have entered the cutter head, but they are not sucked up for some reason and will (eventually) leave the cutter head again. This is the type of spillage that is investigated in this research.

The mixture forming process (and thus the spillage) is influenced by: the formation type, the geometry of the cutter head, the shape of the suction mouth and the operational parameters. For a cutter suction dredge the operational parameters are:

- the rotational velocity of the cutter head
- the suction flow (or mixture velocity)
- the haul velocity

The latter is the velocity with which the cutter head translates through the breach (see Figure 1.5). Reducing the spillage can be achieved in two ways. By optimizing the cutter geometry and by adjusting the operational parameters. The cutter head design is still strongly based on trial and error methods. Adaptations of the cutter head which prove to be successful are passed on to following designs. A method like this is far from ideal. First of all it is very time consuming and secondly a trial and error method misses flexibility. Adjusting the operational parameters is the only way of manipulating the spillage during the dredging operation itself. Still this is very difficult as there is no direct feedback on the productivity of the cutter head. Density meters are placed along the pipeline but this only gives an indication of the production. Especially when the cut particles are large, segregation of the particles, fluctuations in the flow and the slip between the water and the particles make it difficult to determine the production. Moreover, the density meter is usually placed at a significant distance from the cutter head, increasing the delay time. This makes it even more difficult to control the production process.

Research on cutter head spillage has been carried out by the dredging industry in the past in cooperation with WL|Delft Hydraulics. However, this research mainly concerned spillage while cutting sand and clay and not the hard formations that are considered here (though, for hard formations, a lot of research has been carried out on the cutting process).

When cutting sand, the particles will follow the water flow more easily compared to the cutting of hard formations. Then, the cut particles will be larger and consequently have a certain freedom of motion with respect to the water flow. It appeared that for sand there is a distinct relationship between the productivity of a cutter head and the ratio of the suction flow and the rotational velocity of the cutter head. Here the productivity is defined as the percentage of the total cut material that is actually sucked up. Naturally, the sum of the spillage percentage and the productivity equals 100%. As resulted from tests at WL|Delft Hydraulics by Mol (1977a) and Moret (1977a), the ratio of the suction flow and the rotational velocity of the cutter head determines the flow inside the cutter head. This was confirmed by extensive research and measurements on the flow inside the cutter head by Steinbusch et al. (1999) and Dekker et al. (1999). For the cutting of fine sand, the production is mainly (or to a large extent) determined by the ratio of the suction flow and the rotational velocity of the

cutter head. A dimensionless parameter derived from this ratio is the flow number as proposed by Steinbusch et al. (1999), i.e. $Q_s/\omega_c R_c^3$. In this flow number Q_s denotes the suction flow, ω_c is the angular velocity of the cutter head and R_c is the radius of the cutter ring. The flow number is an important scale parameter for performing model tests where uniformity of flow is required.

When the cut particles are relatively large, gravitational and inertial forces are expected to be more dominant in comparison with the cutting of sand. In that case, the spillage is determined by the individual values for the suction flow and the rotational velocity of the cutter head (and particle diameter and density) rather than the flow number only as is verified in Chapter 6.

Tests have been carried out at WL|Delft Hydraulics to determine the flow field inside the cutter head and measure the water velocities in and around the cutter head (see Chapter 2). These tests were carried out with a cutter head rotating in water without the presence of particles. The tests led to a very important aspect of a cutter head. It appeared that for every suction flow there is a transition value for the angular velocity of the cutter head. Below this transition value there is an ingoing flow along the entire contour of the cutter head that equals the suction flow.

However, when the rotational velocity of the cutter head is higher than the transition value, an outgoing flow starts to develop near the cutter ring. Consequently, the total ingoing flow is larger than the suction flow as this ingoing flow equals the sum of the outgoing flow and the suction flow. The test results also showed that the ratio between the transition value for the angular velocity of the cutter head and the suction flow appeared to be fairly constant. In other words, for flow numbers beyond a certain value there is always an ingoing flow, while below this value an outgoing flow will develop near the cutter ring.

The outgoing flow results from the fact that the cutter head works like a pump or actually a combination of two pumps: an axial pump and a centrifugal pump. The front part of the cutter head (i.e. near the hub) works like an axial pump due to the shape of the blades, comparable with a screw propeller (see Figure 1.2). It sucks in water from the front and accelerates this water towards the cutter ring. If the amount of water that is sucked in by the axial pump effect exceeds the suction flow water will have to leave the cutter head, which happens near the ring. Furthermore, the outgoing flow increases when the rotational velocity of the cutter head increases.

Because of the strong rotation of the water and consequently the large centrifugal forces, water is thrown out of the cutter head near the cutter ring. This can be seen as a centrifugal pump effect and the outgoing water flow can be the cause of spillage as it will drag along particles. As water is thrown out of the cutter head near the ring, the cutter head will suck in more water from the front because of continuity. In this way the centrifugal pump

effect directly affects (amplifies) the axial pump effect. In fact, the axial and centrifugal pump effects are so much linked with each other that they can not be seen as separate effects or modeled as two pumps in series. The term ‘pump effect’ is used because it is the commonly accepted term for this phenomena in the dredging industry. Although the flow of water induced by the pump effect may be significant, the pressure rise over the blades (pump head) will be negligible in comparison with the vacuum (or under pressure) caused by the suction flow (or rather the centrifugal pump on the cutter suction dredge). Thus the pump effect of the cutter head does not refer to a pressure rise inside the cutter head.

Some studies have been carried out in order to determine the influence of modifications on the geometry of the cutter head and the suction mouth on cutter head performance (Joanknecht, 1976; Slotta et al., 1977; Miltenburg, 1983; Slotta, 1984). Slotta showed that the height of the cutter head has a big influence on its productivity. Taller cutter heads are less productive because the particles located in the deepest part of the cutter head can not be picked up by the suction flow due to its limited influence. Only in the vicinity of the suction mouth, the suction force acting on the particle is considerable. Miltenburg showed that the use of skirts on the blades can have a positive effect on the productivity. Skirts are simple steel plates, welded on the blades at the trailing edge. Then, the blades basically become wider, narrowing the gap between successive blades. This will decrease the probability that particles can escape from the cutter head.

Although these studies were useful, the cutter head itself still remains a black box. Little is still known about the processes taking place inside the cutter head. The aim of this study is therefore to identify and describe the processes associated with spillage for cutting of relatively hard formations. The cutting process itself is not subject of this research. An important aspect in this is the performance of laboratory tests. Not only the measurements themselves will provide valuable data, but visualizations tests will be as equally important. They comprise an important part of this research as it is still unknown what happens inside the cutter head.

1.4 Scope and outline of thesis

In order to perform tests on a model scale, the relevant processes need to be scaled uniformly. Two aspects that can be distinguished in this are: the flow inside the cutter head and the behavior of the particles in this flow. The flow inside the cutter head is governed by the Navier-Stokes equations and the trajectory of a particle by its equations of motion. The models developed in this thesis mainly focus on the behavior of a single particle inside the cutter head. This means that the behavior of a single particle is assumed to be representative for a large number of particles, neglecting particle-particle interactions and the disturbance of

the flow due to the presence of the particles. Obviously this is a strong simplification of reality.

Under some conditions a single particle model may suffice but it is likely that, in general, the particle-particle interactions and the disturbance of the flow do play an important role. However, taking them into account at this point would be too ambitious considering the limited available knowledge and the complexity of the problem. Moreover, a single particle model will provide useful information and knowledge on the processes taking place. In this thesis the domain of validity and the limitations of a single particle model are investigated.

Writing the Navier-Stokes equations and the equations of motion of a particle in a dimensionless form shows the relative importance of certain parameters and the appropriate scale laws. The dimensionless Navier-Stokes equations and the dimensionless equations of motion for a single particle in a fluid are given in Appendix A. By means of these dimensionless equations, it is shown that on prototype scale inertia of the particles will play an important role when the particle relaxation time is approximately of the same order of magnitude as the characteristic time scale of the fluid. Furthermore, the particle Reynolds number (Re_p) on prototype scale is well within the turbulent or Newton range ($1\times10^3<Re_p<2\times10^5$). In this range the drag coefficient is independent of Re_p. This yields that, the particle drag coefficient will vary between 0.4 for spherical particles and 1.1 for sand-like particles (van Rijn, 1984).

Tests on model scale should be carried out in the same regime as on prototype scale. This means that the ratio of the relaxation time and the characteristic time scale of the fluid on model scale should have the same order of magnitude as on prototype scale. In addition, the particle Reynolds number should be in the Newton range as well, so that the drag coefficients are equal on both scales.

By means of simple guiding tests with single particles more information is obtained about the behavior of particles inside the cutter head. Residence times of the particles are measured for different values of the operational parameters. Video-recordings are made to observe and compare the particle trajectories. The execution of these tests is described in Chapter 4. This chapter starts with the derivation of the appropriate scale laws.

In Chapter 5 a model is set up in order to simulate the trajectory of a single particle inside the cutter head. The flow inside the cutter head is approximated by a superposition of a forced vortex to represent the rotation of the fluid and a sink to represent the suction flow. Particle trajectories are simulated for different values of the operational parameters and compared with the trajectories resulting from the model tests. Furthermore, the influence of the haul velocity on the particle trajectory is discussed.

Cutting tests are performed on a model scale to determine the production and spillage of the cutter head as a function of the operational parameters. In addition, video-recordings

are made of the processes taking place inside the cutter head in order to obtain a qualitative image. The recordings are used to determine the filling degree of the cutter head and provide useful information on the validity of a single particle model. This is described in Chapter 6. Additional tests are performed to determine the influence of the cutter head inclination angle and the particle diameter on the production percentage.

An important result of the cutting tests is the fact that the production curves have an optimum. This means that an initial increase in rotational velocity of the cutter head results in an increase in production. To determine whether this increase in production was caused by the cutter blade geometry, another series of tests was performed. In these tests the influence of the cutter head geometry on the trend of the production curves is investigated. Tests are performed with a cylindrical cutter head and the crown cutter head that was used in the previous cutting tests. The outcome of these tests is described in Chapter 7.

In Chapter 8 a model is set up to simulate the trajectory of a single particle along a cutter blade. This model is used to verify if the cutter blade geometry is responsible for the increase in production with increasing rotational velocity. Initially, the flow inside the cutter head is represented by a forced vortex and a sink, similar to the flow model used in Chapter 5.

Finally, the conclusions of this research and recommendations for further research are given in Chapter 9.

Chapter 2
Literature Review

2.1 Available literature on scale laws

In 1968 Slotta performed cutter head model tests to visualize the flow near and within a rotating cutter head. The tests have been performed on a cutter head with a ring diameter of 16.5 cm. Streams of hydrogen bubbles produced by electrolysis of water were used to visualize the fluid stream. The flow visualization study emphasized the improved efficiency of the cutter suction dredge when a back plate is installed before the suction mouth.

Slotta, also set up similitude criteria for cutter head models based on Buckingham's Pi Theorem. Amongst the Reynolds and the Froude numbers, the normalized velocity was mentioned as an important parameter. The normalized velocity represents the ratio of the rotational velocity of the cutter head and the mixture velocity (velocity in the suction pipe).

Similarity rules have also been set up by Joanknecht (1976), making a sub-division between the cutting process and the transportation of particles towards the suction mouth. The tests focused on the cutting of sand with a d_{50} of 200 μm. For the cutting process he used the Froude scaling as it is governed by gravitational and inertia forces. For the transportation of particles he used the ratio of the terminal velocity and the mixture velocity as the scale law.

2.2 Research performed at WL|Delft Hydraulics

In the seventies, extensive research was performed on dredge cutter head performance. Dutch contractors, combined in the association CSB (Combinatie Speurwerk Baggertechniek) and Rijkswaterstaat, have performed a series of tests at and in cooperation with WL|Delft Hydraulics. The research was subdivided into research on the flow near and inside the cutter head and on the cutting process. In all these tests the entire cutter head, including back plate and suction mouth, were geometrically scaled. The fluid velocities were scaled according to

the Froude number, i.e. the square root of the length scale. In all the tests the cutter head inclination angle was 30º. Important results of the tests concerning the flow inside the cutter head were:

- The cutter head works like a combination of an axial and centrifugal pump. It sucks in water from the front and accelerates it towards the back plate (axial pump effect). Near the back plate or cutter ring the centrifugal pump effect becomes important, by which water is thrown out of the cutter head. The combination of the axial and centrifugal pump action results in a flow inside the cutter head as shown in Figure 2.1.

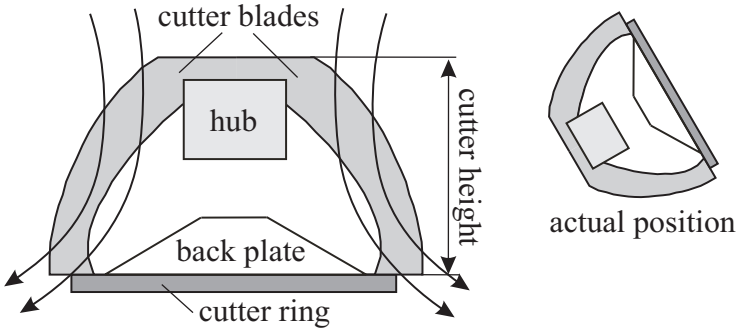

Figure 2.1: Combination of the axial and centrifugal pump action of the crown cutter head

- For every mixture velocity there appeared to be a transition value for the rotational velocity of the cutter head. Below this transition value there was an inward flow along the entire contour of the cutter head. Beyond the transition value an outward flow starts to develop near the cutter ring. This outward flow increased with increasing rotational velocity.
- The ratio of the transition value for the rotational velocity and the mixture velocity was fairly constant; i.e. $\omega_c R_c / v_m = 0.42$ for a cutter head with a diameter of 0.6 m. This value was almost identical in both under-cut and over-cut situation.
- The flow field inside the cutter head in under-cut situation clearly differed from the flow field in over-cut situation. However, varying the rotational velocity and mixture velocity in either the under-cut or over-cut situation did not have a large influence on the flow field. It did have an effect on the magnitude of the velocities. (Moret, 1977a).

- Tests with a freely rotating (not placed in a bank) cutter head that was hauled, showed that the transition value for the rotational velocity had increased in both under and over-cut situation; i.e. $\omega_c R_c / v_m = 0.5$ and 0.6 respectively. In other words, placed in a bank the fluid moves out of the cutter head easier and with a higher flow rate.
- According to Mol (1977a), the influence of the haul velocity could be accounted for by superposing the haul velocity on the flow field of the stationary situation. The haul velocity facilitated the fluid flow out of the cutter head near the cutter ring.

- Tests where plastic particles (ρ_p = 1118 kg/m^3, d_p = 0.02 m) were injected in the cutter head (no haul velocity) showed that the trajectory of the particles depended on the velocity ratio $\omega_c R_c/v_m$.
- In both under and over-cut situation the amount of particles sucked up depended on $\omega_c R_c/v_m$. The production percentage, P, plotted as function of $\omega_c R_c/v_m$ showed the following trend in both under and over-cut situation.

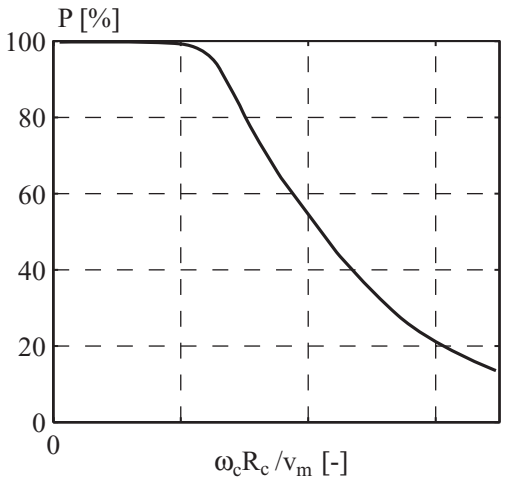

Figure 2.2: General trend for the production percentage as function of the velocity ratio for the cutting of sand

Here P is defined as the ratio of the number of particles sucked up and the number of injected particles.

- In the over-cut situation the production was less than in the under-cut situation.
- The influence of the mixture velocity on the absolute particle velocity was negligible (Mol, 1977b).

- Injections with coarse sand (d_{50} = 500 μm) and fine gravel (d_{50} = 1800 μm) showed that gravity had more influence on the particle trajectories when the size of the particles increased (the cutter head inclination angle was 30º). The trajectories of the particles with the larger diameter deviated more from the streamlines of the fluid than the paths of the smaller particles.
- In under-cut situation the drag force and the gravitational force could cancel each other at some parts of the cutter head.
- In over-cut situation the gravitational force always had a negative influence on the number of particles that was sucked up (Moret, 1977b).

Actual cutting tests in sand (d_{50} = 120 μm) in both under and over-cut have been performed at WL|Delft Hydraulics with a 0.6 m diameter cutter head (Mol, 1977c). The haul velocity, mixture velocity and rotational velocity of the cutter head were varied in these tests. The production rate (in m^3/s) was measured as a function of these variables. It appeared that in under-cut situation the production rate was proportional to the haul velocity. This was ascribed to the fact that in under-cut a more or less homogeneous mixture is present inside the cutter head, while the haul velocity does not have a significant influence on the flow inside the cutter head. In over-cut situation however, the production rate was almost independent of the haul velocity. The poor mixing capacity of the cutter head in over-cut and the influence of gravity were mentioned as possible causes. In all cases the production rate was higher in under-cut than in over-cut.

The shape of the curves for the production percentage plotted against $\omega_c R_c/v_m$ did not differ much from the production curves previously found for the injections with plastic particles (see Figure 2.2). The production percentage was defined as the amount of sand sucked up divided by the amount of sand cut off. In the under-cut situation the haul velocity did not seem to have an effect on the production percentage. In over-cut, on the other hand, the production percentage increased with increasing haul velocity.

2.3 Research performed at the Laboratory of Dredging Technology

Slotta et al. (1977) performed additional tests at the laboratory of Dredging Technology at the Delft University of Technology, focusing on the production percentage as affected by the cutter height. He used several different types of cutter heads with varying heights (see Figure 2.1 for the definition of cutter height). The inner ring diameter of the cutter heads was 0.38 m. He performed tests in both banks of sand (d_{50} = 200 μm) and cemented gravel (20 mm < d_p < 30 mm). Besides the geometry of the cutter head, the haul velocity and the rotational velocity of the cutter head were varied. The cutter head inclination angle was 45º. The tests in sand showed somewhat different results compared with the tests performed at WL|Delft Hydraulics. In both the under-cut and over-cut situation an increase in haul velocity resulted in an (almost linear) increase in production rate. The production percentage (or efficiency) was almost independent of the haul velocity in the over-cut situation, while in the under-cut situation the production percentage decreased with increasing haul velocity. In addition the tests showed that in under-cut the shorter cutter heads often have a higher production rate and production percentage than taller cutter heads. In over-cut the difference between short or tall cutter heads was not as significant.

The anomaly with the tests performed at WL|Delft Hydraulics could result from many factors. First of all the cutter heads were not exactly scaled geometrically. Furthermore, the average diameter of the sand particles used by Slotta was much larger (a factor 1.7), while the scale of the cutter head was a factor 1.5 smaller. In other words, the relative influence of the

particle diameter was much larger in the tests performed by Slotta. Secondly, a factor that also played a role is the way the cutter head was placed in the bank since the ratio of the step size and cutting depth also differed from each other in both tests. Additionally, the ladder inclination angle that was used in the tests at WL|Delft Hydraulics and the tests by Slotta differed from each other (i.e. 30º and 45º degrees respectively). This will also have a large effect on the production percentage.

The tests in the gravel banks, which were only performed in under-cut situation, showed that the production rate increased with increasing haul velocity. The production percentage decreased with increasing haul velocity. Both the production rate and percentage were generally higher for the short cutter head than for the tall cutter head.

Miltenburg (1983) has performed tests at the Laboratory of Dredging Technology studying both the flow inside the cutter head and the mixture forming while cutting sand. The diameter of the cutter heads that were used varied between 0.32 m and 0.4 m. Froude scale laws were applied to scale the fluid velocities inside the cutter head. Tests concerning the flow have been performed on an open and a closed crown cutter head (the same that is used in the tests described in Chapter 6 and Chapter 7), an open cutter head without teeth, an open and a closed cylindrical cutter head. In addition different geometries for the back plates and suction mouths were tested. Basically the same conclusions were drawn as from the tests performed at WL|Delft Hydraulics. Most important being the pump action of the crown cutter head.

The cutting tests have been performed on sand with a d_{50} of 180 μm while varying the rotational velocity of the cutter head, the mixture velocity and the haul velocity. The production appeared to be strongly dependent on the velocity ratio $\omega_c R_c/v_m$. The curves for the production percentage plotted as a function of $\omega_c R_c/v_m$ showed the same trends as shown in Figure 2.2. In under-cut situation the production percentage was always higher than in over-cut.

Miltenburg did not find a clear relationship between the production percentage and the haul velocity and considered this relationship as uncorrelated. The haul velocities Miltenburg tested (i.e. 0.1 m/s, 0.2 m/s and 0.3 m/s) were a factor 2 larger than the haul velocities tested by Slotta. The haul velocities tested by Slotta and WL|Delft Hydraulics were comparable, considering the scale difference.

Some basic modifications on the cutter head geometry and back plate could improve the production percentage by 10%.

Summarizing, the most important conclusions were the existence of a pump effect of the cutter head and the relationship between the production percentage and the ratio $\omega_c R_c/v_m$. Furthermore, in under-cut situation the production percentage is higher than in over-cut situation. Quantitative comparison of the test results is difficult since many important factors differed in the tests (e.g. cutter head geometry, diameter of the sand etc.).

The conclusions that were drawn particularly apply to the cutting of sand. For the cutting of rock where larger particles are present in the cutter head, no data is available except for the tests performed by Slotta. As this is the field of interest in this thesis, the execution of model tests will be eminent in order to obtain more insight in the mixture forming processes taking place inside the cutter head. A more profound understanding of the scale laws and determining the domain of validity of these scale laws is a first requirement. This is described in the next chapter.

Chapter 3
Dimensional Analysis, Governing Parameters and Scale Laws

As a significant part of this research deals with the execution of laboratory tests, it is important to know what processes dominate the behavior of the particles and how these processes are scaled. This is done in the following paragraphs by investigating the governing equations for the fluid flow and the equations of motion of the particle. The scale laws derived focus on the behavior of a single particle only.

3.1 Dimensional analysis and scale laws for laboratory tests

Dimensional analysis is a method for reducing the number and complexity of experimental variables which affect a given physical phenomenon (White, 1994). Dimensional analysis therefore reduces the number of experiments that have to be performed. Moreover, dimensional analysis also provides scaling laws that give insight in the problem and make it possible to perform the experiments on a model scale instead of a prototype scale. Prototype tests are usually undesirable since they are very costly and often difficult to perform. On a model scale it is easier to control the test conditions and the costs are far less than on a prototype scale. However, performing model tests has its disadvantages too, as different processes taking place at the same time on prototype scale may be scaled according to different scale laws. For interpretation of the model test results it is important to realize that certain processes may be scaled incorrectly and the consequences of this should be evaluated. Often such an evaluation will be an estimation based on the gained insight as the results can not be compared directly with the prototype situation due to the lack of test results on prototype. Nevertheless, model tests are essential as they provide a lot of insight on the different processes taking place and on the appropriate scale laws.

Scale laws ensure that the relevant processes on model scale are similar to those on prototype scale. Three types of similarity are distinguished:

- geometrical similarity
- kinematic similarity
- dynamic similarity

Geometric similarity exists between model and prototype if the ratio of all corresponding dimensions in the model and prototype are equal. Kinematic similarity is the similarity of time as well as geometry. Consequently the velocity-scale ratio will be the same on model and prototype scale. Dynamic similarity exists when the model and prototype have similarity of geometry, time and force. This means that the length-scale ratio, time-scale ratio and force-scale ratios are the same for model and prototype. Often, dynamic similarity sets contradictory demands to the scaling of all the forces and therefore choices for the relevant forces and scale law should be made.

With respect to the mixture forming in cutter heads dimensional analysis has been performed by Slotta (1968) and Joanknecht (1976). While Slotta derives several dimensionless groups according to the Buckingham pi theorem (Buckingham, 1914) , Joanknecht directly states that the external force on the soil particles is gravitational in origin and that Froude is the dominating parameter. Furthermore, he states that the ratio of the fall velocity of the particle and the suction velocity should be equal on prototype scale and model scale. No further physical argumentation is given for this. Therefore the appropriate scale laws will be derived again using the dimensionless Navier-Stokes equations and the dimensionless equations of motion for a single particle in a fluid (see Appendix A).

3.1.1 Dimensionless Euler equation

In Appendix A it is shown that the Reynolds number is large enough to neglect the viscous stresses. Therefore, the dimensionless Navier-Stokes equations can be simplified and reduced to the dimensionless Euler equation (White, 1994)

$$\frac{L}{TU}\frac{\partial \bar{v}_f'}{\partial t'} + \bar{v}_f' \cdot \nabla' \bar{v}_f' = -\frac{P_f}{\rho_f U^2}\nabla' p_d' \tag{3.1}$$

in which ρ_f is the density of the fluid, v'_f is the normalized water velocity, t' is the normalized time scale and p_d' is the normalized pressure scale (for the hydrodynamic pressure). The characteristic length scale, time scale velocity scale and fluid pressure scale (or actually **pressure difference** scale) are represented by L, T, U and P_f respectively. As described in Appendix A, the characteristic time scale for the flow T can either be the residence time of a fluid particle or a specific time based on the cycle of the cutter head. The first is applicable when the suction flow is dominant and the second is applicable when the rotational velocity of the cutter head is dominant. The residence time of a fluid particle is defined as

$$t_r = \frac{V_c}{Q_i} \tag{3.2}$$

in which V_c is the volume of the cutter head and Q_i is the total ingoing flow. For a cutter head with six blades a specific time based on the cycle of the cutter head would be the inverse of the blade frequency

$$t_{blade} = \frac{60}{6 \cdot n_c} \tag{3.3}$$

in which n_c is the rotational velocity of the cutter head in RPM.

In Equation (3.1), the two parameters describing the flow are:

$$St = \frac{L}{TU};\ Eu = \frac{P_f}{\rho_f U^2}$$

where St is the Strouhal number and Eu is the Euler number. The Strouhal number gives the ratio of the local acceleration and the convective acceleration, while the Euler number gives the ratio of the pressure (gradient) and the inertia forces.

Similar flows on model and prototype scale requires that the Strouhal and Euler number are equal on both scales. Scaling according to the Euler number implies that the velocities are scaled according to the square root of the length scale. As the time scale is the ratio of the length scale and velocity scale, it is also scaled according to the square root of the length scale. Consequently, the Strouhal number on model scales equals that on prototype scale when scaling according to the Euler number. It is therefore concluded that the Euler number is the appropriate parameter to scale the flow.

3.1.2 Dimensionless equation of motion for a single particle

Taking into account the drag force, added mass force, pressure gradient force, lift force gravitational force and buoyancy force, the dimensionless equation of motion for a single particle in a fluid can be written as (see Chapter 5)

$$\begin{aligned}\frac{\left(\rho_p + \rho_f C_{AM}\right)}{\rho_f}\frac{U_s}{gT_p}\frac{d\overline{v}_s'}{dt_p'} = &-\frac{3C_d}{4}\frac{U_s^2}{d_p g}\overline{v}_s'\left|\overline{v}_s'\right| \\ &+\frac{\left(\rho_p - \rho_f\right)}{\rho_f}\left(\frac{U_f}{gT_f}\frac{\partial\overline{v}_f'}{\partial t_f'} + \frac{U_f^2}{gL}\overline{v}_f' \cdot \nabla'\overline{v}_f' + \overline{g}'\right) - C_L\frac{U_s}{gT_f}\overline{v}_s' \times \overline{\Omega}'\end{aligned} \tag{3.4}$$

in which v'_f is the normalized water velocity, v'_s is the normalized slip velocity between fluid and particle, Ω' is the normalized vorticity, d_p is the particle diameter, ρ_p is the particle density and g is the acceleration of gravity. Moreover, U_s, U_f, T_p and T_f are the characteristic velocity scale for the slip velocity and for the fluid velocity and the characteristic time scales for the

particle and the fluid. The constants C_d, C_{AM} and C_L are the drag coefficient, the added mass coefficient and the lift coefficient respectively.

Again the Strouhal number and Froude number can be recognized in the dimensionless parameters in Equation (3.4)

$$Fr_p^2 = \frac{U_s^2}{gd_p},\ Fr_f^2 = \frac{U_f^2}{gL},\ St_p = \frac{U_s}{gT_p},\ St_f = \frac{U_f}{gT_f},\ St_{pf} = \frac{U_s}{gT_f}$$

in which the subscripts ‘p’ and ‘f’ denote particle and fluid. Uniform particle trajectories on model and prototype scale requires that the dimensionless equation of motion is equal on both scales. Therefore, the Strouhal and Froude numbers need to be equal on both scales as well as the densities of particle and fluid. In addition, the added mass coefficient, the lift coefficient and the ratio of the drag coefficient and particle diameter need to be equal on both scales.

In addition to the aforementioned dimensionless parameters another important dimensionless parameter is the ratio of the tip speed of the cutter head ($\omega_c R_c$) and the mixture velocity (v_m). On a model scale this ratio needs to equal the value on the prototype scale, since it assures similarity of the flow field inside the cutter head. Implicitly, this demand is also met by Fr_f.

In the dimensionless equation of motion the characteristic time scales for the particle T_p and fluid T_f are written explicitly. The ratio of these two time scales denotes an important parameter, as it a measure for how the particle will react to changes in the flow. The characteristic time scale of the particle can be represented by the particle relaxation time t_p. For relatively heavy particles this particle relaxation time is the ratio of the terminal settling velocity and the acceleration of gravity (Fuchs, 1964), as described in Appendix A.

$$t_p = \frac{v_{ts}}{g} \tag{3.5}$$

The particle relaxation time can be defined as a characteristic time required for a particle to adjust or relax to a new condition of forces (Hinds, 1982).

As mentioned before, the characteristic time scale for the fluid can be represented by the residence time of a particle in the cutter head t_r or by the specific time based on the cycle of the cutter head. If the particle relaxation time is much smaller than the characteristic time scale of the fluid, the particle will follow the fluid as if inertialess. On the other hand, if the particle relaxation time is of the same order of magnitude as the characteristic time scale for the fluid (or larger), inertia will play an important role. Then the particle is less likely to follow the fluid. Therefore, the ratio of the particle relaxation time and the characteristic time scale for the fluid is an important parameter that has to be equal on prototype and model scale. This also follows from the ratio of St_p and St_f.

In the next paragraph the scale laws will be applied to derive the appropriate values for variables during the model tests in this thesis.

3.2 Scaling the relevant parameters

The variables that are of importance and need to be scaled when performing model tests are:

- the diameter of the cutter head D_c [m]
- the rotational velocity of the cutter head n_c [RPM]
- the mixture velocity in the suction pipe v_m [m/s]
- the diameter of the particle d_p [m]
- the density of the particle ρ_p [kg/m^3]

Scaling these variables can be subdivided into scaling of the cutter head, the operational parameters and the particle parameters.

3.2.1 Geometrically scaling the cutter head and scaling the operational parameters

In order to define the model scale, the prototype scale needs to be specified first. In practice, the larger cutter heads used for the cutting of rock have an outer ring diameter of approximately 2.8 m to 3.5 m. Considering the dimensions of the facilities at the Laboratory of Dredging Technology this yields a model scale of 1:8 (see next chapter). All geometrical parameters need to be scaled accordingly including the back plate, size (and shape) of the suction mouth, suction pipe diameter and diameter of the cutter axis.

According to the dimensionless Navier-Stokes equation or Euler equation, the Euler number is the appropriate parameter to scale the flow (see Equation (A.5)). Thus the velocities are scaled according to the square root of the length scale. For the mixture velocity on model scale this implies

$$[v_m]_{model} = [v_m]_{prototype} \sqrt{\frac{1}{8}} = \frac{[v_m]_{prototype}}{\sqrt{8}} \tag{3.6}$$

and for the rotational velocity on model scale

$$[n_c]_{model} = [n_c]_{prototype} \sqrt{8} \tag{3.7}$$

In practice the suction flow is fairly constant during operation and will depend on the size and design of the centrifugal pump on the cutter suction dredge. The rotational velocity of the cutter head on the other hand can be varied during operation, although most of the time it will

operate at its nominal value. Typical values, on prototype scale, for the rotational velocity of the cutter head and mixture velocity are: 30 RPM and 5 m/s.

3.2.2 Scaling the particle parameters

The dimensionless equation of motion shows that all densities have to be equal on model and prototype scale in order to have uniform particle trajectories. In practice the density of the rock may vary from 2000 kg/m^3 to 2650 kg/m^3. Moreover, uniform particle trajectories on model and prototype scale requires that the slip velocity v_s is scaled with the same factor as the fluid velocities. According to Fr_p and Fr_f this yields that the particle diameter should be scaled with the same factor as the cutter head and has to be on a 1:8 scale as well. Additionally the drag coefficient should be equal on both scales. Whether this is the case depends on the geometry of the particle and the particle Reynolds number and is further investigated.

Although the shape of the cut particles may vary in practice due to the cutting process and specific rock characteristics like the presence of fractures and rock structure (Verhoef, 1997), it is assumed that particles are spherical or sand-like. Besides its shape, the diameter of the particles varies as well due to the cutting process. However, a reasonable measure for the largest particles inside the cutter head is the gap between two successive blades. Only particles smaller than this gap can enter the cutter head. Assuming that the average particle size (d_{50}) corresponds with half the distance between two blades (i.e. ≈ 16 cm), the d_{50} of the particles on prototype scale is 8 cm. The particle Reynolds number for a particle with a diameter of 8 cm is in the Newton range when the following condition for the slip velocity is met

$$\mathrm{Re}_p = \frac{|v_s| d_p}{\nu} > 1000, \quad |v_s| > 0.0125 \text{ [m/s]}$$

Considering the typical fluid velocities in the cutter head of 4 to 5 m/s it is fair to assume that this condition is always met and that the particle Reynolds number is in the Newton range. In this range the drag coefficient is 0.4 for a sphere and 1.1 for a sand-like particle (van Rijn, 1984). Thus on model scale, the particle Reynolds number has to be in the Newton range as well. As the particle diameter is 1 cm on model scale the slip velocity needs to be larger than

$$\left[\mathrm{Re}_p\right]_{\mathrm{model}} = \frac{|v_s| 0.01}{\nu} > 1000, \quad |v_s|_{\mathrm{model}} > 0.1 \text{ [m/s]}$$

The terminal settling velocity of a particle with a diameter of 1 cm and a density of 2200 kg/m^3 is in the Newton range and its value is given by Equation (3.8)

$$v_{ts} = \sqrt{\frac{4}{3C_d} \frac{(\rho_p - \rho_f)}{\rho_f} g d_p} \tag{3.8}$$

This means that the terminal settling velocity of the particle has a value of

v_{ts} = 0.34 m/s sand-like particles; C_d = 1.1 [-]
v_{ts} = 0.57 m/s spherical particles; C_d = 0.4 [-]

With typical values for the fluid velocities of 1 to 2 m/s on model scale and the assumption that the slip velocity $|v_s|_{model}$ approximately has the same value as the terminal settling velocity, the condition that $|v_s|_{model} > 0.1$ m/s is always met. This means that the particle Reynolds number is always in the Newton range and the constant drag coefficient of 0.4 for a sphere or 1.1 for a sand-like particle apply.

When the particle Reynolds number is in the Newton range, particle inertia should play a dominant role. A significant parameter describing the influence of particle inertia with respect to the fluid flow is the Stokes number, which is the ratio of the particle relaxation time and the characteristic time scale of a fluid

$$\text{Stokes} = \frac{t_p}{T_f}$$

where t_p is defined as shown in Equation (3.5). Particle inertia has a significant influence on the spillage phenomena, since it increases the freedom of motion of the particle with respect to the water flow. Generally, spillage will be larger when particle inertia is larger.

The Stokes number indicates how a particle will react to changes in the flow. The larger the Stokes number, the more particle inertia plays a role and the more likely it is that the particle Reynolds number is in the Newton range. In Appendix A it is shown that, on a prototype scale, the particle relaxation time has the same order of magnitude as the characteristic time scale for the fluid over a wide range. This implies that particle inertia generally plays an important role on a prototype scale and the particle Reynolds number will be in the Newton range.

On a model scale the Stokes number should not only be large enough, but is should also equal that on prototype scale. In Appendix A it is shown that the characteristic time scale for the fluid can either be the residence time of the fluid (suction flow dominates) or a specific time based on the cycle of the cutter head (rotational velocity dominates). Both are scaled according to the square root of the length scale, which means that in this case

$$T_{f,model} = \frac{T_{f,prototype}}{\sqrt{8}}$$

With the particle relaxation time being defined as in Equation (3.5) and the terminal settling velocity defined as in Equation (3.8), the particle relaxation time also scales according to the square root of the length scale

$$t_{p,model} = \frac{t_{p,prototype}}{\sqrt{8}}$$

This yields that the Stokes number on model scale is equal to that on prototype scale and the particle will react in a similar way to changes in the flow. In addition, as the particle relaxation time has the same order of magnitude as the characteristic time scale for the fluid over a wide range (in analogy with the prototype scale), particle inertia will play a significant role on a model scale. Therefore it is fair to assume that the particle Reynolds number lies in the Newton range on a model scale.

In regions inside the cutter head where fluid velocities are less significant, gravity will be dominant. Whether the particle is still in the Newton range in this case needs to be investigated. The equation of motion for a particle in free fall in quiescent water is solved using the relationship between the drag coefficient and the particle Reynolds number for spherical particles as proposed by Turton and Levenspiel (1986):

$$C_d = \frac{24}{Re_p}\left(1+0.173\,Re_p^{0.657}\right)+\frac{0.413}{\left(1+\left(1.63\times10^4\right)Re_p^{-1.09}\right)} \tag{3.9}$$

The simulations showed that for a particle with a diameter of 0.01 m and a density of 2200 kg/m^3 the particle Reynolds number exceeds 1000 within 0.02 s. Therefore it can be assumed that these particles are within the Newton range almost immediately and a constant drag coefficient of 0.4 (or 1.1) is acceptable. The terminal velocity for these particles is described by Equation (3.8), which assures that the particle trajectories are uniform on model and prototype scale if the flow is scaled according to the Euler number, the particle is geometrically scaled and the density is equal on both scales.

It should be noted that there is a lower limit for the model scale. If the model scale is chosen too small, the particle becomes too small to ensure that its Reynolds number is in the Newton range. The drag coefficient is no longer constant and the demand of uniform particle trajectories on model and prototype scale is no longer satisfied.

As the particles are geometrically scaled the added mass coefficient is equal on both scales. The lift coefficient for non-rotating particles depends on the particle Reynolds number and the Reynolds number based on the velocity gradient. Mei (1992) has proposed an approximate expression for the lift based on the results of Saffman (1965) and Dandy and Dwyer (1990). It appears that increasing Re_p results in a decrease in the lift coefficient until it eventually becomes constant. However, the data presented by Dandy and Dwyer (1990) is valid for $0.1 \leq Re_p \leq 100$. As no further information is present for lift coefficients at larger Reynolds numbers, it is assumed that the lift coefficient remains constant even for $Re_p > 100$. As the

Reynolds number based on the velocity gradient is equal on model and prototype scale and the particle Reynolds number is larger than 100 on both scales, the lift coefficient is equal on both scales.

Summarizing, based on the dimensionless parameters in the Navier-Stokes equations and the dimensionless equation of motion for the particle, it is concluded that the particle size should be scaled geometrically. Then

- the particle Reynolds number is large enough on both scales to assume that it is the Newton range, which implies that the drag coefficient is constant and equal on both scales.
- the fluid velocities are scaled according to the square root of the length scale. The flow is uniform on prototype and model scale as $\omega_c R_c^3/Q_s$ (ratio of circumferential speed and suction flow) is equal on both scales. Furthermore, the Euler number is equal on both scales when assuming similar pressure losses.
- the particle (settling) velocity and the fluid velocities are scaled similarly and thus the particle trajectories are uniform on both scales.
- the ratio of the characteristic times scales for the particle and fluid are equal on both scales. The particle will therefore react in a similar manner to changes in the flow on model scale as on prototype scale.

3.3 Conclusions

In this chapter the appropriate scale laws are identified for laboratory tests when focusing on particle transport inside a cutter head. The governing parameters in the research are: the dimension of the cutter head, the dimension and density of the particles inside the cutter head and the operational parameters of the cutter head.

The Reynolds number for the flow inside the cutter head is large enough to neglect the viscous stresses and thus the Euler equation is the governing equation for the flow. The Euler number is the appropriate parameter for scaling the flow which yields that, on a model scale, the water velocities are scaled according to the square root of the length scale.

For obtaining uniform particle trajectories on model and prototype scale the Froude number is the appropriate scale parameter. This means that the particle needs to be scaled geometrically, while its density and drag coefficient need to equal the corresponding values on prototype scale.

When the flow inside the cutter head is dominated by the suction flow, the characteristic time scale for the fluid is based on the residence time of the fluid. When the flow is dominated by

the rotational velocity of the cutter head, the characteristic time scale for the fluid is based on the cycle of the cutter head. The characteristic time scale for the particle is its relaxation time.

On prototype scale the ratio of the particle relaxation time and the characteristic time scale is large enough to assume that particle inertia will play a dominant role. In addition, the slip velocity between particle and the fluid is large enough to assume that generally the particle Reynolds number is in the Newton range. This means that the drag coefficient is constant on prototype scale.

A 1:8 model scale (the scale on which model tests can be performed) is large enough to assure that the particle Reynolds number is still in the Newton range on model scale. Furthermore, geometrically scaling the particle ensures that the ratio of the particle relaxation time and the characteristic time scale are equal on both scales and thus the particle will react in a similar manner to changes in the flow.

Chapter 4
Laboratory Tests with Single Particles inside the Cutter Head

The type of spillage studied in this research is associated with the particle behavior inside the cutter head. A problem that arises is that in practice it is impossible to see what happens inside in the cutter head. Therefore, little is known about the trajectories of the particles, which makes it difficult to model the spillage phenomena.

In order to obtain more insight on particle behavior and their trajectories inside the cutter head, model tests are performed. In these tests, single particles are injected in a rotating cutter head. The aim of the tests is to determine the percentage of sucked up particles or production percentage, while varying the rotational velocity of the cutter head and suction flow. This will give an indication of the influence of these operational parameters on spillage. Furthermore, the particle trajectories inside the cutter head are filmed using under-water cameras.

As described in Chapter 1 a single particle approach is chosen to model the behavior of the particles inside the cutter head. Acknowledging that this is a strong simplification of reality, the behavior of a single particle is assumed to be representative for a large number of particles, neglecting particle-particle interaction and the disturbance of the flow due to the presence of the particles. Therefore single particles are injected into the cutter head.

In the tests the cutter head is placed in a concrete bank in a flume filled with water. However, the cutter head is not moved (hauled) within this bank. The bank only serves as a boundary to represent the actual situation when a cutter head is cutting. It is assumed that neglecting the haul velocity will not have a significant influence on the behavior of the particles inside the cutter head, as the haul velocity is an order of magnitude lower than the rotational velocity of the cutter head and the mixture velocity.

The parameters varied in the tests are: the rotational velocity of the cutter head, the mixture velocity, the particle diameter and the particle density. From practice it is known that the method of cutting, either under-cut or over-cut, has a large influence on the production. Therefore, tests are performed in both under-cut and over-cut situation. Figure 4.1 shows how the under and over-cut tests are performed in the same bank.

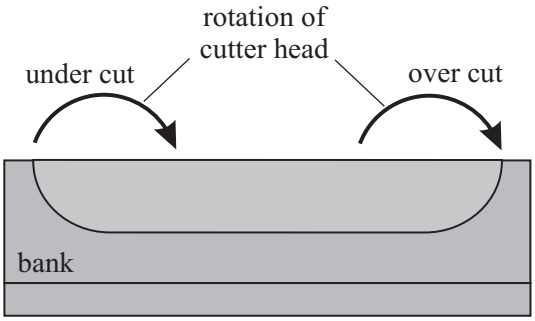

Figure 4.1: Schematic picture of the bank and definition of under-cut and over-cut situations

In order to perform the model tests the appropriate scale laws need to be derived. This is done in the following paragraph.

4.1 Values for the variables on model scale

In order to position the cutter head as near to the breach as possible in the model tests, the model cutter head that was used should not have cutting teeth. Therefore, the model tests have been carried out with a serrated edge cutter head. With this type of cutter heads the tips of the blades consist of serrated edges instead of teeth. In practice, these cutter heads are used in soft formations (clay) and not in rock. The shape of the blades, however, was representative for rock cutter heads, which for these stationary tests (no cutting) is more important. The serrated edge cutter head had an outer ring diameter of 0.32 m and its height was 0.18 m. The diameter of the suction pipe was 0.1 m and the back plate and the suction mouth were identical on model and prototype scale. Considering these dimensions and taking a 2.8 diameter cutter head as prototype, the length scale of the model cutter head is 1:8.75 while the length scale of the suction pipe/ mouth is 1:8. This yields that the dimensions on model scale are not exactly scaled geometrically. As the anomaly is small and these are guiding tests, this is not considered to be a problem. For following applications a general scale of the model cutter head of 1:8 is used.

The table below gives the values for the operational parameters on prototype scale and the according values on model scale derived from equations (3.6) and (3.7).

Table 4.1: Operational parameters on prototype and model scale

	prototype scale	model scale
rotational velocity n_c [RPM]	30	85
mixture velocity v_m [m/s]	5	1.8

The mixture velocities of 5 m/s and 1.8 m/s correspond to suction flows on prototype and model scale of 2.5 m^3/s and 0.014 m^3/s. To determine the influence of the operational parameters on the particle trajectories and production, the rotational velocity of the cutter head and mixture velocity were varied during the tests. The rotational velocity was varied between 20 and 90 RPM and for the mixture velocity the following values were used: 1.5, 2.0, 2.5 and 3.0 m/s.

The particle diameters were geometrically scaled according to scale laws derived in paragraph 3.2. The density on model scale was the same as on prototype scale. This yields the following particle properties on prototype and model scale.

Table 4.2: Particle diameter and density on prototype and model scale

	prototype scale	model scale
particle diameter d_p [m]	0.08	0.01
particle density ρ_p [kg/m^3]	2200-2650	2200-2650

To study the influence of the particle diameter, tests were performed with a diameter of 10 mm but also with a diameter of 6 mm. Furthermore the densities of the particles used are: 1400 kg/m^3, 2200 kg/m^3 and 2650 kg/m^3.

4.2 Test facilities and experimental set up

The tests are performed at the laboratory of Dredging Technology at the Delft University of Technology. A carriage is available for performing tests with cutter heads with a diameter of about 0.3 m to 0.4 m. The dimensions of the test flume in which the tests are performed are: 8×3×1.5 m. The bank, with a length of 6 m, is made of concrete. Figure 4.2 shows the positioning of the cutter head in the bank and the main dimensions of the cutter head and bank. In accordance with the situation in practice, the cutter head is not entirely placed in the bank.

The bank was constructed in such a way that both under-cut and over-cut tests can be performed; i.e. on the right and left side of the bank respectively. An angle for the cutter axis of 45º is chosen as this is the upper limit and the worst case for production. On both sides of the bank, holes are made with a diameter of 2 cm through which particles can be injected. To

ensure free rotation of the cutter head a gap of 5 mm was left between the bank and the cutter head.

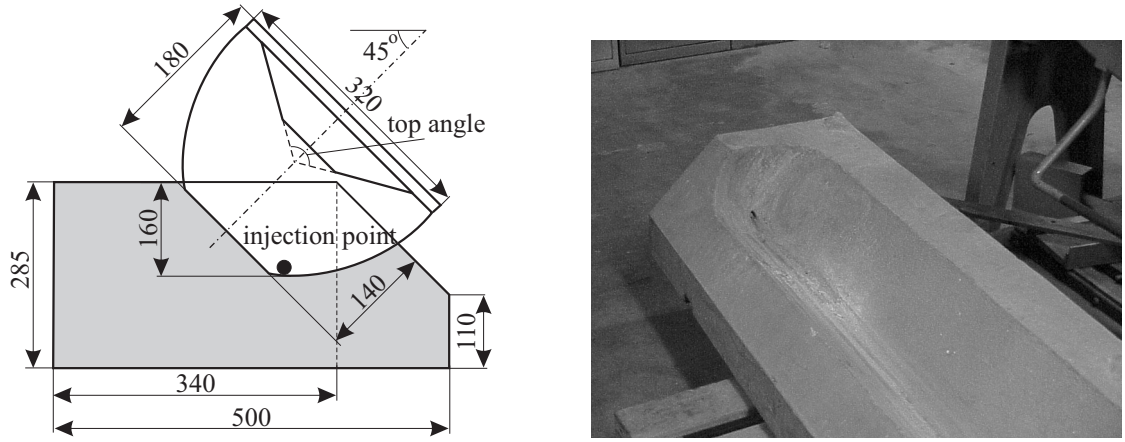

Figure 4.2: Positioning and dimensions of the cutter head in the bank and picture of the left side of the bank showing the position of the injection point

A conical back plate is used with a top angle of 120º. The back plate and the suction mouth are made of perspex, so video recordings can be made from behind the back plate of the particles inside the cutter head. Two digital under-water cameras are used for the recordings. The main purpose of the cameras is to get a qualitative image of the particle behavior. Particle tracking appeared not to be possible due to the relatively low frame rate of 25 Hz of the cameras.

The particles are injected into the cutter head through a tube that is connected with the holes. A jet of water appeared to be necessary to 'push' the particles, in between two passing blades, into the cutter head. This jet of water caused a disturbance of the flow inside the cutter head. However, the water velocity inside the tube was about 0.14 m/s, which corresponds with a flow of 4.4×10^{-5} m^3/s. This is far less than the suction flow. Furthermore, when the rotational velocity of the cutter head varies between 40 RPM and 90 RPM, the circumferential velocity of the cutter head exceeds the velocity of the water jet by a factor 5 to 10. It is therefore reasonable to assume that the injection of the particles does not have a decisive influence on their behavior inside the cutter head.

4.3 Execution of the tests

While performing some preliminary tests, it appeared that the intention of measuring particle production was not a good approach. Often particles that were thrown out of the cutter head were sucked in again which, in general, led to a production of 100%. Still there was a large difference in the time within which the particles were sucked up. In some tests the injected

particles were sucked up immediately, while in other tests this was only after a certain time. Therefore, it was decided to measure the residence time of a particle inside the cutter head instead of the production. The residence time is defined as the moment between injection and the moment the particle is sucked up. An additional advantage of measuring the residence times is that an estimate of the filling degree of the cutter head in practice can be made (assuming that the measured residence times are representative for the situation in practice).

The residence time of a particle under comparable circumstances is not constant. Randomness will play an important role. On the other hand, it is not a completely random process and the residence times will show a certain distribution. The expected probability density function for the residence times should start at zero as none of the particle has a residence time of zero. The probability density function increases with time denoting an increase in the probability that the particle will be sucked up at larger residence times. After the probability density function has reached an optimum it will decrease again and asymptotically reach zero as none of the particles has a larger residence time. The trend of this distribution agrees well with a gamma distribution (see Appendix B). By experiment is was concluded that the injection of 20 particles was enough to get a reproducible probability function.

For the representation of the results in the next paragraphs, one example is given of the gamma cumulative distribution of the measured residence times. The gamma cumulative distributions of all the tests performed are shown in den Burger (1998). In this chapter the average residence times are plotted as a function of the rotational velocity of the cutter head for different mixture velocities. All figures are shown in paragraph 4.3.4. In Appendix B the average residence times and the standard deviations of all the tests performed are shown in tables.

4.3.1 Measured residence times of particles with density of 2600 kg/m^3

Tests in under-cut; d_p = 6 mm

For the mixture velocities of 1.5 m/s and 2.0 m/s and a particle diameter of 6 mm, many particles were not sucked up. At least not within the considered time domain, which was between 0 s and 60 s. If particles were not sucked up in 60 s, the measurement was stopped. Due to the limited number of particles that were sucked up, the average residence times and the standard deviations are not representative for v_m = 1.5 m/s and 2.0 m/s. For mixture velocities of 2.5 m/s and 3.0 m/s nearly all the particles were sucked up and the measurements were representative. Figure 4.3 shows the cumulative gamma distribution of the residence times (Ft) for mixture velocities of 2.5 m/s and 3.0 m/s and particles with a density of 2600 kg/m^3 and a diameter of 6 mm. The markers in the figure are only used to indicate the different curves and do not represent data points.

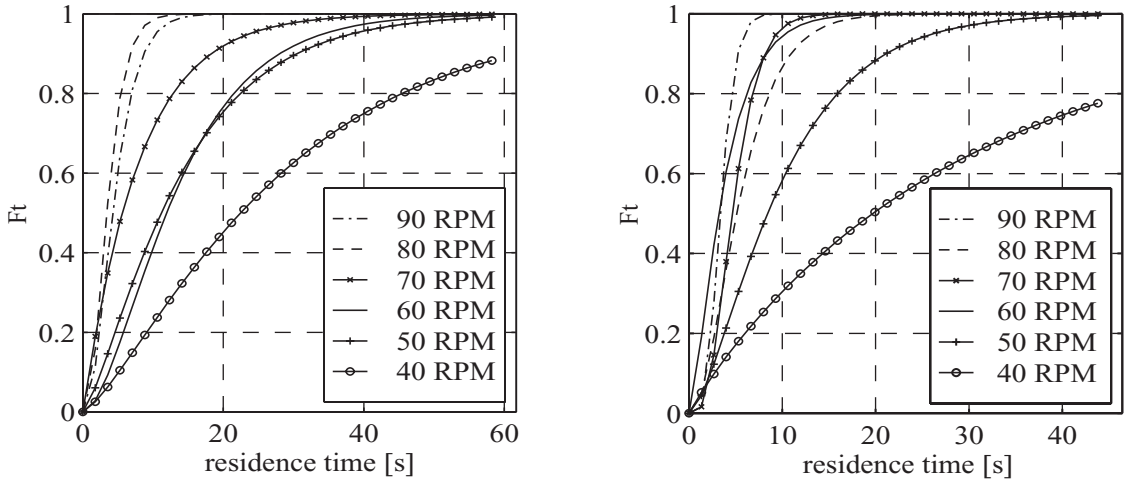

Figure 4.3: Cumulative gamma distributions of the particle residence times for v_m = 2.5 m/s and v_m = 3.0 m/s and a particle diameter of 6 mm

The figure can be interpreted as follows. For a mixture velocity of 3.0 m/s (right hand picture) and a rotational velocity of 40 RPM, the probability is 50% that a particle is sucked up within 20 s. The probability is 100% that a particle is sucked up within 10 s when the rotational velocity is 90 RPM. The cumulative gamma distributions show that in general an increase in rotational velocity of the cutter head results in a decrease in residence time. Furthermore, the deviation of measured residence times becomes significantly smaller when the rotational velocity is increased or when the mixture velocity is increased (see also Table B.1 in Appendix B). It should be noted that for the rotational velocities near the nominal value (say 70 RPM to 90 RPM), the influence of the rotational velocity on the residence times is not that clear. In addition, it is likely that for higher rotational velocities (beyond 90 RPM) the residence times of the particles will increase since more particles will be thrown out of the cutter head and farther away from the cutter head (see paragraph 4.3.3).

The left plot of Figure 4.6 in paragraph 4.3.4 shows the average residence time as a function of the rotational velocity for the 6 mm diameter particles. The figure clearly shows the decrease in average residence time with increasing rotational velocity for both mixture velocities. For a rotational velocity of 40 RPM the average residence time is approximately 30 s while for a rotational velocity of 90 RPM the residence time is approximately 4 s to 5 s.

Using Equation (3.2), a rough estimate of the average residence time of a fluid particle can be given. Suppose the volume of the cutter head is 1.45×10^{-2} m^3 and the diameter of the suction pipe is 0.1 m, the expression for the average residence time of a fluid particle becomes

$$t_r = \frac{1.85}{v_m} \tag{4.1}$$

Thus, for the mixture velocities of 2.5 m/s and 3.0 m/s, the respective residence times of the fluid particle are 0.74 s and 0.62 s. Since the total flow of water inside the cutter head will

often be larger than the suction flow only (as a result of the pump effect of the cutter head), the given residence times indicate an upper limit. This means that the residence times of the particles are always significantly larger than the average residence time of the fluid and thus particle inertia plays an important role.

A better way to determine the average residence time of the fluid would be the use of tracer particles or tracer fluid. Then, a normal camera with 25 frames per second would not suffice and the use of a high speed camera is recommended.

The tests showed the existence of a certain threshold value for the rotational velocity of the cutter head. Below this threshold value for the rotational velocity, the particles more or less rolled over the blades at the deepest point of the bank and the flow inside the cutter head did not seem to have an effect on their motion. None of the particles were sucked up. Beyond the threshold value particles were taken up by the flow due to collisions with the blades, turbulence or lift and particles were sucked up. Naturally, the threshold value for the rotational velocity can not be indicated by a single value, as the transition is not that distinct. The actual transition is a range of rotational velocities near the threshold value. For both mixture velocities the threshold value for the rotational velocity was 40 RPM.

Tests in under-cut; d_p = 10 mm

For the tests with particle diameters of 10 mm the same trends were found as for the particles with a diameter of 6 mm (see the right plot in Figure 4.6 in paragraph 4.3.4). Generally the residence time decreases with increasing rotational velocity. Only for the mixture velocity of 2.0 m/s there seems to be an optimum rotational velocity (≈ 70 RPM) for which the residence time has a minimum. Again the increase in mixture velocity results in a decrease in residence time. Surprisingly, the lowest mixture velocity for which (a sufficient amount of) particles were sucked up was 2.0 m/s instead of 2.5 m/s. The most likely reason for this is that the smaller particles were often located in the gap (5 mm) between the cutter head and the bank. This gap was necessary to ensure free rotation of the cutter head. The suction flow will probably have less influence on these smaller particles as they are more or less screened by the blades. The larger particles will roll over the blades more easily and generally be located inside the cutter head. Hence the suction flow has more influence on their motion. This effect is especially noticeable for the lower rotational velocities, because the particles then roll over the blades and are not taken up by the flow. This explains the large difference in average residence times for particles with a diameter of 6 mm and 10 mm when v_m = 3 m/s and n_c = 40 RPM. For the 6 mm diameter particles it is 29 s while for the 10 mm diameter particle it is 11 s. Even for the higher rotational velocities where the particles were clearly taken up by the flow the residence times for the larger particles are often higher than for the smaller particles. A possible explanation for this is that it is more difficult for the larger particles to escape from the cutter head through the gaps between successive blades.

For both the 6 mm and 10 mm diameter particles the under-water video recording showed that beyond a certain value for the rotational velocity, particles were thrown out of the cutter head. Normally these particles fell on the breach. Due to a strong flow outside the cutter head, directed towards the cutter head, these particles were often dragged towards the cutter head again and could be sucked up (provided that the distance between the particle and cutter head was not too long). This was especially noticeable for the 10 mm diameter particles and a mixture velocity of 2.0 m/s. In this case, more particles were thrown out of the cutter head and further away from the cutter head as the rotational velocity was increased. This is probably the reason why the residence time increases again beyond a rotational velocity of 70 RPM. In paragraph 4.3.3 the trajectories of the particles in both under and over-cut are further explained.

For the mixture velocities of 2.5 m/s and 3.0 m/s it looks as if less particles were thrown out of the cutter head or were located nearer to the cutter head and thus the rotational velocity has less influence on the residence times. Still, comparing the average residence times of the 10 mm diameter particles (4 s to 7 s) with the residence time of the fluid based on the mixture velocity (0.6 s to 0.7 s), it can not be concluded that the mixture velocity is dominating the process.

Tests in over-cut; d_p = 6 mm and 10 mm

Figure 4.7 shows the average residence times for 6 and 10 mm diameter particles in the over-cut situation. Generally, the residence times are lower compared with the same tests in the under-cut situation. This is probably caused by the fact that in over-cut the particles are transported towards the suction mouth by the cutter blades, whereas in under-cut the blades transport the particles away from the suction mouth.

For certain mixture velocities, the residence times tend to decrease as the rotational velocity is increased. However, this trend is not as clear as in the under-cut situation. Moreover, in the over-cut situation there also appeared to be a threshold value for the rotational velocity. For both particle diameters this was 50 RPM. Comparing the results of the 6 mm diameter particles with the 10 mm diameter particles it appears that the largest difference in residence times is found for the lowest mixture velocity, which is 2.0 m/s. In this region, probability plays an important role. The particle has to be brought into the flow directed towards the suction mouth before it can be sucked up. This is done via collisions and friction between the particles and the blades or by the turbulence or lift generated by the blades. The smaller particles are taken up by the flow more easily and once in the suction flow they will follow this flow more easily (due to smaller inertia and lower gravitational force).

The video-recordings showed that most particles moved along the bank and ended up just outside the cutter head. These particles did not lie on the bank motionless. Due to the

disturbances of the flow by the passing blades the particles continuously moved to and away from the cutter head. Most of the time these particles ended up in the cutter head again and could still be sucked up. See paragraph 4.3.3 for the general particle trajectories in the over-cut situation.

4.3.2 Measured residence times of particles with densities of 2200 kg/m^3 and 1400 kg/m^3

For both densities, the residence times of the particles generally decreases with increasing mixture velocity (see Figure 4.8 to Figure 4.11). Comparable with the previous tests the influence of the rotational velocity is not that unambiguous. This is especially true when considering the large variation in measured residence times as shown in the tables in Appendix B.

Generally, the residence times for the particles were lower if the density of the particle was lower. The influence of the particle diameter is difficult to determine from the measurements, although it appears that the increase in particle diameter from 6 mm to 10 mm does not have a significant and consistent influence.

In all the tests there appeared to be a threshold value for the rotational velocity of the cutter head as was the case in the previous tests. This threshold value also seems to decrease with decreasing particle density.

For both the under-cut and over-cut situation particles were thrown out of the cutter head and either fell on the bank or were sucked into the cutter head again. Most of the times the particles that fell on the bank were sucked in again as well due to a strong flow along the bank towards the cutter head. Although the same phenomena take place in under-cut and over-cut situation, the trajectories of the particles are quite different. This is shown in the following paragraph. As the variation of the measured residence times often has the same value as the average residence time and the trends in the residence times are often indistinct, the observed particle trajectories provide useful additional information.

4.3.3 Particle trajectories in under and over-cut and observed phenomena

Although the trajectories of the particles depended on their diameter and density it was still possible to find some general trends in these trajectories. For different particles these similar trajectories were often found for different combinations of the rotational velocity and mixture velocity. In all the tests a threshold value for the rotational velocity was found. Below this threshold value the particles just rolled over the blades in the lowest point of the bank. Above the threshold value the particles were taken up by the flow due to collisions with the blades and the turbulence or lift generated by the blades. The typical trajectories of particles in the under-cut situation for rotational velocities above the threshold value are illustrated in Figure 4.4.

Apart from the fact that above the threshold value for the rotational velocity the particles can taken up by the flow, the particles can also be dragged along by the blades and the flow. This is indicated by trajectory '1'. These particles first move upwards along the breach but fall down again when they are no longer supported by the blade. In this region, the trajectories of the particles are not so much determined by the flow as well as by the gravitational force and contact forces between the blade and particles (friction, collisions and normal force). The normal and friction force are to some extent determined by the centrifugal force acting on a particle. This centrifugal force presses the particle against the blade and hence the particle can stay longer in contact with the blade before it falls down again.

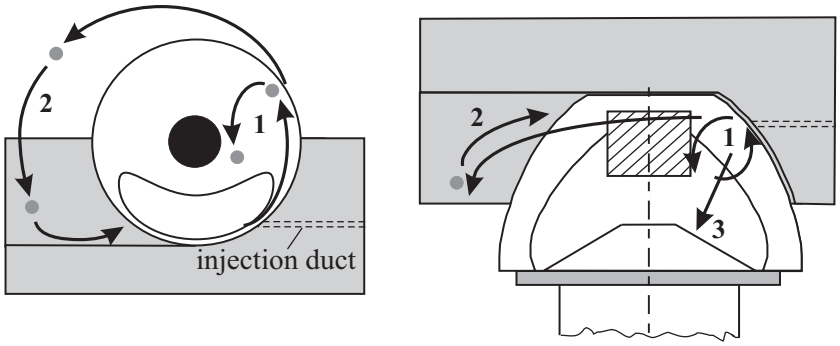

Figure 4.4: General trajectories of the particles in under-cut situation

As the rotational velocity increases, the trajectories indicated by '2' become representative for the particle trajectories. Particles are thrown out of the cutter head because of the large centrifugal forces acting on the particles and many move over the cutter axis. Usually these particles have an axial velocity component as well, directed towards the suction pipe. The particles that are thrown out of the cutter head fall down on the bank and move towards the cutter head again because of the flow towards the cutter head (provided that the distance between the particle and cutter head was not too long). As the rotational velocity increases, more particles are thrown out of the cutter head and further away from the cutter head. Usually these particles are sucked in again as the flow towards the cutter head increases with increasing rotational velocity due to the pump effect of the cutter head.

In the domain where the suction flow was dominant and the residence times were short (relatively large mixture velocity and low rotational velocity), the particles moved towards the suction mouth almost immediately. The trajectories of these particles are indicated by '3'. For the higher residence times the trajectories of the particles that were sucked up could differ significantly from each other (due random processes). Basically a particle was sucked up if it 'coincidentally' came close enough to the suction mouth or entered a distinct flow towards the suction mouth.

In the over-cut situation the particle trajectories differed considerably from the trajectories in under-cut. In the over-cut situation the particles mainly moved along the bank

in the same direction as the rotation of the cutter blades. As the water velocities and the acceleration of gravity have a component in the same direction, these particles had a high velocity and were thrown out of the cutter head most of the time (trajectory '1' in Figure 4.5).

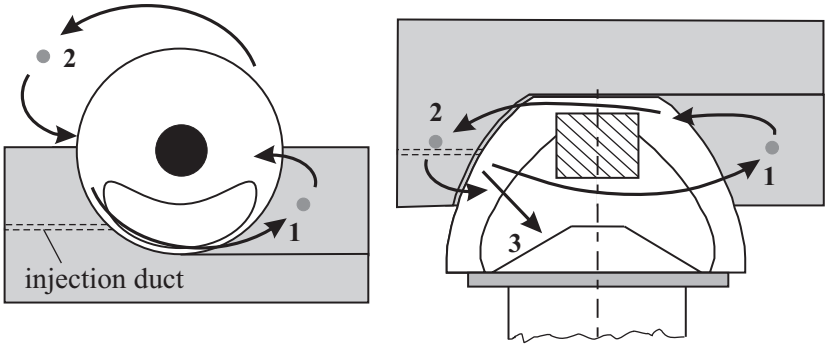

Figure 4.5: General trajectories of the particles in over-cut situation

These particles ended up on the bank on the right side of the cutter head. They did not lie still on the bank but were constantly moving to and away from the cutter head due to the passing blades. Because of the turbulence and eddies generated by the blades particles could enter the cutter head again and be sucked up.

As the rotational velocity of the cutter head was increased more particles were thrown out of the cutter head. On the other hand, these particles were often sucked in again much easier compared with the lower rotational velocities. One reason for this is the pumping effect of the cutter head that caused for a stronger flow towards the cutter head. If the particles ended up in this flow they were immediately transported to the cutter head again. Furthermore, the higher rotational velocity caused for more turbulence and eddies. Hence it was less likely for the particle to fall on the bank and it was in motion continuously. This increased the probability that the particle entered the (or a) flow towards the cutter head and thus the probability that it was sucked up. Moreover, for the higher rotational velocities particles were thrown over the cutter axis and ended up on the bank on the left side of the cutter head (trajectory '2' in Figure 4.5). These particles were often sucked in again as well due to the eddies generated by the blades and/or a flow towards the cutter head.

Comparable with the under-cut situation, the particles with a short residence time moved immediately from the bank towards the suction mouth. However, in this case this was not restricted to the lower rotational velocities but also happened for the higher rotational velocities. For the particles with high residence times there was no well-defined trajectory towards the suction mouth.

For both the under-cut and over-cut situation, the particles that end up outside the cutter head will probably not be sucked in again when the cutter head is hauled. Especially the particles that end up on the bank should be considered as spillage in the actual situation, because the cutter head will move away from these particles. To what extent the measured

residence times are representative for the production and spillage will become clear when actual cutting tests are performed. These actual cutting tests are necessary in order to determine the influence of the haul velocity and a concentration of particles inside the cutter head on the particle trajectories (or rather production). Furthermore, as the models set up in this thesis will focus on the 'behavior' of single particles, the cutting tests will determine the domain of validity of the single particle models. The set up for a model that describes the trajectories of single particles inside the cutter head is given in Chapter 5. In Chapter 6 the results of the actual cutting tests are described.

4.3.4 Figures of the average residence times of all the tests performed

The following figures show the average residence times of the particles (μ_t) plotted against the rotational velocity of the cutter head (n_c) for different mixture velocities (v_m).

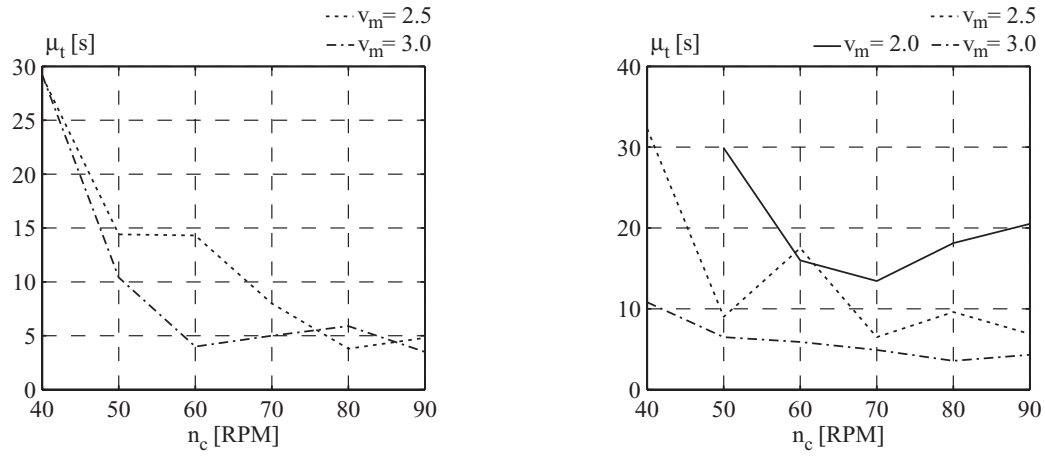

Figure 4.6: Average residence times vs. rotational velocity for particles with a density of 2600 kg/m^3 and diameters of 6 mm (left plot) and 10 mm (right plot) in under-cut situation

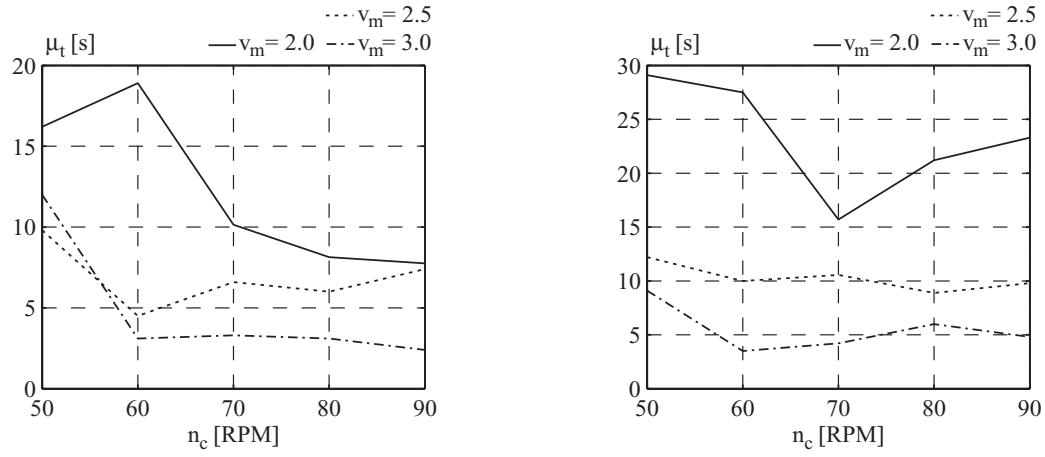

Figure 4.7: Average residence times vs. rotational velocity for particles with a density of 2600 kg/m^3 and diameters of 6 mm (left plot) and 10 mm (right plot) in over-cut situation

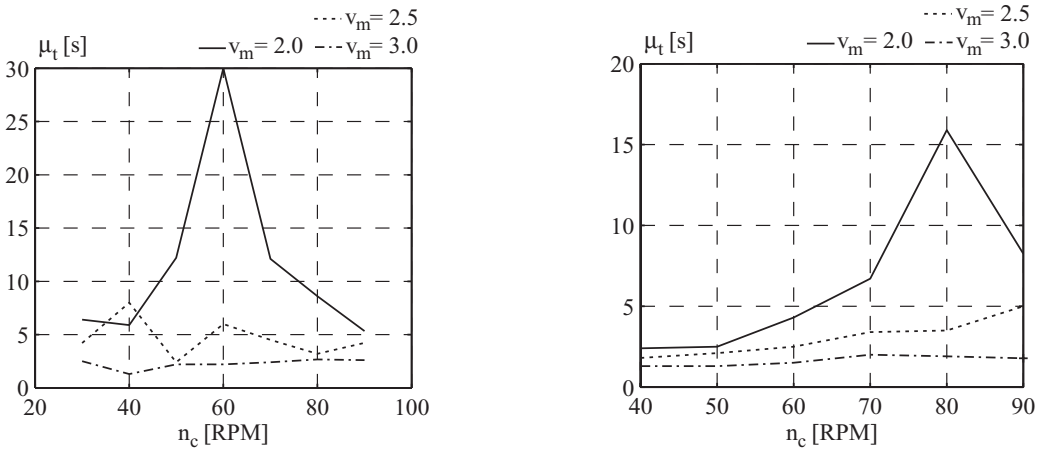

Figure 4.8: Average residence times vs. rotational velocity for particles with a density of 2200 kg/m^3 and diameters of 6 mm (left plot) and 10 mm (right plot) in under-cut situation

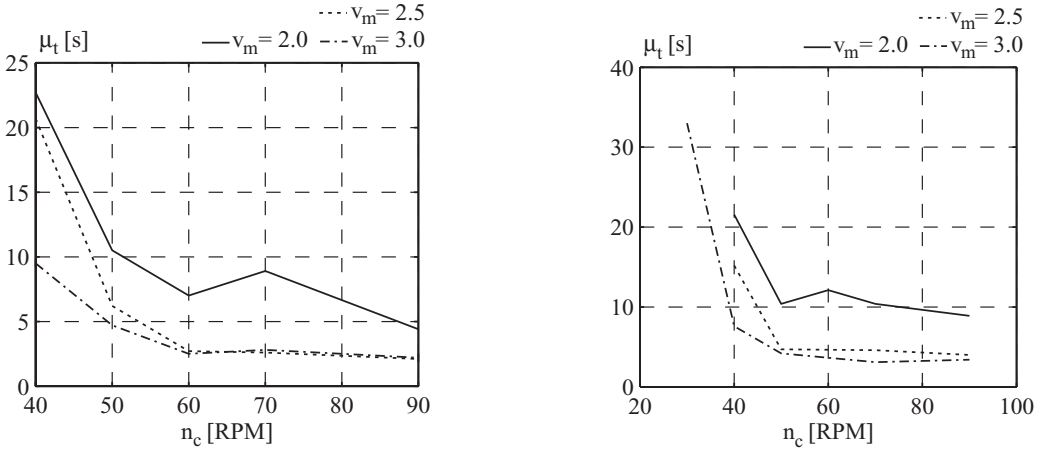

Figure 4.9: Average residence times vs. rotational velocity for particles with a density of 2200 kg/m^3 and diameters of 6 mm (left plot) and 10 mm (right plot) in over-cut situation

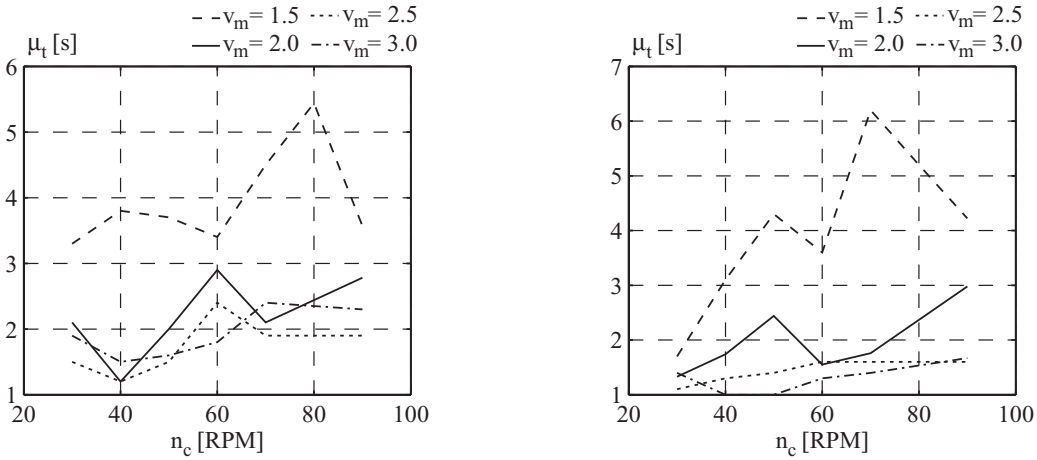

Figure 4.10: Average residence times vs. rotational velocity for particles with a density of 1400 kg/m^3 and diameters of 6 mm (left plot) and 10 mm (right plot) in under-cut situation

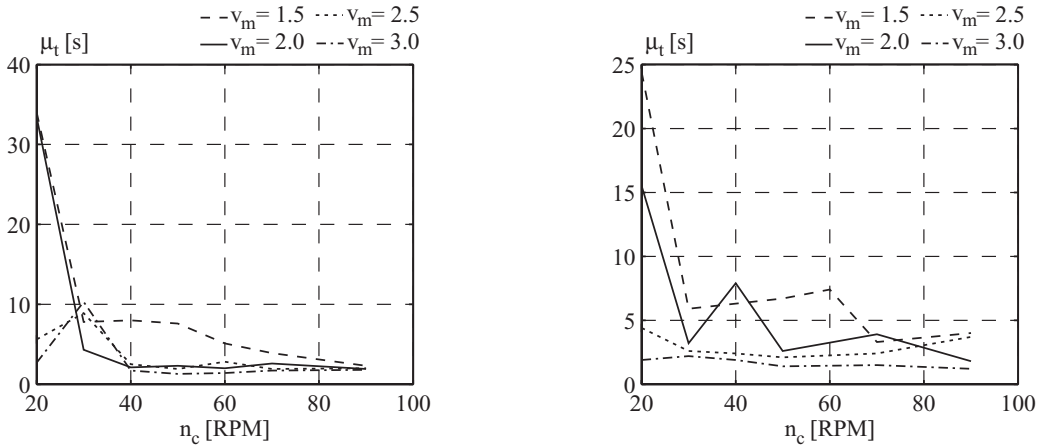

Figure 4.11: Average residence times vs. rotational velocity for particles with a density of 1400 kg/m^3 and diameters of 6 mm (left plot) and 10 mm (right plot) in over-cut situation

4.4 Expected filling degree of the cutter head when cutting

An important parameter is the filling degree of the cutter head, as it indicates to what extent particle-particle interactions will play a role and to what extent the flow is disturbed by the presence of the particles. By means of the measured residence times the filling degree of the cutter head can be estimated, provided that the measured residence times are representative for the situation where the cutter head is hauled and actually cuts the bank.

The filling degree is defined as the ratio between the total volume of material inside the cutter head and internal volume of the cutter head. Suppose that $V_{p,c}$ represents the total volume of material inside the cutter head. Then:

$$V_{p,c} = \mu_t v_h A_{cut} \tag{4.2}$$

where μ_t is the average residence time, v_h is the haul velocity and A_{cut} is the cut off area. For the sake of convenience it is assumed that the density of the material inside the cutter head is equal to that in situ. The following values for the above mentioned parameters apply on a 1:8 scale:

cut off area: $A_{cut} = 0.025$ m^2
haul velocity: $v_h = 0.07$ m/s
volume cutter head: $V_{cutter} = 1.45\times10^{-2}$ m^3

A representative case for the situation in practice is the under-cut tests where:

$\rho_p = 2200$ kg/m^3
$d_p = 10$ mm
$n_c = 90$ RPM
$v_m = 2.0$ m/s

For this test the average residence time (Ft = 0.5) is approximately 7 s. Neglecting the spillage, the total amount of material in the cutter head would be

$$V_{p,c} = 1.2 \times 10^{-2} \text{ m}^3$$

This is 85% of the volume of the cutter head. This is an unrealistically high value, which implies that there has to be a significant amount of spillage. It could also mean that the measured residence times for the single particles do not apply when the cutter head is actually cutting. The haul velocity and particle-particle interaction could decrease the average residence time of a particle. Therefore, a series of cutting tests should be performed where the concentration of particles inside the cutter head is representative for the situation in practice (see Chapter 6).

4.5 Conclusions

Residence times of particles in the cutter head were measured for varying rotational velocities of the cutter head and varying mixture velocities. Both particle diameter and density were varied. For mixture velocities of 1.5 m/s and 2.0 m/s the average residence times and the standard deviations of the residence times were very large. Increasing the mixture velocity generally resulted in a decrease in average residence time and standard deviation. It was not possible to find a general trend in the influence of the rotational velocity on the residence times.

There was a threshold value for the rotational velocity of the cutter head. Below this threshold value none of the injected particles were sucked up and the particles just rolled over the blades in the lowest part of the bank. Beyond the threshold value, the particles were taken up by the flow due to either turbulence, collisions with the blades or lift and could be sucked up.

The difference in tested particle diameters (i.e. 6 mm and 10 mm) was too small and the deviations in measured residence times were too large to notice a significant difference in residence times.

Decreasing the particle density from 2650 kg/m^3 to 2200 kg/m^3 and 1400 kg/m^3 showed a decrease in the residence times of the particles.

The measurements of the residence times confirmed that particle inertia plays an important role, since the residence times of the injected particles were often larger but at least of the same order of magnitude as the residence time of the fluid. The average residence times of the particles varied from approximately 20 s to 30 s in the most unfavorable situation, to

approximately 1 s to 2 s in the most favorable situation. The residence time of the flow varied between 0.6 s and 0.9 s, depending on the suction flow.

Conclusions concerning the video-recordings in under and over-cut

Video-recordings showed that beyond a certain value for the rotational velocity of the cutter head particles were thrown out of the cutter head. These particles could enter the cutter head again because of a strong flow towards the cutter head. This process of particles being thrown out and sucked in again, gives an explanation of the high residence times and standard deviations.

There was a clear difference in particle trajectories in the under and over-cut situation. In the over-cut situation particles were thrown out of the cutter head at lower rotational velocities than in the under-cut situation.

It was clearly visible that the particles with a density of 2650 kg/m^3 and 2200 kg/m^3 were easier thrown out of the cutter head than the particles with a density of 1400 kg/m^3.

General conclusions

Caution is required when interpreting the residence times of the particles and translating them to the situation in practice. Using the measured residence times would imply unrealistically high filling degrees of the cutter head in practice. Therefore, a series of cutting tests should be performed where the number of particles inside the cutter head is representative for the situation in practice.

Chapter 5
Simulated Particle Trajectories inside the Cutter Head

The tests where single particles were injected showed that the residence time of a particle strongly depends on the mixture velocity and the rotational velocity of the cutter head. An increase in mixture velocity resulted in a decrease in residence time, while the influence of the rotational velocity on the residence time was not that clear. A simulation model is set up in order to describe the trajectories of the particles inside the cutter head. Aim of the simulations is to obtain a better understanding of the basic processes taking place inside the cutter head and to verify that the nature of these processes is understood. Thus, the influence of the flow inside the cutter head and the particle-flow interactions are investigated, while particle-particle interactions are neglected. An important factor here is the influence of the different forces acting on the particles.

In addition, the simulations are used to verify whether the trends resulting from the tests can be reproduced. A relatively simple model is used for the flow inside the cutter head, where the pumping effect of the cutter head is not taken into account. The simulations will clarify whether this model will suffice or whether a more elaborate CFD model should be used that takes into account the pumping effect of the cutter head.

5.1 Model for the flow inside the cutter head

The flow inside the cutter head can be subdivided into a flow as a result of the rotation of the cutter head and a flow due to the suction. The flow resulting from the rotation of the cutter head is difficult to determine because of the complex geometry of the cutter head. Furthermore, due to the high rotational velocities of the cutter head the flow will be very turbulent, increasing the complexity of determining the water velocities and pressures. A commercial CFD package could be used for modeling the flow, but this would be a complex

and time consuming operation. Furthermore, at this stage of the research, attention is mainly focused on the basic physics of the particle-fluid interaction for which a simple flow model is more suitable. Besides that, all CFD packages have their limitations, especially when it concerns three-dimensional two-phase flows. Thus without further knowledge on the processes taking place inside the cutter head the results of CFD simulations should be regarded with great caution. This also supports the assumption of starting with a simple flow model.

The flow due to the rotation of the cutter head is represented by a forced vortex (solid body rotation) neglecting turbulence. A justification for neglecting turbulence would be the fact that the time scale of the largest turbulent eddies has the same order of magnitude as the particle relaxation time (see Appendix A). This means that the turbulent eddies have a minor effect on the particle trajectories. The suction flow is represented by a three dimensional sink.

Figure 5.1 shows the cutter head and the coordinate systems used in the flow model. The Z_{sp}-axis of the suction pipe is parallel to the cutter axis and as a first approach the opening of the suction pipe coincides with the cutter ring ($Z_{sp,0} = 0$). In the figure λ denotes the inclination angle of the cutter axis.

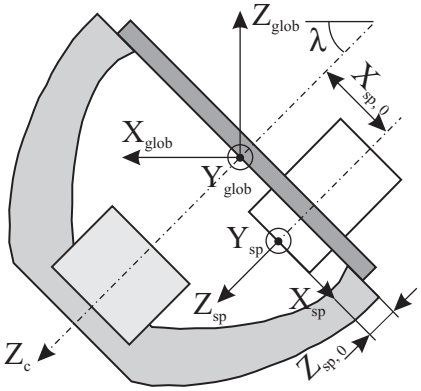

Figure 5.1: Definition of the global coordinate system and coordinate system through suction pipe

Flow due to rotation of the cutter head

Due to the rotation of the cutter head, the water inside the cutter head will rotate as well. The vector for the rotation of the cutter head about the cutter axis (Z_c) is:

$$\bar{\Omega} = \bar{e}_{Zc}\omega_c \tag{5.1}$$

in which $\bar{e}_{Zc}$ is the unity vector in direction of Z_c and ω_c is the angular velocity of the cutter head. The fluid does not necessarily rotate with the same angular velocity. It is more likely that there is a certain amount of slip between the blades and the water. This slip factor is defined as:

$$C_{slip} = 1 - \frac{\omega_f}{\omega_c} \tag{5.2}$$

in which ω_f is the angular velocity of the fluid (water). The vector for the rotation of the water about the Z_c axis equals the definition in Equation (5.1), replacing ω_c with ω_f. Thus, the water velocities due to the rotation, written in the coordinate system of the suction pipe become

$$\overline{v}_{f,vortex} = \overline{\Omega}_f \times \overline{r} \tag{5.3}$$

with $\overline{r} = \left(X_{sp} + X_{sp,0}\right)\overline{e}_{X,sp} + Y_{sp}\overline{e}_{Y,sp}$. Hence

$$\overline{v}_{f,vortex} = \omega_f \left(\left(X_{sp} + X_{sp,0}\right)\overline{e}_{Y,sp} - Y_{sp}\overline{e}_{X,sp}\right) \tag{5.4}$$

Note that because of the forced vortex the flow inside the cutter head is not irrotational ($\nabla \times \overline{v}_f \neq 0$). This means that the flow does not satisfy the theory on potential flows. As the flow is considered to be a solid body rotation, there is no deformation and thus no viscous stresses. The flow can be considered frictionless.

Suction flow

The flow through the suction pipe Q_s is:

$$Q_s = \frac{\pi}{4} D_{sp}^2 v_m \tag{5.5}$$

in which D_{sp} is the diameter of the suction pipe and v_m is the water velocity in the suction pipe (assuming uniform flow). The water velocities in the cutter head due to the suction flow are derived from the continuity equation (Burger, 1997). These are:

$$\overline{v}_{f,suction} = -\frac{Q_s}{2\pi R^2}\overline{e}_R = -\frac{1}{8}\left(\frac{D_{sp}}{R}\right)^2 v_m \overline{e}_R \tag{5.6}$$

where

$$\begin{aligned} \overline{R} &= X_{sp}\overline{e}_{X,sp} + Y_{sp}\overline{e}_{Y,sp} + Z_{sp}\overline{e}_{Z,sp} \\ \overline{e}_R &= \frac{X_{sp}}{R}\overline{e}_{X,sp} + \frac{Y_{sp}}{R}\overline{e}_{Y,sp} + \frac{Z_{sp}}{R}\overline{e}_{Z,sp} \end{aligned} \tag{5.7}$$

This suction flow is a three-dimensional representation of a sink. The flow is frictionless and irrotational, satisfying the theory on potential flows.

Both flows are superposed, satisfying the Euler equation. Superimposing the water velocities induced by to the rotation and the suction flow results in the following velocity components in direction of X_{sp}, Y_{sp} and Z_{sp}

$$v_{f,Xsp} = -\frac{1}{8}\left(\frac{D_{sp}}{R}\right)^2 v_m \frac{X_{sp}}{R} - \omega_f Y_{sp}$$

$$v_{f,Ysp} = -\frac{1}{8}\left(\frac{D_{sp}}{R}\right)^2 v_m \frac{Y_{sp}}{R} + \omega_f \left(X_{sp} + X_{sp,0}\right) \tag{5.8}$$

$$v_{f,Zsp} = -\frac{1}{8}\left(\frac{D_{sp}}{R}\right)^2 v_m \frac{Z_{sp}}{R}$$

With Equation (5.8) the flow inside the cutter head is determined.

The rotation of the flow outside the cutter head could be described by a free vortex. This combination of a forced and free vortex is known as the Rankine vortex and often used to describe cyclones. However, as the trajectories of particles outside the cutter head are not relevant for this research, only the forced vortex is considered.

5.2 Forces acting on a single particle and equation of motion

The forces acting on a single spherical particle are:

- Gravitational force
- Drag force
- Forces due to pressure gradients in the fluid
- Added mass force

The lift force acting on the particle can be neglected, as is shown in Appendix A. Furthermore, the Basset History force is neglected as its value is expected to be much lower than the remaining forces.

Gravitational force

Written in the coordinate system of the suction pipe, the gravitational force acting on the particle is

$$\overline{F}_g = m_p \overline{g} = m_p g\left(\cos\lambda \overline{e}_{Xsp} + \sin\lambda \overline{e}_{Zsp}\right) \tag{5.9}$$

in which m_p is the mass of the particle and g is the acceleration of gravity.

Drag force

The drag force acting on the particle is:

$$\overline{F}_D = \frac{\pi}{8}\rho_f d_p^2 C_d \left(\overline{v}_f - \overline{v}_p\right)\left|\overline{v}_f - \overline{v}_p\right| \tag{5.10}$$

in which ρ_f is the density of the fluid (water), d_p is the particle diameter and C_d is the drag coefficient. Furthermore, v_f represents the fluid velocity and v_p the particle velocity.

Forces due to pressure gradients

The force on a particle due to the pressure gradient is:

$$\overline{F}_{PG} = \rho_f V_p \left(\frac{D\overline{v}_f}{Dt} - \overline{g}\right) \tag{5.11}$$

in which V_p is the volume of the particle and

$$\frac{D}{Dt} = \frac{\partial}{\partial t} + \overline{v}_f \cdot \nabla$$

Added mass force

When a body moves through a fluid it must push a finite mass of fluid out of the way. If the body is accelerated, the surrounding fluid must also be accelerated. The body behaves as if it were heavier by an amount called the added mass of the fluid (White, 1994). The added mass force is defined as:

$$\overline{F}_{AM} = \rho_w V_p C_{AM} \left(\frac{D\overline{v}_f}{Dt} - \frac{d\overline{v}_p}{dt}\right)$$

Then the equation of motion for the particle results in the following set of ordinary differential equations

$$\rho_p V_p \frac{d\overline{v}_p}{dt} = \overline{F}_g + \overline{F}_D + \overline{F}_{PG} + \overline{F}_{AM} \tag{5.12}$$

in which ρ_p is the density of the particle.

5.3 Simulation of the particle trajectories

5.3.1 Variables in the simulation model

The variables in the simulation model are: ρ_p, ρ_w, d_p, C_{AM} and C_d of which the first three can be chosen freely. The added mass coefficient and drag coefficient depend on the respective densities, the particle diameter and the water velocities. Comparable with the tests in the

previous chapter, simulations are performed with particle densities of 2200 and 2650 kg/m^3. Furthermore, particle diameters of 6 mm and 10 mm were used in the simulations.

The added mass coefficient C_{AM} varies between 0.5 and 1.05 for spheres in free fall, depending on the ratio of the density of the particle and surrounding fluid (Odar and Hamilton, 1964). In general, a value of 0.5 is commonly used for spheres. As was shown in Chapter 4, the particle Reynolds number will mainly be in the Newton range thus C_d is 0.4 for spherical particles. However it is possible that initially the velocity difference between water and particle is so small that the particle Reynolds number is in the intermediate regime or even in the Stokes regime. This could have a significant effect on the drag coefficient. Turton and Levenspiel (1986) have proposed a relationship between the drag coefficient and the particle Reynolds number for spherical particles

$$C_d = \frac{24}{Re_p}\left(1+0.173\,Re_p^{0.657}\right)+\frac{0.413}{\left(1+\left(1.63\times10^4\right)Re_p^{-1.09}\right)} \tag{5.13}$$

This relationship covers the Stokes regime for low values of Re_p, the intermediate regime and the Newton's regime for large values of Re_p. The validation of paragraph 5.3.4 shows that the particle Reynolds number is generally large enough to be in the Newton range and a constant value of 0.4 can be used for the drag coefficient.

The flow is considered without slip between the blades and water (C_{slip} = 0). As the rotation of the flow is described by a forced vortex, varying the rotational velocity of the cutter head has the same effect as varying C_{slip}.

Defining the initial position and velocity of the particle, the equation of motion for the particle is solved with a routine in Matlab^{tm} based on an explicit Runge-Kutta method. The relative error tolerance of the simulations is 1×10^{-3} and the absolute tolerance is 1×10^{-6}.

5.3.2 Simulations with ρ_p = 2200 kg/m^3 and d_p = 6 mm

Particles are released from five different locations inside the cutter head. They are released in front of the suction pipe at the inner contour of the blades. The initial velocities of the particles equaled the water velocity at the initial positions.

The first simulation is performed with a rotational velocity of 40 RPM and a mixture velocity of 3 m/s. Figure 5.2 shows the results of this simulation. The two plots show the results of the same simulation viewed from two different angles. The figure also shows the outer and inner contour of the cutter blade, the cutter ring, the hub and the suction pipe. These objects are drawn for representational purposes only and do not have a direct influence on the flow. Furthermore, the cutter head rotates clockwise when looking in the positive direction of Z_c.

Only the three particles closest to the suction pipe are sucked up. The other two particle escape from the cutter head. They do have an initial motion towards the suction pipe,

but as they rotate away from the suction pipe and move towards the exterior (due to the centrifugal forces), the influence of the suction flow decreases rapidly.

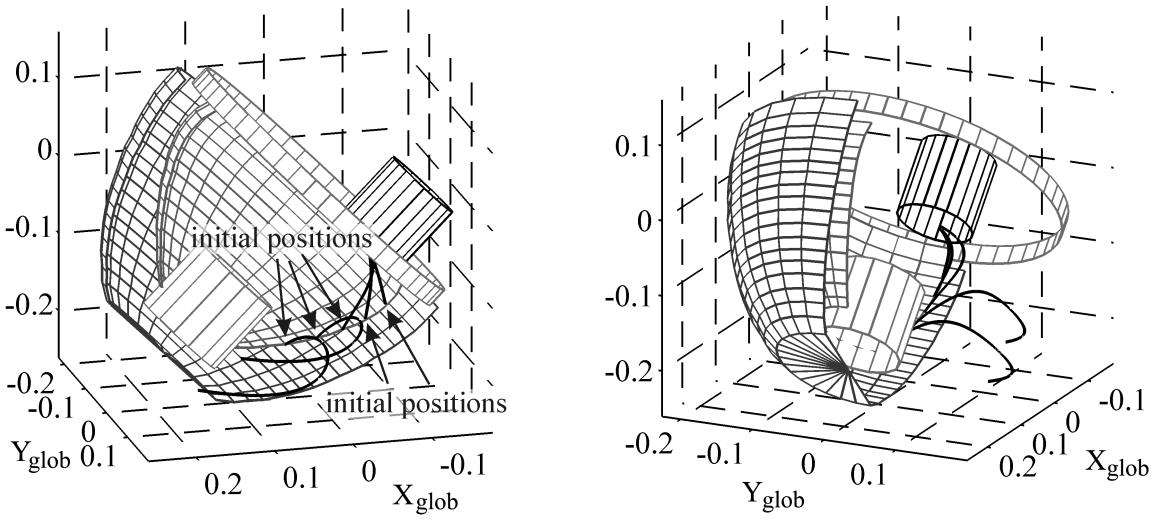

Figure 5.2: Particle trajectories of 5 particles (ρ_p = 2200 kg/m^3) released in front of the suction pipe when n_c = 40 RPM and v_m = 3 m/s

The poor influence of the suction pipe becomes evident when looking at the pressure gradient. Using the velocities as given in Equation (5.8) and neglecting the rotation of the cutter head, the hydrodynamic pressure gradient becomes:

$$\frac{\partial p}{\partial \bar{R}} = \frac{-\frac{1}{2}\rho_w R_{sp}^4 v_m^2}{R^5}\bar{e}_R \tag{5.14}$$

with R_{sp} being the radius of the suction pipe. The pressure gradients decrease with the fifth power of R (the distance towards the origin of the suction mouth). As the particle moves away from the suction pipe and R increases, the pressure gradient decreases significantly. In this case, where R_{sp} = 0.1 m and d_p = 0.01 m, the hydrodynamic pressure gradient already equals $(\rho_p - \rho_w)g$ (i.e. gravity minus buoyancy) at a distance from the suction pipe of 10 particle diameters. Moreover, near the hub ($R \approx 0.25$ m) the hydrodynamic pressure gradient is a factor 35 lower than $(\rho_p - \rho_w)g$ and will thus have no effect on the particle trajectory.

A second simulation is performed with n_c = 90 RPM and v_m = 3 m/s. The results of this simulation are shown in Figure 5.3. It shows that none of the particles are sucked up this time. The rotation of the cutter head is very dominant compared to the suction flow. Therefore the trajectories of the particles are mainly determined by the rotation of the cutter head and gravitation. This is also noticed when looking at the forces acting on the particle, as shown in

Figure 5.4. In this figure the forces acting on the particle closest to the suction pipe are plotted. Furthermore, the figure shows the absolute water and particle velocities.

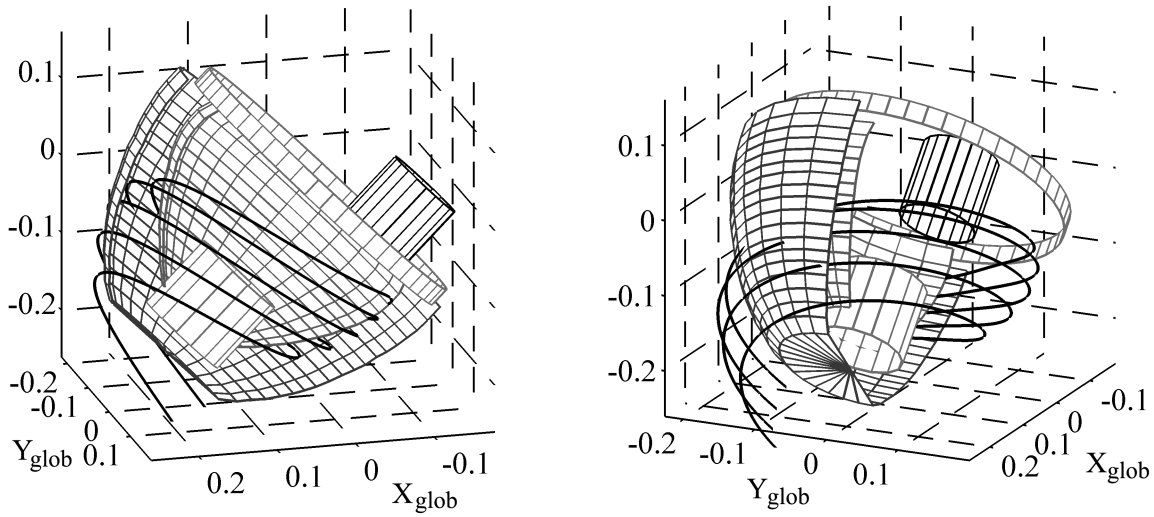

Figure 5.3: Particle trajectories of 5 particles (ρ_p = 2200 kg/m^3) released in front of the suction pipe when n_c = 90 RPM and v_m = 3 m/s

The plots show the components of the forces acting on the particle in three directions, i.e. X_{sp}, Y_{sp} and Z_{sp}. These components are plotted as a function of time. The legend above each plot shows the respective force of which the component is plotted. Furthermore, F_g includes the hydrostatic pressure gradient (buoyancy effect). The last plot shows the absolute velocities in the three directions. The subscripts 'w' and 'p' in the legend stand for water and particle. For convenience the subscript 'sp' is omitted in the legend.

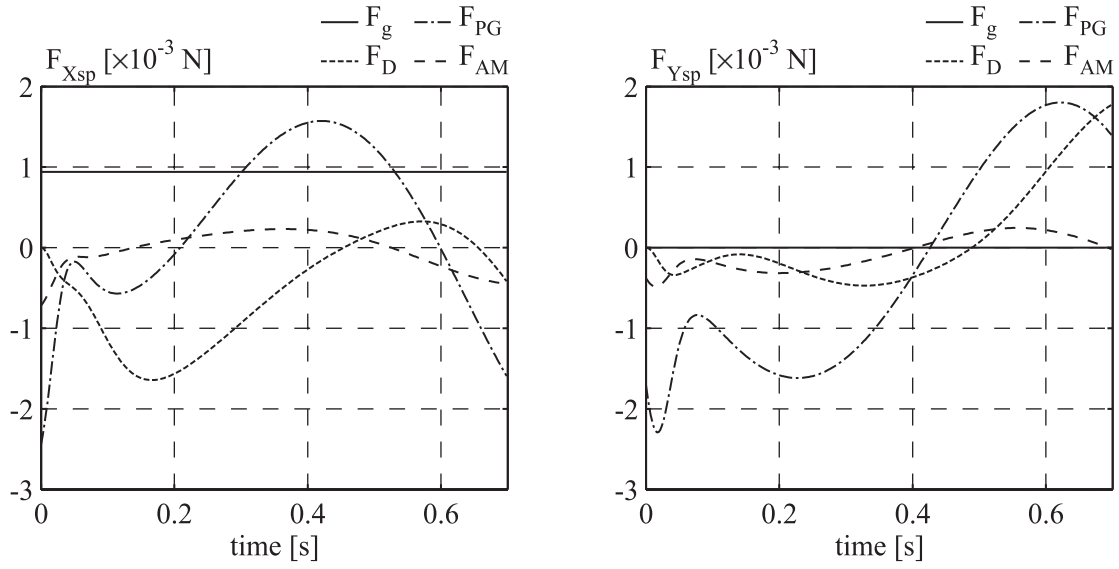

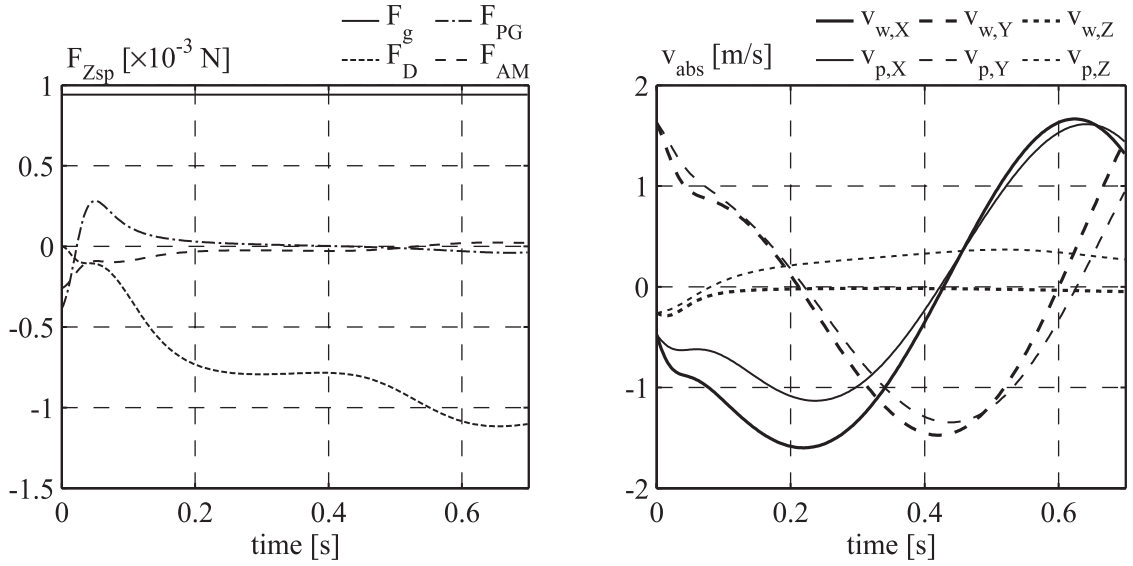

Figure 5.4: Forces acting on the particle (ρ_p = 2200 kg/m^3) and the absolute water and particle velocities when n_c = 90 RPM and v_m = 3 m/s

In the directions of X_{sp} and Y_{sp} the components of the forces are of the same order of magnitude. Most forces are sinusoidal because of the rotation of the particle and the representation in a Cartesian coordinate system.

The pressure gradient is considerable in X_{sp} and Y_{sp} direction but negligible in the direction of Z_{sp}. In direction of Z_{sp}, the pressure gradient is induced by the suction flow only. As shown by Equation (5.14), these pressure gradients are not very relevant. Obviously, the pressure gradients acting on the particle as a result of the rotational flow are significantly larger. The gravitational force (minus buoyancy force) and the drag force are relatively large in the direction of Z_{sp}. The drag force is negative in the direction of Z_{sp} because the term $(v_{f,Zsp} - v_{p,Zsp})$ is negative.

The plot for the absolute velocities show a strong correlation between the particle and water velocities. The particle velocities have a certain delay time with respect to the water velocities. This delay time is a measure for the particle relaxation time or the characteristic time required for a particle to adjust to or relax to a new condition of forces (Hinds, 1982). The velocities in X_{sp} and Y_{sp} direction are sinusoidal. The amplitude of these sinuses increases in time as a forced vortex was used to represent the rotational flow. Particles move in radial direction because of the centrifugal force acting on the particle. As the radial distance of the particle towards the cutter axis increases, the tangential velocity increases as well and thus the centrifugal force. Hence, the trajectories of the particles are spirals where the radial and tangential velocity of the particle continuously increases. Outside the cutter head the use of a forced vortex is incorrect. A free vortex, where the rotational velocity decreases with increasing radius, would be more adequate. However, the trajectory of the particle outside the

cutter head is not of importance and it is more convenient to stop the simulation when the particle leaves the cutter head.

In the plots for the forces only the external forces acting on the particle are plotted. Moreover the forces are plotted in a Cartesian coordinate system. Rewriting the equation of motion in cylindrical coordinates, introducing a rotating axes frame, two additional acceleration terms appear: centrifugal acceleration and the Coriolis acceleration. These accelerations cause for the centrifugal force and Coriolis force. Note that these forces are not external forces but merely a result of the chosen reference system. If a rotating cylindrical coordinate system had been chosen instead of the Cartesian coordinate system, the centrifugal and Coriolis acceleration would become apparent in the equation of motion.

An extended series of simulations was performed varying the values for the operational parameters and the initial position of the particles. It could be concluded that only particles released close enough to the suction pipe were sucked up. With respect to particle being sucked up (production), increasing the rotational velocity always had a negative influence. As the particles were hardly sucked up it is difficult to compare the results with the tests as described in Chapter 4.

The flow of particles indicated by '1' in Figure 4.4, representing the trajectories of particles for relatively low values of n_c could not be reproduced with the simulations. As described in Chapter 4 for the lower values of n_c the contact forces between particle and blade are determinative for the trajectories and not the flow.

The trajectories of particles thrown out of the cutter head as indicated by '2' in Figure 4.4 could be simulated up till the point where they leave the cutter head. In the simulations the particles move in positive direction of Z_{sp} (thus away from the suction pipe) while in the tests most of the particles moved in negative direction of Z_{sp}, especially for large rotational velocities. The most likely reason for this is the combination of the poor influence of the suction flow in the simulations and not taking into account of the pump effect of the cutter head. The pump effect causes for a larger axial flow inside the cutter head in the negative direction of Z_{sp}. Thus compared to simulations, in reality the axial water velocities will be significantly larger (in negative Z_{sp} direction). If large enough the gravitational force can be compensated and the particle has an axial motion in negative direction of Z_{sp}.

5.3.3 Influence of the particle diameter and density on particle trajectories

The simulations were repeated while increasing the particle diameter from 6 mm to 10 mm. This increase in particle diameter first of all resulted in an increase in the velocity difference between particle and water (i.e. the slip velocity). For the lower rotational velocities of the cutter head this is clearly noticeable in the trajectories of the particles. The particles tend to

move more in the negative direction of Z_{glob} due to the larger settling velocity of the particles and the influence of the suction flow on the trajectories of the particles is less significant.

For the higher rotational velocities of the cutter head the larger slip velocity of the 10 mm particle is more apparent in the plane of rotation. The particle still has a circular motion but as the velocity of the particle is smaller, the distance completed by the particle is shorter compared with the 6 mm particle. Furthermore, because of the larger slip velocity of the larger particles and consequently the smaller angular velocity and relative influence of the centrifugal force, the particle tend to stay longer inside the cutter head. At least, when looking in the plane of rotation, thus perpendicular to the cutter axis.

Moreover, increasing the particle diameter results in an increase in particle relaxation time. Hence, it takes longer for larger particles to adjust and these particles are less likely to follow the fluid flow. For the higher rotational velocities of the cutter head, this can be very important. The initial velocity of the particle is an important factor in this. When choosing the initial velocity of the particle far from the homogeneous solution (e.g. a velocity much lower or higher than the fluid velocity at the point of release), the difference in relaxation time will result in a significant difference in particle trajectory.

Increasing the density of the particles from 2200 kg/m^3 to 2650 kg/m^3 resulted in a larger centrifugal acceleration of the particles. Therefore these particles were thrown out of the cutter head faster. This was especially noticeable at higher rotational velocities of the cutter head. As the tangential water velocities increase with increasing radius, the centrifugal acceleration of the particle increases rapidly in time. In addition the increase in density resulted in an increase in fall velocity of the particle and an increase in particle relaxation time.

It is difficult to quantify the influence of increasing either the particle diameter or density on the particle trajectories. Furthermore it is difficult to determine whether the increase in particle diameter or density has a larger influence on the particle trajectory. This strongly depends on the values for the operational parameters and the initial velocity of the particle. Generally speaking however, the particle diameter tends to have a larger influence on the particle trajectory for the lower rotational velocities. Then gravity and thus the settling velocity of the particle is an important parameter. As shown in Equation (3.8), the terminal settling velocity of the particle is proportional with the square root of its diameter and proportional with the density difference between particle and water. Increasing the particle diameter by a certain factor will thus have a larger influence than increasing the particle density by the same factor.

The particle density tends to have a larger influence on the particle trajectory for the higher rotational velocities due to its circular motion and the rapidly increasing centrifugal force acting on the particle. Note that for a rotational velocity of the cutter head of 90 RPM,

the centrifugal acceleration of the particle has the same order of magnitude as the acceleration of gravity. Thus even for the larger rotational velocities gravity can not be neglected.

5.3.4 Variation of C_d and Re_p along the particle trajectory

In the simulations, a constant C_d coefficient of 0.4 has been used, based on the conclusion from paragraph 3.2.2 that the particle Reynolds number will generally be in the Newton range. However, the particle Reynolds number was based on the assumption that considering the large fluid velocities and/or the large terminal settling velocity of the particle, the slip velocity is always large enough for the Reynolds number to be in the Newton range. In the simulations the initial velocity of the particle was equal to the water velocity and thus the slip velocity was zero. In this case the particle Reynolds number will not start in the Newton range and initially the C_d coefficient will be larger than 0.4. It is necessary to check how fast the particle Reynolds number is in the Newton range compared with the time it takes before a particle is sucked up or thrown out of the cutter head. This will show whether it is allowed to use a constant C_d coefficient for the particle trajectory inside the cutter head.

The demand that the particle Reynolds number has to be in the Newton range is especially important for comparison with prototype scale. As the particle Reynolds numbers are not equal on prototype and model scale, the C_d coefficients are different outside the Newton range. This anomaly should then be compensated by changing the particle diameter so that the ratio of C_d and d_p is constant on both scales and uniform particle trajectories are obtained (see dimensionless equation of motion in paragraph 3.1).

A series of simulations is performed where the drag coefficient given by Equation (5.13) is used.

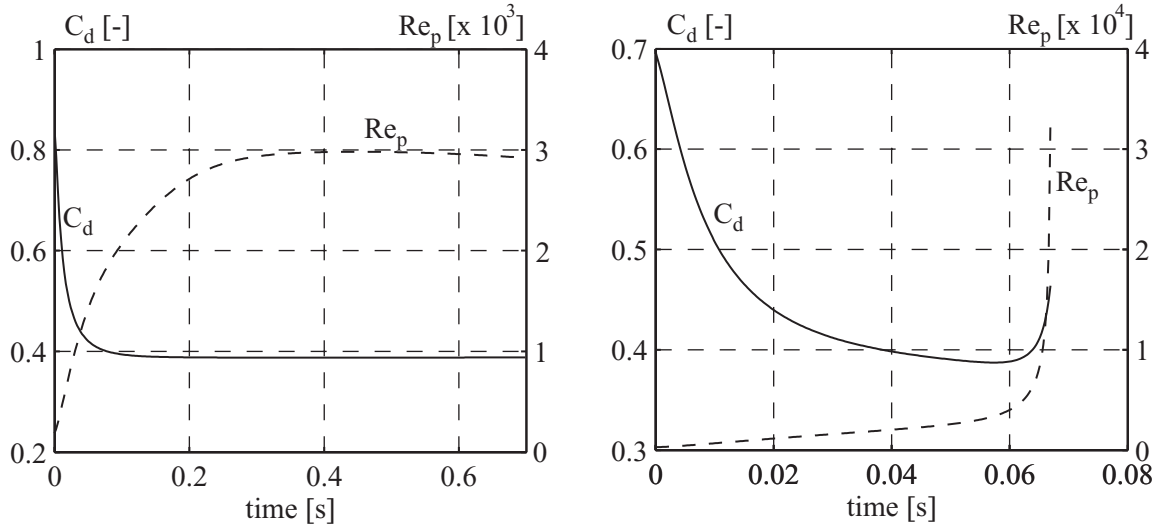

Figure 5.5: Variation of the C_d coefficient and Re_p in time for a particle outside the zone of attraction of the suction flow (left) and a particle that is sucked up (right)

Figure 5.5 shows the variation of the C_d coefficient and Re_p in time for a particle that is released near the hub of the cutter head, thus outside the zone of attraction of the suction flow. The right plot shows variation of the C_d coefficient and Re_p when the particle is released just in front of the suction pipe and will be sucked up. The initial velocity of the particle was taken 0.95 times the velocity of the fluid. A initial velocity equal to the fluid velocity would result in a Re_p of zero and an infinite value for C_d. The rotational velocity of the cutter head in the simulations was 40 RPM and the mixture velocity was 3 m/s. The trajectories of these particles are given by the particle furthest away from the suction pipe and the particle closest to the suction pipe, as was plotted in Figure 5.2.

It appears that for the particle released relatively far away from the suction pipe, the drag coefficient converges rapidly to 0.4. At least compared with the time the particle stays inside the cutter head, which was approximately 0.6 s. In this case it would hardly make any difference for the particle trajectory if C_d was taken to be 0.4 along the entire particle trajectory. For the particle that is sucked up it is not so evident that C_d can be taken to be 0.4 all the time. The value for C_d decreases rapidly from 0.7 to 0.39 as Re_p increases, but as the particle is sucked up so rapidly the C_d coefficient does not have the time to settle. The sudden increase in Re_p and C_d is caused by the small distance between the particle and the suction pipe. As can be seen from Equation (5.6), the fluid velocities will reach infinity when this distance becomes zero.

To check whether a constant value for the C_d coefficient of 0.4 is justified, the velocity of the particle resulting from the simulation with a variable and constant C_d coefficient are compared.

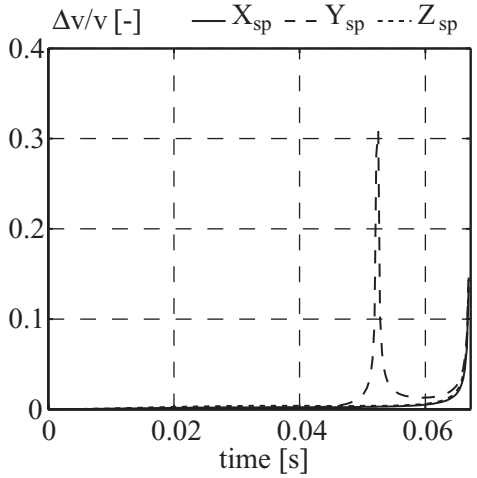

Figure 5.6: Velocity difference between the simulations with a variable and a constant C_d coefficient

In Figure 5.6 the relative velocity difference $\Delta v/v$ is plotted, where Δv is the absolute velocity difference and v is the particle velocity resulting from the simulation with the variable C_d coefficient. The relative velocity difference is plotted in X_{sp}, Y_{sp} and Z_{sp} direction. The figure shows that a variable C_d coefficient results in a negligible difference in simulated particle velocities compared with the constant C_d coefficient of 0.4. Only near 0.045 s the difference in velocity component in Y_{sp} direction shows a peak. This is due to the fact that the velocity in Y_{sp} direction resulting from the simulation with a variable C_d coefficient becomes very small and almost reaches zero. Therefore it can be assumed that for all the particles considered in the simulations, Re_p will be generally be in the Newton range and C_d can be taken to be 0.4.

5.3.5 Scale laws and dimensionless groups

The simulation model makes it possible to validate the scale law that was used in Chapter 4, i.e. Froude scaling for particles and Euler scaling for the flow. If the cutter head (and particles) are geometrically scaled and the operational parameters are scaled according to Equations (3.6) and (3.7), simulations on model and prototype scale should result in the same 'relative' particle trajectories. As a validation, simulations are performed on both scales using the nominal values for the operational parameters as given in Table 4.1. Thus, the respective values for the rotational velocity and mixture velocity on prototype and model scale are: n_c = 30 RPM and 85 RPM; v_m = 5 m/s and 1.8 m/s.

The diameter of the particles was 10 mm on model scale and 80 mm on prototype scale. For these diameters it is fair to assume that the particle Reynolds number is large enough to be in the 'Newton's range'. In this range the terminal velocity of the particle is proportional to the square root of the particle diameter (van Rijn, 1984). Thus geometrically scaling the particle diameter implies that the terminal velocity of the particle is scaled according to the square root of the length scale which is Froude scaling. With all the velocities being scaled in the same manner in all directions, the relative particle trajectory should be the same on both scales.

Figure 5.7 shows the results of the simulations on model and prototype scale. The left plot being the result on model scale and the right plot the result on prototype scale. All particle trajectories show good agreement on both scales and it is concluded that Froude scaling is the appropriate scale law. It should be kept in mind however that this conclusion is based on the forces that are considered in the model. In reality other forces may play a role and have an effect on the scale law.

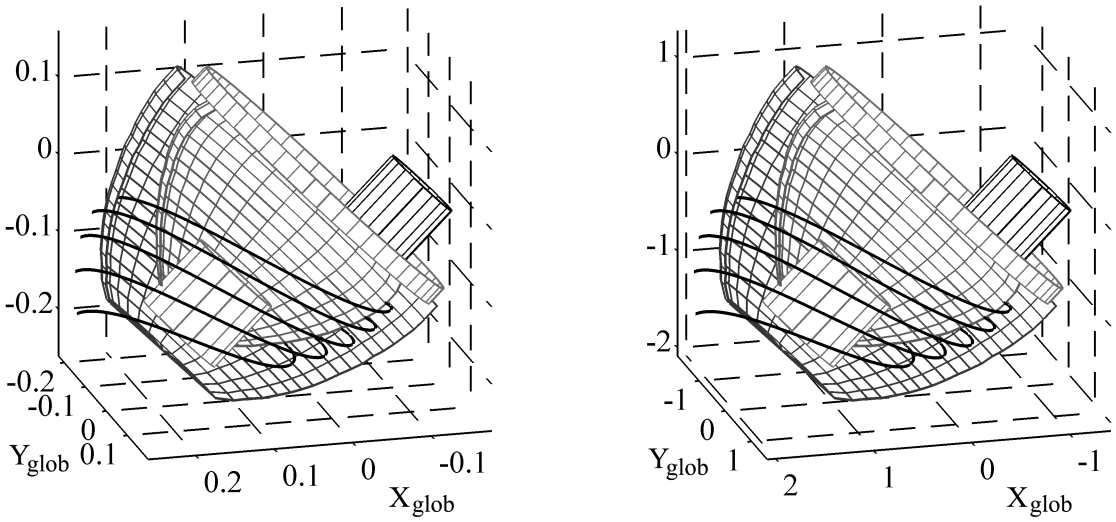

Figure 5.7: Particle trajectories on model and prototype scale when scaling according to Froude

It is not possible to reproduce identical particle trajectories on the same scale by varying the operational parameters. This is only possible when the gravitational force is neglected. Then the particle trajectories are fully determined by the flow and thus by the ratio

$$\frac{\omega_c R_c}{v_m}$$

in which R_c is the radius of the cutter ring.

The tests performed at WL|Delft Hydraulics (see Chapter 2) also showed that this ratio is decisive for the fluid flow and for the production when cutting fine sand. In that case the influence of the gravitational force on the particle trajectory may be neglected and production is determined by the flow inside the cutter head.

5.4 Influence of the haul velocity on particle trajectories

In the previous simulations the particles were all released in front of the suction pipe. For the under-cut situation this is the point where the teeth enter the breach when the cutter head is hauled. In the over-cut situation the teeth enter the breach at the top of the breach (see also Figure 4.5). The difference in under-cut and over-cut situation becomes clear when the haul velocity is taken into account.

Figure 5.8 shows the trajectories of the particles for the under-cut (left plot) and over-cut situation (right plot). The cutter head rotates clockwise when looking in the positive direction of Z_c with a rotational velocity of 40 RPM. The mixture velocity is 3 m/s and the haul velocity is 0.2 m/s. In the under-cut situation the haul velocity is in positive direction of Y_{glob} (see Figure 5.1) and in the over-cut situation in opposite direction. The haul velocity of

0.2 m/s is higher than the nominal value (≈ 0.07 m/s on model scale). This is done to make the difference more visible. The particle density and diameter were 2650 kg/m^3 and 6 mm respectively.

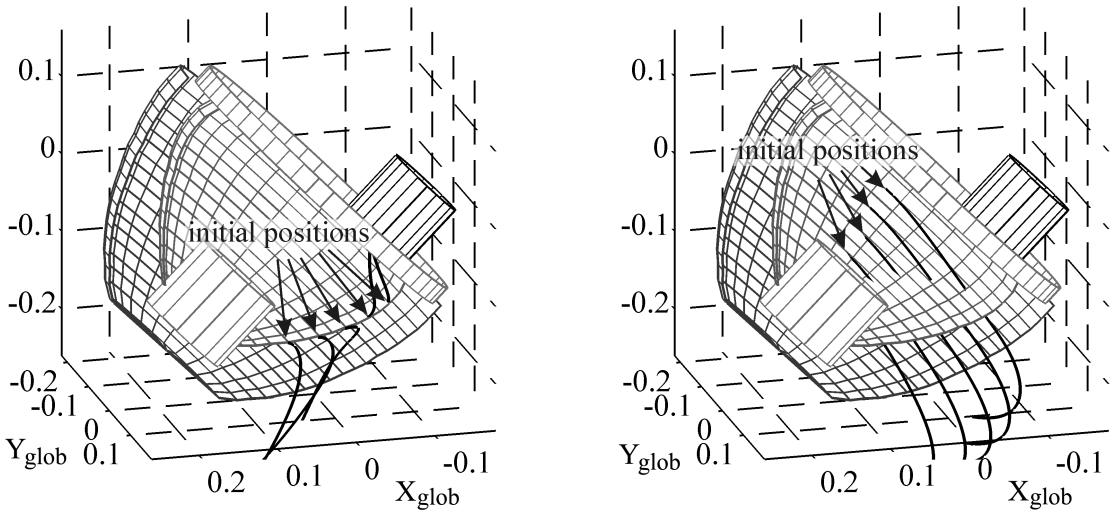

Figure 5.8: Particle trajectories of 5 particles (ρ_p = 2200 kg/m^3) released in front of the suction pipe for under-cut (left plot) and over-cut (right plot) situation when n_c = 40 and v_h = 0.2 m/s. Haul velocity is directed in positive and negative direction of Y_{glob} respectively

The particle trajectories are plotted in a relative global coordinate system, i.e. a coordinate system that is moving along with the cutter head. In comparison with the simulation where the haul velocity was zero, the particle second closest to the suction mouth is sucked up as well. This can be explained by the fact that the cutter head is moving in the same direction as the particles, which is in positive direction of Y_{glob}. Therefore the distance between the particles and the suction mouth is shorter on average and thus the probability of sucking up the particle is larger. Furthermore, the time that the suction flow has its influence on the particle is larger. For the over-cut situation the opposite is the case. The particles move in positive direction of Y_{glob} but the cutter head moves in negative direction. This means that in direction of Y_{glob} there is a large velocity difference between the particles and the suction mouth. Therefore the time span that the particles are in a region where the suction flow has an influence is much shorter than in the case of under-cut.

Another disadvantage of the over-cut situation is that the particles are cut at the side of the cutter head where the blades move in the same direction as gravity. Therefore the particles will be accelerated significantly and the particle velocity will be very high when it passes the suction mouth. If the velocity of the particle is too high the suction flow is not strong enough to suck the particle in. For the under-cut situation, the particles are cut at the side of the cutter head where the blades move in opposite direction of gravity. The velocities of the particles

will therefore be lower and the suction flow has more influence. Furthermore, due to the different manners the particles are cut, the particles are mixed better in the under-cut situation. In the over-cut situation the particles will mainly lie on the blades due to gravity and the large centrifugal forces and be thrown out of the cutter head as they pass the suction mouth (see Figure 5.8).

The difference in particle velocities for the under-cut and over-cut situation is emphasized by plotting the particle velocities resulting from the simulations. As an example the velocities of the second particle from the suction pipe is taken and the velocities in under-cut and over-cut situation are plotted (see Figure 5.9). For convenience the velocities are plotted in cylindrical coordinates in the suction pipe coordinate system. According to the right hand coordinate system the general transformation from Cartesian to polar coordinates is

$$\begin{bmatrix} v_R \\ v_\varphi \\ v_Z \end{bmatrix} = \begin{bmatrix} \cos\varphi & \sin\varphi & 0 \\ -\sin\varphi & \cos\varphi & 0 \\ 0 & 0 & 1 \end{bmatrix} \begin{bmatrix} v_X \\ v_Y \\ v_Z \end{bmatrix} \tag{5.15}$$

The left plot shows the velocities in the under-cut situation and the right plot in over-cut situation. The subscripts ‘w’ and ‘p’ stand for water and particle, while R and φ represent the radial and tangential direction. Note that φ is positive when rotating from X_{sp} to Y_{sp} axis. Z is the axis of the suction pipe Z_{sp}.

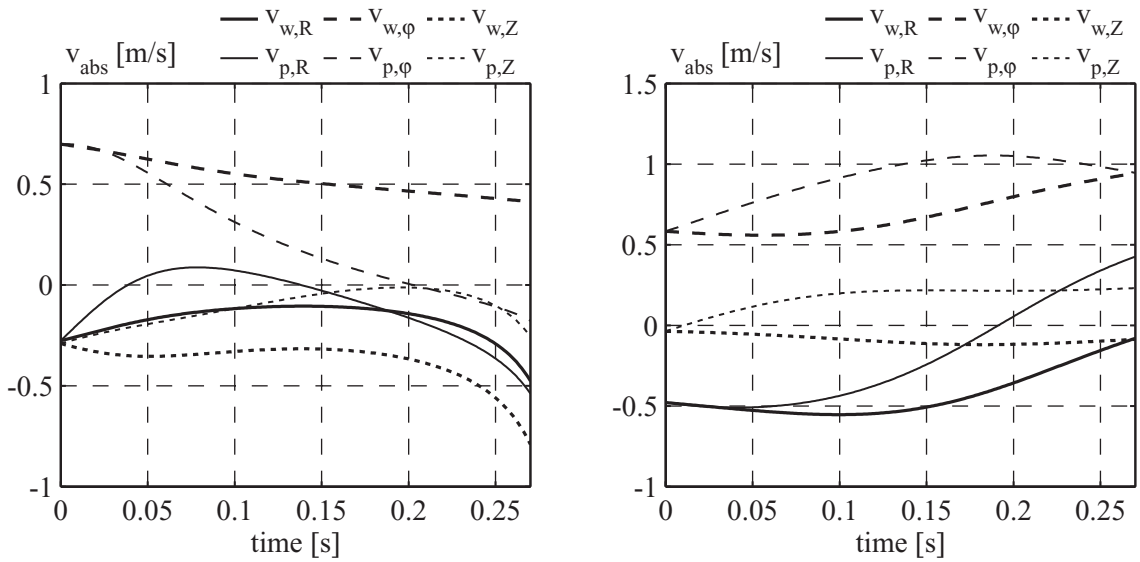

Figure 5.9: Particle velocity for under-cut and over-cut situation when n_c = 40 and v_h = 0.2 m/s

It is clearly shown in Figure 5.9 that in the under-cut situation the tangential velocity of the particle ($v_{p,\varphi}$) is much lower than in the over cut situation. This results from the fact that both the water velocities and the gravitational force accelerate the particle. Furthermore, the axial

velocity of the particle ($v_{p,Z}$) in under-cut situation has a negative value during the entire simulation, indicating that it moves towards the suction mouth. In the over-cut situation on the other hand, the axial particle velocity becomes positive rapidly, indicating that it moves away from the suction mouth.

The simulations in under and over-cut are repeated with zero haul velocity in order to illustrate the influence of the haul velocity on the velocities of the particles. The water and particle velocities resulting from these simulations of the second particle from the suction pipe are plotted in Figure 5.10. Here it should be noted that in the under-cut situation (left plot in Figure 5.10) the particle is not sucked up as opposed to the simulation with the haul velocity of 0.2 m/s. Thus, for this particle the hypothesis that the haul velocity can be beneficial in the under-cut situation is supported.

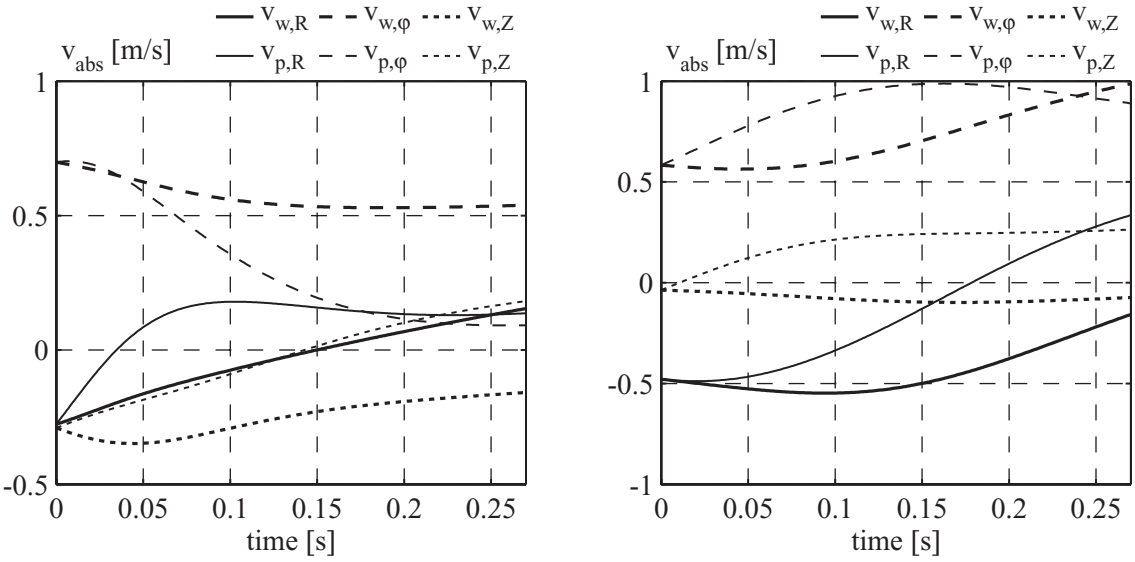

Figure 5.10: Particle velocity for under-cut and over-cut situation when $n_c = 40$ and $v_h = 0$ m/s

Comparing the velocities in the under-cut situation with the velocities in the over-cut situation it shows that there is a large difference between the under-cut and over-cut situation. Figures 5.9 and 5.10 clearly show that whereas the tangential velocity of the particle in the under-cut situation decreases, it increases in the over-cut situation. Furthermore, in the under-cut situation the axial velocity is directed towards the suction pipe all the time (Figure 5.9) or a significant part of the time (Figure 5.10). In the over-cut situation on the other hand, the radial and axial velocity of the particle are positive during the entire simulation, which means that the particle immediately moves away from the suction pipe. As the flow inside the cutter head is identical in under and over-cut situation, the difference in particle velocities is caused by the different initial position of the particles.

The difference in under and over-cut is further illustrated by plotting the forces in the direction of Z_{sp} as shown in Figure 5.11. The left plot shows the forces on the particle in the under-cut situation and the right plot the forces in the over-cut situation for the simulation where v_h = 0.2 m/s. At first notice it may appear as if there is little difference between the forces in Z_{sp} direction resulting from the simulation in under and over-cut respectively. The forces due to the pressure gradients are somewhat larger in the under-cut situation compared with the over-cut situation, but not significantly. Furthermore, in both the under and over-cut situation the drag force increases (in an absolute sense) in time. However, Figure 5.9 shows that in the under-cut situation the drag force increases due to the increasing velocity difference in Z_{sp} direction between the particle and water, but the particle velocity is directed towards the suction mouth all the time. This is caused by the relatively larger water velocities directed towards the suction mouth (and the initial velocity of the particle). The strong increase in the pressure gradient force and drag force for t > 0.25 s indicates that the particle is sucked up.

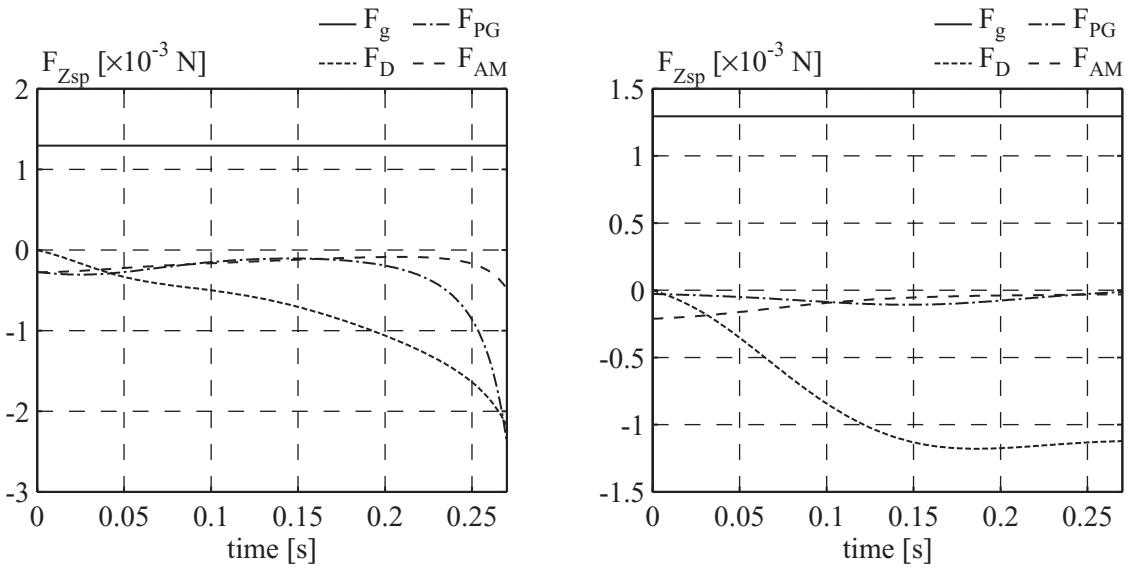

Figure 5.11: Forces in Z_{sp}-direction for under and over-cut when n_c = 40 and v_h = 0.2 m/s

In the over-cut situation, the velocity difference between particle and water increases as the particle moves away from the suction pipe. For t > 0.15 s the sum of the components in Z_{sp} direction of the drag force, pressure gradient force and added mass force almost equal the gravity component and the particle velocity in Z_{sp} direction will reach a constant value (see Figure 5.9).

For the over-cut situation, the particle velocities resulting from the simulation with a haul velocity of 0.2 m/s do not differ a lot from the particle velocities resulting from the simulation with no haul velocity. Gravity and the rotational velocity of the cutter head are the dominant

parameters that cause for a strong rotational velocity of the particle. The haul velocity of the cutter head does not have a significant influence on this. In the under-cut situation the influence of the haul velocity was significant, as in the case of a haul velocity of 0.2 m/s the particle was sucked up which did not happen when there was no haul velocity. The fact that the suction pipe moves in the same direction as the particle enables a stronger 'suction force' on the particle and over a longer period of time. In other words, the work done by the suction flow can be significantly larger when the suction pipe moves in the same direction as the particle. However, this positive effect strongly depends on the ratio of the rotational velocity of the cutter head and the haul velocity. If the rotational velocity of the cutter head is too large, the particle velocity will be significantly larger than the haul velocity. Consequently the particle moves away from the suction pipe rapidly and the influence of the haul velocity will be negligible.

The difference between the under-cut and over-cut situation can also be explained by looking at the work done by the suction flow. The work done is defined as

$$U_{sp} = \int \left(F_{Xsp} dX_{sp} + F_{Ysp} dY_{sp} + F_{Zsp} dZ_{sp} \right) \tag{5.16}$$

where F_{Xsp}, F_{Ysp} and F_{Zsp} are the forces acting on the particle induced by the suction flow (i.e. pressure gradient force and drag force) in the three directions. The displacement of the particle is given by dX_{sp}, dY_{sp} and dZ_{sp}.

As an example, the work done by the suction flow (U_{sp}) is plotted for the under and over-cut situation (see Figure 5.12) for the simulations where n_c = 40 RPM and v_h = 0.2 m/s. Figures 5.9 and 5.11 show the respective velocities and forces.

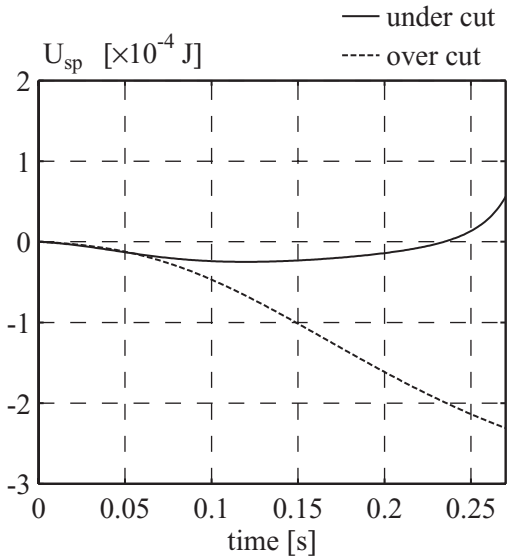

Figure 5.12: Work done by the suction flow in axial direction for the under-cut and over-cut situation when n_c = 40 and v_h = 0.2 m/s

In the figure U_{Zsp} represents the work done in direction of Z_{sp}. Only the influence of the suction flow (i.e. pressure gradient and drag force) is taken into account for determining the work done. The influence of gravity is left out of consideration. As in the under-cut situation both the displacement of the particle and the forces acting on the particle are negative, the work done in Z_{sp} direction is positive. In the over-cut situation the work done is negative as the displacement of the particle is opposite to direction of the forces. Therefore it is concluded that the suction flow has less influence on the particle in the over-cut situation than in the under-cut situation. The difference in work done by the suction flow in over and under-cut diminishes as the rotational velocity of the cutter head increases. Then the suction flow has little influence on the particle trajectory in either case.

The influence of the haul velocity on the situation in practice can also be clarified by plotting the general particle trajectories in under and over-cut situation (see Figure 5.13). The left plot shows the under-cut situation and the right plot the over-cut situation.

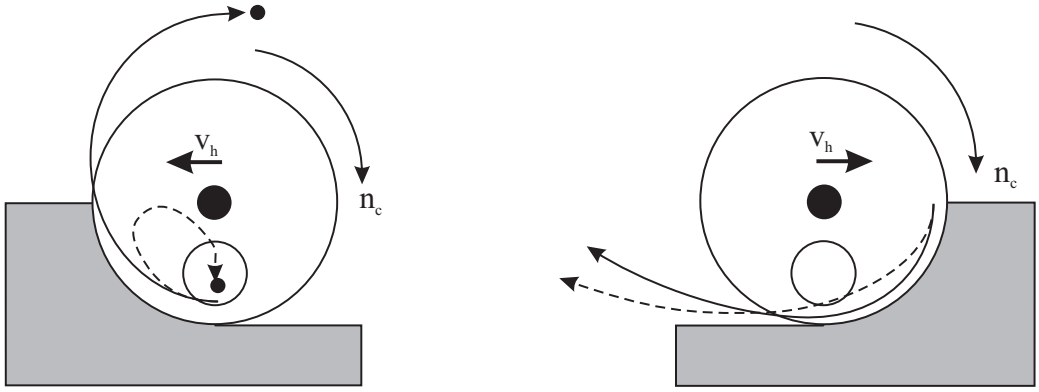

Figure 5.13: Influence of the haul velocity on the particle trajectories for under and over-cut

The gray area is the breach, while the smaller white circle represents the suction pipe. In both plots the solid lines represents the case where $v_h = 0$ and the dashed lines represent the case where v_h equals the nominal value. These dashed lines are plotted in a relative coordinate system moving along with the cutter head (i.e. moving with velocity v_h).

From the left plot it becomes clear that the cutter head moves in the same direction as the particle in the under-cut situation. Therefore, the average distance between the particle and the suction pipe is generally shorter when the haul velocity equals the nominal value compared to the situation where $v_h = 0$. Moreover, gravity works in opposite direction of the rotation of the cutter head over a certain period of time, decreasing the rotational velocity of the particle. Then, the suction flow will have more influence on the trajectory of the particle.

In over-cut situation the particles are accelerated due to gravity up to the moment they pass the suction pipe. Therefore the particles will have such a high velocity that the influence

of the suction flow is often not large enough to suck the particle up. This becomes even worse when the cutter head is hauled. Then the difference in speed between the suction pipe and particle is so large that the particles just pass by the suction pipe as shown in Figure 5.13. This phenomenon is most likely the reason that in practice the production in over-cut situation is 2 to 3 times lower than in under-cut situation.

5.5 Reflections on the flow model used in the simulations

The simulations performed in this chapter showed the limitations of the relatively simple flow model that was used. Especially the absence of the pump effect of the cutter head in the flow model could be crucial for determining the particle trajectories. Therefore it was decided that a separate research investigation should be set up in order to determine the flow inside the cutter head. This research investigation was set up in cooperation with the section Engineering Fluid Dynamics of the Department of Mechanical Engineering of the University of Twente. Expertise is available at the section of Engineering Fluid Dynamics on successfully setting up three-dimensional CFD models for determining the flow in axial fans, mixed-flow pumps and centrifugal pumps (Kruyt et al. 1999). Considering their expertise, the analogy between cutter heads and the different kinds of pumps plus the results of the models set up by the section of Engineering Fluid Dynamics, this strategy was preferred over the use of a commercial CFD package.

The CFD model is based on the theory for incompressible potential flows. This theory is valid if the Reynolds number is large enough, the incoming water flow is irrotational and no massive boundary layer separation occurs (Dekker et al., 2002). The Navier-Stokes equations are then simplified to the unsteady Bernouilli equation and the governing equations are solved numerically using a three-dimensional finite-element method. Once the model is set up, the particle trajectories are simulated in a comparable way as is done in this chapter. The flow field is given in an Eulerian framework, while the particle trajectories are solved in a Lagrangian framework. Thus, the presence of the particles does not have an influence on the flow inside the cutter head.

For more detailed information on the set-up of the CFD model and validation tests of the model, the reader is referred to the concerning literature. However, initial results of the flow simulations are used to determine the trajectories of particles along the inner surface of a cutter blade. This is described in Appendix F.

5.6 Conclusions

A model has been set up that determines the trajectories of particles inside the cutter head. The influence of the blade geometry on the flow is neglected, as well as the contact between a

particle and a blade. The flow inside the cutter head is represented by the superposition of a forced vortex and a sink. As the flow is considered frictionless, the Euler equation is the governing equation.

The forces acting on the particle taken into account are: gravitational force, drag force, forces due to the pressure gradient and the added mass force. Simulations showed that the particle Reynolds number was generally in the Newton range and a constant C_d coefficient of 0.4 was allowed.

Simulations showed that, due to the poor influence of the suction flow, only particles released close enough to the suction mouth were sucked up. The pressure gradients resulting from the suction flow and the fluid velocities towards the suction pipe decrease rapidly with increasing distance from the suction pipe. This was not entirely in accordance with the tests results of the single particles (Chapter 4) where particles could be sucked up from larger distances. As particles were hardly sucked up in the simulations it was not possible to compare the residence times of the particles in the simulations with the test results.

The flow model used for the simulations is too simplistic. The influence of the cutter head geometry on the flow inside the cutter head should be taken into account. Especially the absence of the pump effect of the cutter head in the flow model forms a significant deficiency.

Performing the simulations on two different scales and using the scale laws derived in Chapter 3 showed that the Euler number for scaling the flow and Froude number for particle give uniform particle trajectories.

Simulations representing the under and over-cut situation gave a qualitative explanation for the low production in over-cut situation as experienced in practice. As a particle is cut in the over-cut situation, the water velocities and the gravitational force are in the same direction over a large part of the particle trajectory. The particle is continuously accelerated and has a high velocity as it passes the suction mouth. In addition, the suction mouth (or cutter head) moves in opposite direction of the particle, which means that the particle is in the area of influence of the suction flow for a very short period of time. The suction flow is not strong enough to deflect the particle towards the suction mouth in such a short period of time. In the under-cut situation the particle velocity is lower than in the over-cut situation and particle initially moves in the same direction as the suction mouth. Therefore, the suction flow has a stronger influence on the particle and over a longer period of time.

Chapter 6
Cutting Tests in Cemented Banks of Gravel

6.1 Introduction

The tests where single particles were injected in the cutter head (see Chapter 4) showed that the residence times of the particles were very high. In practice, when actually cutting a bank, these high residence times for the particles would imply that the cutter head fills up with particles. As it is known from practice that this does not happen, the processes inside the cutter head will be different when a bank is actually cut. In order to determine what really happens and to determine the influence of a concentration of particles inside the cutter head, actual cutting tests have been performed on a model scale. Here an artificial bank made of gravel has been cut.

Performing cutting tests made it also possible to determine the production and spillage as a function of the operational parameters (i.e. the rotational velocity of the cutter head and the mixture velocity). In the stationary tests this was not possible as often particles that were thrown out of the cutter head could enter the cutter head again because of the strong flow towards the cutter head and the absence of a haul velocity.

The aim of the tests was to focus on the mixture forming processes rather than the cutting process. Furthermore, the tests had to be representative for the cutting of rock or hard clay, where inertial forces play an important role. Therefore, the artificial bank was made of weakly cemented gravel. That way, the cutting forces would never become dominant and the available torque on the cutter head drive shaft was not the limiting factor. Moreover, the density of gravel was 2650 kg/m^3 and thus representative for cutting of rock or hard clay and comparable with particles used in the tests where single particle were injected in the cutter head. By weakly cementing the gravel particles it was expected that single particles would enter the cutter head.

The tests have been performed on a 1:8 scale in relation to the large cutter suction dredges. This scale was not chosen freely, but it results from the available test facilities and cutter heads. Both the under and over-cut situation were investigated. In order to compare the simulated particle trajectories with the particle trajectories resulting from the cutting tests, a transparent back plate was used (see Figure 6.2 for the position and dimensions of the back plate). This made it possible to film inside the cutter head and visualize the processes taking place inside the cutter head.

6.2 Test facilities and equipment

The tests have been carried out at the Laboratory of Dredging Technology of the Delft University of Technology. Figure 6.1 shows the cross section of the cutting tank and the towing carriage. The different numbers in the figure indicate:

1. radioactive density meter
2. suction pipe
3. cutter head
4. cemented gravel bank
5. main cutting tank
6. collecting tank (used for collecting the production during tests)

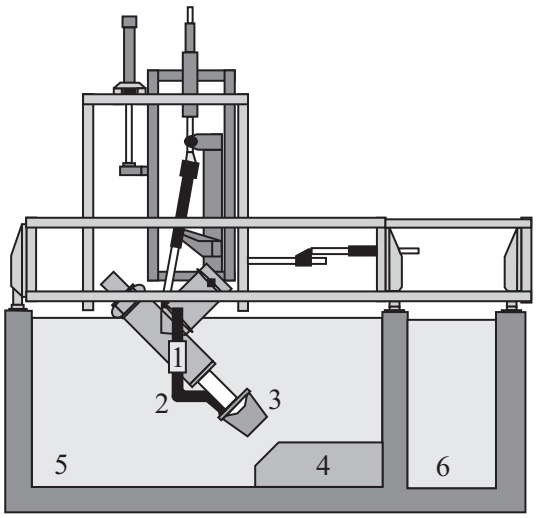

Figure 6.1: Cross section of the cutting tank and towing carriage

The part of the tank that has been used was 8 m long with a width of 3 m and a depth of 1.5 m. The maximum haul velocity of the carriage was 1.25 m/s, while the angular velocity of the cutter head was adjustable between 0 and 180 RPM approximately. The suction and delivery

pipeline had a diameter of 0.1 m resulting in a maximum mixture velocity of 6.0 m/s. A radioactive density meter has been placed in the suction pipe 2 m after the suction mouth.

All tests have been carried out with the same cutter head. This was a six bladed crown cutter head, with an outside ring diameter of 0.4 m. The height of the cutter head is 0.29 m including the ring (0.265 m. without the ring). A conical back plate has been used with a diameter of 0.32 m and a top angle of 120º. Figure 6.2 gives the geometry and the most important measures of the cutter head (dimensions in mm).

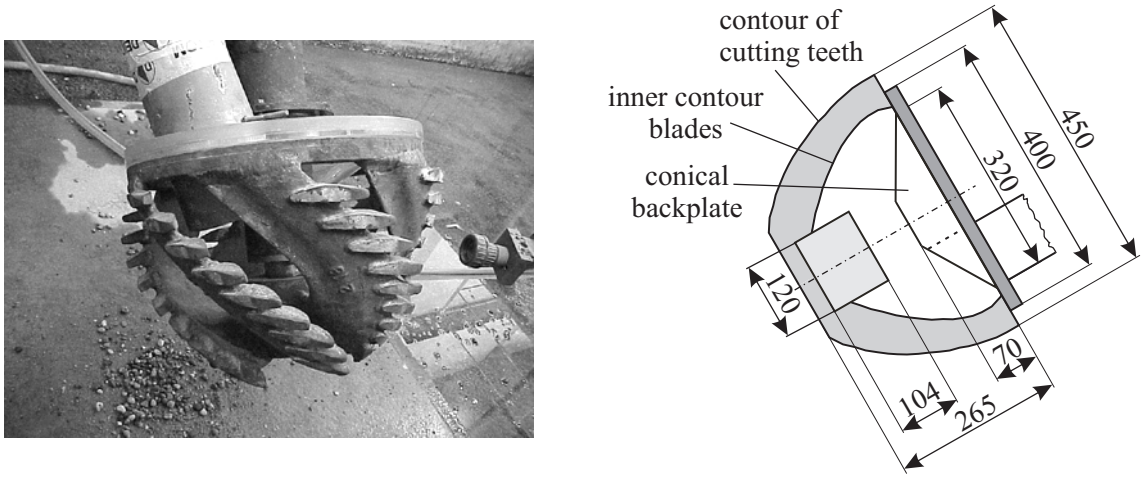

Figure 6.2: Geometry and dimensions of the cutter head

The suction mouth was shaped like a banana and the area of its cross section was 1.25 times the area of the cross section of the suction pipe (see for instance Figure 4.5 for the shape of the suction mouth). Both the conical back plate and the suction mouth were transparent so that video recordings could be made under-water from behind the back plate. Therefore, two digital cameras have been placed behind the back plate, one on each side of the cutter drive shaft in order to film the processes in the cutter head. A third analog camera has been placed above the cutter head to have a total view.

The length of the cemented gravel banks was 2.16 m. A cross section of the cemented gravel bank is shown in Figure 6.3 (dimensions in mm).

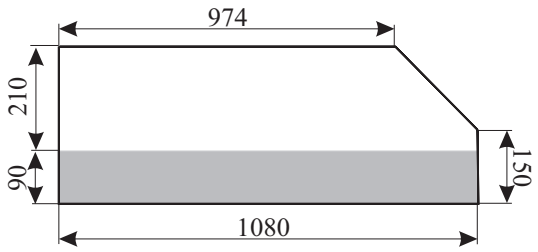

Figure 6.3: Cross section and dimensions of the cemented gravel bank

At the bottom of each block a layer of 9 cm of reinforced concrete was used for creating sufficient stiffness to enable hoisting of the banks. The average grain size of the gravel particles in the bank was 1 cm, in accordance with the scale laws derived in paragraph 3.2.2 and the simulations that have been performed in Chapter 5. The density of the gravel bank was 1700 kg/m^3 in air which corresponds with a density of 2058 kg/m^3 in water when all the pores are filled with water. With each bank it was possible to perform four consecutive cuts.

6.3 Applied scale laws for cutting tests

6.3.1 Scaling the rotational velocity of the cutter head and suction flow

In order to determine the values of the operational parameters on a model scale their values on prototype scale need to be defined. For the prototype cutter head the parameters based on the cutter suction dredge Ursa have been used, as shown in the following table. The table also gives the dimensions of the cutter head on model scale and the properties of the gravel bank.

	prototype scale	model scale
Diameter suction pipe: D_{sp}	0.95 [m]	0.1 [m]
Diameter ring cutter head: D_c	3.12 [m]	0.4 [m]
Density rock: ρ_r	2200 [kg/m^3]	
Density gravel bank: ρ_b		1700 [kg/m^3]
Density gravel grain: ρ_g		2650 [kg/m^3]
Suction flow: Q_s	3.0 [m^3/s]	-
(mixture velocity: v_m)	(4.2 m/s)	
Rotational velocity: n_c	30 [RPM]	-
Haul velocity: v_h	0.2 [m/s]	-

The model cutter head is not exactly scaled geometrically, since the diameter of the cutter head is scaled with a different factor than the diameter of the suction pipe. The diameter of the suction pipe on a model scale is 9.5 times smaller than on a prototype scale, while the diameter of the ring of the model cutter head is 7.8 times smaller. Furthermore, the densities of the cut material on model and prototype scale are not alike. For the density of rock a value of 2200 kg/m^3 is taken while the gravel particles have a density of 2650 kg/m^3.

On a model scale there is the additional issue that the density of the bank differs from the density of a single gravel grain. This has some consequences for the filling degree of the

cutter head and thus on the scaling of the haul velocity, which will be dealt with in paragraph 6.3.2.

Directly applying the Froude scale for determining the values of the operational parameters on model scale will give a certain abnormality due to the fact that the cutter head is not exactly scaled geometrically. This can be avoided by realizing that scaling according to the Froude number is a way of realizing dynamic similarity on prototype and model scale. This means that all the relevant force ratios are equal on both scales. Therefore dynamic similarity can also be achieved by determining the (expected) dominant forces and keeping their ratios constant. Supported by the results of the tests with single particles and the simulations described in Chapter 5, it is assumed that the trajectories of the particles is governed by: gravitational force F_g, centrifugal force F_{cf} and the suction force F_s. This means that two dimensionless groups can be formed by the ratio of forces. First of all

$$\frac{F_{cf}}{F_g} \sim \frac{m_p R_c \omega_c^2}{(\rho_p - \rho_w) V_p g} \sim \frac{\rho_p}{(\rho_p - \rho_w)} \frac{R_c \omega_c^2}{g} \tag{6.1}$$

in which m_p is the mass of the particle, R_c is the radius of the cutter ring, ω_c is the angular velocity of the cutter head, ρ_p is the density of the particle, ρ_w is the density of water, V_p is the volume of the particle and g is the acceleration of gravity. Note that the buoyancy effect is included in the gravitational force. In the latter fraction the Froude number can be recognized.

The second dimensionless group is formed by the ratio of the centrifugal force and the suction force. The magnitude of the suction force acting on the particle equals the pressure gradient as given by Equation (5.14) multiplied by the volume of the particle. The ratio becomes

$$\frac{F_{cf}}{F_s} \sim \frac{\rho_p}{\rho_w} \left(\frac{\omega_c R_c^3}{v_m R_{sp}^2} \right)^2 \tag{6.2}$$

in which v_m is the mixture velocity and R_{sp} is the radius of the suction pipe.

The term between brackets represents the flow number as described in Chapter 1. It is the ratio of two flows namely: the flow generated by the cutter head itself (pump effect governed by $\omega_c R_c^3$) and the suction flow. For equal values of this flow parameter there is similarity of the flow inside the cutter head (Steinbusch et al., 1999).

In Equations (6.1) and (6.2), the dissimilarity in geometrical scale factors is taken into account as the dimensions for the cutter head and suction pipe appear in the equations. Furthermore, the difference in densities of the cut particles on both scales is taken into account. Using the ratios of the forces as the appropriate scale laws results in the following nominal values for the rotational velocity and mixture velocity on model scale.

rotational velocity:	$n_c = 90$	[RPM]
Suction flow:	$Q_s = 0.021$	[m^3/s]
	($v_m = 2.64$ m/s)	

6.3.2 Scaling the haul velocity

The haul velocity and the cutoff area determine the amount of material that is cut per unit of time and thus the amount, or rather concentration, of particles inside the cutter head. Here the cutoff area is the area perpendicular to the haul velocity, determined by the contour of the cutting teeth and the positioning of the cutter head in the bank. The concentration of particles inside the cutter head is important for the processes taking place inside the cutter head. It will determine the proportion of the following generalized forces:

- Forces due to fluid-particle interaction
- Inter particle forces (such as friction or inter-particle collision)

Furthermore, the interaction between particles and the blades (friction, collisions) depends on the concentration of particles inside the cutter head. These forces are of the same category as the inter-particle forces. An important additional effect of large concentration of particles is the fact that the flow will be disturbed. This may have a significant influence on the production.

In order to have the same effects on model scale as on prototype scale, the filling degree of the cutter head (concentration) needs to be equal on model and prototype scale. This yields that the ratio of the mass flow of particles into the cutter head and the mass flow of particles through the suction pipe (discharge) needs to be equal on model and prototype scale. Thus

$$\frac{\rho_b v_h A_{cut}}{c_t \rho_p Q_s} = \text{constant} \tag{6.3}$$

in which A_{cut} is the cutoff area and c_t is the transport concentration of particles in the suction pipe. With equal c_t on prototype and model scale, the haul velocity on a model scale becomes

$$\left[v_h\right]_m = \frac{\left[A_{cut}\right]_p}{\left[A_{cut}\right]_m}\left[\frac{\rho_p Q_s}{\rho_b}\right]_m\left[\frac{v_h}{Q_s}\right]_p \tag{6.4}$$

in which the subscript ‘m’ and ‘p’ stand for model and prototype. In the equation, the ratio between the density of the particles and the bank on model scale appears. This is because the density of the bank is different than that of the individual gravel particles, because of the pore volume between the particles (35% of the banks consists of pores filled with water).

Supposing that on a model scale the cutter head is positioned the same way as on a prototype scale, the cutoff area is geometrically scaled. Taking the cutter ring diameter as the

normative size, the cutoff area on model scale is a factor 7.8 squared smaller than on a prototype scale. Substituting the values for the different parameters in Equation (6.4) results in the following haul velocity on model scale:

$$[v_h]_m = 0.13 \text{ m/s}$$

Directly scaling the haul velocity according to the Froude number and thus to the square root of the length scale, would have resulted in a haul velocity of 0.07 m/s. Where it is assumed that the average model scale is 1:8. Apparently scaling the haul velocity in such a way that the expected filling degree of the cutter head is equal on model and prototype scale results in a haul velocity that is almost twice as large as when it is scaled according to Froude. This difference is mainly caused by the difference in densities (on model scale) of the particle and bank.

Compared with the mixture velocity and the rotational velocity, both being approximately 2 m/s, the haul velocity is still relatively small. Therefore it may be assumed that the increase in haul velocity will not have a significant influence on the flow inside the cutter head.

Positioning of the cutter head in the bank

For a prototype cutter head with a outer ring diameter of 3.12 m and a cutter axis inclination angle of 45º, a reasonable cutting depth would be 1.1 m with a step size of 1.5 m (i.e. for cutting of hard rock). Then the average cutoff area is approximately 1.4 m^2. On a model scale this corresponds with a cutting depth of 0.14 m, a step size of 0.19 m and thus a cutoff area of 0.023 m^2. The mass flow of particles into the cutter head then becomes:

$$\dot{M}_{in} = A_{cut} v_h \rho_b = 0.023 \cdot 0.13 \cdot 1700 = 5.1 \text{ kg/s}$$

However one of the demands during the tests was that single gravel grains would enter the cutter head instead of clusters of gravel grains. This means that the thickness of the cut (h) is limited. The equation for h is:

$$h \approx \frac{60 v_h \sin \alpha_{cut}}{n_c q} \tag{6.5}$$

where α_{cut} is the angle between the tip of a tooth and the vertical axis and q is the number of arms on the cutter head. The 60 appears in the equation as n_c is defined as revolutions per minute. Equation (6.5) is further explained by Figure 6.4. The figure shows two successive teeth that are placed on two successive blades. Assuming that the cutter head has six blades the angle between the teeth is 60˚. The tooth just entering the bank will follow the path indicated by the dashed line. The thickness of the cut reaches a maximum (h_{max}) when the tooth is almost at the top of the bank. When h_{max} is too large, a cluster of gravel grains will break out instead of single gravel grains.

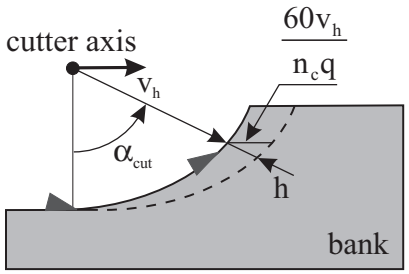

Figure 6.4: Thickness of the cut h as a function of the angle of cut α_{cut}

Preliminary tests the indicated that if $h_{max} \approx 1.7$ cm, the gravel grains (1 cm diameter) will still enter the cutter head separately. For a rotational speed of 90 RPM this means that the haul velocity is limited to 10 cm/s instead of the calculated 13 cm/s. Furthermore, for the lower rotational speeds (lower than 70 RPM) it appeared to be difficult to reach the required haul velocity due to the higher cutting forces. Therefore the haul velocity was kept at 10 cm/s throughout the tests. As the haul velocity is much lower than the mixture velocity and the rotational velocity, it can be assumed that the change in haul velocity does not have a significant influence on the processes inside the cutter head, as long as the mass flow of gravel into the cutter head is equal.

In order to get the same mass flow of gravel into the cutter head, the theoretical cut-off area should be increased from 0.023 m^2 to 0.03 m^2. This is realized by increasing the cutting depth to 16 cm and the step size to 20.5 cm instead of the 14 cm and 19 cm. This means that the cutter head is positioned in the bank as shown in Figure 6.5.

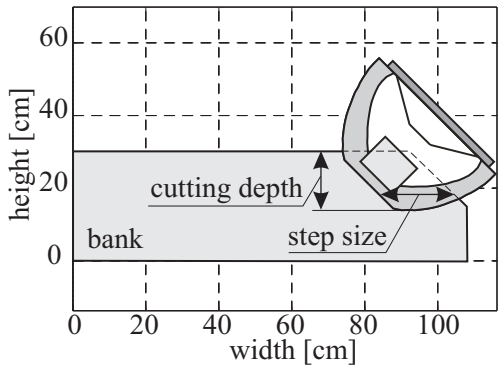

Figure 6.5: Positioning of the cutter head in the cemented gravel bank

Summarizing, the properties on prototype and model scale are as shown in Table 6.1.

Table 6.1: Properties on prototype and model scale

	prototype scale	model scale
Diameter suction pipe: D_{sp}	0.95 [m]	0.1 [m]
Diameter ring cutter head: D_c	3.12 [m]	0.4 [m]
Density rock: ρ_r	2200 [kg/m^3]	
Density gravel bank: ρ_b		1700 [kg/m^3]
Density gravel grain: ρ_g		2650 [kg/m^3]
Suction flow: Q_s	3.0 [m^3/s]	0.021 [m^3/s]
(mixture velocity: v_m)	(4.2 m/s)	(2.6 m/s)
Rotational velocity: n_c	30 [RPM]	90 [RPM]
Haul velocity: v_h	0.2 [m/s]	0.1 [m/s]
Cut off area: A_{cut}	1.4 [m^2]	0.023 [m^2]
Cutter inclination angle: λ	45 [º]	45 [º]

6.4 Results of the cutting tests in cemented gravel banks

Primary tests were performed where the rotational velocity of the cutter head and the mixture velocity were varied around their nominal values. The haul velocity was kept constant at 0.10 m/s in all the tests. Both the under-cut and over-cut situation have been investigated. Furthermore, additional tests have been carried out with gravel grains with a d_{50} of 1.5 cm and a cutter inclination angle of 25º. An overview of all the tests performed is shown in Appendix C. During each test, the sucked up gravel grains were dumped in the collecting tank (see Figure 6.1). After each test the spillage was collected and weighed as was the sucked up material. The production percentage P is defined as:

$$P = \frac{\text{weight of sucked up material}}{\text{total weight of cut material}} \times 100\%$$

6.4.1 Test results for the under-cut situation

The result of the tests in under-cut situation are shown in the following figure. In the left plot the production percentage is plotted against the rotational velocity. The different markers correspond with different mixture velocities and indicate the measured points. The measured points at similar mixture velocities are connected by dashed lines (second order polynomial fit). These lines are merely used for representation purpose and hold no physical background. The plot shows that the production curves at constant mixture velocity do have optimum values. An initial increase in rotational velocity results in an increase in production. After a

certain optimum has been reached, further increasing the rotational velocity causes for a decrease in production. Increasing the mixture velocity (at constant rotational velocity) always results in an increase in production. The plot also shows that the nominal values of the operational parameters (n_c = 90 RPM, v_m = 2.6 m/s) do lie near the optimum.

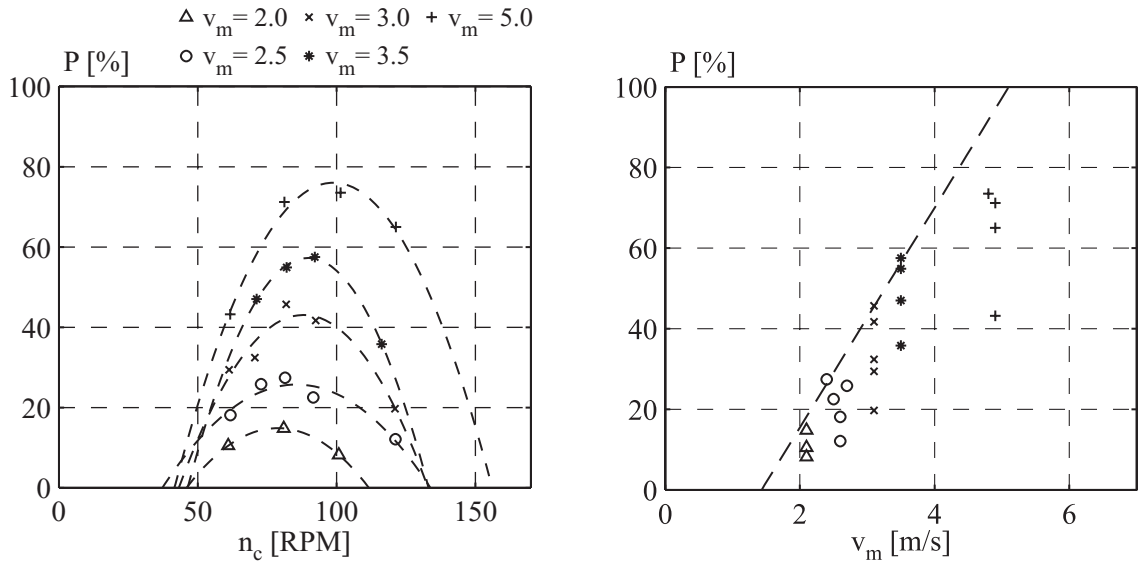

Figure 6.6: Production percentage vs. the rotational velocity and mixture velocity in the undercut situation

In the plot on the right, the production percentage is plotted against the mixture velocity for the different rotational velocities. The plot shows that the maximum production percentage varies almost linearly with the mixture velocity between mixture velocities of 2 m/s and 3.5 m/s (indicated by the dashed line). Beyond a mixture velocity of about 3.5 m/s, the maximum attainable production starts to deviate from the dashed line.

The reason that the production percentage decreases when the rotational velocity becomes too high is first of all the larger centrifugal forces acting on the particles. Because of the large centrifugal forces the particles are thrown out of the cutter head (segregation). The higher the rotational velocity of the cutter head the higher the centrifugal forces and the lower the production percentage. Secondly, the increasing rotational velocities cause for an increasing pump effect of the cutter head and thus an increasing outgoing flow when the suction flow remains constant. Therefore, more particles will escape from the cutter head as they are dragged along with this outgoing flow.

The increase in production with increasing rotational velocity is more difficult to explain. At low rotational velocities the gravitational forces are clearly dominant and most particles will

gather at the lowest point in the cutter head and can be considered as spillage. The most likely reasons for the increase in production percentage with increasing rotational velocity are:

- better mixing of the particles due to collisions of particles with the blades
- positive change of flow inside the cutter head

As the rotational velocity of the cutter head increases, the intensity of the collisions between particles and the blades increases. Therefore it is plausible that more particles are kept or even brought into suspension and consequently sucked up more easily.

Increasing the rotational velocity can also result in more favorable flow pattern inside the cutter head. In the area where the particles are cut, between the breach and the cutter head axis, the drag force acting on a particle has a component working in opposite direction of the gravitational force. This means that for higher rotational velocities of the cutter head, the larger drag force could compensate for the (negative) influence of the gravitational force. Of course this effect is limited, as the centrifugal force acting on a particle will increase as well with increasing rotational velocity of the cutter head. Another positive change in the flow could be caused by the (axial) pump effect of the cutter head. This pump effect will induce higher axial velocities inside the cutter head directed towards the suction pipe and thus transport particles in the direction of the suction pipe. Consequently the probability that a particle will be sucked up is increased.

Production percentage against flow number

More insight in the test result is obtained by plotting the production percentage against the dimensionless parameters as given by Equations (6.1) and (6.2). As the density of the particles is not varied, plotting the production percentage against the dimensionless group in Equation (6.1) will not produce further information compared with Figure 6.6. Plotting the production percentage against the ratio of flows given by Equation (6.2), which is the inverse of the flow number, results in the left plot of Figure 6.7. Tests performed by WL|Delft Hydraulics indicated that an inward flow along the entire cutter contour is achieved for flow numbers larger than 0.47 (see Chapter 2) and thus inverse flow numbers smaller than 2. This means that most of the tests have been executed at values for the operational parameters where an outward flow exists.

For rotational velocities beyond the optimum, the measured production percentages almost lie on one line (indicated by the gray line). This means that for these rotational velocities, the production percentage is determined by the (inverse) flow number and not by the individual values of the mixture velocity and rotational velocity. The same trend was noticed in the tests performed at WL|Delft Hydraulics (Mol, 1977a) where plastic particles were injected in the cutter head and the cutting tests in sand performed by Miltenburg (1983).

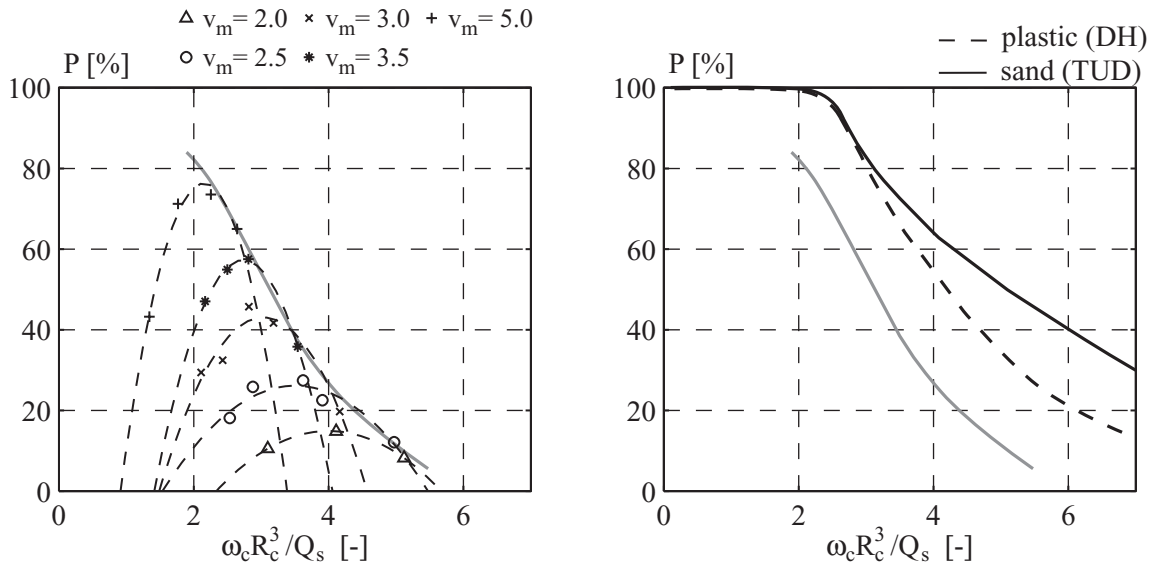

Figure 6.7: Production percentage vs. inverse of the flow number in the under-cut situation for cutting of gravel (left plot) and the results of the sand and plastic particles (right plot)

The production curves resulting from these two tests, that were already mentioned in Chapter 2, are shown in the right plot in Figure 6.7. For comparison, the results of the current gravel tests are plotted as well. It should be noted that the tests with the plastic particles, performed at WL|Delft Hydraulics, were executed on a larger scale as the diameter of the cutter ring was 0.6 m instead of the 0.4 m. For comparing the results, the plastic particles with a diameter of 2 cm were geometrically scaled to the 1:8 scale. This means that on a 1:8 scale the particle diameter is 1.3 cm. The right plot in Figure 6.7 is clarified by the properties in the following table. The columns successively represent: particle diameter, particle density, terminal settling velocity, drag coefficient, particle relaxation time and the ratio of the centrifugal force and the gravitational force minus buoyancy force.

Table 6.2: Particle properties in the different tests

	d_p [mm]	ρ_p [kg/m^3]	v_{ts} [m/s]	C_d	t_p [s]	$F_{cf}/(F_g-F_{buo})$ [-]
sand	180×10^{-3}	2650	0.02	9	3.5×10^{-3}	2.8
plastic	13	1118	0.21	0.4	0.23	13.5
gravel	10	2650	0.73	0.4	0.07	1.08

In order to determine the particle relaxation time of the sand and plastic particles the general equation for the particle relaxation time as given by Equation (A.11) in Appendix A is used. For the sake of simplicity it is here assumed that the slip velocity approximately has the same value as the terminal settling velocity and that the drag coefficient is constant. The particle relaxation time of the gravel particle is derived by using Equation (3.5). Therefore the determined particle relaxation times (t_p) only give a rough estimation. For determining the

centrifugal force it is assumed that the tangential velocity of the particle equals the tangential water velocity minus the terminal settling velocity of the particle, i.e. ($\omega_c R_c - v_{ts}$). Furthermore, the centrifugal force was determined for a rotational velocity of the cutter head of 90 RPM. For this rotational velocity and using Equation (3.3), the characteristic time scale for the fluid T_f becomes 0.11 s.

By means of the values shown in Table 6.2 it is concluded that although the trends of the different curves are similar for the higher rotational velocities, the processes behind the trend are different. Considering the small value of the particle relaxation time for sand with respect to the characteristic time scale for the fluid ($t_p/T_f << 1$) it may be presumed that particle inertia can be neglected with respect to the hydrodynamic forces. This is verified by large drag coefficient. This implies that the decrease in production with increasing inverse flow number is mainly caused by pump effect of the cutter head and thus the outgoing flow dragging along particles. For the plastic particles inertia does play an important role, considering the relatively large particle relaxation time. Particles are thrown out of the cutter head as a result of this inertia and additionally because of the outgoing flow. This causes for the shift downwards of the production curve. Considering the ratio of the centrifugal force and the gravitational force compensated for buoyancy, which will only be higher for larger rotational velocities, gravity will not play a dominant role. For the gravel particles both particle inertia and gravity play a dominant role.

Table 6.2 shows that for the cutting tests with gravel particles, the ratio of the centrifugal force acting on the particle and the gravitational force minus buoyancy force is 1.08. This ratio was estimated for a rotational velocity of the cutter head of 90 RPM. As the centrifugal force acting on the particle is approximately quadratically proportional to the rotational velocity of the cutter head, this ratio will about 2 for a rotational velocity of 120 RPM. Considering this value it can be assumed that in the tested region between 90 RPM and 120 RPM, where the production decreases with increasing rotational velocity, the influence of the gravitational force can not entirely be neglected. Gravity will therefore still have a considerable influence on the spillage percentage.

Qualitative information by the video-recordings

The video-recordings provided a lot of useful information on the processes taking place in the cutter head. The video-recordings showed that in all the tests in under-cut situation the concentration of particles inside the cutter head was much larger on the right side of the cutter head, where the particles were cut, than on the left side. This is illustrated in Figure 6.8 where two stills of the video-recordings are plotted for the situation that n_c = 100 RPM and v_m = 5 m/s.

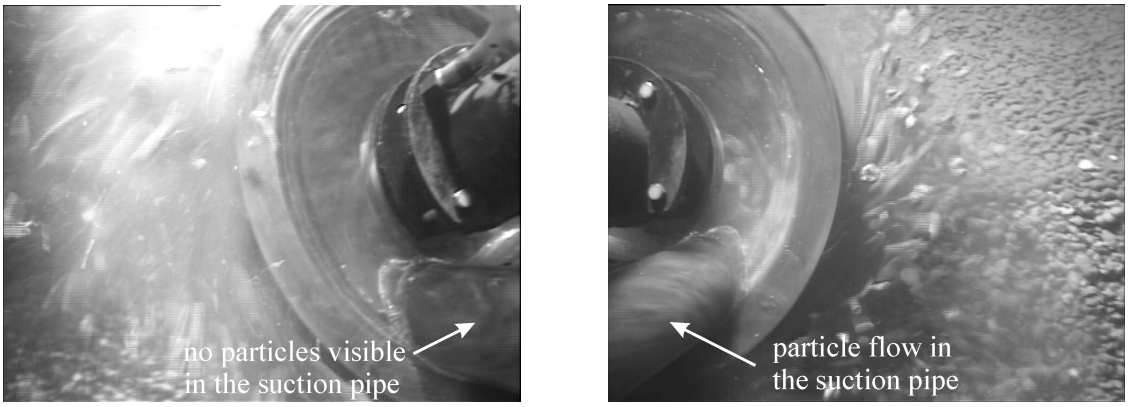

Figure 6.8: Video stills of the situation inside the cutter head for the under-cut situation

Moreover, on the left side of the suction mouth clearly fewer particles are sucked up than on the right side of the suction mouth. This was also noticed during the other tests in under-cut situation. The particle trajectories that generally could be observed, depending on the rotational velocity of the cutter head and the mixture velocity, are shown in Figure 6.9.

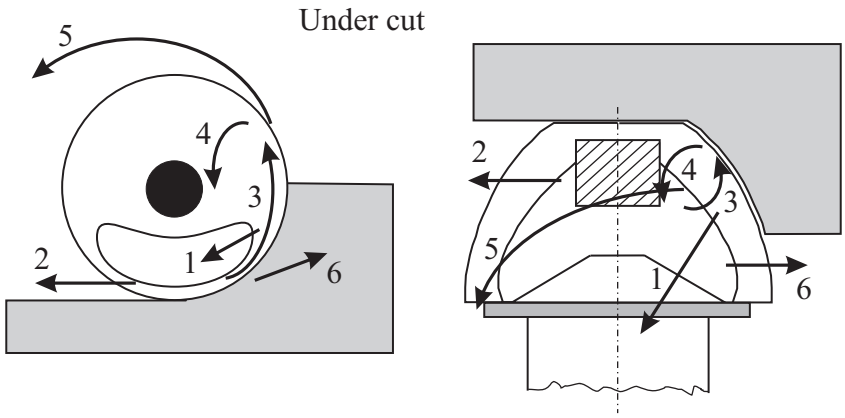

Figure 6.9: General trajectories of the gravel particles in under-cut situation

Basically three stages could be observed:

1. Relatively low rotational velocity
   The particles are hardly mixed and most particles gather at the lowest point in the cutter head. It seems that the particles that are sucked up immediately move towards the suction mouth (trajectory 1) and thus have a very short residence time. The particles that gather at the lowest point of the cutter head disappear through the openings between the cutter blades (trajectory 2). To some extent trajectory 3 can be observed. These particles are initially lifted by the blades but will fall off the blades again when they are no longer supported by the blades. Trajectory 5 mainly consists of particles that are thrown away due to the cutting process and never really entered the cutter head.

2. Optimum rotational velocity
   There is a distinct flow of particles towards the suction mouth. On the other hand, many particles also move upwards along the breach (trajectory 3) and either fall down again (trajectory 4) or they are thrown out of the cutter head because of the centrifugal forces acting on the particles (trajectory 5). Besides the particles that are thrown out of the cutter head, trajectory 5 also consists of particles that are thrown away due to the cutting process. Near the ring, at the right of the suction mouth, particles also leave the cutter head (trajectory 6). This flow of particles probably exists of particles that have made a full rotation in the cutter head and were thrown out. Possibly, trajectory 6 could also consist of particles that were deflected from trajectory 1.

3. High rotational velocity
   Segregation occurs because of the high centrifugal forces. Trajectory 4 is no longer observed and the magnitude of the particle flows 2, 3, 5 and 6 becomes bigger. Trajectory 1 is still observed but the magnitude of this particle flow becomes smaller.

Trajectory 5 had an axial component which became larger when the rotational velocity of the cutter head was increased. This was noticed visually during the tests and also by inspecting the spillage after the tests. With low rotational velocities the spillage mainly lay on the bank, while for the high rotational velocity a large amount ended up in front of the bank.

The video-recordings also showed that when the cutter head entered the bank, particles were not immediately sucked up. Apparently the cutter head needs to fill up with particles first before a distinct flow of particles towards the suction mouth is established. By means of the measured volumetric concentration (or density) it can be examined whether a stationary flow of particles towards the suction mouth is attained. In Figure 6.10 an example is shown of the measured volumetric concentration c_v and the measured torque T_c on the cutter head drive shaft for the situation that v_m = 3 m/s and n_c = 80 RPM. The measured torque is scaled in order to fit in the plot for the volumetric concentration and is only used to indicate when the cutter head enters and leaves the bank. Furthermore, the density meter was placed in the vertical section of the suction pipe 2 meters after the suction mouth (see Figure 6.1). The plot clearly shows that the volumetric concentration is shifted to the right with respect to the measured torque. When the cutter head enters the bank (sudden increase in torque) it takes about 7 seconds before a more or less stationary production flow is attained. Besides the fact that it takes time for the cutter head to fill up with particles this is also caused by the distance between the suction mouth and the density meter and the integration time of the density meter

(which was 1 s). When the cutter head leaves the bank there are still particles left in the cutter head and it takes some time before all particles are sucked up. This is also shown by the video-recordings.

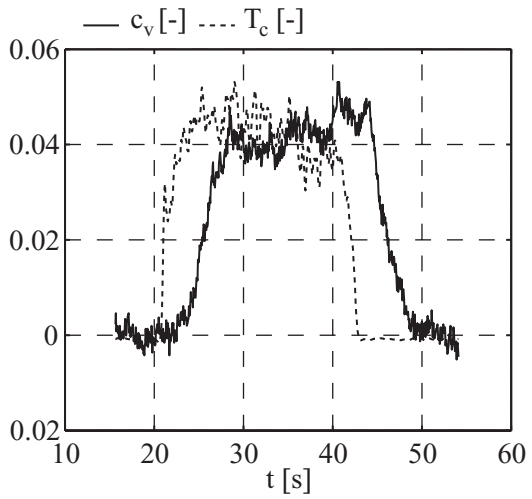

Figure 6.10: Measured volumetric concentration and scaled torque for v_m = 3 m/s and n_c = 80 RPM

The concentration shown in Figure 6.10 is a volumetric concentration which is the fraction of the mixture volume which is occupied by the gravel particles in the pipeline. Due to the relatively large slip velocity between the particles and water, the volumetric concentration can not directly be used to determine the production. Instead the delivered concentration or transport concentration should be used. In Appendix B the time averaged volumetric and transport concentrations are plotted for all the tests in under-cut situation.

Although it was not clearly visible in the video recordings, it looks as if the filling degree of the cutter head is fairly constant in the stationary domain. At least, obvious large fluctuations were not observed. This would imply that the spillage flow of particles is also fairly constant in the stationary domain. Furthermore, the filling degree of the cutter head was much less than the 85% that was derived from the tests with single particles as mentioned in paragraph 4.4. This means that there is a certain anomaly between the tests with single particles and the actual cutting tests. The difference most likely results from the fact that while cutting the cutter head is filled with particles near the hub. The curvature of the blades is largest near the hub and the gap between the blades is smallest, so escaping of particles is complicated in this region. As the spaces between the blades near the hub are blocked with particles, the internal volume of the cutter head is actually reduced and thus the relative influence of the suction flow in the ‘free’ volume increases. Particles in this volume then have a higher probability of being sucked up. This actually implies that the filling of the cutter head is a self-regulating

system. If the amount of particles inside the cutter head increases, the increasing influence of the suction flow will reduce the amount of particles in the cutter head again. The filling degree of the cutter head is then fluctuating around a constant value and the processes are almost stationary (assuming that the spillage flow is also constant in time). In terms of residence times a distinction should be made between the residence times of particles that are sucked up and particles that can be considered as spillage. The latter being much larger in general.

In the simulations with single particles described in the previous chapter, the decrease in internal volume is not accounted for. Consequently, the influence of the suction flow is underestimated in the simulations. Besides the alleged absence of the pump effect, this is another reason why the particles are hardly sucked up in the simulations. The large influence of the filling degree on the production is also noticed in the tests described in the next chapter.

The test results and particularly the video-recordings have shown that for modeling the mixture forming processes, particle-particle interaction should be taken into account. Furthermore, the presence of the particles has a significant influence on the flow inside the cutter head which should be considered. Tracking all individual particles in a simulation model may be limited by the availability of sufficient computational power. Anyway the simulation of the particle trajectories will be very time consuming. A possible alternative approach that needs to be considered for future research is the use of a continuum model instead of the Lagrangian model. In a continuum model the differential equations are averaged over certain control volumes. The advantage of a continuum model is the possibility of describing the main particle flows as shown in Figure 6.9 and thus determining production percentages without tracking all individual particles. For describing the main flows of particles along the blade a continuum model is also more suitable. However, a problem that may arise is the particle size and the necessary dimensions of a control volume. For accurate averaging, a sufficient number of particles within a control volume is needed. As the particles are relatively large, the control volume may become too large to take into account the details of the flow.

6.4.2 Test results for the over-cut situation

The test result in over-cut situation are shown in Figure 6.11. The production percentage in over-cut situation is a factor 2 to 4 lower than in the under-cut situation. This is in agreement with the experience from practice. Comparable with the situation in under-cut, the production percentage increases with increasing mixture velocity. Furthermore, it looks as if the rotational velocity does not have such a significant influence on the production percentage as in the under-cut situation. However, it should be noted that with each mixture velocity only two different rotational velocity were tested. It is therefore difficult to define a general trend with respect to the influence of the rotational velocity.

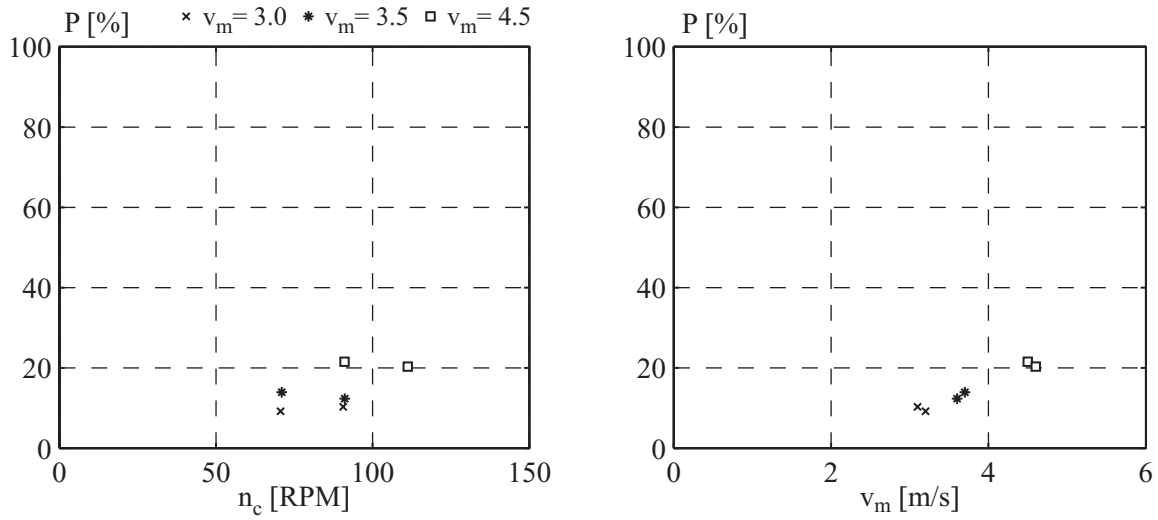

Figure 6.11: Production percentage vs. the rotational velocity and mixture velocity in the over-cut situation

The reason for the high spillage percentage in over-cut situation became clear after studying the video-recordings. They showed that in the over-cut situation most particles traveled along the breach and were then thrown out of the cutter head. The observed particle trajectories are shown in Figure 6.12. They agree well with the trajectories that were simulated in paragraph 5.4.

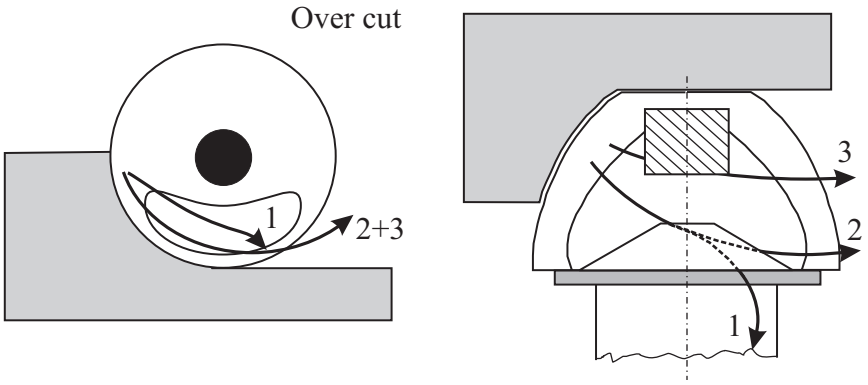

Figure 6.12: General trajectories of the gravel particles in over-cut situation

Trajectories 2 and 3 mainly consist of particles with a high rotational velocity due to the fact that the gravitational force and the fluid velocities are in the same direction for most part of the particle trajectory. Consequently, for most of these particles the suction force was not strong enough to bend their trajectories towards the suction mouth in such a short time span. Trajectory 1 consists of particles that were close enough to the suction mouth so that the

suction force was strong enough to suck in the particles. The video-recordings showed that the cutter blades often played an important role at the right side of the suction mouth. Particles that followed trajectory 2 often collided with the blades and their velocity was suddenly reduced. Because of this, the relative influence of the suction flow increased and particles were sucked up. Depending on the mixture velocity and rotational velocity particles sometimes accumulated near the ring on the right side of the suction mouth (between trajectories 1 and 2).

Inspecting the spillage after each test showed that almost all particles lay on the breach. The rotational velocity did not have a significant influence on the distribution of the spillage. This implies that the spillage flow is mostly generated by trajectory 3.

Comparable with the under-cut situation most particles were sucked up by the right side of the suction mouth. On the left side of the suction mouth hardly any particle was visible. This can be explained by the fact that the rotational velocity is relatively large and the suction force would have to be extremely high to immediately bend the particles towards the suction mouth. Moreover the movement of the cutter head is mainly in opposite direction of the movement of the particles (see also paragraph 5.4). An adaptation of the cutter head geometry that is sometimes applied in practice is the rotation of the suction mouth by a certain angle, in the direction of rotation of the cutter head (i.e. counterclockwise in the figures above). The suction mouth is then mainly working on the right side of the cutter head, which can be beneficial in both under-cut and over-cut situation according to the test results. Miltenburg (1983) has performed cutting tests in sand (d_{50} = 180 μm) where the suction mouth was rotated by an angle of 30º in the direction of rotation of the cutter head. In both under and over-cut situation this proved to be beneficial for the spillage percentage which could be reduced by maximally 7%. To what extent this is also valid for the larger gravel or rock particles needs to be investigated.

6.5 Tests with lower cutter axis inclination angle and larger particles

Additional tests have been performed to investigate the effect of decreasing the cutter axis inclination angle and the effect of increasing the average particle diameter. The cutter axis inclination angle was lowered from 45º to 25º degrees, which was the lowest possible angle. One bank was made of gravel with an average diameter of 15 mm, which made it possible to perform four tests with the coarser gravel. These cutting tests have only been performed in the under-cut situation.

6.5.1 Additional tests with lower cutter axis inclination angle

An overview of the tests performed with the cutter axis inclination angle of 25º is given in Appendix C. The average diameter of the gravel particles was 10 mm. In Figure 6.13 the

results of these tests are plotted. The figure also shows the results from the comparable test with the inclination angle of 45º.

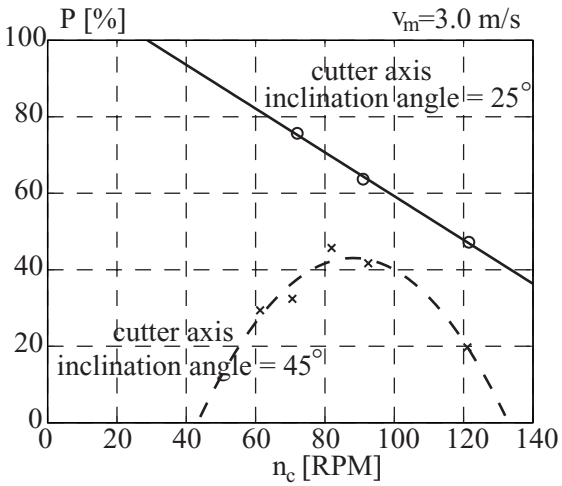

Figure 6.13: Influence of decreasing the cutter axis inclination angle from 45º to 25º on the production percentage (d_p = 10 mm)

Decreasing the cutter head inclination angle from 45º to 25º has a large positive effect on the production. A production percentage of 75% was reached at 70 RPM which is a factor 2.5 larger than the production percentage with the inclination angle of 45º. Furthermore, the trend of the production curve has changed. Due to the limited amount of tests it is not possible to define the trend over a wide range of rotational velocities, but it is clear that the position of the optimum rotational velocity has changed. Whether this optimum lies between 0 and 70 RPM or whether the production curve continuously increases for decreasing rotational velocities can not be deduced from the tests.

The higher production percentage for the lower cutter axis inclination angle is the result of a combination of factors:

- First of all the negative influence of the gravitational force on the particles is smaller. The vertical distance the particles have to travel to reach the suction mouth is shorter for the lower inclination angle (see Figure 6.14). Thus, in comparison, the influence of the suction flow will be larger. The gravitational force can even play a positive role for the particles on the blades near the hub. Due to the conical shape of the blades these particles can slide towards a position closer to the suction mouth (see right plot Figure 6.14). Because of the shorter distance to the suction mouth, these particles are sucked up easier.

- Due to the way the cutter head is positioned in the bank, the average distance between the bank and the suction mouth is smaller for the lower inclination angle. Therefore, the relative influence of the suction flow on the particles is larger.

- The change in positioning of the cutter head in the bank also caused for a more beneficial flow inside the cutter head. This is further explained in Figure 6.14.

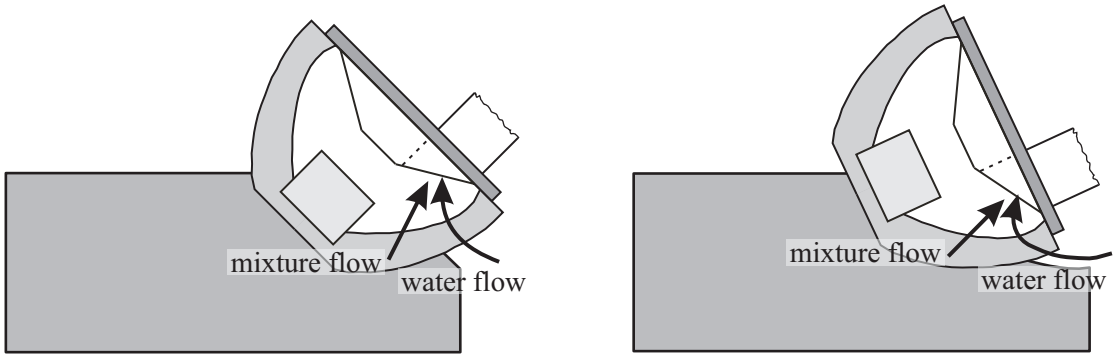

Figure 6.14: Positioning of the cutter head with 45º and 25º cutter axis inclination angle

The (vertical) gap between the suction mouth and the bank is smaller for the tests with 25º cutter head inclination angle, which means that less water will be sucked in from behind the cutter head (see arrows in Figure 6.14). This flow of water is undesirable, as it blocks the mixture flow towards the suction mouth which results in a lower production. In other words, the suction flow is used more efficiently when the cutter head inclination angle is 25º.

By studying the results in Figure 6.13 it can also be concluded that the flow inside the cutter head will change significantly when the ladder inclination angle is reduced. Looking at the results for a rotational velocity of 120 RPM it appears that the production increases from 20% to 48% when the cutter axis inclination angle decreases from 45º to 25º. In this region the hydraulic forces acting on the particle are much higher than the gravitational forces. The magnitude of the resultant force acting on the particle is therefore determined by the values of the operational parameters and will not depend on the inclination angle. However, the direction of this resultant force (and thus the direction of the flow) will depend on the inclination angle. For the lower inclination angle the flow is more directed towards the suction mouth as appears from the increase in production. Flow measurements inside the cutter head and the simulation model that is being set up should verify these assumptions (Dekker et al., 1999).

6.5.2 Additional tests with larger gravel grains

An overview of the tests performed with the gravel particles with an average diameter of 15 mm is given in Appendix C. The results of these tests are plotted in Figure 6.15. This figure also shows the results of the comparable tests with an average particle diameter of 10 mm. Both tests were performed with an cutter axis inclination angle of 45º. Again a second order polynomial was used in order to fit the data for representational purposes.

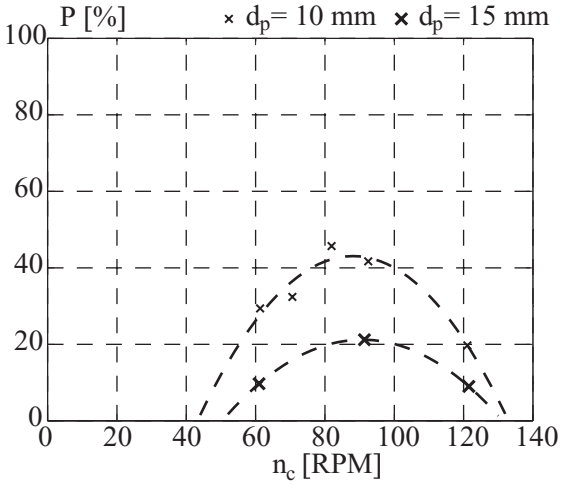

Figure 6.15: Influence of the gravel particle diameter on the production percentage

The production curve for the gravel particles with an average diameter of 15 mm shows the same trend as for the gravel particles with an average diameter of 10 mm. The influence on the production percentage however is enormous. The production percentage is reduced by a factor 2 to 3. The most likely explanations for this reduction are the influence of gravity and the increase in particle inertia. As the particle diameter is a factor 1.5 larger (on average) the gravitational force is a factor 1.5^3 (≈ 3.4) larger. Furthermore, due to the increase in particle inertia, particles are less likely to follow the fluid. Once it has obtained a significant rotational velocity, the suction flow will not be strong enough to deflect the particle trajectory. Moreover, it looks as if the increase in particle diameter has a larger influence on the production for the lower rotational velocities than for the higher rotational velocities. Although this can not be stated with certainty, considering the limited amount of tests that have been performed.

Apparently, the increase in particle diameter did not to have a significant influence on the optimum rotational velocity. This was still 90 RPM approximately. Again it should be noted that only a limited amount of tests have been performed and therefore it is difficult to make a clear statement regarding the optimum rotational velocity.

6.6 Influence of particle collisions and gravitational stresses

In Chapter 4 it was concluded that particle inertia plays a dominant role. This conclusion was based on the behavior of a single particle. For a concentration of particles the Bagnold number gives a good indication whether particle inertia or fluid viscosity dominates (Bagnold, 1954). The Bagnold number is defined as

$$N_{Bag} = \frac{\sqrt{\lambda_c}\rho_p d_p^2 \dot{\gamma}}{\mu_f} \tag{6.6}$$

in which λ_c is the linear concentration, ρ_p is the particle density, d_p is the particle diameter, $\dot{\gamma}$ is the shear rate and μ_f is the dynamic viscosity. The linear concentration, λ_c, represents the ratio of the particle diameter and the free distance between the particles.

According to Bagnold, particle inertia dominates if $N_{Bag} > 440$ and fluid viscosity dominates if $N_{Bag} < 40$. The region between Bagnold numbers of 40 and 440 is called the transition region.

The linear concentration can also be written as

$$\lambda_c = \left[\left(\frac{c_{v,max}}{c_v} \right)^{1/3} - 1 \right]^{-1} \tag{6.7}$$

in which c_v is the volumetric concentration and $c_{v,\,max}$ is the maximum possible volumetric concentration (which is 0.74 for spheres). The linear concentration and thus the Bagnold number will depend on the position inside the cutter head and the values for the operational parameters. As the aim is to verify that particle inertia generally dominates, the minimum (reasonable) value for the Bagnold number is determined. This implies a low rotational velocity of the cutter head (low shear rate) and low volumetric concentration. Considering the low production percentages the lowest volumetric concentration is found in the particle flow towards the suction mouth. Using the results from Figure D.1 in Appendix D a volumetric concentration of 0.02 is a reasonable assumption for a rotational velocity of 60 RPM. The linear concentration then becomes $\lambda_c = 0.43$. The shear rate is difficult to determine, but it is assumed that it at least has the same order of magnitude as the angular velocity of the cutter head. For a rotational velocity of 60 RPM this yields: $\dot{\gamma} = 6.3$ 1/s. The Bagnold number becomes

$$N_{Bag} = \frac{\sqrt{0.43} \cdot 2650 \cdot 0.01^2 \cdot 6.3}{1 \times 10^{-3}} = 1095 \tag{6.8}$$

This means that it is reasonable to assume that in the tests particle inertia generally dominates over the effects of fluid viscosity. As the Bagnold number can also be interpreted as a dimensionless number that estimates the ratio of grain-collision stresses to viscous shear stresses in a granular mixture it can be assumed that particles collisions play a significant role.

The Bagnold number does not take into account the gravitational stresses at grain contacts. Savage (1984) introduced a dimensionless number that takes account of gravity stresses, N_{Sav}. It estimates the ratio of grain-collision stresses to gravitational (or frictional) stresses. Taking into account the effects of buoyancy the Savage number is defined as:

$$N_{Sav} = \frac{\rho_p \dot{\gamma}^2 d_p^2}{(\rho_p - \rho_w) g h \tan \varphi_i} \tag{6.9}$$

in which h is the height of the particle flow and φ_i is the angle of internal friction ($\approx 42^o$ for gravel). Although the Savage number actually applies for steady gravity driven flows, it gives a fair indication of the importance of the respective stresses. From the video-recordings it is concluded that a layer with a height of 6 particles on the cutter blades is a reasonable assumption. For a rotational velocity of the cutter head of 60 RPM the Savage number will have a value of

$$N_{Sav} = \frac{2650 \cdot 6.3^2 \cdot 0.01^2}{1650 \cdot 9.81 \cdot 0.06} = 0.01$$

According to tests performed by Savage and Hutter (1989), grain-collision stresses become important when $N_{Sav} > 0.1$. Otherwise, gravity dominates stresses at grain contacts. Although not entirely comparable with the situation of Savage and Hutter, the low value for N_{Sav} indicates that gravity will probably dominate the stresses. However, the value for the Savage number was derived at a relatively low rotational velocity of the cutter head. As the rotational velocity can reach values of up to 120 RPM, the shear rate and thus the Savage number can increase significantly. It is very likely that for the higher rotational velocities the Savage number will approach or even exceed the experimentally determined value by Savage and Hutter of 0.1. Thus, for these higher rotational velocities the influence of the grain-collision stresses may become important and the grain-collision stresses at least have the same order of magnitude as the gravitational stresses. Still it is arguable what the nett effect of the grain-collisions will be. Especially near the hub, movement of the particles is restricted by the presence of the blades.

Summarizing it is concluded that inertia or grain-collision stresses and the gravitational stresses always dominate over the viscous stresses. For the lower rotational velocities of the cutter head gravitational stresses dominate over grain-collision stresses, while for the higher rotational velocities the grain-collision stresses at least have the same order of magnitude as the gravitational stresses. Whether grain-collision or gravitational stresses dominate will to a large extent depend on the position inside the cutter head.

6.7 Translating the tests results to the situation in practice

One of the important conclusions from the tests with a cutter head inclination angle of 45º and gravel particles with a diameter of 10 mm was the existence of an optimum rotational velocity. Below this optimum rotational velocity the production percentage increased with increasing rotational velocity while beyond the optimum rotational velocity the production percentage decreased with increasing rotational velocity. The results of these tests are valid for particles with an average diameter of 10 mm. Furthermore, the particle diameter was constant during the tests, which is not the case in practice when cutting rock. Then, the particle size differs due to the cutting process. Moreover, the haul velocity and the rotational velocity do have an influence on the size of the particles as shown by Equation (6.5). In practice, when cutting rock, increasing the rotational velocity of the cutter head will result in smaller particles when the haul velocity remains constant. Considering the relatively large influence of the particle diameter on the production percentage, as resulted from the additional tests, it is expected that in practice the production curves (for constant haul velocities) will differ from the test results.

Assuming that in practice, for a 3 m diameter cutter head, the maximum increase in rotational velocity is from 20 RPM to 40 RPM this yields that the particle size can be decreased by a factor 2 (for a constant haul velocity). As the relationship between the particles on prototype and model scale is linear, the same conclusions can be drawn for the particle size on a model scale. On a 1:8 model scale, the corresponding increase in rotational velocity is from 57 RPM to 113 RPM. Figure 6.15 showed the influence of an increase in particle diameter by a factor 1.5 on the production percentage. The results in this figure are used to study the following case.

Suppose that on a 1:8 model scale rock is cut. The mixture velocity is 3 m/s, the haul velocity is 0.1 m/s and the average particle diameter in the cutter head is 15 mm. Then Figure 6.15 shows that the production percentage is 10% at 60 RPM. Increasing the rotational velocity from 60 RPM to 90 RPM (a factor 1.5) results in a decrease in average particle diameter from 15 mm to 10 mm, as was shown by Equation (6.5). Figure 6.15 shows that for particles with an average diameter of 10 mm and a rotational velocity of 90 RPM, the production percentage is approximately 42%. If the particle diameter would not have decreased and remained 15 mm, the production percentage would have been 21%. Suppose that the rotational velocity of the cutter head is further increased to 120 RPM. The average particle diameter then becomes 7.5 mm. In analogy with the tests results of the 10 mm and 15 mm diameter particles, it is assumed that the production curve shows the same trend for the 7.5 mm diameter particle, while the production percentage is generally higher. If it is also assumed that the value for the optimum rotational velocity is approximately the same, the production curve is as shown in Figure 6.16. In addition, the figure shows the production percentages for the different particle

diameters when the rotational velocity is increased from 60 RPM to 120 RPM (indicated by '×'). Thus, the (gray dashed) curve fitted through the points indicated by '×' represents the production curve for the situation that the particle size depends on the rotational velocity of the cutter head and the haul velocity is constant.

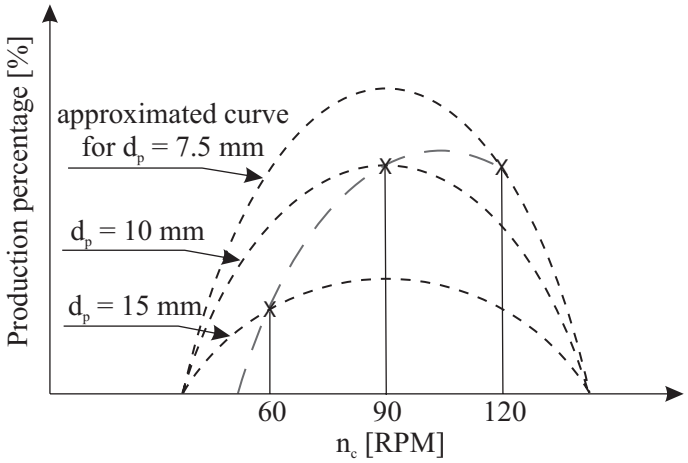

Figure 6.16: Change in production curve when the particle size is dependent on the rotational velocity of the cutter head and the haul velocity is constant

The figure shows that due the decrease in average particle diameter with increasing rotational velocity, the curve shifts to the right just like the optimum rotational velocity.

Although in practice reducing the rotational velocity with constant haul velocity is limited due to the consequent increase in cutting forces and the available torque on the cutter head drive shaft, the same conclusion can be drawn. For a constant haul velocity and increasing rotational velocity the average particle diameter decreases and the production curve may shift to the right resulting in a higher optimum rotational velocity. Varying the haul velocity with constant rotational velocity of the cutter head basically results in the same shift in the production curve, although reversely proportional.

It should be noted that the conclusion drawn above merely give the relative influence for the situation in practice. To what extent the production curve may shift to the right and the exact value for the optimum rotational velocity depends on the actual particle sizes. Furthermore, the conclusions apply for a 45º cutter axis inclination angle where the influence of particle diameter is relatively large as gravity is dominant. For the 25º cutter axis inclination angle more tests are needed to determine the influence of an increase in rotational velocity and the consequent decrease in particle size on the production percentage.

6.8 Conclusions

Tests in under-cut situation showed that increasing the mixture velocity always resulted in an increase in production. In addition, for every mixture velocity there is an optimum rotational

velocity of the cutter head. Initially the production increases with increasing rotational velocity just until an optimum has been reached. Beyond the optimum rotational velocity the production decreases with increasing rotational velocity. This is mainly caused by the difference in density between the gravel particles and water and the consequently large centrifugal forces acting on the particles.

The reason for the increase in production with increasing rotational velocity is not clear yet and will be further investigated in the next chapters. The most likely possibilities for the increase in production that will be examined are:

- better mixing of the particles due to collisions of particles with the blades
- positive change of flow inside the cutter head

In over-cut situation the production also increased with increasing mixture velocity. However, this increase was not as significant as in the under-cut situation. Due to the limited amount of tests no clear relationship between rotational velocity and production could be established. In general the production was 2 to 4 times lower than in the under-cut situation, which for the material tested is in good agreement with experience from practice.

By means of the video-recordings the particles trajectories were identified in both under-cut and over-cut situation. These trajectories gave good qualitative support of the tests results and clearly showed the difference between under-cut and over-cut.

Additional tests performed in under-cut situation where the particle diameter was 1.5 times larger showed a general decrease in production by a factor 2 to 3. This decreases can be imputed to the increase in gravitational force and the increase in particle inertia. The general trend of the production curve did not change and the optimum rotational velocity was the same as for the smaller particles.

Decreasing the cutter head inclination angle from 45º to 25º showed a significant increase in production. This was caused by a better inclusion of the cutter head in the bank, which had a positive effect on the flow inside the cutter head. Furthermore, as the particles had to be transported more horizontally than vertically, the relative influence of the gravitational force was less. Lowering the cutter head inclination angle also decreased the average distance between the particles and the suction mouth.

For a concentration of suspended particles the Bagnold number is large enough to assume that particle inertia and particle collisions dominate over the effects of fluid viscosity. In addition, the Savage number showed that for the lower rotational velocities (about 60 RPM) gravitational stresses dominate over grain-collision stresses. For high rotational velocities

(120 RPM) the grain-collision stresses at least have the same order of magnitude as the gravitational stresses.

Even though the centrifugal forces acting on the particles are the main cause for the decrease in production for rotational velocities beyond 90 RPM approximately, gravity can not entirely be neglected in this region. For rotational velocities between 90 RPM and 150 RPM, the ratio of the centrifugal acceleration and the acceleration of gravity varies between 2 and 5.

Chapter 7
Tests Focusing on the Increase in Production with Increasing Rotational Velocity

7.1 Introduction

An important result of the cutting tests described in the previous chapter is the initial increase in production with increasing rotational velocity in the under-cut situation. As described in paragraph 6.4.1 the most likely reasons for the increase in production percentage are:

- better mixing of the particles due to collisions of particles with the blades
- positive change of the flow inside the cutter head

As the rotational velocity of the cutter head increases, the intensity of the collisions between particles and the blades increases. Therefore it is plausible that more particles are brought into suspension and sucked up more easily.

Increasing the rotational velocity can also result in a more favorable flow pattern inside the cutter head. In particular the (axial) pump effect of the cutter head could, initially, have a positive effect as the axial velocities inside the cutter head are increased. The transport of particles in the direction of the suction pipe is increased and possibly the probability that a particle is sucked up.

In this chapter the several possibilities mentioned above are studied via a series of laboratory tests comparable with the previous cutting tests. In order to study the influence of the collisions between the gravel particles and the cutter blades, the tests have been carried out with a cylindrical cutter head with straight adjustable blades. All tests have been carried out in under-cut for comparison with the results of the cutting tests in under-cut situation.

As the angle of the cutter blades was adjustable, the blades could be put in any desired position varying from tangential to radial. By increasing the angle of the cutter blades, the

amount (or intensity) of collisions of particles with the blades could be increased and the influence on the production. The advantage of a cylindrical cutter head is the absence of an axial pump effect. This makes it easier to attribute changes in production to changes in fluid flow or to interaction of the particles with the blades. As it was not possible to perform cutting tests with the cylindrical cutter head due to its limited strength, an alternative method was used to bring the gravel particles into the cutter head. This is described in the next paragraph.

The tests have also been carried out with the crown cutter head that was used in the cutting tests described in Chapter 6. This way the influence of the blade geometry could be investigated by comparing the results of both cutter heads. In addition video-recordings were made to visualize the particle behavior inside the cutter heads and determine the difference. Another reason for using the crown cutter head is that in this way the influence of the alternative method of bringing in the gravel particles could be determined by comparing the results with the results of the cutting tests.

7.2 Test set up

Due to the limited strength of the cylindrical cutter head it was not possible to perform cutting tests. Instead, the gravel was injected into the cutter head through the back plate via a silo and a tube. The gravel that was used in these tests had an average diameter of 10 mm. The experimental set up is show in Figure 7.1. In all the tests described, the cutter head inclination angle was 45º.

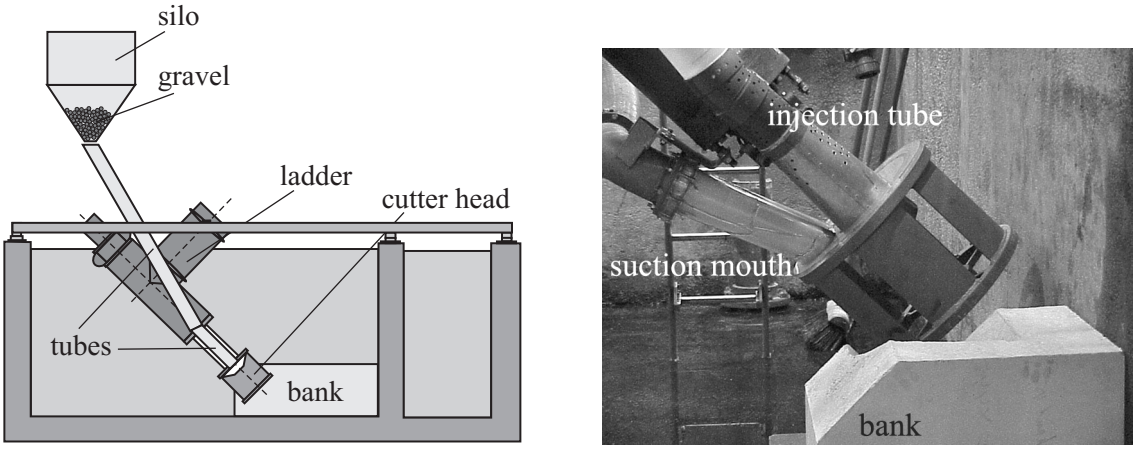

Figure 7.1: Schematic representation of the test set up and the cylindrical cutter head with the injection tube, suction mouth and bank

Underneath the silo that contained the gravel, a valve was placed that enabled adjustment of the flow of gravel particles. The mass flow of particles was identical to the mass flow during the previous cutting tests, which was 5.1 kg/s (see paragraph 6.3.2). The mass flow was determined by a dynamometer that measured the decrease in weight of the silo. Measurements

of the dynamometer showed that the average mass flow of the different tests was 5.1 kg/s ± 0.4 kg/s. The deviation was usually caused by the difference in opening of the valve.

The experimental set up consisted of two transparent tubes: a tube with a diameter of 160 mm placed under an angle of 30º with the vertical axis and a tube with a diameter of 100 mm placed under an angle of 45º with the vertical axis. The inclination of the tubes was necessary to reduce the speed with which the gravel particles entered the cutter head. As the tubes were transparent, the velocity of the gravel particles could be estimated by using colored gravel particles and filming the trajectories at the end of the smaller tube. Analyzing the video-recordings it appeared that the particles left the smaller tube with a velocity of approximately 0.7 m/s. With a mass flow of 5.1 kg/s this yields that the concentration of particles entering the cutter head was approximately 35%. In comparison with the actual cutting tests this is quite a difference. During the cutting tests the area over which the particles were brought in was 0.03 m^2. The velocity with which the particles entered the cutter head was 0.1 m/s and thus the concentration of particles was 65% (corresponding with a density of the bank of 1700 kg/m^3, see paragraph 6.3.2). In other words, in order to reach the required mass flow of 5.1 kg/s, the smaller inlet area and concentration of particles, resulting from the use of an inlet tube, is compensated by a larger inlet velocity of the particles.

To distribute the particle more evenly over the right side of the cutter head, a conical piece with a similar shape as the suction mouth was placed at the end of the tube (see left plot in Figure 7.2). The surface of the opening of this conical piece was 1.3 times larger than the area of the 100 mm tube.

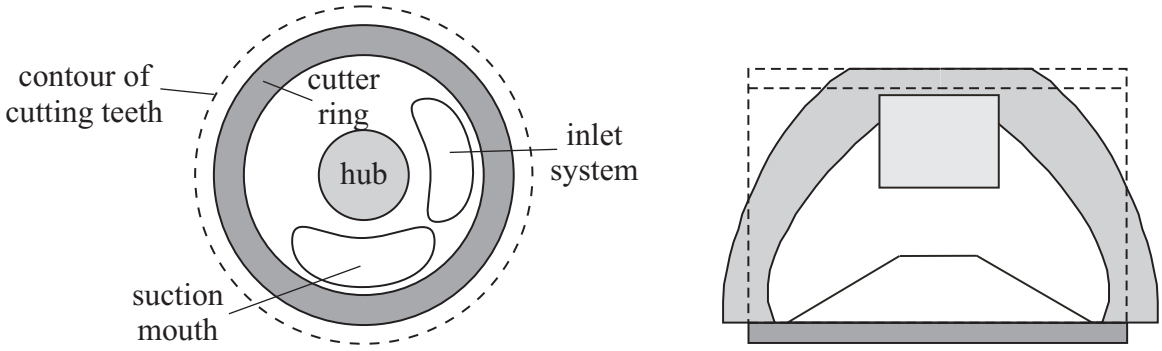

Figure 7.2: Position of the inlet system when looking from cutter ring to hub (left plot) and the dimensions of the cylindrical cutter head in comparison with the crown cutter head

The main dimensions of the cylindrical cutter head were identical to the dimensions of the crown cutter head; i.e. an outer ring diameter of 0.4 m and a total height of 0.29 m. Due to the conical shape of the crown cutter head and the curvature of the blades its internal volume was smaller than the internal volume of the cylindrical cutter head. The right plot in Figure 7.2

shows the cylindrical cutter head (dashed lines) plotted on top of the crown cutter head and. Due to the larger internal volume of the cylindrical cutter head it is expected that the production percentage will be lower in comparison with the tests with the crown cutter head. This is not of importance as the research focuses on the relative influence of the blades and not on the absolute production percentages.

The back plate that was used during the tests was identical to the back plate used in the cutting tests except for the opening (inlet system) through which the particles were brought in. The production and spillage percentages were again determined by weighing the production and spillage after each test and dividing each by the total weight of particles. The bank only enclosed the right side of the cutter head which made it possible for the spillage to fall on the bottom of the tank on the left side of the cutter head.

7.3 Results of the tests

7.3.1 Results of the tests with the cylindrical cutter head

Tests have been performed with the cylindrical cutter head with blade angles of 0° and 20° (see Figure 7.3 for the definition of the blade angle). The tests that have been performed are shown in Table 7.1. In this table v_m denotes the mixture velocity and n_c the rotational velocity of the cutter head. The gray background in a cell denotes that these tests could not be performed, usually due to blockage of the tubes.

Table 7.1: Test matrix for cylindrical cutter head

	v_m [m/s]	n_c [RPM]					
blade angle 0°	4	1	-	50	70	90	-
blade angle 20°	4	1	25	50	70	90	120

Preliminary tests indicated that when the cutter head was not rotating the production depended on the position of the cutter head. There was a significant difference in production if a blade was positioned right underneath the suction of mouth or if the opening between two blades was underneath the suction mouth. In the first situation the production was higher as the particles were blocked by the blades and particles gathered right in front of the suction mouth. In the second situation it was somewhat easier for the particles to slip between the blades and thus the production was lower. Therefore, in the tests, the lowest rotational velocity was 1 RPM.

The right plot in Figure 7.3 shows the results of the tests with both blade angles. The horizontal axis shows the rotational velocity of the cutter head and the vertical axis the production percentage.

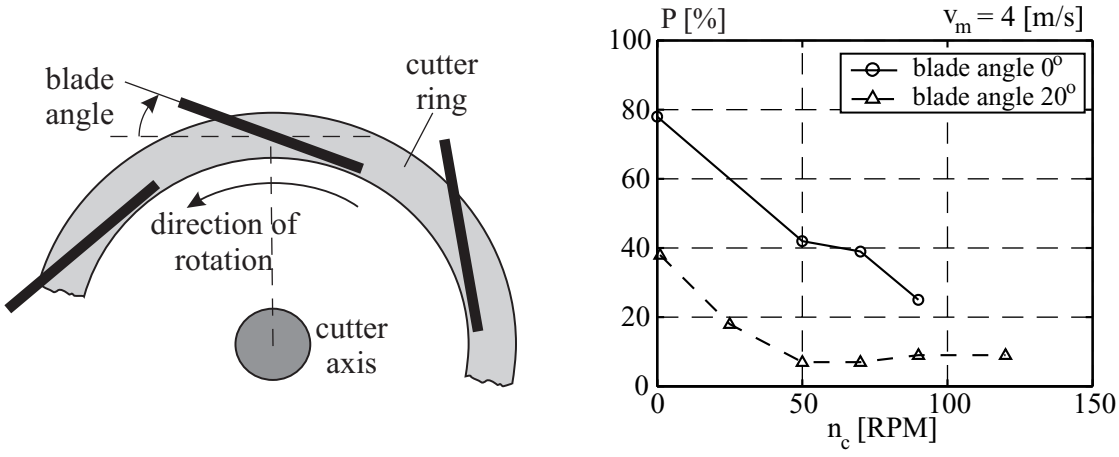

Figure 7.3: Definition of the blade angle and results of the tests with the cylindrical cutter head for both blade angles

The production curves show different trends in comparison with the cutting tests from Chapter 6. In both cases the production percentage decreases with increasing rotational velocity and the optimum lies at the lowest rotational velocity. The relatively high production percentage for the rotational velocity of 1 RPM can be explained by the fact that in this case the cutter head is rapidly filled with particles. As the cutter head hardly rotates it is more difficult for the particles to fall through the gaps between the blades (bridge forming of particles may occur). By rotating the cutter head the outflow of particles is facilitated. When the rotational velocity is further increases the centrifugal forces become dominant and most particles are thrown out of the cutter head. This explains the low production percentage for the higher rotational velocities. By increasing the blade angle to 20º, the gap between the blades is increased and the particles can fall out of the cutter head more easily. This explains the large difference in production percentage between the tests with both blade angles.

Aim of increasing the blade angle was to intensify the amount and impact of the collisions of gravel particles with the blades, which could be the reason for the increase in production with increasing rotational velocity. The tests results first of all did not show this increase in production. In addition the video-recordings showed no evidence that collisions were taking place. To what extent the experimental set up influences the test results in comparison with actual cutting tests becomes clear after repeating the tests with the crown cutter head.

7.3.2 Results of the tests with the crown cutter head

The test matrix for the crown cutter head is given in Table 7.2. A picture of the crown cutter head and the results of the tests are given in Figure 7.4. This time the test results do show an increase in production with increasing rotational velocity. Especially for the mixture velocity of 2.5 m/s, the increase in production is clearly noticeable. Moreover, for this mixture velocity

the optimum rotational velocity appears to be approximately 90 RPM, which is comparable with the optimum in the cutting tests (then it was approximately 80 RPM).

Table 7.2: Test matrix for the crown cutter head

v_m [m/s]	n_c [RPM]					
2.5	-	25	50	70	90	120
4	1	25	50	70	90	120

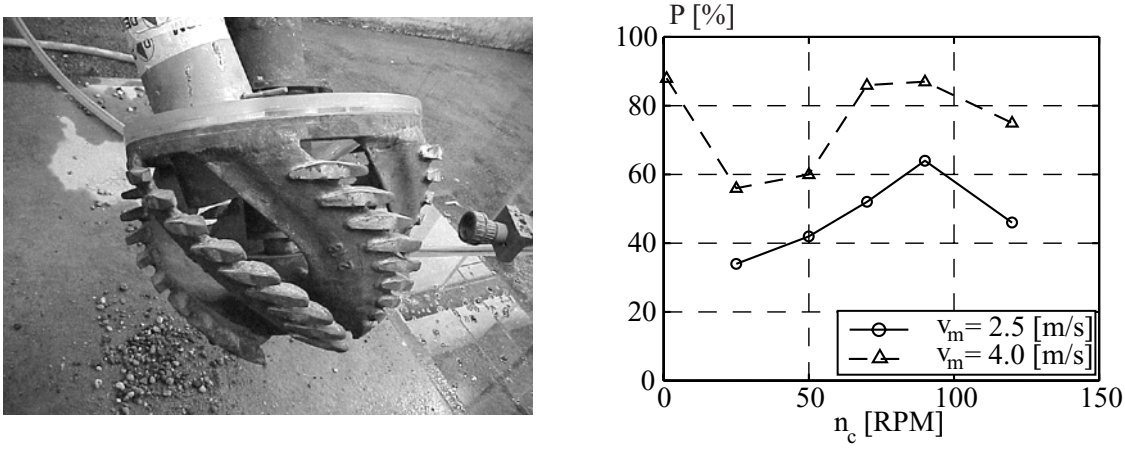

Figure 7.4: The crown cutter head and the results of the tests for mixture velocities of 2.5 m/s and 4.0 m/s

Beyond 90 RPM the production percentage decreases with increasing rotational velocity as particles are thrown out of the cutter head due to the large centrifugal forces. The fact that the optimum rotational velocity is approximately 90 RPM again indicates that this parameter is presumably related to cutter head design. Moreover, the way the particles enter the cutter head does apparently not have a significant influence on the value for the optimum rotational velocity. It does have an influence on the absolute value for the production and spillage percentages, which becomes clear by comparing the results from Figure 7.4 with the results from Figure 6.6.

For the mixture velocity of 4.0 m/s the production percentages are so large in general that near the optimum rotational velocity only small differences in production percentages are possible. Therefore the increase in production percentage is not as distinct as for the mixture velocity of 2.5 m/s. Similar as in the tests with the cylindrical cutter head the production percentage is large for a rotational velocity of 1 RPM. Again this is caused by the fact that the cutter head is rapidly filled up. Rotating the cutter head with 25 RPM is apparently enough to facilitate the outflow of particles (spillage flow) and the production percentage decreases from 90% to 58%. Beyond 90 RPM the production percentage decreases, which is again caused by the centrifugal forces acting on the particles.

Examining the video-recordings of all tests with the crown cutter head, collisions of particles with the blades could not be observed. The video-recordings did show a sort of sliding motion of the particles along the blades towards the cutter ring for rotational velocities beyond 50 RPM approximately. Furthermore, it seemed that for the larger rotational velocities the particles were in contact with the blades for a longer time, as they were more or less pushed against the cutter blade due to the centrifugal forces. As the increase in production is present in the tests with the crown cutter head, it is likely that this is caused by the cutter head geometry. The fact that in the tests with the crown cutter head the optimum rotational velocity hardly changes in comparison with the cutting tests strengthens this assumption. The mechanism behind the increase in production with increasing rotational velocity is clarified in Figure 7.5.

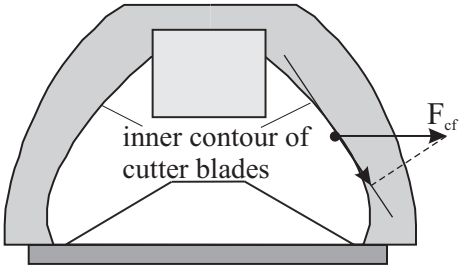

Figure 7.5: Component of the centrifugal force along the inner contour of the cutter blade

A centrifugal force, F_{cf}, is acting on a particle in contact with the cutter blade and rotating about the cutter axis. Due to the geometry of the blade the centrifugal force has a component along the blade's surface that is directed towards the cutter ring. If this component is large enough the particle may move towards the cutter ring and thus closer to the suction mouth. The probability that the particle is sucked up is increased. Clearly this effect depends, to a large extent, on the flow inside the cutter head. First of all the fluid rotation (rotational velocity of the cutter head) needs to be large enough to develop a centrifugal force that is significant enough to drive the particle towards the cutter ring. Furthermore, the difference between the rotational velocity of the fluid and the rotational velocity of the blade can not be too large, otherwise the particle will leave the blade at the leading or trailing edge after a short period of time. Then, the particle will not have the time to move in axial direction towards the cutter ring even if the centrifugal force is large enough.

Furthermore, the axial pump effect may support the axial motion of the particles. On the other hand, the pump effect of the cutter head may also cause for a outflow near the ring, dragging along particles. A model that determines the trajectory of a single particle along the inner surface of a cutter blade is set up in Chapter 8. Aim is to validate that the combination of the centrifugal force acting on a particle and the blade's geometry is (partly) responsible for the axial motion of particles towards the cutter ring.

7.4 Qualitative information by the video-recordings

For both the cylindrical and the crown cutter head there was no evidence that collisions of particles with the blades were taking place. However, the video-recordings did provide other valuable information. Tests have been performed where the cutter head was not placed in the bank, but was rotating freely. A camera was placed on the right-hand side of the cutter head to film through the gaps between the blades. Figure 7.6 shows the filling of the crown cutter head and the cylindrical cutter head (blade angle 20º) for a rotational velocity of 1 RPM and a mixture velocity of 2.5 m/s.

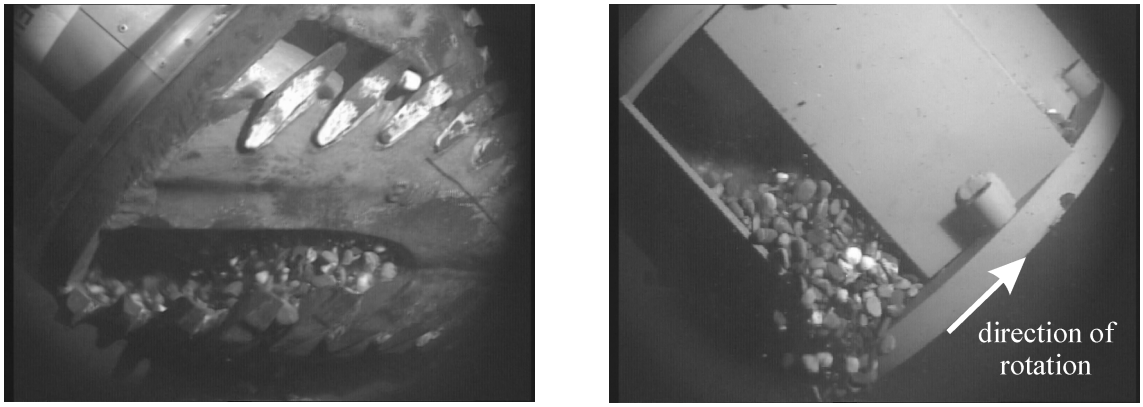

Figure 7.6: Filling of the crown and cylindrical cutter heads for a rotational velocity of 1 RPM and a mixture velocity of 2.5 m/s

For both cases it is clear that the inner volume of the cutter head is effectively decreased as particles block a large part of the openings between the blades. Furthermore, due to conical shape of the crown cutter head, its inner volume is smaller than the inner volume of the cylindrical cutter head. Particles are generally closer to the suction mouth, which explains the higher production percentage for the crown cutter head in comparison with the cylindrical cutter head. Due to the geometry of the crown cutter blade, the inner surface almost lies vertical when the blade is positioned right underneath the suction mouth. In the case of the cylindrical cutter head the particle will slight away from the suction mouth due to gravity.

Increasing the rotational velocity to 90 RPM showed the influence of the cutter blade geometry. In the case of the cylindrical cutter head the particles were thrown out over the entire length of the cutter head but mainly near the hub. In the case of the crown cutter head most particles were thrown out of the cutter head near the ring and hardly any particle was thrown out of near the hub. Moreover, with the crown cutter head there was a significant axial motion of the particles noticeable that was directed towards the cutter ring. This is clearly shown in Figure 7.7.

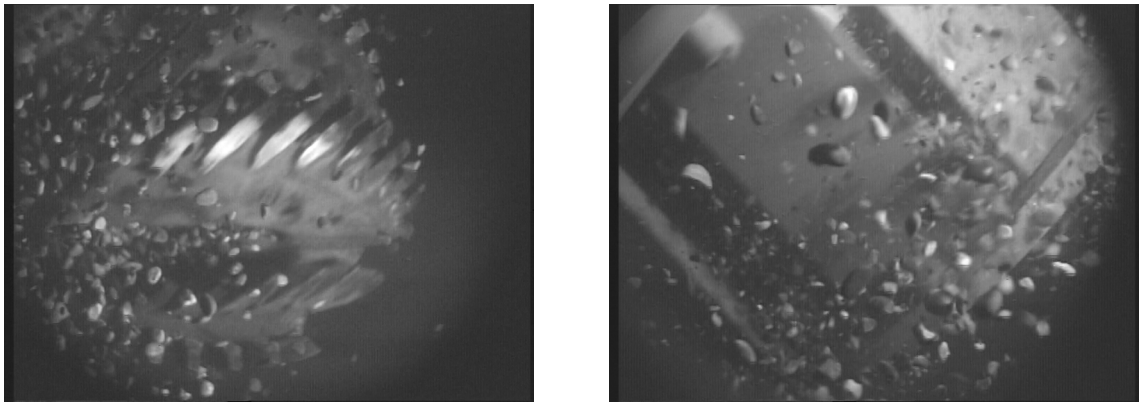

Figure 7.7: Particles thrown out of the cutter head for a rotational velocity of 90 RPM and a mixture velocity of 2.5 m/s

The motion of the particles that are thrown out of the cutter head confirms the assumption that for the crown cutter head the particles are moving axially towards the cutter ring when the rotational velocity is large enough. To what extent this is caused by the component of the centrifugal force along the blade's inner surface or the axial pump effect is not clear yet. In Chapter 8 this will be further examined.

Additional tests were performed with particles with an average diameter of 3 mm. With these smaller particles the axial pump effect of the cutter head became especially clear as shown in Figure 7.8.

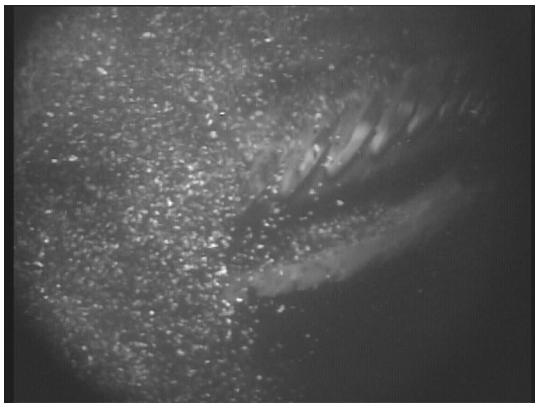

Figure 7.8: Particles with a diameter of 3 mm thrown out of the cutter head for a rotational velocity of 90 RPM and a mixture velocity of 2.5 m/s

7.5 Comparing the results of the cutting tests with the silo tests

As described in paragraph 1.3 the total spillage percentage consists of:

- spillage resulting from the cutting process

- spillage resulting from the mixture forming process

The first topic mentioned consists of particles that are thrown away immediately and never entered the cutter head. The second topic consists of particles that have entered the cutter head but were, for some reason, not sucked up. As the cutting process is absent in the tests described in this chapter, there is no spillage resulting from the cutting process. By comparing the results of Figure 7.4 with the results of the cutting tests shown in the previous chapter (Figure 6.6), an estimate is possible of the respective spillage components mentioned above.

From the right plot in Figure 6.6 it can be seen that the maximum possible production starts to deviate from the straight line for higher mixture velocities. The maximum production will asymptotically reach 100% for higher mixture velocities. Considering the results of the cutting tests, it is reasonable to assume that the spillage resulting from the cutting process varies between 0% and 30%, for rotational velocities of the cutter head up to 120 RPM. This assumption is additionally based on the knowledge that an inward flow along the entire cutter contour is achieved when the flow number, $Q_s/\omega_c R_c^3$, is larger than 0.47 as followed from the tests performed at WL|Delft Hydraulics (see Chapter 2). For the maximum rotational velocity of 120 RPM this implies that the mixture velocity has to be larger than 6 m/s. A zero percentage of spillage as a result of the mixing forming processes requires at least a canceling of the outflow and thus a mixture velocity of at least 6 m/s. Taking into account the results in Figure 6.6, it is reasonable to assume that for this mixture velocity the total spillage percentage is about 30%. Since the spillage resulting from the cutting process increases with increasing rotational velocity, the maximum spillage resulting from the cutting process will be lower than 30% for rotational velocities lower than 120 RPM.

It is interesting to see what percentage of the gravel that enters the cutter head is actually sucked up and what percentage is spillage (resulting from the mixture forming process). For both the cutting tests and the tests with the silo, these percentages are compared when using the crown cutter head. The total spillage S_{tot} is defined as

$$S_{mixture} + S_{cut} = S_{tot} \tag{7.1}$$

in which $S_{mixture}$ is the spillage resulting from the mixture forming process and S_{cut} is the spillage resulting from the cutting process. The production P is a certain percentage (c_{prod}) of the total amount of gravel entering the cutter head. In fractions the total amount of gravel in the cutter head is 1-S_{cut}. Thus

$$c_{prod}\left(1-S_{cut}\right) = P \tag{7.2}$$

For the tests with the silo c_{prod} equals P, since there is no spillage as a result of the cutting process. The table below gives the determined values for c_{prod} for the tests with a mixture velocity of 2.5 m/s.

Table 7.3: Percentage of material inside the cutter head that is sucked up

	c_{prod} [%]	
n_c [RPM]	Cutting test	Silo test
50	21	41
70	32	52
90	29	62

It is here assumed that the spillage as a result of the cutting process S_{cut} was 20% in all the cutting tests, independent of the rotational velocity. The table shows the large difference in percentages. Not only is the amount of particles entering the cutter head larger in the tests with the silo, the percentage of this amount that is actually sucked up is also significantly larger. This results from the fact that in the case of the silo tests the particles are entering the cutter head much closer to the suction mouth (see Figure 7.2) and the filling degree of the cutter head was much larger. The test results emphasize the importance of reducing the distance between the particles and the suction mouth. Increasing the filling degree can contribute to this.

7.6 Conclusions

The tests with the cylindrical cutter head did not show an increase in production with increasing rotational velocity. Increasing the blade angle in order to increase the amount of collisions of particles with the blades only had a negative effect on the production percentage. Moreover, video-recordings did not show evidence of particle collisions with the blades.

Tests with the crown cutter head did show the increase in production with increasing rotational velocity. Moreover, the optimum rotational velocity was comparable with the optimum in the cutting tests. Beyond the optimum rotational velocity the production percentage decreased with increasing rotational velocity. Again video-recordings did not show evidence of particle collisions with the blades. The recordings did show that for increasing rotational velocities the particles were increasingly thrown out of the cutter head near the ring with a significant axial velocity. This was caused by the component of the centrifugal force acting along the blade's inner surface or the pump effect of the cutter head or most likely a combination of both. Due to the shape of the cutter blade's the centrifugal force acting on particles in contact with the blade has a component directed towards the cutter ring. If this component is large enough the particles can be forced towards the cutter ring and will thus have an axial velocity component. The axial pump effect of the cutter head can increase this axial velocity of the particles. It is assumed that the axial transportation of particles is the cause for the increase in production with increasing rotational velocity. As the particles are transported axially towards the cutter ring, they get closer to the suction mouth and thus the probability that they are sucked up increases. Video-recordings showed that a significant

number of particles was in contact with the blades and ‘sliding’ of particles along the cutter blade was noticeable.

A model will be set up that describes the trajectory of a particle along the inner surface of a cutter blade. Aim is to validate that the combination of the centrifugal force acting on a particle and the blade’s geometry is (partly) responsible for the axial motion of particles towards the cutter ring.

Chapter 8
Model for Particle Trajectories along a Cutter Blade

A dynamic model is set up that describes the trajectory of a particle along the inner surface of a cutter blade for a cutter head rotating in a fluid. The main purpose of the model is to verify that the component of the centrifugal force acting along the surface of a cutter blade can be responsible for the motion of particles towards the cutter ring. The model is set up in such a way that it is not restricted to a single geometry of a blade, but can be used for any reasonable blade geometry. An Eulerian-Lagrangian approach is chosen for the dynamic model. The Eulerian framework to describe the flow field inside the cutter head and the Lagrangian framework for the rigid particles. The particle is represented by a point mass with finite size. The forces acting on a particle that are of concern are described in the following paragraph. From these forces the equation of motion for the particle is derived.

The model is set up for single particles that slide (not roll) along the blade's surface. Considering the elliptical shape of the gravel particles it is fair to assume that the particles do not roll over the blades. The absence of multiple particles in the model can be justified by the fact that attention is focused on the influence of the centrifugal force acting on a particle in combination with the blade's geometry on the axial motion of a particle towards the cutter ring. For both single and multiple particles this effect should be present, although to different extents.

The simulations in this chapter are performed on a 1:8 model scale, which enables a direct comparison with the tests performed in the previous chapters.

8.1 Forces acting on the particle

In the dynamic model three coordinate systems are used: a global coordinate system, a cutter coordinate system and a blade coordinate system. Figure 8.1 gives a schematic representation

of the cutter head, showing the inner and outer contour of the cutter blades, the cutter ring, back plate and hub. In this figure the global coordinate system and the cutter coordinate system are drawn.

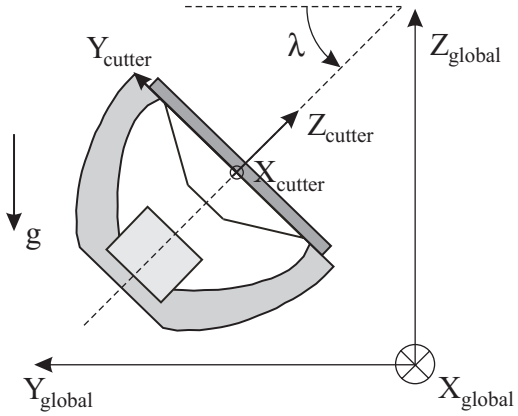

Figure 8.1: Definition of global and cutter coordinate system

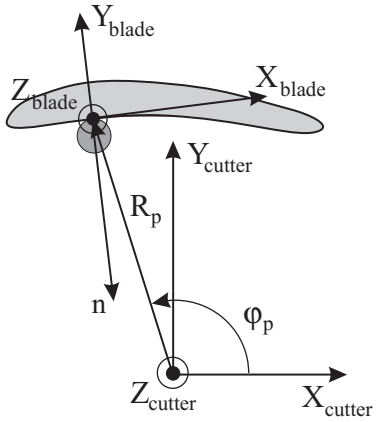

Figure 8.2: Definition of blade coordinate system

In addition the motion of the particle is described in a rotating reference frame in cylindrical coordinates ($R_{p,cutter}$; $\varphi_{p,cutter}$; $Z_{p,cutter}$). Figure 8.2 shows the cross-section of a particle in contact with a blade. The cutter coordinate system, the blade coordinate system and the rotating particle coordinate system are drawn (note that the subscript 'cutter' is omitted in the figure). In the blade coordinate system the direction Y_{blade} is defined as parallel to the normal vector n (normal to the blade's surface in the specific point) and directed outwards.

The forces acting on the particle are the same as mentioned in Chapter 5. In addition, the normal force and friction force resulting from the contact between particle and cutter blade are taken into account. Thus the considered forces acting on the particle are:

Gravitational force

For a cutter head with a cutter axis inclination angle λ, the gravitational force F_g acting on the particle, written in vector notation, is:

$$\overline{F}_g = m_p \overline{g} = -m_p g \left(\cos\lambda \overline{e}_{Ycutter} + \sin\lambda \overline{e}_{Zcutter} \right) \tag{8.1}$$

in which m_p is the mass of the particle and g is the acceleration of gravity.

Normal force

The normal force acting on the particle is defined as

$$\overline{F}_n = -F_n \overline{e}_{Yblade} \tag{8.2}$$

Thus positive when directed inwards. The normal force is a reaction force that results from the contact between particle and blade. The magnitude of F_n is not known beforehand, but will be derived by solving the equation of motion as shown in Equation (8.13).

Friction force

The friction force F_f is also a reaction force that results from the friction between particle and blade. This force is directed along the blade's surface and it is opposite to the relative velocity of the particle (i.e. relative to the velocity of the blade). The relative velocity of the particle in the blade coordinate system is:

$$\bar{v}_{p,blade,rel} = v_{p,Xblade,rel}\bar{e}_{Xblade} + v_{p,Zblade,rel}\bar{e}_{Zblade} \tag{8.3}$$

in which the subscript 'p' denotes particle. The friction force thus becomes

$$\bar{F}_f = -\mu F_n \frac{v_{p,Xblade,rel}\bar{e}_{Xblade} + v_{p,Zblade,rel}\bar{e}_{Zblade}}{\left|\bar{v}_{p,blade,rel}\right|} \tag{8.4}$$

in which μ is the mechanical friction coefficient between the particle and the blade. Actually the thin water film between the particle and the blade will reduce the coefficient of friction, but this will not be taken into account.

Forces due to fluid flow

The forces on the particle caused by the fluid flow can be subdivided into: drag forces and forces due to pressure gradients in the fluid.

The drag force F_D on a particle is:

$$\bar{F}_D = \frac{\pi}{8}\rho_f d_p^2 C_d \left(\bar{v}_f - \bar{v}_p\right)\left|\bar{v}_f - \bar{v}_p\right| \tag{8.5}$$

in which ρ_f is the density of the fluid (water), d_p is the particle diameter, C_d is the drag coefficient. It is assumed that this expression for the drag force is also valid for a particle moving along a wall (in this case the blade). The wall effect is taken into account in the drag coefficient (see paragraph 8.4.2).

The force on a particle due to the pressure gradient is:

$$\bar{F}_{PG} = \rho_f V_p \left(\frac{D\bar{v}_f}{Dt} - \bar{g}\right) \tag{8.6}$$

in which V_p is the volume of the particle and

$$\frac{D}{Dt} = \frac{\partial}{\partial t} + \overline{v}_f \cdot \nabla$$

Note that the buoyancy effect (Archimedes) is taken into account in this force. The force on the particle due to the pressure gradient given here is strongly simplified, as the influence of the particles on the flow round the particles is not taken into account.

Added mass force

The added mass force is defined as:

$$\overline{F}_{AM} = \rho_f V_p C_{AM} \left(\frac{D\overline{v}_f}{Dt} - \frac{d\overline{v}_p}{dt} \right) \tag{8.7}$$

in which C_{AM} is the added mass coefficient and

$$\frac{d}{dt} = \frac{\partial}{\partial t} + \overline{v}_p \cdot \nabla$$

The influence of the Basset History force is neglected as its value is expected to be much lower than that of the remaining forces. The lift force acting on the particle is also neglected based on its estimated order of magnitude as shown in Appendix A. For any known flow field inside the cutter head, the equation of motion for the particle can now be derived.

8.2 Equation of motion for a particle moving along a blade

For convenience sake, the position for the particle along the blade is written in cylindrical coordinates ($R_{p,cutter}$; $\varphi_{p,cutter}$; $Z_{p,cutter}$) in a rotating reference frame where (see Figure 8.2)

$$\begin{aligned} X_{p,cutter} &= R_{p,cutter} \cos\varphi_{p,cutter} \\ Y_{p,cutter} &= R_{p,cutter} \sin\varphi_{p,cutter} \end{aligned} \tag{8.8}$$

The accelerations terms for the particle at the position defined by $R_{p,cutter}$, $\varphi_{p,cutter}$ and $Z_{p,cutter}$ in the directions of X_{blade}, Y_{blade} and Z_{blade} are:

$$\begin{aligned} a_{p,Xblade} &= A_{11}\left(a_{Rp}\cos\varphi_p - a_{\varphi p}\sin\varphi_p\right) + A_{21}\left(a_{Rp}\sin\varphi_p + a_{\varphi p}\cos\varphi_p\right) + A_{31}\ddot{Z}_p \\ a_{p,Yblade} &= A_{12}\left(a_{Rp}\cos\varphi_p - a_{\varphi p}\sin\varphi_p\right) + A_{22}\left(a_{Rp}\sin\varphi_p + a_{\varphi p}\cos\varphi_p\right) + A_{32}\ddot{Z}_p \\ a_{p,Zblade} &= A_{13}\left(a_{Rp}\cos\varphi_p - a_{\varphi p}\sin\varphi_p\right) + A_{23}\left(a_{Rp}\sin\varphi_p + a_{\varphi p}\cos\varphi_p\right) + A_{33}\ddot{Z}_p \end{aligned} \tag{8.9}$$

in which A_{11} to A_{33} represent certain constants depending on the geometry of the blade at the position of the particle (see Appendix E). For readability the subscript ‘p,cutter’ is replaced by just ‘p’. Furthermore,

$$\begin{aligned} a_{Rp} &= \ddot{R}_p - R_p\dot{\varphi}_p^2 \\ a_{\varphi p} &= R_p\ddot{\varphi}_p + 2\dot{R}_p\dot{\varphi}_p \end{aligned} \tag{8.10}$$

The mass of the particle multiplied by the above mentioned acceleration terms has to equal the sum of all external forces. Furthermore, the component of the relative particle acceleration perpendicular to the blade's surface has to be zero. Or

$$\left(\ddot{R}_p\,\bar{e}_{Rp} + R_p\ddot{\varphi}_p\,\bar{e}_{\varphi p} + \ddot{Z}_p\,\bar{e}_{Zp}\right)\cdot\bar{e}_{Yblade} = 0 \tag{8.11}$$

Rewriting the condition above yields that

$$\left(A_{12}\cos\varphi_p + A_{22}\sin\varphi_p\right)\ddot{R}_p + \left(A_{22}\cos\varphi_p - A_{12}\sin\varphi_p\right)R_p\ddot{\varphi}_p + A_{32}\ddot{Z}_p = 0 \tag{8.12}$$

Written in the blade coordinate system and adding the above mentioned condition, the dimensionless equation of motion becomes (see Appendix E for a more elaborate derivation of this equation):

$$\left(1+\frac{C_{AM}}{S_s}\right)\frac{\boldsymbol{M}}{g}\begin{bmatrix}\ddot{R}_p\\ R_p\ddot{\varphi}_p\\ \ddot{Z}_p\\ \dfrac{F_n}{m_p}\end{bmatrix} = \left(1+\frac{C_{AM}}{S_s}\right)\boldsymbol{N} + \begin{bmatrix}Const_7\\ Const_8\\ Const_9\\ 0\end{bmatrix} +$$

$$+Const_{10}\begin{bmatrix}\left(v_w - v_p\right)_{Xblade,abs}\left|\bar{v}_w - \bar{v}_p\right|\\ 0\\ \left(v_w - v_p\right)_{Zblade,abs}\left|\bar{v}_w - \bar{v}_p\right|\\ 0\end{bmatrix} + \frac{\left(1+C_{AM}\right)}{gS_s}\begin{bmatrix}\dfrac{Dv_{w,Xblade}}{Dt}\\ \dfrac{Dv_{w,Yblade}}{Dt}\\ \dfrac{Dv_{w,Zblade}}{Dt}\\ 0\end{bmatrix} \tag{8.13}$$

with

$$\boldsymbol{M} = \begin{bmatrix} Const_1 & Const_2 & A_{31} & \mu\dfrac{v_{p,Xblade,rel}}{\left|\bar{v}_{p,rel}\right|}\dfrac{S_s}{\left(S_s+C_{AM}\right)}\\ Const_3 & Const_4 & A_{32} & \dfrac{S_s}{\left(S_s+C_{AM}\right)}\\ Const_5 & Const_6 & A_{33} & \mu\dfrac{v_{p,Zblade,rel}}{\left|\bar{v}_{p,rel}\right|}\dfrac{S_s}{\left(S_s+C_{AM}\right)}\\ gConst_3 & gConst_4 & gA_{32} & 0\end{bmatrix} \tag{8.14}$$

and

$$\boldsymbol{N} = \begin{bmatrix} \left(\frac{R_p \dot{\varphi}_p^2}{g} \mathrm{Const}_1 - \frac{2\dot{R}_p \dot{\varphi}_p}{g} \mathrm{Const}_2 \right) \\ \left(\frac{R_p \dot{\varphi}_p^2}{g} \mathrm{Const}_3 - \frac{2\dot{R}_p \dot{\varphi}_p}{g} \mathrm{Const}_4 \right) \\ \left(\frac{R_p \dot{\varphi}_p^2}{g} \mathrm{Const}_5 - \frac{2\dot{R}_p \dot{\varphi}_p}{g} \mathrm{Const}_6 \right) \\ 0 \end{bmatrix} \tag{8.15}$$

The constants in the matrices ***M*** and ***N*** are:

$$\mathrm{Const}_1 = \left(A_{11} \cos\varphi_p + A_{21} \sin\varphi_p \right) \qquad \mathrm{Const}_2 = \left(A_{21} \cos\varphi_p - A_{11} \sin\varphi_p \right)$$

$$\mathrm{Const}_3 = \left(A_{12} \cos\varphi_p + A_{22} \sin\varphi_p \right) \qquad \mathrm{Const}_4 = \left(A_{22} \cos\varphi_p - A_{12} \sin\varphi_p \right)$$

$$\mathrm{Const}_5 = \left(A_{13} \cos\varphi_p + A_{23} \sin\varphi_p \right) \qquad \mathrm{Const}_6 = \left(A_{23} \cos\varphi_p - A_{13} \sin\varphi_p \right)$$

$$\mathrm{Const}_7 = \left(A_{21} \cos\lambda + A_{31} \sin\lambda \right) \left(\frac{1 - S_s}{S_s} \right) \qquad \mathrm{Const}_8 = \left(A_{22} \cos\lambda + A_{32} \sin\lambda \right) \left(\frac{1 - S_s}{S_s} \right)$$

$$\mathrm{Const}_9 = \left(A_{23} \cos\lambda + A_{33} \sin\lambda \right) \left(\frac{1 - S_s}{S_s} \right) \qquad \mathrm{Const}_{10} = \frac{3}{4} \frac{C_d}{g d_p S_s}$$

Here S_s is the specific density: ρ_p/ρ_w.

The matrix ***M*** mainly contains constants determining the direction of the acceleration along the blade's surface and the matrix ***N*** contains the centrifugal and Coriolis accelerations. The second term on the right hand side of the equal sign denotes the gravity force compensated for buoyancy. The third term represents the drag forces and the last term on the right hand side represents the pressure gradient and the added mass forces. The equation of motion is written in a dimensionless form by dividing it by the mass of the particle and the acceleration of gravity.

If the initial position and the initial velocity of the particle are known and the flow field inside the cutter head is known, this equation can be solved numerically.

Special attention should be paid to the situation where the relative velocity of the particle is zero, i.e. the situation where the particle is fixed to the blade. The particle will only start to move if the driving force exceeds the friction force. If not, the particle will stay fixed to the blade. The driving forces acting on the particle along the cutter blade surface are:

$$F_{df,Xblade} = m_p\left(1+\frac{C_{AM}}{S_s}\right)\left(Const_1 R_p\dot{\varphi}_p^2 - Const_2\, 2\dot{R}_p\dot{\varphi}_p\right) - m_p g Const_7 + \\ + \frac{\pi}{8}\rho_w d_p^2 C_d\left(v_{w,Xblade} - v_{p,Xblade}\right)\left|\bar{v}_w - \bar{v}_p\right| + \rho_w V_p(1+C_{AM})\frac{Dv_{w,Xblade}}{Dt} \tag{8.16}$$

$$F_{df,Zblade} = m_p\left(1+\frac{C_{AM}}{S_s}\right)\left(Const_5 R_p\dot{\varphi}_p^2 - Const_6\, 2\dot{R}_p\dot{\varphi}_p\right) - m_p g Const_9 + \\ + \frac{\pi}{8}\rho_w d_p^2 C_d\left(v_{w,Zblade} - v_{p,Zblade}\right)\left|\bar{v}_w - \bar{v}_p\right| + \rho_w V_p(1+C_{AM})\frac{Dv_{w,Zblade}}{Dt} \tag{8.17}$$

When the relative velocity of the particle is zero, the friction force is defined as opposite to the driving force. Thus,

$$\bar{F}_f = -\mu F_n \frac{F_{df,Xblade}\bar{e}_{Xblade} + F_{df,Zblade}\bar{e}_{Zblade}}{\left|\bar{F}_{df}\right|} \tag{8.18}$$

8.2.1 Scale laws with respect to the particle trajectory along the cutter blade

In paragraph 3.1.2 it was shown that the trajectories of particles were uniform on prototype and model scale if the particle was scaled geometrically and the fluid velocities were scaled according to Euler (square root of the length scale). This is valid because the particle Reynolds number lies within the Newton range on both scales and thus the drag coefficient is equal on both scales.

For the trajectory of a particle along the blade the same conclusions apply. The additional forces with respect to the equation of motion for the particle in the free flow are the normal force and the friction force, which are both proportional with the radius, $R_{p,}$ and the square of the angular velocity of the particle. Scaling the velocities according to the square root of the length scale will ensure that the dimensionless equation of motion is equal on model and prototype scale (see Equation (8.13)). Here it is assumed that the drag coefficient and the friction coefficient are equal on prototype and model scale.

8.3 Implementation of the equation of motion and testing the simulation model

In order to validate the simulation model, the flow field as described in Chapter 5 is used. This means that the flow field inside the cutter head is represented by a forced vortex and a sink. One adaptation that has to be made to this flow field is that the relative water velocities perpendicular to the blade's surface need to be zero. By setting these velocities in the

direction of Y_{blade} to zero, the flow field does not satisfy the Euler equation for inviscid flows anymore. At this point this is not considered to be a major problem. The flow field that is now used will eventually be replaced by a more accurate one. The error that is made in the flow field is not believed to have an effect on the validity of the equation of motion of the particle, which is the main concern at this point.

The equation of motion is basically the same system of non-linear, second-order differential equations as given in Chapter 5. Only the restriction that the particle has to move along the surface of the blade (as long as it stays in contact with the blade) and the friction force are added. This equation can be solved with a Euler, Heun or Runge-Kutta method. Chapter 5 showed that for a small enough time step the difference in solutions between the Runge-Kutta and the forward Euler or Heun method (trapezoidal rule) was negligible. However, to get the same order of accuracy the Euler method is generally more time consuming than the higher order Runge-Kutta method as a smaller time step is needed. On the other hand, for a first approach it is justified to use a forward Euler method with a small time step as the main purpose in the following paragraphs is to validate the equation of motion. The solution method could be improved if necessary (see also paragraph 8.4.5). The flow chart for the simulation model is given in Appendix E.

First of all the simulation routine is checked by using a cylindrical cutter blade instead of the crown cutter blade. That way, the calculated forces acting on the particle and the particle velocities are easier to verify.

8.3.1 Simulations with a cylindrical cutter blade

A straightforward test case is a particle that is sliding down the blade with no initial velocity. The cutter head does not rotate and there is no suction flow, thus the particle moves in a quiescent fluid.

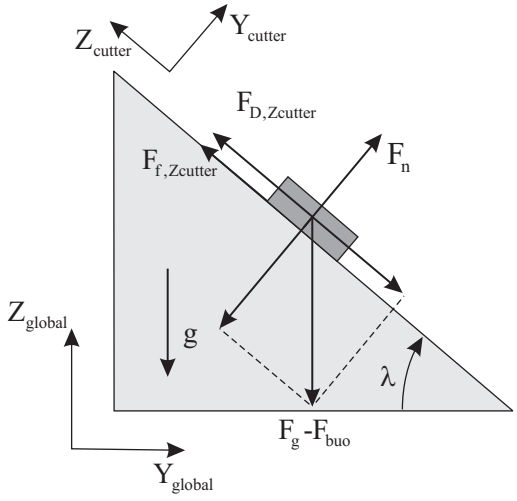

Figure 8.3: Particle sliding down an incline

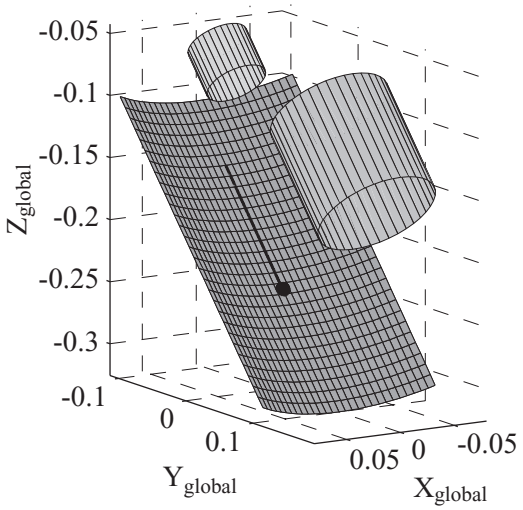

Figure 8.4: Particle sliding down a cylindrical blade

This situation can be represented by a particle sliding down an incline under-water as shown in Figure 8.3, where F_{buo} is the buoyancy force. In this figure the particle is drawn as a disk to emphasize the fact that gravel particles are more disk-like than spherical and thus more likely to slide along the blade than to roll. Note that in following figures the particle may still be represented as a sphere. Figure 8.4 shows the result of the simulation. The gray cylindrical surface represents the cylindrical cutter blade. The large cylinder represents the hub, while the smaller cylinder represents the suction pipe. The black line shows the trajectory of the particle, that is depicted by the black dot. There is only a displacement and velocity of the particle in the direction of Z_{cutter}. In time, the particle velocity will converge to a constant value, the asymptotic solution. This asymptotic solution will be determined analytically and compared with the value resulting from the simulation. Disregarding the added mass force, the equation of motion for the particle sliding down the incline is:

$$m_p \ddot{Z}_{p,cutter} = F_{D,cutter} + F_{f,cutter} - \left(F_g - F_{buo}\right)\cos\lambda \tag{8.19}$$

or

$$\ddot{Z}_{p,cutter} = \frac{3}{4}\frac{\rho_w}{\rho_p}\frac{C_d}{d_p} v_{p,Zcutter}^2 + \frac{\rho_p - \rho_w}{\rho_p} g\left(\mu \sin\lambda - \cos\lambda\right) \tag{8.20}$$

This is basically the equation for a settling particle with an extra term for the friction. Accordingly, the particle velocity will converge to a value of:

$$v_{p,Zcutter} = \pm\sqrt{\frac{4}{3}\frac{\rho_p - \rho_w}{\rho_w}\frac{d_p}{C_d} g\left(\cos\lambda - \mu\sin\lambda\right)} = \pm 0.276 \text{ [m/s]}$$

with d_p = 0.01 m, C_d = 1.4, ρ_p = 2650 kg/m^3, μ = 0.3 and λ = 45°.

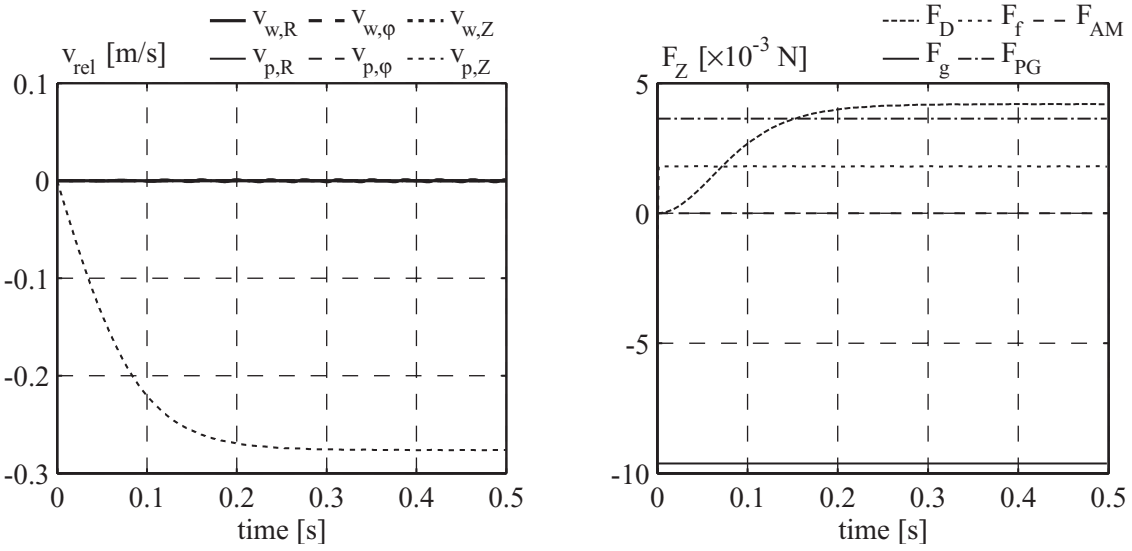

Figure 8.5: Relative velocity components for water and particle and axial components of the forces acting on the particle

Figure 8.5 shows the simulated particle velocity and the forces in direction of Z_{cutter} acting on the particle. Note that in this figure (and all following figures) the subscripts 'cutter' or 'blade' are omitted for convenience sake. In the plot for the forces the legend above the figure on the right shows the respective force while the legend on the left shows the component of the force that is plotted. The particle velocity in direction of Z_{cutter} matches the analytically determined value of -0.276 m/s.

The drag force in direction of Z_{cutter} converges to a value of

$$F_{D,Zcutter} = \frac{\pi}{8}\rho_w d_p^2 C_d v_{p,Zcutter}^2 = 4.2\times10^{-3} \text{ [N]}$$

The gravitational force, friction force and pressure gradient force are constant in time.

$$F_{g,Zcutter} = -m_p g\cos\lambda = -9.6\times10^{-3} \text{ [N]}$$

$$F_{PG,Zcutter} = \rho_w V_p g\cos\lambda = 3.6\times10^{-3} \text{ [N]}$$

$$F_{f,Zcutter} = \mu\left(\rho_p - \rho_w\right) V_p g\sin\lambda = 1.8\times10^{-3} \text{ [N]}$$

These values agree well with the values resulting from the simulation. It may be assumed that the basic equation of motion is solved properly in the simulations.

A second simulation is performed with the cylindrical cutter blade. This time the cutter blade is positioned vertically and the acceleration of gravity is set to zero. The cutter head is rotating with 90 RPM and there is no suction flow. The slip factor between blade and water is 0.3 and the particle's initial velocity is half the fluid velocity.

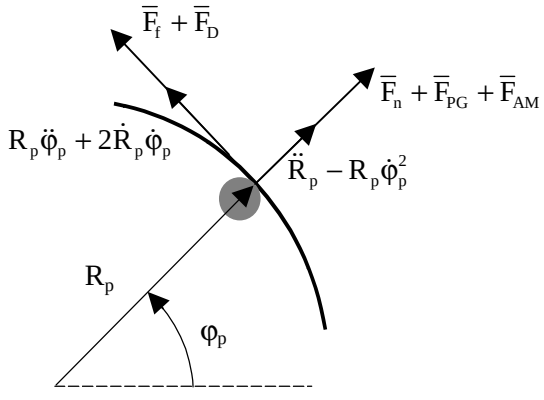

Figure 8.6: Schematic representation of particle in contact with cylindrical blade

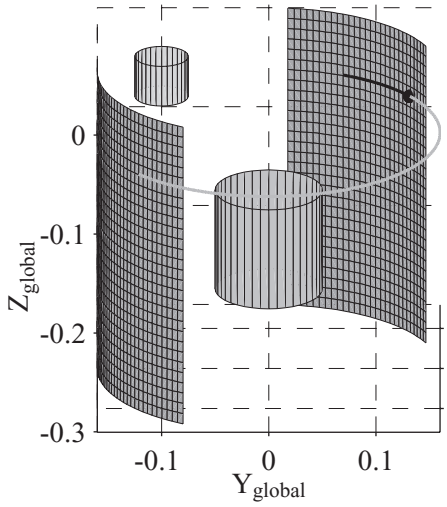

Figure 8.7: Simulated particle trajectory along the cylindrical blade

As there are no forces acting on the particle in axial direction, the force equilibrium on the particle can be represented as in Figure 8.6.

Figure 8.7 shows the trajectory of the particle when the initial velocity of the particle is $0.9v_w$. The two blades give the initial and final position of the blade (the blade on the left gives the initial position). The small cylinder represents the suction pipe and the large cylinder the hub. The black line shows the relative trajectory of the particle (i.e. relative to the blade), while the gray line shows the global trajectory. Furthermore, the black dot represents the particle in its final position. Being confined by the cylindrical blade, the particle makes a circular motion and there is no displacement in axial direction. Figure 8.7 also shows that the angular velocity of the blade is larger than the angular velocity of the particle. This means that eventually the particle will leave the blade at the trailing edge of the blade.

Again the asymptotic solution is compared with the numerical solution to check whether the forces on the particle and velocities of the particle are determined correctly in the simulation. Comparable with the previous case, the particle will not be accelerated anymore after a certain time, which means that its angular velocity will be constant. The equilibrium of forces on the particle in tangential and radial direction is then:

Tangential

$$0 = \mu F_n + \frac{\pi}{8}\rho_w d_p^2 C_d \left(R_p\omega_f - R_p\dot{\varphi}_p\right)\left|R_p\omega_f - R_p\dot{\varphi}_p\right| \tag{8.21}$$

Radial

$$m_p\left(-R_p\dot{\varphi}_p^2\right) = -F_n + \rho_w V_p\left(-R_p\omega_f^2\right) + \rho_w V_p C_{AM}\left(-R_p\omega_f^2 + R_p\dot{\varphi}_p^2\right) \tag{8.22}$$

Note that the normal force is defined as

$$\overline{F}_n = -F_n\overline{e}_{Rp} \tag{8.23}$$

There are two equations with two unknowns, i.e. the normal force F_n and the angular velocity of the particle $\dot{\varphi}_p$. Solving these equations gives

$F_n = 0.0124$ [N]

$\dot{\varphi}_p = 8.22$ [rad/s]

with $R_p = 0.16$ m, $d_p = 0.01$ m, $C_{AM} = 0.5$, $C_d = 1.4$, $\rho_p = 2650$ kg/m^3, $\mu = 0.3$, $\omega_c = 9.425$ rad/s and $\omega_f = 0.7\omega_c$ rad/s.

The relative water and particle velocity in tangential direction are:

$v_{w,rel} = R_p(\omega_f - \omega_c) = 0.16(6.597 - 9.425) = -0.45$ [m/s]

$$v_{p,rel} = R_p(\dot{\varphi}_p - \omega_c) = 0.16(8.22 - 9.425) = -0.19 \text{ [m/s]}$$

Accordingly, the forces acting on the particle are

$F_f = 0.0037$ [N]
$F_D = -0.0037$ [N]
$F_{PG} = -0.0036$ [N]
$F_{AM} = 0.001$ [N]

Figure 8.8 shows the water and particle velocities and the forces acting on the particle resulting from the simulation.

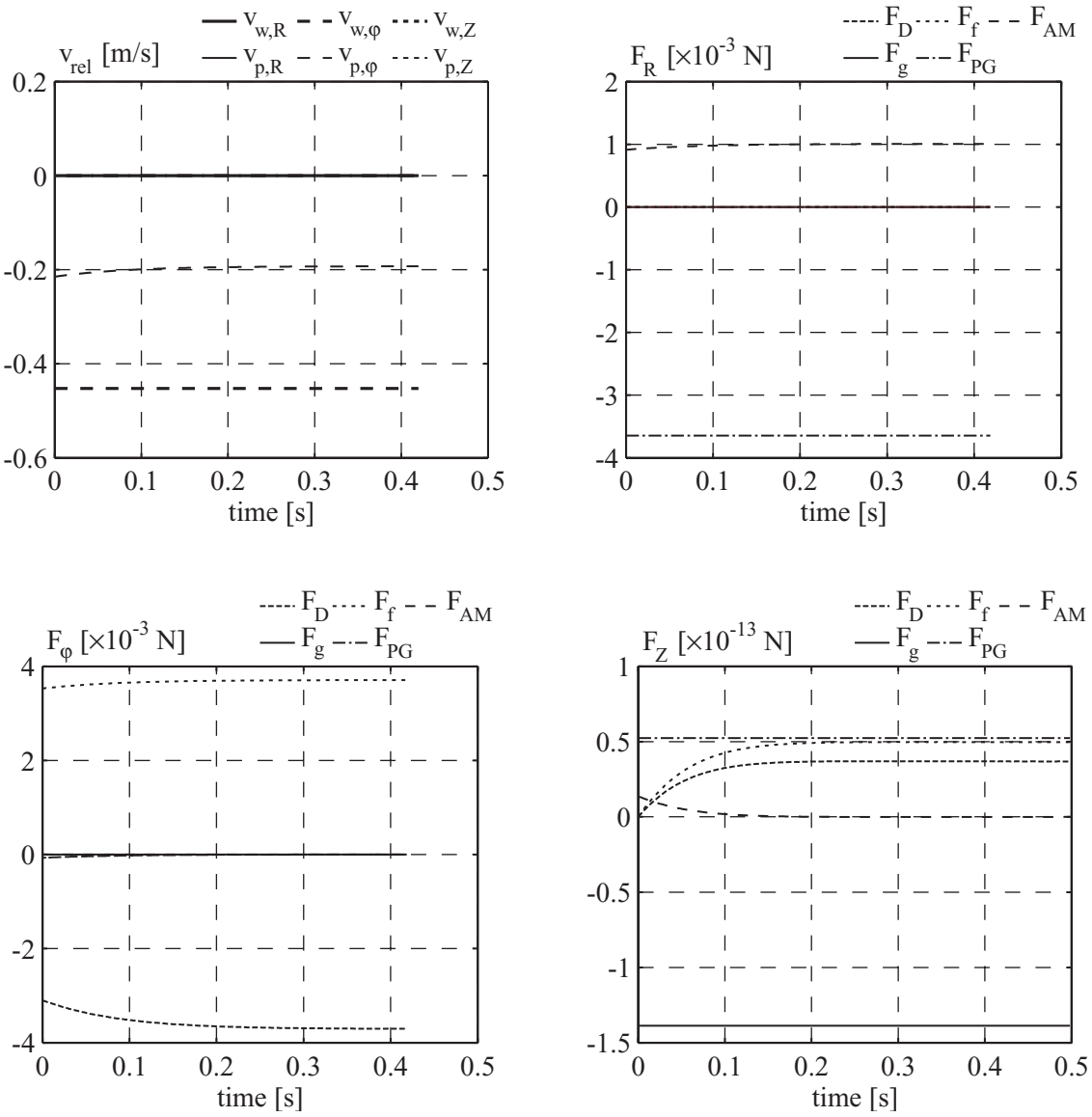

Figure 8.8: Axial, radial and tangential components of the relative water and particle velocity and the forces acting on the particle

The first plot shows the radial, tangential and axial components of the relative water and particle velocity. The second, third and fourth plot show the radial, tangential and axial components respectively of the forces acting on the particle. The simulated velocities and forces match their analytically determined values. However, the axial forces acting on the particle are not exactly zero. This is mainly caused by the fact that the acceleration of gravity was not exactly zero but set to 1×10^{-10}. This was done to avoid a division by zero as the equation of motion is set up in dimensionless form. Thus, the gravitational force has an order of magnitude of 1×10^{-13}. As the forces are coupled in the equation of motion, the remaining forces will have the same order of magnitude.

8.3.2 Simulations with a crown cutter blade

For the following simulations the blade geometry of a crown cutter head has been used. In comparison with the cylindrical blade the blade of a crown cutter head is curved in three dimensions and has a helical shape (see Figure 8.9 or Figure 1.2). The cutter blade that has been used in the simulations had the same shape as the blades of cutter head used in the CFD model for determining the water velocities and pressures inside the cutter head (see paragraph 5.5). In order to match the scale used in the previous simulations, the cutter head was geometrically downscaled by a factor 2. Then it also matches the scale of the cutter head used for the cutting tests in cemented banks of gravel and the stationary tests, i.e. the tests with the silo. Again the flow field inside the cutter head is represented by a forced vortex and a sink. The velocity components perpendicular to the blade's surface were set to zero. As a result of this action, the flow field does not satisfy the Euler equation, or rather continuum equation, anymore. However, for validation of the model this is not considered to be a problem.

Particle sliding down the inner surface of the blade

In the first simulation, the cutter head is placed in a vertical position and a particle is released from a point near the cutter ring. The cutter head does not rotate and there is no suction flow. Furthermore the particle is released with zero initial velocity. The simulated trajectory of this particle is shown in Figure 8.9. The two cylinders in the plots represent the hub and the suction pipe again. The black line denotes the trajectory of the particle and the black dot represents the particle in its final position, when it leaves the blade. As it is impossible to find an analytical solution for this case, the particle trajectory has to be evaluated in a numerical way.

The figure shows that the particle follows the blade's inner surface and its trajectory is fairly plausible. In the left plot it looks as if the particle moves down in an almost straight line. The right plot however, shows that its trajectory is deviated near the hub due to the strong curvature of the blades at that location. The simulated particle trajectory could be validated experimentally by filming its trajectory using underwater cameras. This validation has not been performed yet and is recommended for further research.

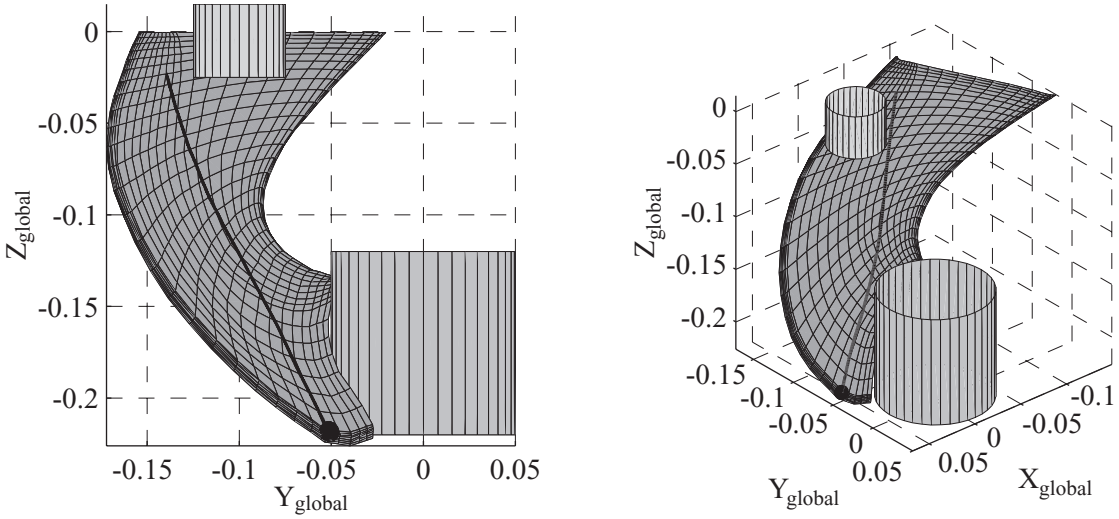

Figure 8.9: Particle sliding down the crown cutter blade (side and top view)

The calculated particle velocity and forces on the particle can give more insight on the validity of the model. As the water velocities inside the cutter head are zero, the particle will slide down because of the gravity. This will also be the dominant force. Figure 8.10 shows the relative water and particle velocity and the forces acting on the particle resulting from the simulation. Between 0.1 and 0.5 s the figures show strong fluctuations in the calculated values for the velocities and forces. These fluctuations are mainly caused by the discrete build up of the blade (see Appendix E.3). The geometry of the blade is not described analytically, but determined by 30×28 measured points. Because of errors during measurements and the relatively small amount of measured points to describe the blade's surface, the normal vector may not vary smoothly from one point to another. As the normal vector is used in the simulation to define the blade's surface in a specific point, the blade's surface may therefore appear bumpy.

The figure for the velocity shows that the particle initially has a relatively large axial acceleration. This is due to the fact that the blade's surface is almost vertical and the gravitational force is very dominant. When the particle comes closer to the hub, the slope of the blade starts to change and the axial velocity decreases. This trend is also shown by the radial particle velocity. The particle is first accelerated towards the hub (smaller radius thus negative radial velocity) but when it reaches the curved area of the blade, the acceleration changes sign and eventually the particle will even move away from the hub (positive radial velocity). The tangential velocity, on the other hand, increases continuously. The reason for this becomes clear when looking at the slope (especially near the hub) of the blade in Figure 8.9.

The forces plotted in Figure 8.10 show that the gravitational force and the drag force are indeed the dominant forces. As there is no water flow, the pressure gradient force consists only of the buoyancy force.

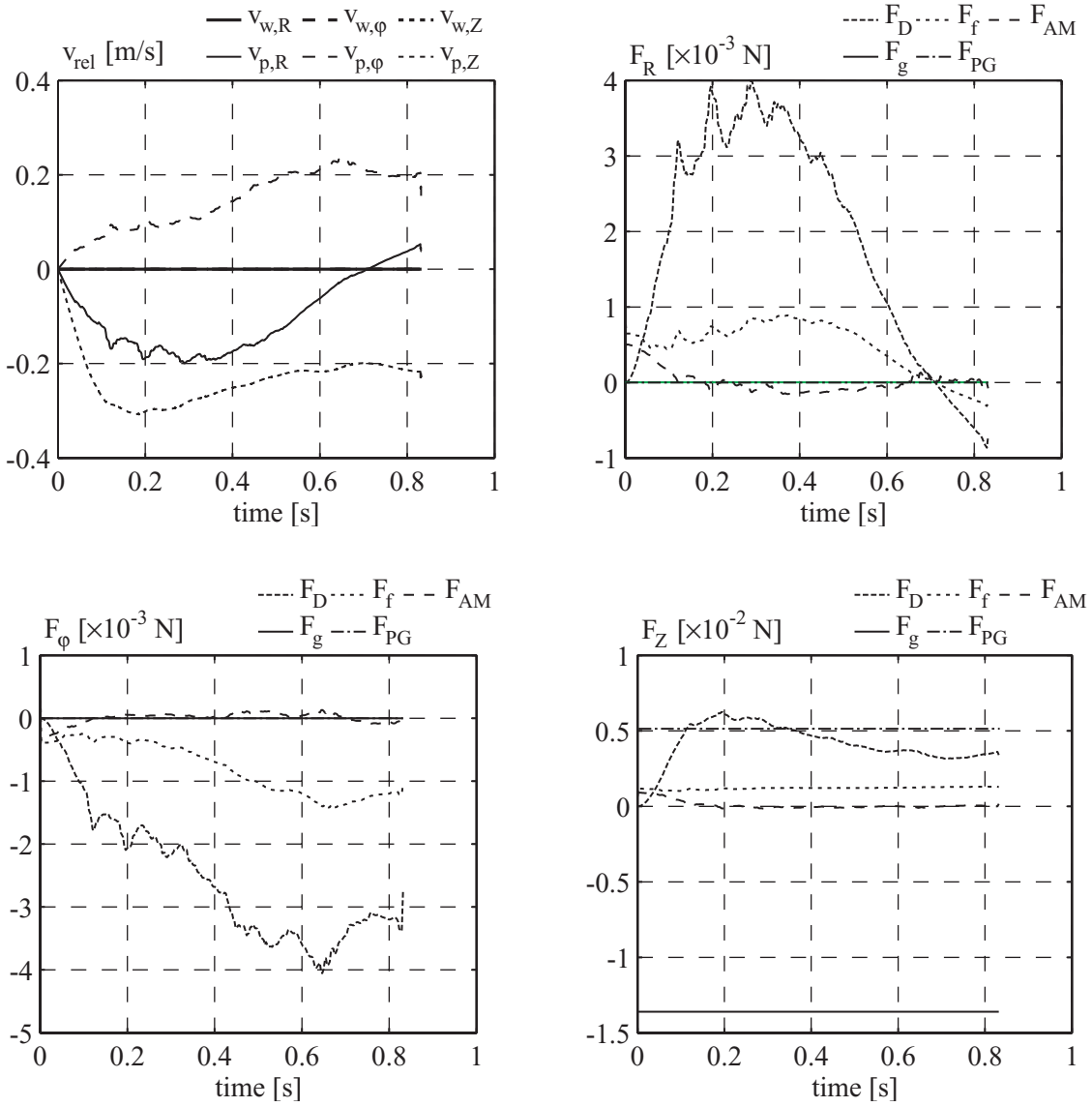

Figure 8.10: Axial, radial and tangential components of the relative water and particle velocity and the forces acting on the particle

Simulation with zero gravity

A simulation is performed where the acceleration of gravity is set to zero. Nominal values were taken for the rotational velocity of the cutter head and the mixture velocity i.e.: 90 RPM and 3 m/s respectively. The variables in the simulation model had the values as indicated in Table 8.1.

Table 8.1: Values for the variables in the simulation model

$\rho_p = 2650$ [kg/m^3]	$C_{AM} = 0.5$ [-]	$c_{slip} = 0.3$ [-]	$\mu_{stat} = 0.3$ [-]	$\lambda = 45$ [°]
$\rho_w = 1000$ [kg/m^3]	$C_d = 1.4$ [-]	$d_p = 0.01$ [m]	$\mu_{dyn} = 0.3$ [-]	

The initial velocity of the particle was:

$$\overline{v}_{p,t=0} = 0.7\overline{v}_w$$

in which v_w is the water velocity at the initial position of the particle. The following figures show the simulated particle trajectory along the blade.

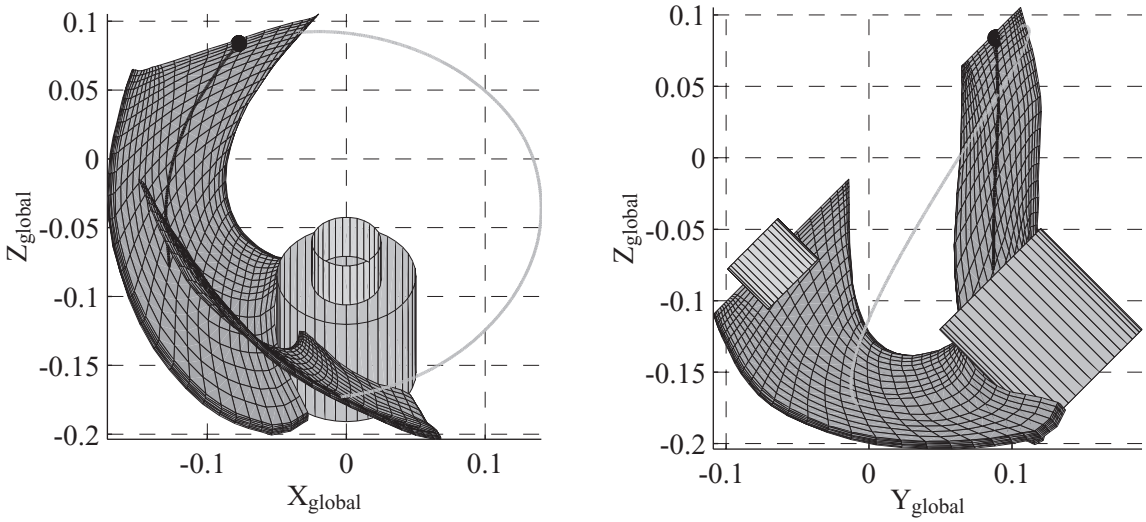

Figure 8.11: Particle trajectory along a blade resulting from the simulation with zero gravity

The blade right underneath the suction pipe corresponds with the initial position of the blade, while the other blade gives its final position, i.e. the position at the end of the simulation. Furthermore, the figure shows two particle trajectories. A global trajectory of the particle, depicted by the gray line and a relative trajectory depicted by the black line. In which relative means relative to the blade.

The particle was released approximately halfway the cutter head in the region where the cutter head is enclosed by the breach. Although there is no gravity to force the particle towards the hub, the particle is, apparently, still not transported towards the suction pipe. This is an indication of the poor influence of the suction flow. The particle does however have an axial motion towards the cutter ring. The reason for this is found by looking at the particle velocity and the forces acting on the particle as shown in Figure 8.12.

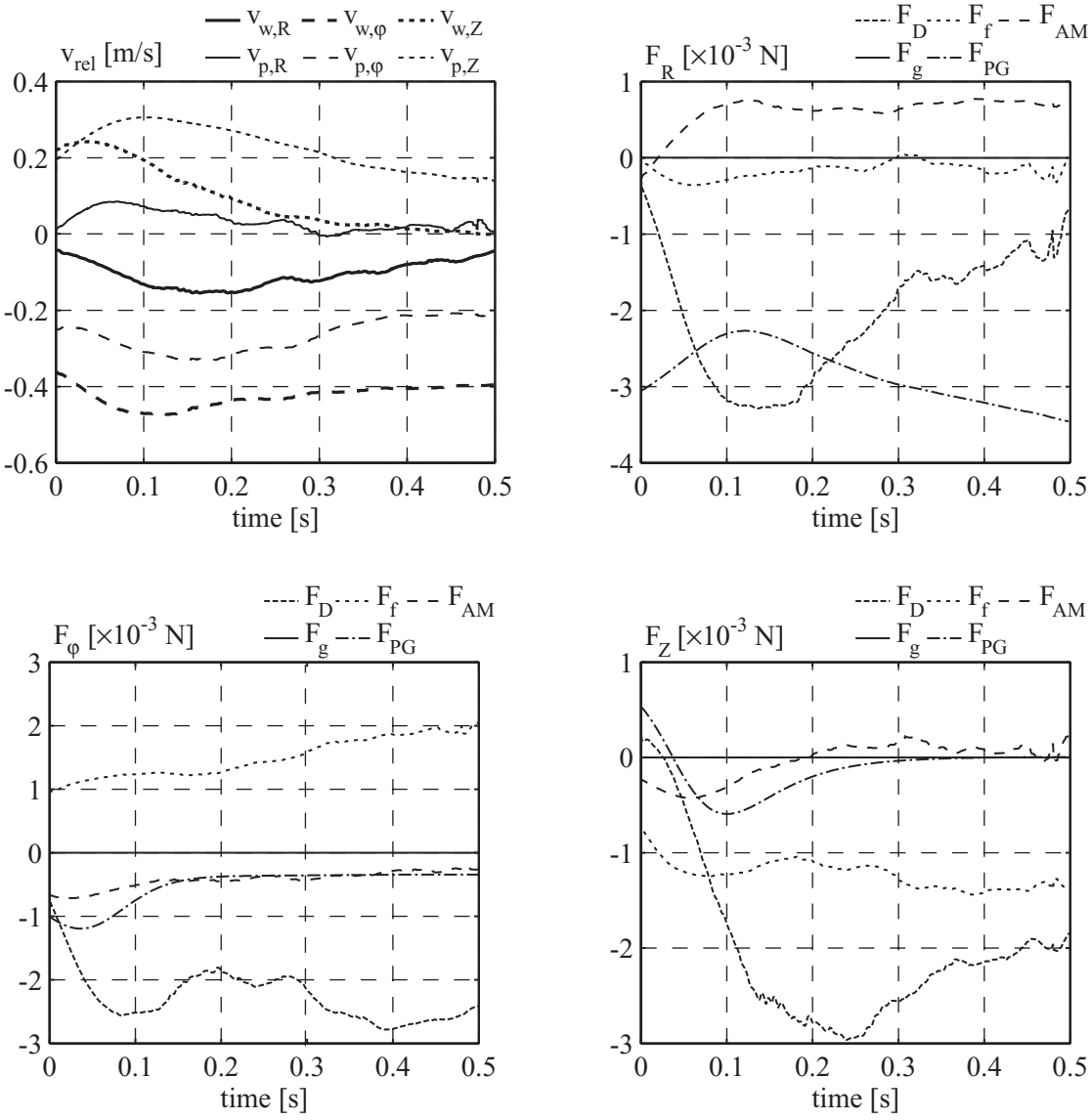

Figure 8.12: Radial, tangential and axial components of the relative water and particle velocity and the forces acting on the particle

Indeed, the axial velocity of the particle is positive implying that it is moving towards the cutter ring. According to the axial forces in Figure 8.12, the resultant force is negative thus directed towards the hub. Still the particle moves towards the cutter ring. This can be explained by the relatively large centrifugal force acting on the particle or actually centrifugal acceleration of the particle. The left plot in Figure 8.13 shows a simplified case of a particle moving along the surface of the blade. All other forces besides the forces due to acceleration of the particle and the normal force are neglected. The particle can move along the surface frictionless. As the situation is axially symmetrical, the problem can be considered two dimensional. Then, the horizontal acceleration of the particle equals the radial acceleration in the rotating coordinate system.

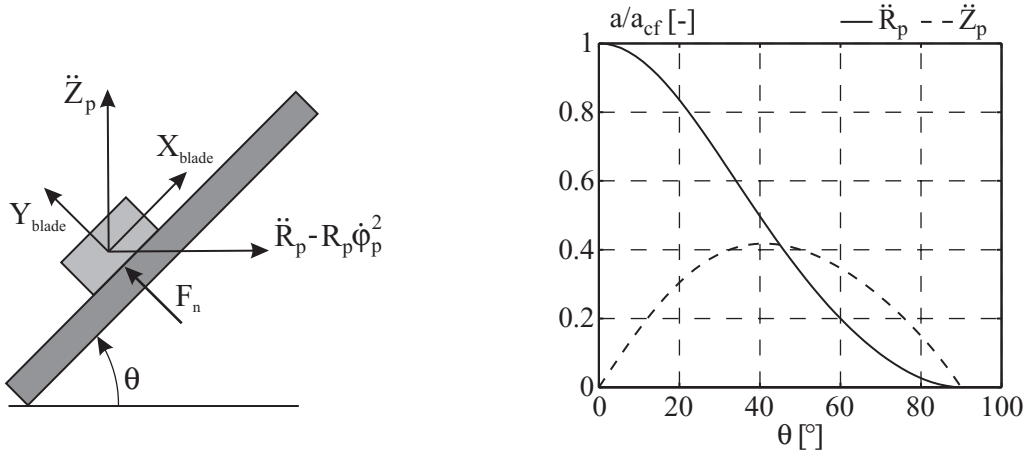

Figure 8.13: Influence of the centrifugal acceleration on the radial and axial acceleration of the particle and the accelerations plotted as a function of the blade angle θ

The equation of motion for the particle in the direction of X_{blade} and Y_{blade} is (and adding the restriction of movement along the surface):

$$\begin{aligned} &m_p\left(\left(\ddot{R}_p - R_p\dot{\varphi}_p^2\right)\cos\theta - \ddot{Z}_p\sin\theta\right) = 0 \\ &m_p\left(-\left(\ddot{R}_p - R_p\dot{\varphi}_p^2\right)\sin\theta + \ddot{Z}_p\cos\theta\right) = F_n \\ &\ddot{Z}_p = \ddot{R}_p\tan\theta \end{aligned} \tag{8.24}$$

or

$$\begin{aligned} &\ddot{R}_p = R_p\dot{\varphi}_p^2\frac{\cos^2\theta}{\cos\theta + \sin^2\theta} \\ &\ddot{Z}_p = \ddot{R}_p\tan\theta \\ &F_n = m_p R\dot{\varphi}_p^2\sin\theta \end{aligned} \tag{8.25}$$

Thus, the acceleration in Z_p direction is proportional to the centrifugal acceleration, a_{cf}, defined as

$$a_{cf} = R_p\dot{\varphi}_p^2$$

Furthermore, the relationship between the acceleration in Z_p direction and the angle θ is parabolic as shown in the right plot of Figure 8.13. The vertical axis in this plot shows the acceleration of the particle in radial and axial direction normalized by the centrifugal acceleration, a_{cf}. For $\theta = 0$ and $\theta = \pi/2$ the acceleration in Z_p direction is 0, while the

maximum acceleration is found near $\theta = 0.72$ rad ($\approx 41^o$). The maximum acceleration in Z_p direction is 0.42 times the centrifugal acceleration.

Figure 8.14 shows the centrifugal force F_{cf} (i.e. the centrifugal acceleration multiplied by the particle mass) resulting from the simulation with zero gravity.

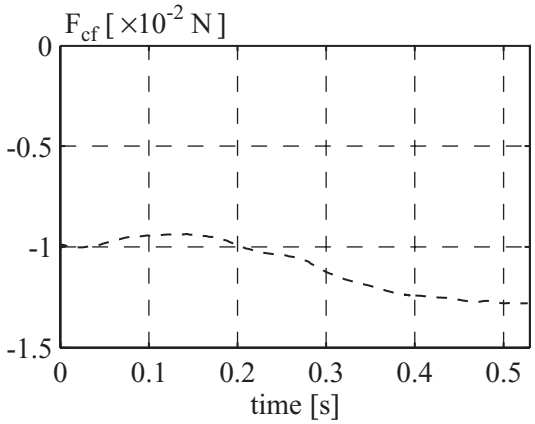

Figure 8.14: Magnitude of the centrifugal force in the simulation with zero gravity

Comparison of the magnitudes of the centrifugal force with the forces shown in Figure 8.12 indicates that the centrifugal acceleration is well capable of forcing the particle towards the cutter ring. In addition, the particle moves towards the cutter ring with such a high velocity that it exceeds the water velocities in axial direction. Therefore the component of the drag force in axial direction is negative.

As the slip factor between water and blade is 0.3, the angular velocity of the water is smaller than the angular velocity of the blade. Therefore the tangential water velocity is negative. The tangential velocity of the particle is also negative but larger than the tangential water velocity. This means that the particle is rotating faster (about the cutter axis) than the water but slower than the cutter blade, which is confirmed by the positive tangential component of the friction force. This is also caused by the centrifugal force acting on the particle, that has a component along the blade's surface in the direction of the rotation of the cutter head. Because of this component the particle wants to move towards the tip of the blade.

Simulation with high friction coefficient

In the next simulation the rotational velocity of the cutter head was 120 RPM and the mixture velocity was 3 m/s. The friction coefficient between particle and blade was increased from 0.3 to 5. With such a high friction coefficient the particle is expected to stay fixed to the blade. The same values for the remaining variables were taken as given in Table 8.1. The initial velocity of the particle was half the water velocity in the point of release. Figure 8.15 shows the simulated particle trajectory.

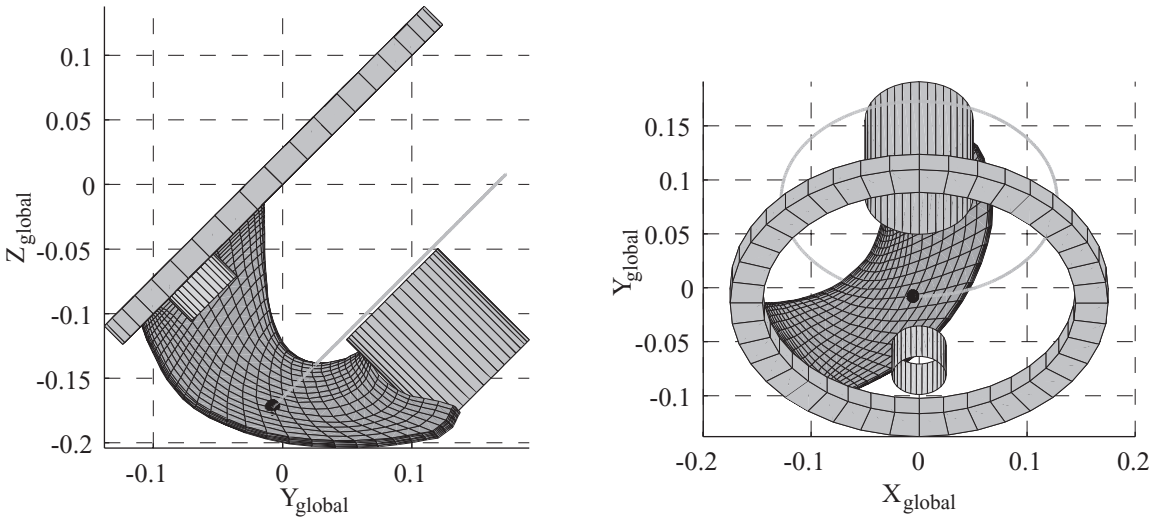

Figure 8.15: Particle trajectory along a blade resulting from the simulation with μ = 5 [-]

The simulation was stopped after a full rotation of the cutter head. It may appear as if the particle trajectory, given by the gray line, stops before a full rotation is completed. In reality the line continues behind the blade and ends at the point indicated by the black sphere which represents the particle in its final position. Thus, the particle was indeed fixed to the blade and has completed a full circle. The relative velocity components of the particle given in Figure 8.16 give a confirmation of this.

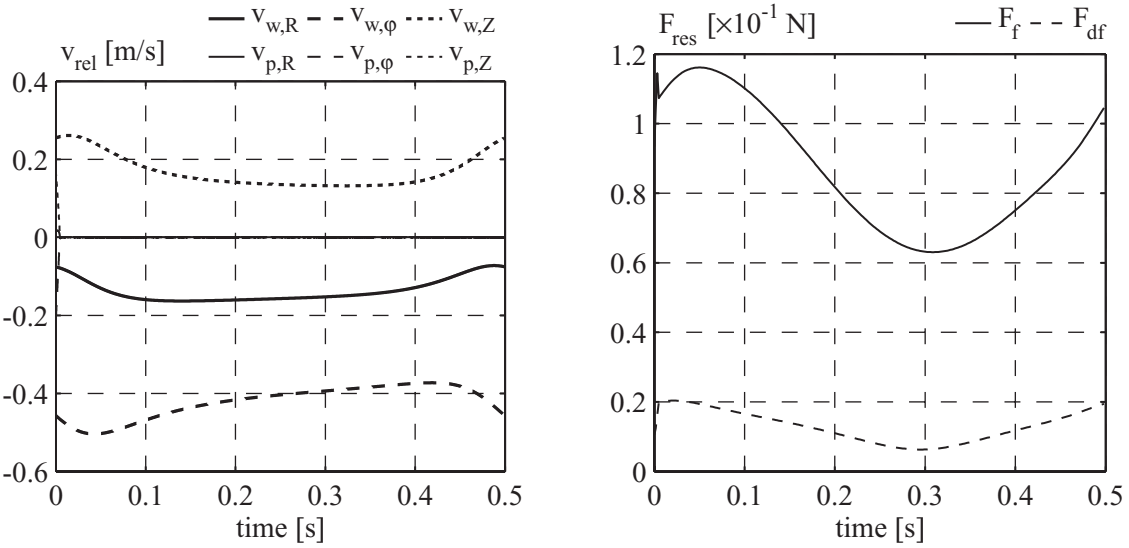

Figure 8.16: Axial, radial and tangential components of the relative water and particle velocity and the resultant driving and friction force acting on the particle

These velocity components are all zero except for a short period at the beginning during which the particle velocity adjusts to match the blade's velocity.

The particle was fixed to the blade because the friction force was larger than the driving force acting on the particle (see equations (8.16) and (8.17)). This is also shown in Figure 8.16. The second plot shows the resultant friction force F_f acting on the particle and the resultant driving force F_{df}. The friction force is about 5 to 6 times larger than the driving force which means that the particle can not move with respect to the cutter blade.

8.4 Simulations with the flow represented by a forced vortex and a sink

In this section a series of simulations is performed where the flow inside the cutter head is represented by a superposition of a forced vortex and a sink. These simulations aim to clarify and give more insight on the test results from Chapter 7. In particular the increase in production percentage with increasing rotational velocity is subject of research. As stated in Chapter 7 this is thought to be the result of an increasing centrifugal force acting on the particle, forcing the particle along the surface of the blade towards the suction mouth.

As only the trajectory of a single particle along the blade is simulated and a production percentage can not be determined yet, the comparison with the test results is done in a qualitative way. Attention is mainly focused on the change in particle trajectories along the cutter blades as a result of an increase in rotational velocity of the cutter head in the range of 40 RPM to 90 RPM. Increasing the rotational velocity in this range is expected to enhance the transport of particles along the cutter blades towards the suction mouth. In addition, the influence of the variables in the model on the particle trajectory is investigated. However, not all variables in the model are changed as the simulations focus on trajectories of gravel particles with equal diameter in water. Basically the list of variables can be subdivided into constants and variables in the simulations.

8.4.1 Constants in the simulations

The constants in the simulations include:

- Mechanical friction coefficient μ
- Density of the particle ρ_p
- Density of the fluid ρ_w
- Diameter of the particle d_p
- Added mass coefficient C_{AM}

Mechanical friction coefficient μ

It is difficult to give an exact value for the mechanical friction coefficient as this variable is dependent on many factors. For instance, the roughness of the blade can affect the friction coefficient significantly. Nevertheless, according to practical experience a value of 0.3 is

reasonable. This value is used for both the static and dynamic friction coefficient, although in the simulation model a distinction can be made between the static and the dynamic friction coefficient.

Particle and fluid properties ρ_p, ρ_w and d_p

For the density and diameter of the particle the same values were used as in the tests described in Chapter 6 and Chapter 7; i.e. $\rho_p = 2650$ kg/m^3 and $d_p = 0.01$ m. The density of the fluid is the density of water: $\rho_w = 1000$ kg/m^3.

Added mass coefficient C_{AM}

According to Odar and Hamilton (1964), the added mass coefficient C_{AM} ranges from 0.5 to 1.05 for spheres in free fall and depends on the ratio of the density of the particle and the density of the fluid. For the density ratio of 2.65 an added mass coefficient of 1 would be appropriate.

However, the gravel particles are not spherical but can be ellipsoidal or disk-like. In that case, C_{AM} is a tensor depending not only on the shape of the gravel particle but also on the relative orientation of the particle to the flow (Batchelor, 1967). Assuming that the particle is disk-like or a circular cylinder moving normal to its axis (most likely situation for the particle sliding along the blade), C_{AM} also equals 1 (Batchelor, 1967).

Attention should be paid to the fact that the gravel particles are not in free fall but that they are bounded by the surface of the blade. Jan and Chen (1997) studied the movement of a sphere rolling down an incline and showed that the proximity of a wall causes for an increase in C_{AM} as well as the drag coefficient C_d. According to their numerical results, a C_{AM} of 2 shows the best agreement with their experimental results. As opposed to the spherical particles used by Jan and Chen, the gravel particles are not likely to roll over the blade due to their ellipsoidal shape. It is more likely that they will only slide along the blades. In that case the total kinetic energy of the fluid relative to the particle will be lower as there is no rotation energy (Batchelor, 1967). This would yield a lower value for C_{AM} than 2.

Taking everything into account, it can be assumed that the lower limit for C_{AM} is 1 and the upper limit is 2. In order to limit the amount of simulations that have to be performed, only the lower limit for C_{AM} is used in the simulations at first. This is done with the assumption that the added mass force will not be the dominating force. However, if proved necessary, additional simulations can be performed varying C_{AM} in the range of 1 to 2.

8.4.2 Variables in the simulation

Besides the operational variables such as: suction flow, rotational velocity of the cutter head and cutter inclination angle, the variables in the simulation model include:

- Drag coefficient C_d
- Slip factor between water and blade C_{slip}

- Initial position of the particle on the blade
- Initial position of the blade
- Initial velocity of the particle

Drag coefficient C_d

For the ellipsoidal gravel particles, the drag coefficient C_d also depends on the relative orientation of the particle to the flow. Furthermore the proximity of the blade will cause an increase in C_d. According to the experimental results by Jan and Cheng (1977), the C_d value for a sphere rolling down a smooth incline is about 1 when the particle Reynolds number has order of magnitude 1×10^3. This is a significant increase, as compared to a C_d of 0.4 that applies to a sphere in free fall. Jan and Cheng attributed this increase in C_d to the existence of an overpressure in the corner between the plane and the lower front part of the sphere, which can not evacuate. This overpressure will be dependent on the rotational velocity of the particle. Generally speaking, the faster the particle rotates the higher the overpressure. As the gravel particles are not likely to rotate, only slide, a same increase in C_d coefficient as for rolling spheres is not expected. On the other hand, due to lack of data on sliding particles and considering the range of possible particle shapes, the C_d value of 1 resulting from the experiments by Jan and Chen can be used as an upper limit for C_d.

A lower limit for C_d would be the case of a disk-like particle moving normal to its axis of rotation symmetry and along the blade. Neglecting the presence of the blade, the C_d coefficient is then approximately 0.2 (White, 1994). This means that the C_d coefficient may vary between 0.2 and 1. Simulations are performed with the minimum and maximum value for the C_d coefficient.

Slip factor between water and blade C_{slip}

The slip factor C_{slip} is a measure for the difference in velocity between the blade and water. Exactly on the blade, water will have the same velocity as the blade but in the viscous boundary layer water velocities will drop rapidly. At first, the assumption is made that the boundary layer is small enough to assume a velocity difference between blade and water. As the blade only has a velocity in tangential direction, C_{slip} is only defined in tangential direction. The following definition for C_{slip} is used to define the difference in velocity.

$$C_{slip} = 1 - \frac{v_{\varphi,w}}{\omega_c R_{blade}} \tag{8.26}$$

in which $v_{\varphi,w}$ is the tangential velocity of the water, ω_c is the angular velocity of the cutter head and R_{blade} is the radial distance from the cutter axis to the concerned point on the blade. Note that equation (8.26) is not necessarily restricted to points on the blade. Replacing R_{blade} by the radial distance to any arbitrary point inside the cutter head gives the slip factor in that specific point. The slip factor then defines the difference between the actual tangential

velocity in a point compared to the tangential velocity in that point considering a forced vortex with angular velocity ω_c.

Velocity measurements at different positions inside the cutter head near the blades showed that C_{slip} may vary within a wide range (Dekker, 2001). These measurements were performed at stationary positions, meaning that the measuring device did not rotate with the cutter head. Not only did C_{slip} depend on the absolute position inside the cutter head but also on the relative position of the cutter blades with respect to the measuring device. This is understandable as a higher tangential velocity will be measured when a blade is passing the measuring device than when the gap between two blades passes by. The slip factor was however independent of the flow number ξ.

It was difficult to find a general trend for C_{slip}. Therefore simulations were performed with three different values for C_{slip} based on the velocity measurements. The values for C_{slip} that were used are: 0.5, 0.1 and –0.2. Here it is assumed that C_{slip} applies for every position inside the cutter head. The negative value for C_{slip} indicates that the water rotates faster than the blade which implies an outgoing flow.

Initial position of the particle on the blade

Particles are released at six different positions on the cutter blade. First of all, three positions near the leading edge of the blade and 3 positions halfway the leading and trailing edge of the blade.

Initial position of the blade

A cutter blade enters the breach right underneath the suction mouth. This is the first initial position of the blade examined in the simulations. Other initial position are given by rotating the blade about the cutter axis according to the direction of rotation of the cutter head (i.e. counterclockwise for the under-cut situation).

Initial velocity of the particle

Both the cutting test in cemented banks of gravel and the tests where the gravel was supplied by means of a silo showed the same trend. An initial increase in production with increasing rotational velocity of the cutter head. Furthermore, in both cases the optimum rotational velocity was the same. The way the particles enter the cutter head are entirely different. In the cutting tests the particles enter the cutter head radial with a large tangential velocity component, while during the tests with the silo the particles enter the cutter head axially. Obviously, the initial velocity with which the particles reach the blade will differ in both cases. It is therefore assumed that the initial velocity of the particle will not play a decisive role in the aforementioned trend.

The initial velocity of a particle is a vector, which means that not only its magnitude needs to be defined but also the direction. The following initial velocities for a particle on a blade at a certain position (R_p, φ_p, Z_p) were used in the simulations:

$$\overline{v}_p\left(R_p, \varphi_p, Z_p\right) = 0$$

$$\overline{v}_p\left(R_p, \varphi_p, Z_p\right) = \overline{v}_w\left(R_p, \varphi_p, Z_p\right)$$

$$\overline{v}_p\left(R_p, \varphi_p, Z_p\right) = \overline{v}_{blade}\left(R_p, \varphi_p, Z_p\right)$$

Thus an initial velocity of the particle of 0, an initial velocity equal to the water velocity and an initial velocity equal to the velocity of the blade.

8.4.3 Operational parameters

The operational parameters are parameters that can be varied during the cutting process. These parameters are:

- Rotational velocity of the cutter head n_c
- Mixture velocity v_m
- Haul velocity v_h
- Cutter axis inclination angle λ

Only the rotational velocity of the cutter head will be varied in the simulations. Three values chosen for the rotational velocity are: 40, 90 and 120 RPM. This implies a rotational velocity below optimum, a rotational velocity near the optimum and a rotational velocity beyond optimum.

A mixture velocity of 3 m/s, which is the nominal value, and a cutter axis inclination angle of 45° are taken. The haul velocity was zero in all simulations, comparable with the stationary tests with the silo.

8.4.4 Detailed description of typical simulated particle trajectories

As it is not possible to show the results of all the simulations that have been performed, a selection is made of some typical simulated particle trajectories. These specific trajectories are explained in detail in this paragraph, while in the next paragraph the general trends of the simulations are described.

Simulations with a large slip factor

The influence of changing the slip factor C_{slip} was significant. The simulations with the relatively large slip factor of 0.5 showed that the blade always rotates faster than the particle. Therefore, the particle leaves the blade at the trailing edge or it comes off the blade (negative normal force in the simulation). Furthermore, the particle is in contact with the blade over a relatively short time because of the large difference in rotational velocity between water and

the blade. Figure 8.17 shows a typical trajectory of a particle for a simulation with C_{slip} = 0.5. The rotational velocity of the cutter head was 90 RPM and the initial position of the blade was right underneath the suction pipe.

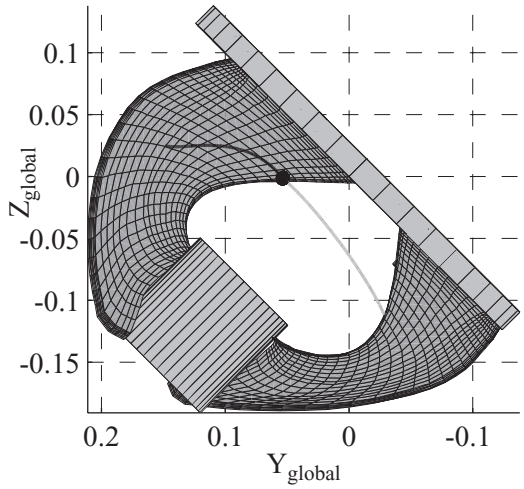

Figure 8.17: The trajectory of a particle for a simulation with C_{slip} = 0.5, n_c = 90 RPM and v_m = 3 m/s

The relative trajectory of the particle (black line) is shown on the blade in its final position of the simulation. The particle was released with an initial velocity of zero (absolute) and its drag coefficient was C_d = 0.2. Due to the large velocity difference between water and blade, the large drag force acting on the particle will prevent it from moving along with the blade. Therefore, the blade rotates faster than the particle. In addition, the gravitational force also slows down the rotational velocity of the particle because of which it will leave the particle at the trailing edge.

Figure 8.17 shows that the particle has an axial motion towards the cutter ring. This same axial motion was found when the rotational velocity of the cutter head was increased to 120 RPM. The simulation with a rotational velocity of 40 RPM did not show this axial motion towards the cutter ring. Instead the particle slid down towards the hub along the surface of the blade. The reason for this axial motion of the particle towards the cutter ring was explained in paragraph 7.3.2. The centrifugal force acting on the particle has a component along the blade's inner surface directed towards the cutter ring that is large enough to exceed the forces in opposite direction.

Changing the initial velocity or the drag coefficient did have an effect on the particle trajectories but it did not change the aforementioned trend. In general it can be concluded that for the simulations with C_{slip} = 0.5 the particles tend to stay within the cutter head. They leave the blade at the trailing edge or come off the blade where they are picked up by the free flow.

The flow inside the cutter head will then determine the further trajectory of the particle. The axial movement of the particles towards the cutter ring is less significant as expected due to the large velocity difference between water and blade.

These simulation with the large slip factor represent the case where the influence of the blades on the water flow is small. The flow inside the cutter head is than mainly determined by the suction flow, keeping the particles inside the cutter head. Compared with the actual situation, the water velocities between the blades are underestimated in the simulation as the presence of the blades is not taken into account. As the space between the blades form 6 channels and the total surface through which the water can flow towards the suction pipe is narrowed, the axial and radial water velocity will be higher in reality. A rough estimation of the space occupied by the blades, hub and cutter axis would suggest that the axial and radial velocities can be increased with up to 10%.

The simulations performed with the large slip factor and relatively high rotational velocities resemble the corresponding simulations where the flow inside the cutter head was determined by the CFD model (see paragraph 5.5). Results of these simulations are described in Appendix F. The simulations additionally show that for lower rotational velocities of the cutter head particles are sucked up.

Simulations with a negative slip factor

The opposite case would be when the blades have a large influence on the flow inside the cutter head. For instance when the pumping effect of the cutter head is large and there is an outgoing flow (near the cutter ring). This implies that in this region the water rotates faster than the cutter blades and thus a negative slip factor should be used in the simulation model. Simulations with C_{slip} = -0.2 showed different trajectories for the particles as compared to the simulations with C_{slip} = 0.5. The variations were especially significant when the rotational velocity of the cutter head was 90 or 120 RPM. Most of the times, the particles were longer in contact with the blade. This resulted in trajectories of the particles describing a full or nearly full rotation. Furthermore the particle generally left the blade at the leading edge which means that they were thrown out of the cutter head.

However, when C_d was 0.2 it was still possible that the particle left the blade at the trailing edge. This was mainly due to the fact that the drag forces were lower and thus the rotational velocity of the particle was lower as illustrated in Figure 8.18. The left plot shows the simulated particle trajectory, while C_d = 0.2 and the right plot the particle trajectory while C_d = 1. In the right plot the blade has made one full rotation and thus the initial and final position of the blade coincide. The particles were released from the same point with an initial velocity equal to the velocity of the blade. The rotational velocity of the cutter head was 90 RPM, the mixture velocity was 3 m/s and the slip factor was –0.2.

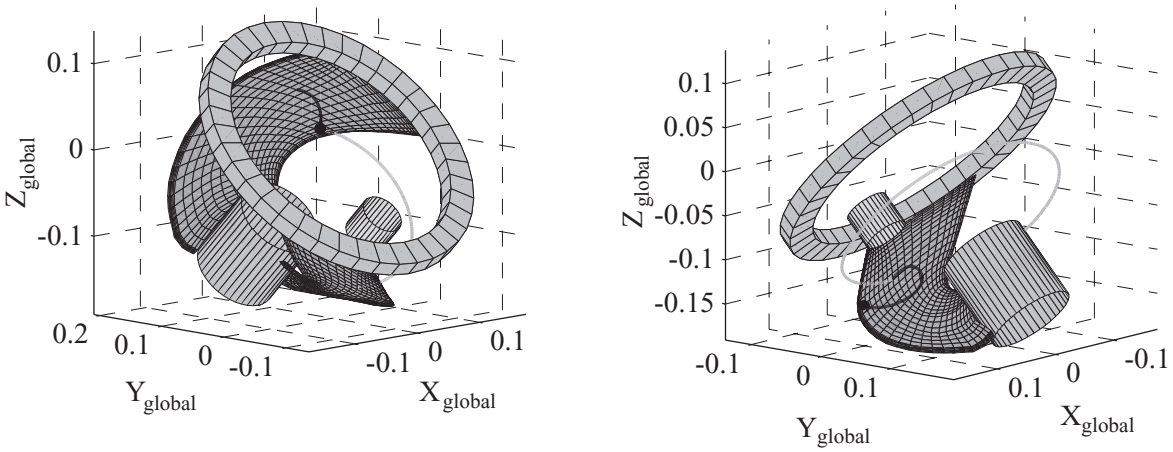

Figure 8.18: The trajectories of a particle with C_d coefficients of 0.2 (left) and 1 (right) respectively, while n_c = 90 RPM, v_m = 3 m/s and C_{slip} = -0.2

The simulation with C_d = 0.2 shows the same trend as the previous simulation. As the blade rotates faster than the particle, it leaves the blade at the trailing edge. In the simulation where C_d = 1 the particle describes a different trajectory. The relative trajectory appears to be elliptical. Initially the particle moves towards the trailing edge of the blade just like the situation where C_d = 0.2. The relative motion of the particle slightly changes direction and after a while the particle starts to move towards the leading edge of the blade. The reason for this is that when the particle starts to move downwards, the gravitational force and the drag force have a large component acting in the direction of rotation of the blade. Because of this the particle is accelerating towards the leading edge of the blade. The differences in trajectories of the particles can be further explained by examining the (relative) velocities of the particle. Figure 8.19 shows these relative velocities for both cases. For comparison the axes have a similar scale.

The particle velocities initially show the same trend in both cases. The relative tangential particle velocity shows that in the simulation where C_d = 1 the particle moves somewhat slower towards the trailing edge of the blade than when C_d = 0.2. As the particle is released underneath the suction pipe it will immediately experience the influence of the suction flow. Hence, the initial positive value for the relative axial particle and water velocity.

The influence of the suction flow is also clear for the axial particle and water velocity. These velocities have a positive value when the particle passes the suction pipe, which means that it moves towards the suction pipe (in axial direction).

Although the relative tangential particle and water velocities are negative, their absolute values are positive, for the rotational velocity of the blade has order of magnitude of 1 m/s when n_c = 90 RPM. At 0.05 s the axial particle velocity is 0.08 m/s while the absolute tangential particle velocity will be about 0.75 m/s. Thus, the absolute tangential particle velocity is much larger than the axial particle velocity. This explains why the particle does not show a distinct movement towards the suction pipe in Figure 8.18.

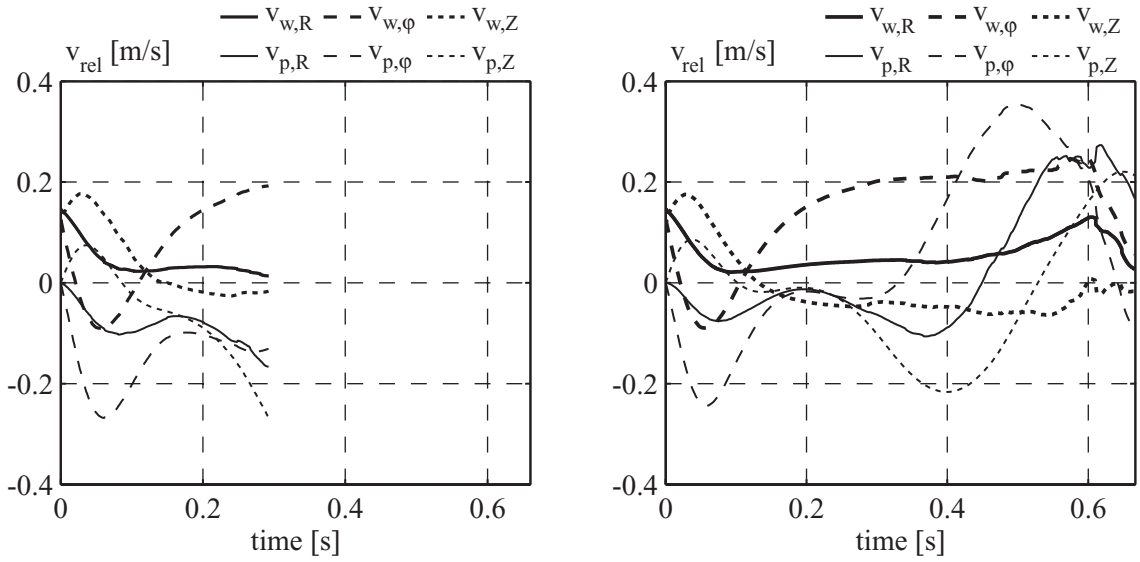

Figure 8.19: The relative velocities of a particle with C_d coefficients of 0.2 (left) and 1 (right) respectively, while n_c = 90 RPM, v_m = 3 m/s and C_{slip} = -0.2

As the particle moves slower towards the trailing edge of the blade when C_d = 1 the particle stays on the blade. While moving away from the suction pipe the influence of the suction pipe becomes smaller and the relative tangential water velocity becomes positive. The positive sign of the relative water velocity is the result of the negative slip factor of –0.2, letting the water rotate faster than the blade. Therefore, the relative particle velocity increases and becomes positive. It now moves towards the leading edge of the blade. The particle is even further accelerated towards the leading edge when the tangential component of the gravitational force becomes positive (see Figure 8.19). At a certain moment the tangential particle velocity is even larger than the tangential water velocity (between 0.4 s and 0.6 s).

The trajectory of a particle is determined by the sum of all external forces acting on the particle and its initial condition. Figure 8.20 shows the components in cylinder coordinates of the total external force acting on the particle for the simulations with C_d = 0.2 and C_d = 1 respectively.

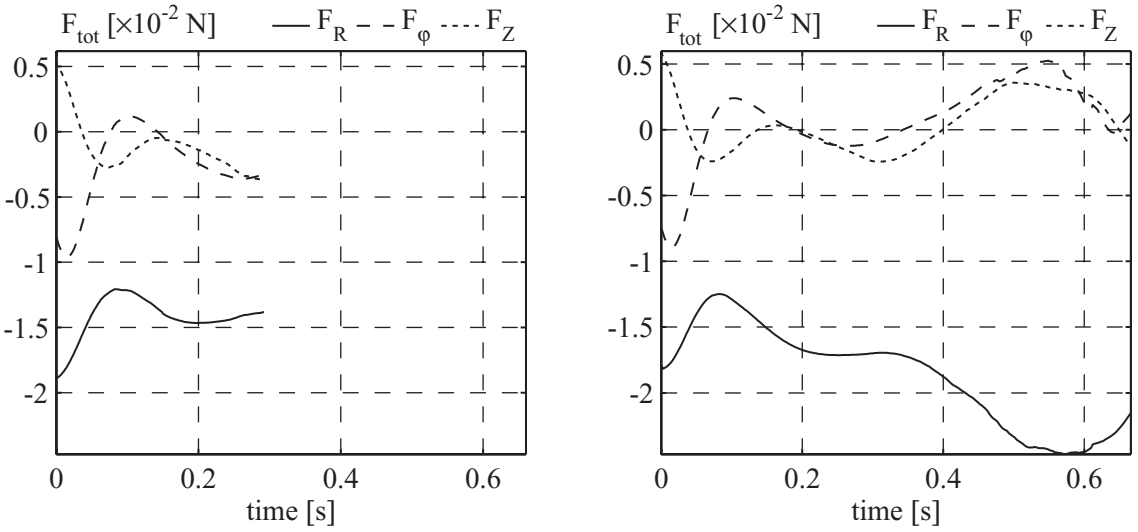

Figure 8.20: The total radial, tangential and axial forces on a particle with C_d coefficients of 0.2 and 1 respectively, while n_c = 90 RPM, v_m = 3 m/s and C_{slip} = -0.2

The total external force equals the mass of the particle multiplied by the acceleration terms. In tangential and radial direction these acceleration terms a_R and a_φ are defined as in Equation (8.10) and shown in Figure 8.21.

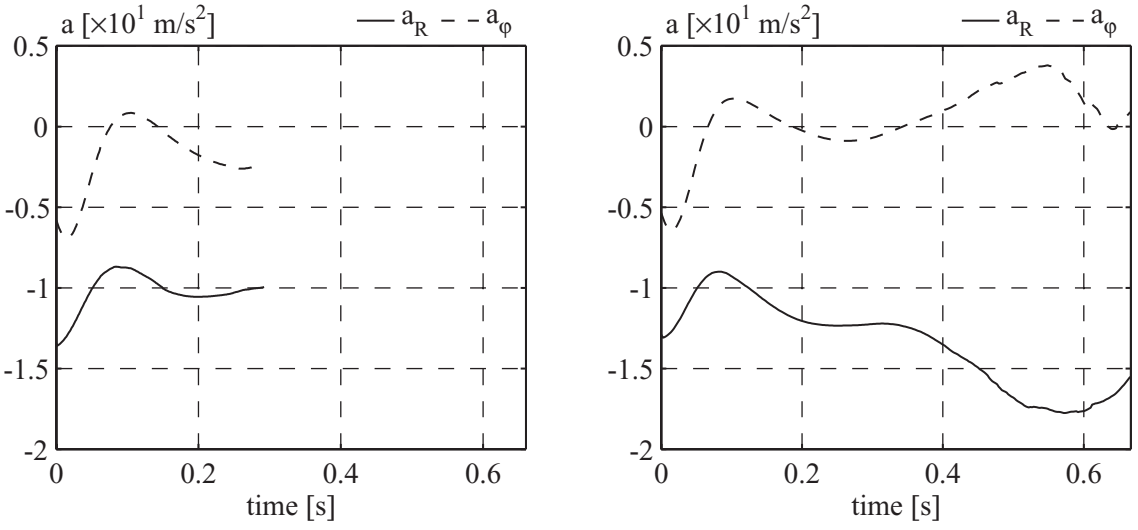

Figure 8.21: The radial and tangential acceleration terms for the simulations with C_d coefficients of 0.2 and 1 respectively, while n_c = 90 RPM, v_m = 3 m/s and C_{slip} = -0.2

Multiplied by the particle mass of 1.4×10^{-3} kg the acceleration terms equal the radial and tangential components of the total external force.

As shown in Equation (8.10) the radial acceleration term consists of the radial acceleration of the particle and the centrifugal acceleration. The tangential acceleration term consists of the tangential acceleration of the particle and the Coriolis acceleration. These centrifugal and Coriolis accelerations are shown in the following figure, where

$$\begin{aligned} \bar{a}_{cf} &= -R_p \dot{\varphi}_p^2 \bar{e}_R \\ \bar{a}_{cor} &= 2\dot{R}_p \dot{\varphi}_p \bar{e}_\varphi \end{aligned} \tag{8.27}$$

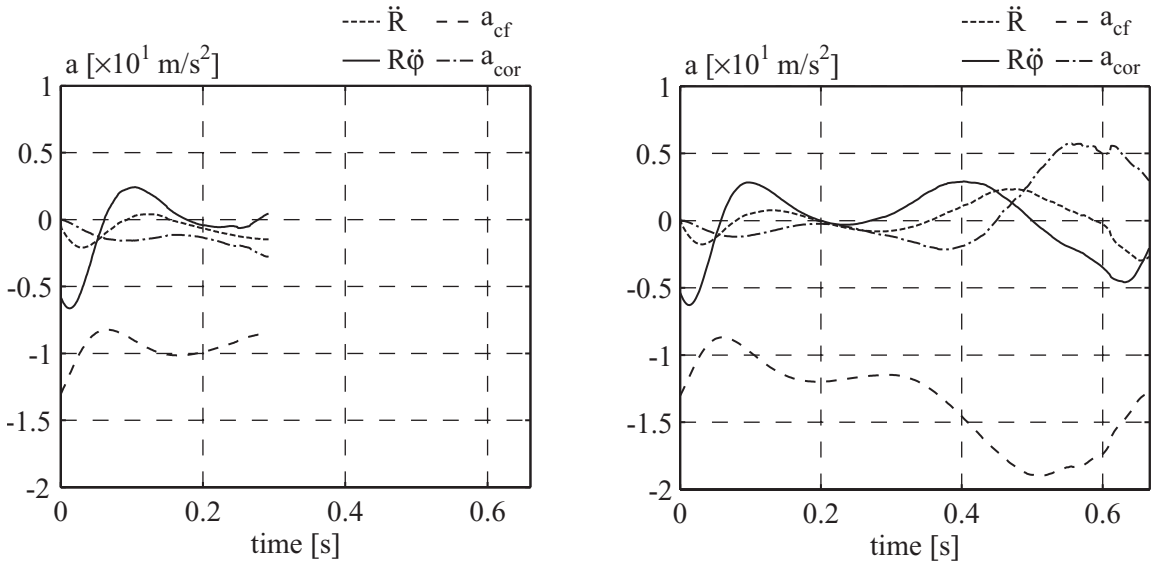

Figure 8.22: The acceleration components of a particle with C_d coefficients of 0.2 and 1 respectively, while n_c = 90 RPM, v_m = 3 m/s and C_{slip} = -0.2

The centrifugal acceleration is the dominant acceleration of the particle, which is mainly caused by the relatively large angular velocity of the particle. It is the centrifugal force that forces the particle to move in radial direction. Being restricted by the presence of the blade, the particle will not only move in radial direction, but it will slide along the surface of the blade towards the cutter ring.

The total external forces were shown in Figure 8.20 in cylindrical coordinates. Figure 8.23 and Figure 8.24 show the radial, tangential and axial components of the individual forces on the particle. The forces, in both simulations, do not differ that much from each other. As the particle is released underneath the suction pipe, the pressure gradient force is relatively large at the beginning of both simulations. While the particle moves away from the suction pipe the pressure gradient force decreases. Overall, the gravitational force is significant in all directions. The components in radial and tangential direction are sine curves because they are shown in a cylindrical coordinate system.

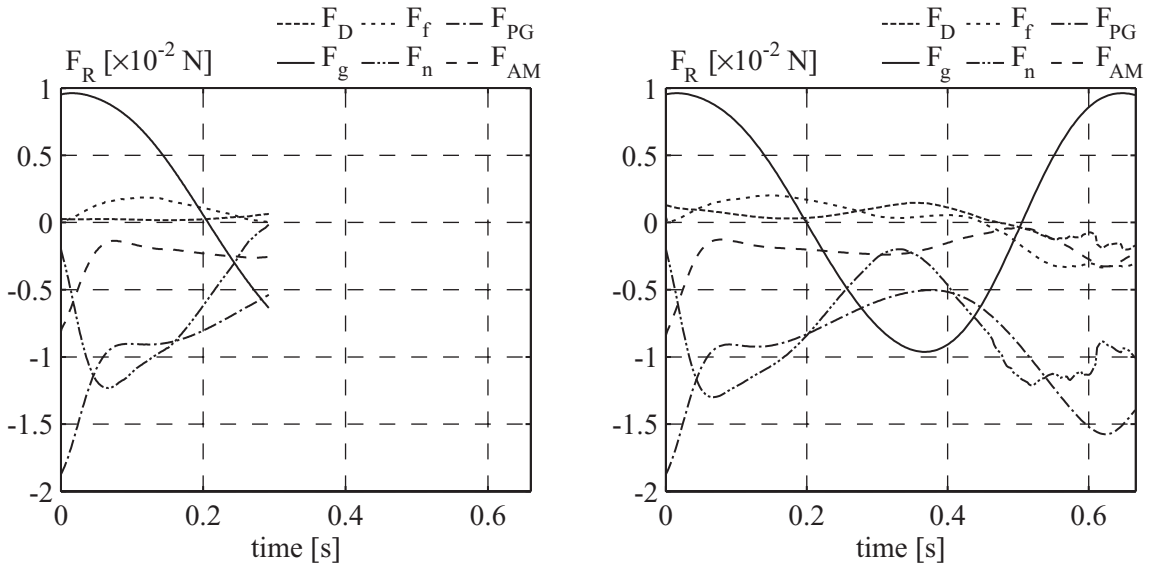

Figure 8.23: The radial components of the forces on the particle with C_d coefficients of 0.2 and 1 respectively, while n_c = 90 RPM, v_m = 3 m/s and C_{slip} = -0.2

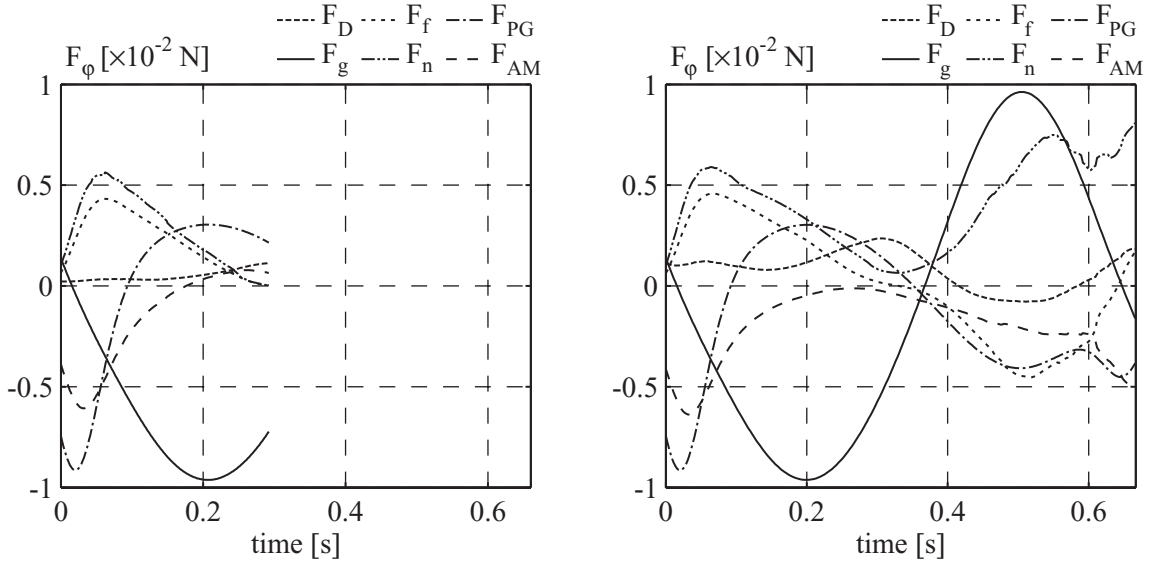

Figure 8.24: The tangential components of the forces on a particle with C_d coefficients of 0.2 and 1 respectively, while n_c = 90 RPM, v_m = 3 m/s and C_{slip} = -0.2

In both simulations the drag force is remarkably low in all directions. This is surprising as the rotational velocity of the cutter head is 90 RPM. The drag force is small because of the small difference in particle and water velocity as shown in Figure 8.19. The centrifugal forces in the simulations are so large ($\approx 1.4\times10^{-2}$ N) that the particle is 'pressed' against the blade and dragged along by the blade. Furthermore, due to the shape of the blade the centrifugal force has a component along the blade directed towards the leading edge of the blade. For parts of the particle trajectory this component compensates the gravitational force to some extent. So

apparently the particle is never accelerated or decelerated that much that its velocity will deviate significantly from the water velocities.

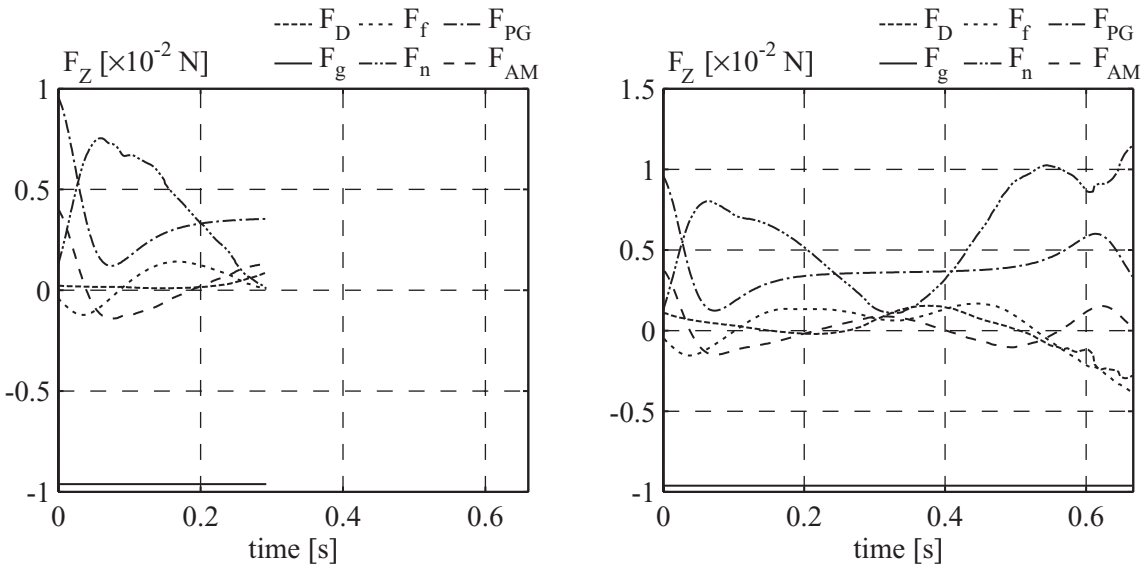

Figure 8.25: The axial components of the forces on a particle with C_d coefficients of 0.2 and 1 respectively, while n_c = 90 RPM, v_m = 3 m/s and C_{slip} = -0.2

The simulation with C_d = 0.2 stops after 0.3 s because the normal force becomes zero at this point. This means that the particle will no longer be in contact with the blade. The reason that the simulation with C_d = 1 does not stop at this point is that the drag force and consequently the angular particle velocity are higher than when C_d = 0.2. As the angular particle velocity is higher, the centrifugal force will be higher as well. In this case the centrifugal force is large enough to compensate the gravitational force (around t = 0.3 s) and keep the particle pressed against the blade.

Simulations with a relatively small slip factor

In the next simulation a particle with a C_d coefficient of 1 is released near the leading edge of the blade while the slip factor was 0.1. The rotational velocity of the cutter head was 120 RPM and the mixture velocity was 3 m/s. The particle was released right underneath the suction pipe with an initial velocity equal to the velocity of the blade. This simulation is not meant as a typical trajectory of a particle when the slip factor is low. It merely shows that under certain conditions the particle can leave the cutter blade at the leading edge of the blade, even though the slip factor is positive and the relative water velocity is directed towards the trailing edge. This is shown in Figure 8.26.

The relatively large centrifugal acceleration of the particle and the geometry of the blade are again the reasons for the movement of the particle towards the leading edge of the blade.

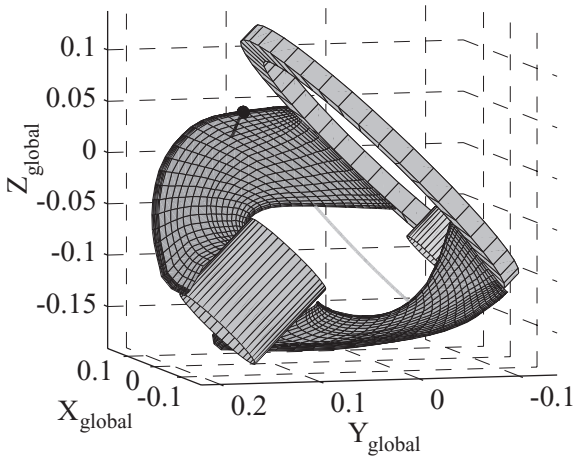

Figure 8.26: The trajectory of a particle for a simulation with $C_{slip} = 0.1$, $C_d = 1$, $n_c = 120$ RPM and $v_m = 3$ m/s

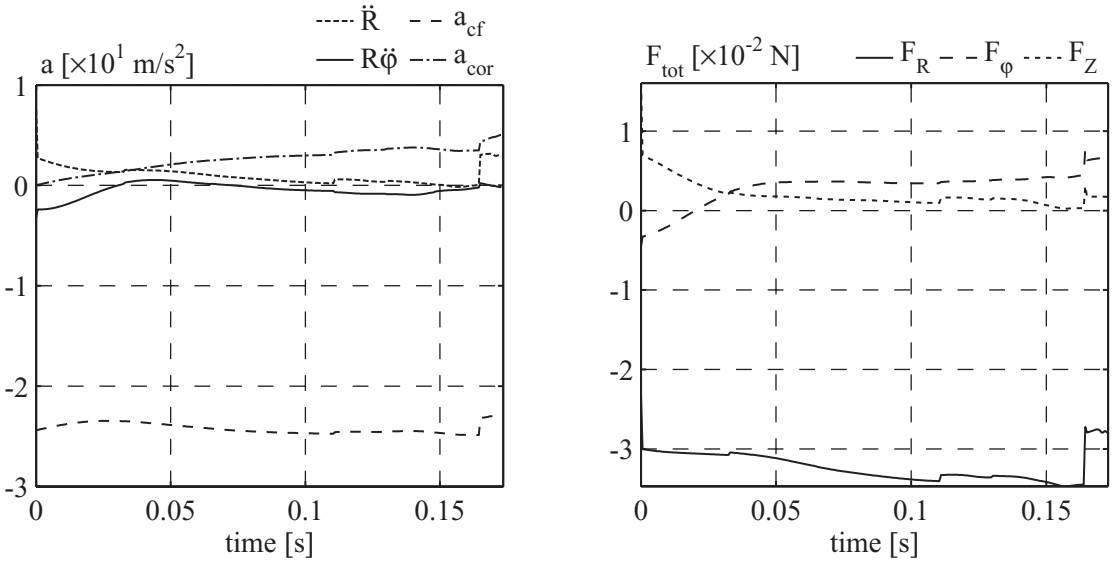

Figure 8.27: The accelerations and the radial components of the total resulting force acting on the particle for a simulation with $C_{slip} = 0.1$, $C_d = 1$, $n_c = 120$ RPM and $v_m = 3$ m/s

In the left plot of Figure 8.27 the body, the Coriolis and the centrifugal acceleration of the particle are shown (the subscript 'p', denoting particle, is omitted in the legend). As expected, the centrifugal acceleration is by far the largest and approximately 2.5 times the acceleration of gravity. In addition, the component of the centrifugal acceleration directed towards the leading edge of the blade is large enough to overcome the friction force, the drag force and the pressure gradient force. Therefore, the radial body acceleration $\ddot{R}_p$ is positive (shown in the left plot of Figure 8.27), although the resultant radial component of the external forces

$F_{R,tot}$ has a negative value (shown in the right plot of Figure 8.27). This is also clarified in Figure 8.28. The left plot illustrates that a positive radial acceleration of the particle corresponds with a movement of the particle towards the leading edge due to the offset of the blade angle (provided that the initial radial velocity of the particle is zero). In the right plot in Figure 8.28 the component of the centrifugal force towards the leading edge is represented by $\overline{F}_{cf} \cdot \overline{e}_{Xblade}$.

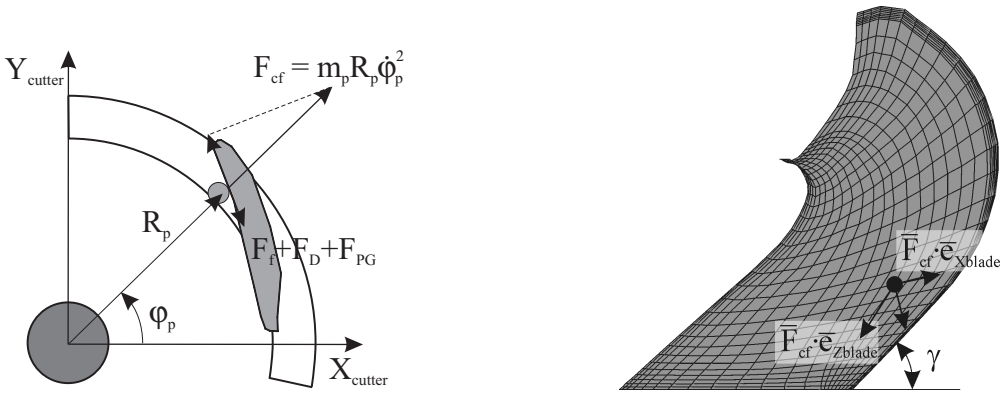

Figure 8.28: Movement of the particle towards the leading edge of the blade due to the large centrifugal acceleration and the geometry of the cutter blade

The right plot also shows that the component of the centrifugal force directed towards the cutter ring (indicated by $\overline{F}_{cf} \cdot \overline{e}_{Zblade}$) forces the particle towards the leading edge as well, due to the helical shape of the blade. Thus, besides the component of the centrifugal force along the blade, the helix angle γ will also have a significant influence on whether the particle will leave the blade at the leading edge. The generally negative value of the tangential body acceleration of the particle $R_p \ddot{\varphi}_p$ (see left plot in Figure 8.27) might seem contradictory to its motion towards the leading edge. This can be clarified by looking at the trajectory of the particle in the cutter coordinate system.

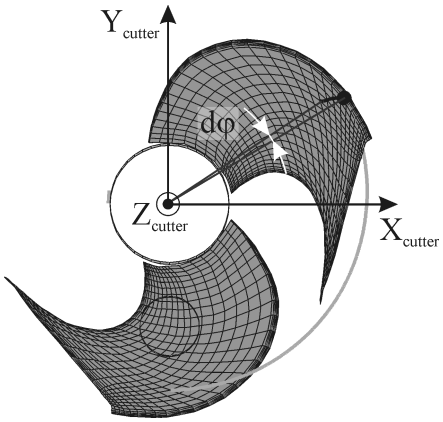

Figure 8.29: Trajectory of the particle viewed in the cutter coordinate system

Figure 8.29 shows that, with respect to its initial position, the relative angle of rotation $d\varphi$ at the end of the simulation has a negative value. This means that on average the particle's angular velocity has declined (initial angular velocity of the particle was ω_c) and the tangential body acceleration has a negative value.

8.4.5 Qualitative description of simulation results in relation to test results

In this paragraph a qualitative description is given of the simulations that have been performed. The results are compared with the test results.

In order to transport particles along the cutter blade towards the suction mouth a mixture velocity of about 5 m/s in the simulations was necessary. This is almost twice as high as the nominal mixture velocity. In addition, the particles had to be released close enough to the suction mouth, otherwise the suction flow did not have a relevant effect on the particle trajectory. This is comparable with the simulated particle trajectories in the free flow described in Chapter 5.

For slip factors, C_{slip}, higher than approximately 0.1 (indicating an inward flow) the particle always moved towards the trailing edge of the blade. The drag force acting on the particle was too large in comparison with the centrifugal force and the particle was decelerated with respect to the angular velocity of the blade. For a nominal mixture velocity of 2.5 to 3 m/s and rotational velocities beyond approximately 80 RPM, particles were transported towards the leading edge for slip factors of 0.1 and smaller. This means that for rotational velocities beyond 80 RPM, particles can be thrown out of the cutter head even though there is a (small) inward flow. Particles were thrown out of the cutter head more easily when the slip factor was negative, indicating an outward flow.

As described in Chapter 2, a fully inward flow only exists if the flow number $Q_s/\omega_c R_c^3$ is larger than 0.47 (or inverse flow number lower than 2.1). For the cutting tests performed and described in Chapter 6, this denotes that a fully inward flow only existed for the tests with a mixture velocity of 5 m/s and rotational velocities of 60 RPM and 80 RPM (see Figures 6.6 and 6.7). The large number of particles that were thrown out of the cutter head during the tests for rotational velocities beyond 80 RPM agrees qualitatively with the simulation results.

Whether the particle moved towards the leading edge of the cutter blade also depended on the initial position of the particle on the blade. The radius R_p has to be large enough, otherwise the centrifugal force is not large enough to overcome the drag and friction forces. The largest radius R_p is found near the cutter ring and near the tip of the blade as can be seen from Figure 8.29. Therefore, particles with initial positions close to the leading edge of the blade will be thrown out of the cutter head first. During the cutting tests and the tests with the silo, the video-recordings showed that particles could be thrown out of the cutter head along the entire contour of the cutter head. This was confirmed by the simulations. If the particles

were released near the leading edge of the blade, they could be thrown out of the cutter head within a short period of time. Particles that are cut right underneath the suction pipe can be thrown out of the cutter head within a quarter rotation of the cutter head. The flow of these particles can be represented by the trajectories indicated by '6' in Figure 6.9. On the other hand, this flow of particles may also consist of particles that have completed a full rotation about the cutter axis. Particles that are cut and initially move towards the trailing edge of the blade are accelerated towards the leading edge by the gravitational force when the blade is moving in the direction of gravity (moving downwards). This was also illustrated by the right plot in Figure 8.18. As the centrifugal acceleration of these particles increases, the axial transport of particles towards the cutter ring also increases. In several simulations it was possible to have the particle complete a full rotation about the cutter axis while transporting it axially towards the cutter ring and near the suction mouth. Being close to the suction mouth, the probability that the particle is sucked up is substantial. The particle trajectories resulting from the cutting tests and described in Figure 6.9 should be added with this 'possible' trajectory. In Figure 8.30 the trajectory is represented by the dashed line indicated by '7'.

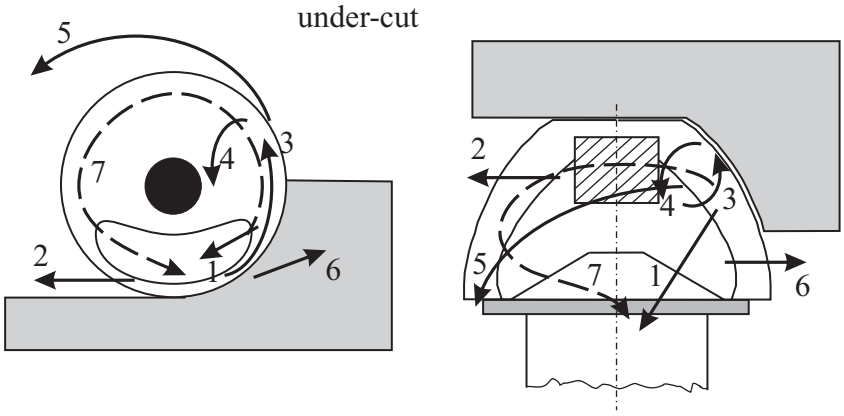

Figure 8.30: Particle trajectories resulting from the cutting tests added with the particle trajectory resulting from the simulations (dashed line indicated by '7')

The trajectory could not be observed from the video-recordings as it was impossible to trace single particles. Thus, the actual presence of trajectory '7' can not be validated although it is plausible. It may be possible that when trajectory '1' exists it has a positive effect on trajectory '7' as it prevents the particles from escaping (trajectory '6') and may drag them towards the suction mouth. Trajectory '1' should not be seen as the trajectory of a single particle but more of a layer of particles.

The presence of trajectories '1', '6' and '7' at the same time will strongly depend on the rotational velocity of the cutter head. A considerable rotational velocity is necessary to effectuate trajectories '6' and '7'. If the rotational velocity is too large, trajectory '1' will not exist as the suction flow will not be able to bend the particles towards the suction mouth in such a short time. It could be possible that trajectory '1' gives the general trajectories of the

productive particles when the rotational velocity is relatively small. If the rotational velocity is relatively large, the general trajectories of the productive particles gradually changes to trajectory '7'.

Most of the simulations have been performed with an initial position of the blade right underneath the suction mouth. This is the point where the blade enters the bank. As the blade moves farther into the breach it moves away from the suction mouth. The particles that are cut at these positions of the blade can only be sucked up directly if the ratio of the mixture velocity and rotational velocity is large enough. If not, the particle will have to describe a trajectory similar to trajectory '7' in Figure 8.30 in order to reach the suction mouth. This also resulted from simulations where the initial position of the blade was halfway between the points of entering and leaving the bank. Usually, a particle would have an initial motion towards the trailing edge of the cutter blade. At a certain point the particle will move towards the leading edge under influence of the gravitational force. As the particle is accelerated and the centrifugal force becomes large enough, the particle can move along the blade in axial direction towards the cutter ring.

As mentioned before, most of the time the flow number is smaller than 0.47 (certainly near the nominal values of the operational parameters). This means that most of the time an outward flow exists near the cutter ring and an inward flow exist near the hub. To improve the representation of the flow inside the cutter head a positive slip factor can be used near the hub while a negative slip factor can be used near the cutter ring, which is clarified in Figure 8.31. In the figure the relative water velocity is given; i.e. $(\omega_f - \omega_c)R_2$. The thick gray lines represent cross-sections of the blades near the hub (at distance R_1) and near the cutter ring (at distance R_2).

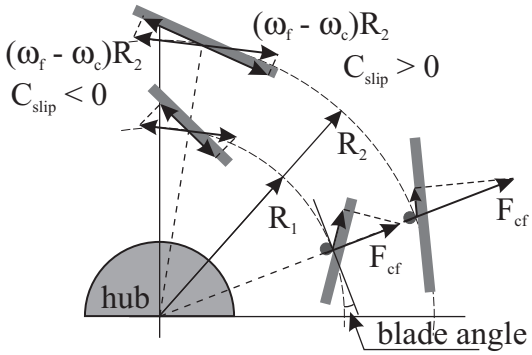

Figure 8.31: Modeling an inward or outward flow by means of varying C_{slip} and the effect of the centrifugal force for a particle near the hub and near the cutter ring

A negative value for C_{slip} indicates that the water rotates faster than the cutter blade; where C_{slip} is defined as in Equation (5.2).

$$C_{slip} = 1 - \frac{\omega_f}{\omega_c}$$

Setting the water velocity perpendicular to the blade's surface to zero will result in an outward flow (or inward if C_{slip} is positive).

Simulations with a rotational velocity of 90 RPM and 120 RPM have been performed in order to check the influence of the inward flow near the hub on the transport of particles along the cutter blade. As usually only half the cutter head is used to cut the rock the particle will have to travel over a large axial distance to reach the suction mouth. In the simulations that have been performed a value of 0.5 was used for the slip factor. It appeared that the axial transport of particles along the blade towards the cutter ring was clearly present for C_d coefficients of 0.2 (and 0.4). For a C_d coefficient of 1 the axial transport along the blade was also present but not as clear because the particle left the blade at the trailing edge after a short period of time. The subsequent trajectory of the particle will depend on the flow inside the cutter head.

The average velocity differences between water and blade resulting from the simulations were significant; i.e. about 0.6 m/s for the simulations with 90 RPM and 0.85 m/s for the simulation with 120 RPM. The reason that the particles were still able to move in axial direction for the lower values of the C_d coefficient is a combination of different factors:

- As the blade angle is larger near the hub than near the cutter ring, the component of centrifugal force directed towards the leading edge of the blade is comparatively larger. This was also illustrated in Figure 8.31. The drag force and the gravitational force can be compensated by this component of the centrifugal force where the resultant force towards either the leading or trailing edge is small.

- The larger blade angle causes a larger normal force and thus a larger friction force, which obstructs the movement of the particle towards the trailing edge.

- Due to the strong curvature of the blades in axial direction, the component of the centrifugal force along the blade which forces it towards the cutter ring is large. This can also be deduced from Figure 7.5. The more horizontal the inner contour of the cutter blades (which is near the hub), the larger the component of the centrifugal force along this contour. However, the radius R_p and thus the centrifugal acceleration will be smaller near the hub.

Thus, provided that the centrifugal force is large enough, the axial transport of particles near the hub is larger than near the cutter ring.

In the simulations the pump effect was not taken into account. The rotational velocity of the cutter head did not have an influence on the axial water velocities inside the cutter head. Therefore, the axial water velocities used in the simulations give an underestimation of

the actual axial water velocities. Taking into account the pump effect of the cutter head in the simulations will increase the axial transport of particles towards the cutter ring. Whether this will increase the production will depend on the magnitude of the centrifugal forces acting on the particles. Because of the larger centrifugal forces the particles are thrown out of the cutter head more easily. Furthermore, the outward water flow near the ring resulting from the pump effect can drag along particles as well.

Influence of the initial particle velocity

From simulations where the initial particle velocity has been varied it was concluded that the initial particle velocity has a significant effect on the particle trajectory. The initial particle velocities used in the simulations were: 0, equal to the water velocity and equal to the blade velocity. In reality (in the cutting tests that have been performed) the initial velocity of the particle can vary between the values as mentioned above, depending on the history of the particle and position on the blade. The simulations did show that independent of the initial velocity of the particle an axial motion of the particle towards the cutter ring was present to a certain extent. This is validated by the tests where the particles were brought in the cutter head by means of a silo and a tube. In these tests the initial velocity was clearly different compared with the actual cutting tests. Nevertheless, the production percentage did increase with increasing rotational velocity and the optimum rotational velocity was the same in both tests. It is therefore concluded that the initial velocity of the particles can not have a decisive influence on the increase in production with increasing rotational velocity.

Cutter head design aspects resulting from the simulations

It is not possible to give precise recommendations concerning the design of the cutter head as it depends on so many factors; many of which are not fully understood yet. Besides, the simulations have been performed with a simplified flow model and focused on the interaction between particle and the blade only. However, at this point it is possible to emphasize some aspects of the cutter head design that should be paid attention to.

- First of all, the cutter blades should be designed to guide the particles towards the suction mouth. The blade angle, the curvature of the blades and the conical shape of the cutter head play an important role in this.

- The movement of particles towards the leading edge of the blade should be avoided as much as possible. As the particle also moves in axial direction, the helix angle of the blade is an important factor in this.

- To facilitate the flow of particles through the suction mouth, the cutter blades should smoothly connect to the suction mouth. This means that possible blockage by the cutter ring should be avoided.

- Increasing the axial transport of particles along the blade should rather be accomplished by increasing the axial component of the centrifugal force along the cutter blade than by increasing the centrifugal force itself. The negative effects of a large rotational velocity on the production percentage clearly result from the cutting tests. Increasing the diameter of the cutter head will increase the centrifugal force acting on the particles but it will also increase the centrifugal pump action of the cutter head. This will increase the amount of particles thrown out of the cutter head. In addition, increasing the diameter of the cutter head will decrease the relative influence of the suction flow. This was also noticed in the tests performed by Slotta (1984).

Comments on the Euler integration scheme

For solving the differential equations the forward (explicit) Euler method has been used. Basically this method is instable and small time steps are needed (Press, 1999). For simulating the trajectory of a single particle, a small time step is not considered a problem when regarding the computing time. Furthermore, the time step has to be small anyway because of the discontinuity of the equation of motion. The discontinuity is caused by the repositioning of the particle on the blade after each time step (see Appendix E.3). Larger time steps and thus larger displacements of the particle would result in larger errors when reposition the particle on the blade.

However for future development of the model it is worthwhile to study other integration methods, at least for stability. A method that is absolutely stable is the backward Euler (or implicit) scheme. This method comes down to the following scheme:

$$y(t+\Delta t) = y(t) + \Delta t \dot{y}(t+\Delta t) \tag{8.28}$$

As the velocity at time t+Δt is used to calculate the position at time t+Δt it is called the backward Euler method. Off course for accuracy the time step size Δt can not be too large but stability is always ensured.

Another method to solve the set of differential equation would be the use of the Newmark Algorithm. The general Newmark algorithm (Newmark, 1959) is given by

$$\begin{aligned} y(t+\Delta t) &= y(t) + \Delta t^2 \left(\tfrac{1}{2} - \beta\right) \ddot{y}(t) + \Delta t^2 \beta \ddot{y}(t+\Delta t) \\ \dot{y}(t+\Delta t) &= \dot{y}(t) + \Delta t (1-\gamma) \ddot{y}(t) + \Delta t \gamma \ddot{y}(t+\Delta t) \end{aligned} \tag{8.29}$$

where β and γ are constant integration parameters depending on assumptions on $\ddot{y}$ within the time step and determine integration accuracy and stability. When taking β = 0 and γ = ½, the Newmark algorithm results in the well known central difference scheme.

Whether these algorithms will really make it possible to use larger time steps without affecting the accuracy needs to be determined by trial and error (implementation in the

simulation model). At least these algorithms will increase the stability of the integration method.

8.5 Conclusions

Scaling the fluid according to the Euler number and geometrically scaling the particle ensures similarity of the particle trajectories on prototype and model scale. General values have been used for the drag, added mass and the mechanical friction coefficient without taking into account the particle shape and the presence of the blade in great detail. As the particle Reynolds number lies within the Newton range on prototype scale, equal drag coefficients requires that the particle Reynolds number is in the Newton range as well on model scale.

In the equation of motion the lift force acting on the particle is neglected, as it is an order of magnitude lower than the other forces. In practice the lift force may have a larger (and significant) influence as the vorticity of the fluid may be larger in reality. This is especially true in front of the suction pipe where the rotational flow and suction flow have perpendicular directions.

The imposed flow field was simplified considerably as the influence of the blades on the flow field (pump effect) was not taken into account. Nonetheless, some basic trends and the influence of the variables on the particle trajectories could be established.

Simulations describing the trajectory of a particle along the cutter blade show that the blade's geometry in combination with the centrifugal force can be responsible for the axial motion of particles towards the cutter ring. This could explain the increase in production with increasing rotational velocity as resulted from the cutting tests. The axial motion is certainly visible for rotational velocities of the cutter head beyond 80 RPM on model scale (which corresponds with 28 RPM on prototype scale). The axial transport of particles along the blade is generally higher near the hub due to the larger blade angle and the strong curvature of the blades near the hub. Therefore, in this region, the component of the centrifugal force along the blade's surface is larger.

The slip factor had a significant influence on the particle trajectory. For slip factors beyond 0.1 the particles always left the blade at the trailing edge. For these large slip factors the time the particle was in contact with the blade was relatively short. Therefore, the axial motion of the particle along the blade was less distinct. For slip factors smaller than 0.1 (negative values indicate an outward flow) particles could leave the blade at the leading edge which implies that they are thrown out of the cutter head. Comparable with the cutting tests this happened

near the cutter ring. Due to the helix angle of the blade the particle reached the leading edge of the blade sooner as it moved towards the cutter ring.

The influence of the drag coefficient was significant but not unambiguous, as it is closely related to the flow inside the cutter head. The drag coefficient and the slip velocity are determinative for the value (and direction) of the drag force. For large drag coefficients the particle is more inclined to follow the fluid and its trajectory will strongly depend on the flow field inside the cutter head.

The simulations showed that instead of a trajectory directly towards the suction mouth, the particles that were sucked up could also have made a full rotation. This requires that these particles are in contact with the blade for a relatively long period of time.

The trajectories have been determined for single particles only. When a concentration of particles is present, the flow inside the cutter head may alter significantly. In addition, particle-particle interaction should be accounted for. Nonetheless, the component of the centrifugal force acting along the surface of the blade will still be present and can force the particles towards the cutter ring.

Most of the time the forces acting on the particle have the same order of magnitude. However, for relatively low rotational velocities on model scale (i.e. 40 RPM) the gravitational force is dominant. For large rotational velocities (i.e. 120 RPM), the centrifugal force acting on the particle is usually the largest force but only exceeding the gravitational force by a factor 2 to 3.

Chapter 9
Conclusions and Recommendations

Main conclusion regarding this research:

- Particles trajectories are similar on model and prototype scale if the flow inside the cutter head is scaled according to the Euler number and the particles are scaled geometrically. Additionally, in accordance with prototype scale the particle Reynolds number has to be in the Newton range on a model scale as well. This demand determines the lower limit for the model scale.

- Tests where single particles were injected in a rotating cutter head showed large fluctuations of the particle residence times. Whereas increasing the mixture velocity resulted in a decrease in residence time, the influence of the rotational velocity of the cutter head was not that unambiguous. However, for every rotational velocity there appeared to be a threshold value below which none of the injected particles was sucked up. Considering the high residence times of single particles inside the cutter head, it is unlikely that the processes inside the cutter head can completely be represented by single particle models.

- Simulations of the particle trajectories showed that the superposition of a forced vortex and a sink to represent the flow inside the cutter head was too simplistic. The absence of the pump effect of the cutter head results in an underestimation of the axial water velocities. The influence of the suction flow decreases rapidly as the distance towards the suction mouth increases. For the lower rotational velocities the gravitational force is generally the dominant force. For larger rotational velocities there is no distinct dominant external force. The lower production in over-cut situation as experienced in practice could be explained by the larger velocity of the particles as they pass the suction mouth. In

under-cut situation the suction flow acts on the particle over a longer period of time (work done by the suction flow is larger in under-cut than in over-cut).

- Cutting tests in under-cut situation with a crown cutter head showed that an increase in mixture velocity always resulted in an increase in production percentage. For every mixture velocity there is an optimum rotational velocity. The production percentage initially increases with increasing rotational velocity. Beyond the optimum rotational velocity the production percentage decreases with increasing rotational velocity as a result of the increasing magnitude of the centrifugal forces acting on the particles. The increase in production percentage with increasing rotational velocity is most likely caused by the component of the centrifugal force acting along the blade and directed towards the cutter ring. The pump effect of the cutter head, and especially the increasing axial water velocities, may be responsible as well for the initial increase in production.
- When entering the bank the cutter head appears to fill up with particles first before a production rate is established. Then the production rate increases until a stationary situation has been reached. At this point the filling degree of the cutter head is nearly constant, assuming a constant spillage flow. In addition, the filling degree of the cutter head does have an influence on the production percentage. This means that the single particle model will neglect processes that actually should be accounted for.
- Decreasing the ladder inclination angle results in a significant increase in production. This is caused by a decreasing influence of gravity and a better inclusion of the cutter head in the bank.
- Particle inertia and particle collisions dominate over the effects of fluid viscosity. For lower rotational velocities gravitational stresses dominate over grain-collisions stresses, while for higher rotational velocities the grain-collisions stresses at least have the same order of magnitude as the gravitational stresses.

- Tests with a cylindrical cutter head did not show the increase in production with increasing rotational velocity verifying the significant influence of the crown cutter blade geometry.

- Simulations describing the trajectory of a particle along the cutter blade shows that the blade's geometry in combination with the centrifugal force can be responsible for the axial motion of particles. The slip factor (a measure for the velocity difference between water and blade), had a large influence on the particle trajectories. For slip factors beyond 0.1 (indicating large inward flow) the particles always left the blade at the trailing edge within a short period of time and the axial motion along the blade was less distinct. For slip factors smaller than 0.1 (negative value indicating an outward flow) particles could leave the blade at the leading edge, which implies that they are thrown out of the cutter head.

The axial transport of particles is clearly visible for rotational velocities beyond 80 RPM (on model scale) and larger near the hub due to the strong curvature of the blades.

- Particle trajectories are uniform on model and prototype scale if the fluid flow is scaled according to the Euler number and the particle is scaled according to the Froude number. On both scales the particle Reynolds number will be in the Newton range, which ensures equal drag coefficients.
- For lower rotational velocities gravitational forces are dominant, while for the larger rotational velocities (beyond 90 RPM) the external forces approximately have the same order of magnitude. Between 90 RPM and 120 RPM, the centrifugal acceleration varies from approximately the same value as the acceleration of gravity up to three times the acceleration of gravity.
- The drag coefficient, initial velocity and initial position of the particle have a significant influence on the exact particle trajectory.
- Particles that are sucked up could have made a full rotation while staying in contact with the blade. This could not be verified by the video-recordings of the cutting tests, as the view was often obstructed and individual particles could not be traced.

- The CFD model that has been set up, parallel to this study, to determine the flow inside the cutter head does not give acceptable results for higher rotational velocities as the pump effect is not correctly taken into account. To what extent the CFD model gives acceptable results for lower rotational velocities needs to be investigated further.

Recommendations:

- The model for particle trajectories should include the influence of particle-particle interaction. The feasibility of a continuum model for the particles in suspension needs to be investigated. Instead of focusing on single particles in contact with the blades, layers of particles should be described.
- The model for particle trajectories along the cutter blades and the model for the particle trajectories in the free flow should be coupled (hybrid model).
- Further research is needed on the flow inside the cutter head, especially for higher rotational velocities. The use of alternative (commercial) CFD software is recommended. The influence of the particle on the flow should be accounted for, especially the particle layers on the blades.
- The influence of the particle shape should be accounted for in the model. Then the freedom of motion of the particle should be extended to enable particle rotation. This means that the equation of motion for the particle should be extended with the equations for the torque in three directions.

- More research is needed on the influence of the blade geometry on particle trajectories and cutter head production.

- Tests on a larger scale should be performed to validate the scale laws.
- By measuring the production and spillage only, the cutter head still remains a black box. Under-water cameras provide useful information on general particle flows but individual particles can not be traced. Additional measurements while cutting (e.g. particle tracking and residence time measurements) would significantly increase the knowledge on the processes taking place inside the cutter head.
- For an initial comparison of the productivity of cutter heads with different geometries the test set up where particles were brought in the cutter head by means of a silo can be used. It is less time consuming than actual cutting tests and more cost-effective.

Appendix A
Dimensionless Navier-Stokes Equations

A.1 Dimensionless Navier-Stokes equations

Performing scale tests requires a geometrical scaling of the cutter head. Furthermore, the cutter head will have to produce similar flow patterns on both scales. These demands are satisfied when the Navier-Stokes equations describing the flow produce analogous results on both scales. The full Navier-Stokes equations (for incompressible and non-diffusive fluid) are

$$\rho_f \frac{\partial \bar{v}_f}{\partial t} + \rho_f \bar{v}_f \cdot \nabla \bar{v}_f = -\nabla p + \mu \nabla^2 \bar{v}_f + \rho_f \bar{g} \qquad \text{(A.1)}$$

in which ρ_f is the fluid density, v_f is the fluid velocity, p is the fluid pressure, μ is the coefficient of viscosity and g is the acceleration of gravity. The terms on the left hand side of the equation denote the acceleration of a volume of fluid. The first term on the right hand side gives the forces on the volume of fluid due to the pressure gradient. The second term on the right hand side results from the shear stresses and the third term gives the volume force due to gravity. The bar above the parameters implies that these are vectors.

When the variations in density that occur in the cutter head are taken into account the fluid density ρ_f consist of a hydrostatic (ρ_0) and a hydrodynamic component (i.e. variation $\Delta\rho$). Then the Navier-Stokes equations can be written as:

$$\left(1 + \frac{\Delta\rho}{\rho_0}\right)\left(\frac{\partial \bar{v}_f}{\partial t} + \bar{v}_f \cdot \nabla \bar{v}_f\right) = -\frac{1}{\rho_0}\nabla p + \frac{\mu}{\rho_0}\nabla^2 \bar{v}_f + \left(1 + \frac{\Delta\rho}{\rho_0}\right)\bar{g} \qquad \text{(A.2)}$$

Furthermore, the total pressure, p, is the sum of the hydrostatic (p_s) and the hydrodynamic pressure (p_d). In the Navier-Stokes equations the total pressure can be replaced by the hydrodynamic pressure p_d ($p_d = p - p_s$). And thus

$$\left(1+\frac{\Delta\rho}{\rho_0}\right)\left(\frac{\partial\overline{v}_f}{\partial t}+\overline{v}_f\cdot\nabla\overline{v}_f\right)=-\frac{1}{\rho_0}\nabla p_d+\frac{\mu}{\rho_0}\nabla^2\overline{v}_f+\frac{\Delta\rho}{\rho_0}\overline{g} \tag{A.3}$$

As the Navier-Stokes equations are too complex to obtain general solutions, it is better to normalize these equations by means of certain relevant scales. Normalization will lead to dimensionless parameters which represent the relative importance of various parts of the full equations. The following parameters are introduced to represent the typical scales: L for length scale, U for velocity scale, T for time scale, P_f for fluid pressure scale (or rather pressure difference). Note that the pressure scale P_f is yet unknown. This results in the following dimensionless variables

$$\overline{v}_f' = \overline{v}_f / U,\ t' = t/T,\ \overline{x}' = \overline{x}/L,\ p_d' = p_d / P_f,\ \overline{g}' = \overline{g}/g$$

The dimensionless Navier-Stokes equations now become

$$\left(1+\frac{\Delta\rho}{\rho_0}\right)\left(\frac{L}{TU}\frac{\partial\overline{v}_f'}{\partial t'}+\overline{v}_f'\cdot\nabla'\overline{v}_f'\right)=-\frac{P_f}{\rho_0 U^2}\nabla' p_d'+\frac{\nu}{UL}\nabla'^2\overline{v}_f'+\frac{\Delta\rho}{\rho_0}\frac{gL}{U^2}\overline{g}' \tag{A.4}$$

where ν is the kinematic viscosity of the fluid. In the equation the following dimensionless parameters are recognized.

$$\frac{UL}{\nu} = \text{Reynolds number} = \text{Re} \sim \frac{\text{inertia}}{\text{viscous force}}$$

$$\frac{P_f}{\rho_f U^2} = \text{Euler number} = \text{Eu} \sim \frac{\text{pressure}}{\text{inertia}}$$

$$\frac{L}{TU} = \text{Strouhal number} = \text{St} \sim \frac{\text{local acceleration}}{\text{convective acceleration}}$$

$$\frac{\rho_0}{\Delta\rho}\frac{U^2}{gL} = (\text{densimetric}) \text{ Froude number}^2 = \text{Fr}^2 \sim \frac{\text{inertia}}{\text{gravity}}$$

Reynolds number

Analogous flow patterns are achieved when the dimensionless parameters in Equation (A.4) are equal on prototype and model scale. For a prototype cutter head with a diameter of 3 m, a nominal rotational velocity of 30 RPM and a suction flow of 4 m^3/s, a typical value for the velocity scale U is 4 m/s. With the cutter head diameter representing the typical length scale L, the Reynolds number has order of magnitude

$$\text{Re} \approx 1\times10^7$$

Hence, the Reynolds number is large enough to ignore the viscous stresses.

Euler number

The Euler number gives the ratio of the pressure and inertia forces. According to Bernoulli the pressure difference (P_f) in the cutter head is proportional with ($\frac{1}{2}\rho U^2$. Assuming that the pressure losses are small, the Euler number has order of magnitude

$$Eu \approx 1$$

Note that the Euler number indirectly demands for a geometrical scaling of the cutter head as well. The pressure difference P_f is scaled correctly with ρU^2 if the coefficients for pressure losses are equal on both scales. Large abnormalities in the geometries on both scales could result in different values for these coefficients and thus in pressure losses that are scaled incorrectly.

Strouhal number

For determining the Strouhal number it is initially assumed that the time scale T is governed by the residence time of the fluid in the cutter head. For the above mentioned cutter head with an internal volume of 5 m^3 the residence time of the fluid depends on the total ingoing flow Q_i (i.e. the sum of the suction flow Q_s and the outgoing flow Q_o). Assuming that the outgoing flow varies between 0 and the same value as the suction flow the residence time t_r varies between (Q_s = 4 m^3/s)

$$\frac{V_c}{2Q_s} \le t_r \le \frac{V_c}{Q_s}, \text{ or } \quad 0.63 \text{ s} \le t_r \le 1.25 \text{ s}$$

Therefore a typical value for the time scale would be 1 s. Then, the Strouhal number becomes

$$St = \frac{L}{TU} = \frac{3}{1 \cdot 4} = 0.75$$

For the characteristic time scale of the flow T, the residence time of a fluid particle was chosen. This is acceptable for (almost) stationary flows where the suction flow is dominant and the rotational velocity of the cutter head is low. For high rotational velocities of the cutter head the flow is not stationary and T is governed by the time scale of changes in the flow. Roughly, the following classification for the rotational velocity of the cutter head on prototype scale can be used

- low rotational velocity: 20 RPM
- nominal rotational velocity: 30 RPM
- high rotational velocity: 40 RPM

In the case of a high rotational velocity the specific time based on the cycle of the cutter head would be the characteristic time scale. Then, for a cutter head with 6 blades, the characteristic time scale for the fluid is 0.25 s. This is a factor 2.5 to 5 smaller than when the characteristic time scale is governed by the residence time. Then the Strouhal number becomes:

$$St = \frac{L}{TU} = \frac{3}{0.25 \cdot 4} = 3$$

Which indicates that for larger rotational velocities the Strouhal number becomes more important.

Densimetric Froude number

The densimetric Froude number gives an indication of the effect of the density differences in the fluid. This can be significant for phenomena competing with buoyancy or settling processes. Large density differences over large length scales can lead to significant density currents. Experience from practice indicates that for the cutting of rock the maximum density is about 1170 kg/m^3. As only half the cutter head is placed in the bank a representative value for the length scale L is 1.5 m. Then the Froude number becomes

$$Fr^2 = \frac{\rho_0}{\Delta\rho}\frac{U^2}{gL} = \frac{1000}{170}\frac{4^2}{9.81 \cdot 1.5} = 6.4$$

indicating that the inertial forces are dominant over the gravitational forces. The inverse of the Froude number (the latter term in the dimensionless Navier-Stokes equations) has a value of 1/6.4 = 0.16. This is a factor 5 to 19 lower (for low and high rotational velocities respectively) than the Strouhal number and a factor 5 lower than Euler number.

For the single particle model that is set up in this thesis an Eulerian-Langrangian approach is chosen. The flow inside the cutter head is modeled as if only water is present. The particles have no influence on the flow and the density variations in the fluid due to the presence of the particles are neglected. Neglecting the density variations in the term before the fluid accelerations on the left side of the Navier-Stokes equations (Boussinesq approximation) can be reasoned by noting that:

$$\frac{\Delta\rho}{\rho_0} = 0.17$$

which is significantly smaller than 1. Besides, this is considered to be a maximum value. In general the relative density variations will be smaller than 0.17. For the latter term on the right hand side of the Navier-Stokes equations, neglecting the density variations will cause an inaccuracy of 20% at most (as the densimetric Froude number is a factor 5 lower than the Euler number). Without the density variations the Navier-Stokes equations can be simplified to result in the following dimensionless Euler equation

$$\frac{L}{TU}\frac{\partial \overline{v}_f'}{\partial t'} + \overline{v}_f' \cdot \nabla' \overline{v}_f' = \frac{P_f}{\rho_f U^2} \nabla' p_d' \tag{A.5}$$

Hence the relevant parameters for scaling the flow are the Strouhal and Euler number. As it is fair to assume that the time scale is proportional with the ratio of the length scale and velocity scale, the demand for equal Strouhal numbers is automatically met. Hence, the parameter for scaling the flow is the Euler number.

A.2 General equation of motion for particle in fluid

Taking into account the drag force, added mass force, pressure gradient force, lift force gravitational force and buoyancy force, the equation of motion for a single particle in a fluid can be written as (see Chapter 5)

$$\begin{aligned}\rho_p \frac{d\overline{v}_p}{dt} = {} & \frac{3}{4}\frac{C_d}{d_p}\rho_f \left(\overline{v}_f - \overline{v}_p\right)\left|\overline{v}_f - \overline{v}_p\right| + \rho_f C_{AM}\left(\frac{D\overline{v}_f}{Dt} - \frac{d\overline{v}_p}{dt}\right) + \rho_f \frac{D\overline{v}_f}{Dt} \\ & + C_L \rho_f \left(\overline{v}_f - \overline{v}_p\right) \times \overline{\Omega} + \left(\rho_p - \rho_f\right)\overline{g}\end{aligned} \tag{A.6}$$

in which ρ_p is the density of the particle, v_p is the particle velocity, v_f is the fluid velocity, d_p is the particle diameter, C_d is the drag coefficient, C_{AM} is the added mass coefficient, C_L is the lift coefficient and $\overline{\Omega}$ is the vorticity. Furthermore

$$\frac{d}{dt} = \frac{\partial}{\partial t} + \overline{v}_p \cdot \nabla \quad \text{and} \quad \frac{D}{Dt} = \frac{\partial}{\partial t} + \overline{v}_f \cdot \nabla \tag{A.7}$$

Substituting

$$\overline{v}_s = \overline{v}_f - \overline{v}_p$$

in which v_s is the slip velocity, gives

$$\begin{aligned}\left(\rho_p + \rho_f C_{AM}\right)\frac{d\overline{v}_s}{dt} = {} & -\frac{3}{4}\frac{C_d}{d_p}\rho_f \overline{v}_s \left|\overline{v}_s\right| + \left(\rho_p - \rho_f\right)\left(\frac{D\overline{v}_f}{Dt} + \overline{g}\right) \\ & - C_L \rho_f \overline{v}_s \times \overline{\Omega}\end{aligned} \tag{A.8}$$

The equation of motion is made dimensionless by using the following definitions

$$\overline{v}_f' = \overline{v}_f / U_f,\ \overline{v}_s' = \overline{v}_s / U_s,\ \overline{x}' = \overline{x} / L,\ t_f' = t / T_f,\ t_p' = t / T_p,\ \overline{\Omega}' = \overline{\Omega} T_f,\ \overline{g}' = \overline{g} / g$$

Note that a specific time scale for both the particle and the fluid is introduced. Here T_f denotes the time scale for changes in the flow with respect to the moving particle and T_p the time scale for the moving particle.

The dimensionless equation of motion becomes

$$\left(\rho_p+\rho_f C_{AM}\right)\frac{U_s}{T_p}\frac{d\overline{v}_s'}{dt_p'}=-\frac{3\rho_f C_d}{4}\frac{U_s^2}{d_p}\overline{v}_s'\left|\overline{v}_s'\right|+\left(\rho_p-\rho_f\right)\left(\frac{U_f}{T_f}\frac{\partial\overline{v}_f'}{\partial t_f'}+\frac{U_f^2}{L}\overline{v}_f'\cdot\nabla'\overline{v}_f'+g\overline{g}'\right)$$
$$-C_L\rho_f\frac{U_s}{T_f}\overline{v}_s'\times\overline{\Omega}' \qquad \text{(A.9)}$$

and divided by $\rho_f g$

$$\frac{\left(\rho_p+\rho_f C_{AM}\right)}{\rho_f}\frac{U_s}{gT_p}\frac{d\overline{v}_s'}{dt_p'}=-\frac{3C_d}{4}\frac{U_s^2}{d_p g}\overline{v}_s'\left|\overline{v}_s'\right|$$
$$+\frac{\left(\rho_p-\rho_f\right)}{\rho_f}\left(\frac{U_f}{gT_f}\frac{\partial\overline{v}_f'}{\partial t_f'}+\frac{U_f^2}{gL}\overline{v}_f'\cdot\nabla'\overline{v}_f'+\overline{g}'\right)-C_L\frac{U_s}{gT_f}\overline{v}_s'\times\overline{\Omega}' \qquad \text{(A.10)}$$

Again the Strouhal number and Froude number can be recognized in the dimensionless parameters when considering ‘g’ as a length scale divided by the squared time scale. Generalizing, they can be subdivided into Strouhal and Froude numbers for the particle and the flow, i.e.

$$Fr_p^2=\frac{U_s^2}{gd_p},\quad Fr_f^2=\frac{U_f^2}{gL},\quad St_p=\frac{U_s}{gT_p},\quad St_f=\frac{U_f}{gT_f},\quad St_{pf}=\frac{U_s}{gT_f}$$

From the dimensionless equation of motion is can be seen that when performing scale tests ρ_p, ρ_f, C_{AM} and C_L need to be equal on prototype and model scale. Furthermore, U_s and U_f need to be scaled correspondingly for dynamic (and kinematic) similarity and thus the characteristic time scales for both particle and fluid need to be scaled correspondingly. The particle Froude number states that the diameter of the particle is scaled according to the same length scale L provided that the drag coefficient C_d is equal on both scales. As the drag coefficient is a function of the particle Reynolds number and thus on its diameter this is not evident.

Drag coefficient and particle inertia

The drag coefficient of a particle is determined by the particle Reynolds number Re_p

$$Re_p=\frac{\left|v_s\right|d_p}{\nu}$$

In the Newton range (Re_p >1000) the drag coefficient is a constant. On a prototype scale, a characteristic measure for the particle diameter is 0.08 m. If the particle Reynolds number is in the Newton range the slip velocity needs to be larger than

$$Re_p=\frac{\left|v_s\right|d_p}{\nu}>1000,\quad \left|v_s\right|>0.0125\ \text{[m/s]}$$

Since the typical water velocity in the cutter head is 4 m/s it is fair to assume that the difference in velocity between water and particle is larger than 0.0125 m/s. In the Newton range the drag coefficient is 0.4 for spherical particles and 1.1 for irregularly shaped particles (van Rijn, 1984).

An important parameter for the behavior of the particles in the flow is the ratio of the particle relaxation time and the characteristic time scale for the flow. With the particle relaxation time being a characteristic time required for a particle to adjust or relax to a new condition of forces (Hinds, 1982). If this relaxation time is much smaller than the characteristic time scale for the flow, the particle will follow the fluid as if inertialess. On the other hand, the larger this ratio the more inertia will play a role and the less the particle is likely to follow the fluid. The general definition for the relaxation time of a particle in a fluid is

$$t_p = \frac{4}{3}\frac{\rho_p}{\rho_f}\frac{1}{C_d}\frac{d_p}{\left|v_f - v_p\right|} \tag{A.11}$$

A more practical definition for the particle relaxation time for heavy particles is the ratio of the terminal settling velocity and the acceleration of gravity (Fuchs, 1964).

$$t_p = \frac{v_{ts}}{g} \tag{A.12}$$

Assuming the following typical values on prototype scale

$\rho_p = 2650$	[kg/m^3]
$\rho_f = 1000$	[kg/m^3]
$d_p = 0.08$	[m]
$C_d = 0.4 - 1.1$	[-]
$v_{ts} = 1.3 – 2.1$	[m/s]

and using Equation (A.12), the particle relaxation time lies between

$$0.13 \text{ s} < t_p < 0.21 \text{ s}$$

The characteristic time scale for the flow can either be the residence time of the fluid or the specific time based on the cycle of the cutter head. The residence time of a fluid particle varies between 0.63 s and 1.25 s and the specific time based on the cycle of a cutter head is about 0.25 s. This means that the particle relaxation time and the characteristic time scale for the flow are approximately of the same order of magnitude over a wide range. Therefore, particle inertia will play an important role on prototype scale.

Conclusions on scaling parameters

Based on the dimensionless parameters in the Navier-Stokes equations and the dimensionless equation of motion for the particle, it is concluded that the particle size should be scaled geometrically. Then

- the particle Reynolds number is large enough on both scales to assume that it is the Newton range, which implies that the drag coefficient is constant and equal on both scales.
- the fluid velocities are scaled according to the square root of the length scale. The flow is uniform on prototype and model scale as $\omega_c R_c^3/Q_s$ (ratio of circumferential speed and suction flow) is equal on both scales. Furthermore, the Euler number is equal on both scales when assuming similar pressure losses.
- the particle (settling) velocity and the fluid velocities are scaled similarly and thus the particle trajectories are uniform on both scales.
- the ratio of the characteristic times scales for the particle and fluid are equal on both scales. The particle will therefore react in a similar manner to changes in the flow on model scale as on prototype scale.

A.3 Influence of turbulence on particle motion

As shown before, the Reynolds number of the flow inside the cutter head has order of magnitude 1×10^7 on prototype scale. As the cutter blades are not designed for optimal flow conditions as is the case for instance with impeller blades, it is likely that the flow does not leave the trailing edge smoothly. Therefore the flow inside the cutter head will be highly turbulent. The effect of the turbulent eddies on the particle motion can be represented by the ratio of the particle relaxation time and the time scale of the turbulent eddies (i.e the Stokes number). If the particle relaxation time is much smaller than the time scale of the turbulent eddies, turbulence will have an effect on the particle's motion.

It was shown that on a prototype scale the relaxation time of the particle varies between

$$0.13 \text{ s} < t_p < 0.21 \text{ s}$$

The times scale of the turbulent eddies t_e is defined as

$$t_e = \frac{l_e}{u'} \tag{A.13}$$

in which l_e represents the eddy length scale and u' the turbulent velocity fluctuation. Only eddies with a large enough length scale ($l_e > d_p$) will have a significant influence on the particle trajectory. Due to the lack of sufficient knowledge on the flow in cutter heads the actual size of the largest eddies and the corresponding velocity fluctuations are not known.

On the other hand, it is reasonable to assume that the largest eddies are determined by the cutter head geometry. This means that the eddies at the trailing edges of the blades approximately equal the radius of the cutter ring as shown in Figure A.1.

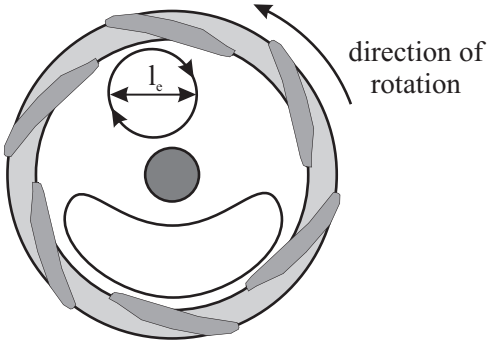

Figure A.1: Large eddy at the trailing edge of a cutter blade

The turbulent velocity fluctuations associated with these macro eddies are assumed to have the same order of magnitude as the average fluid velocity (say $0.5\omega_c R_c$). The time scale of the eddies then becomes

$$t_e = \frac{R_c}{0.5\omega_c R_c} = \frac{1}{0.5\omega_c}$$

As on a prototype scale the rotational velocities vary between 20 RPM and 40 RPM, the time scale of the turbulent eddies varies between:

$$0.48\ s < t_e < 0.95\ s$$

This means that the Stokes number (t_p/t_e) varies between

$$0.14 < \text{Stokes} < 0.44$$

Turbulence will have an effect on the particle's motion if the Stokes number is small (Stokes<<1). According to the values of the Stokes number derived above, this is not the case. Here it should be taken into account that the size of the turbulent eddies will generally be smaller than is assumed here. Consequently the time scale of the turbulent eddies will generally be lower and the Stokes number will be higher. Thus it is fair to assume that the turbulent velocity fluctuations will not have a significant effect on the particle's motion. The inertia of the particle is too large to follow the turbulent fluid fluctuations.

It should be noted that turbulence may be enhanced by the large size of the particles due to the wake of the particles or vortex shedding (Hetsroni, 1989).

Order of magnitude of the dimensionless groups in the equation of motion

Using the dimensionless equation of motion and characteristic values for the different parameters on prototype scale, the relative importance of the forces acting on the particle can be determined. The dimensionless equation of motion was:

$$\frac{\left(\rho_p+\rho_f C_{AM}\right)}{\rho_f}\frac{U_s}{gT_p}\frac{d\overline{v}_s'}{dt_p'}=-\frac{3C_d}{4}\frac{U_s^2}{d_p g}\overline{v}_s'\left|\overline{v}_s'\right| + \frac{\left(\rho_p-\rho_f\right)}{\rho_f}\left(\frac{U_f}{gT_f}\frac{\partial\overline{v}_f'}{\partial t_f'}+\frac{U_f^2}{gL}\overline{v}_f'\cdot\nabla'\overline{v}_f'+\overline{g}'\right)-C_L\frac{U_s}{gT_f}\overline{v}_s'\times\overline{\Omega}'$$

On a prototype scale the following values are applicable.

ρ_p = 2650 kg/m^3	U_s = 2 m/s	L = 3 m	C_{AM} = 0.5
ρ_f = 1000 kg/m^3	U_f = 4 m/s	d_p = 0.08 m	C_D = 0.4 – 1.1
	T_f = 0.3 – 1.3 s	g = 9.81 m/s^2	C_L = 0.2
	T_p = 0.2 s		

The characteristic scale for the slip velocity, U_s, is supposed to have the same order of magnitude as the terminal settling velocity of the particle. The characteristic time scale for the fluid is based on a rotational velocity of the cutter head of 30 RPM (T_f = 0.3 s) and the residence time of fluid in the cutter head (T_f = 1.3 s). For the lift coefficient the generally accepted value for spherical particles of 0.2 is taken. This value is slightly arbitrary as according to Kurose et al. (2001) the lift coefficient for solid particles at large particle Reynolds numbers (Re_p > 100) can even be lower than 0.2. The dimensionless groups have the following values:

$$\frac{\left(\rho_p+\rho_f C_{AM}\right)}{\rho_f}\frac{U_s}{gT_p}=3.2 \qquad \frac{\left(\rho_p-\rho_f\right)}{\rho_f}\frac{U_f^2}{gL}=0.9$$

$$\frac{3C_d}{4}\frac{U_s^2}{gd_p}=1.5-4.2 \qquad \frac{\left(\rho_p-\rho_f\right)}{\rho_f}=1.65$$

$$\frac{\left(\rho_p-\rho_f\right)}{\rho_f}\frac{U_f}{gT_f}=0.5-2.2 \qquad C_L\frac{U_s}{gT_f}=0.03-0.14$$

Considering these values it is justified to neglect the lift force in comparison with the other forces.

Appendix B
Additional Information on the Residence Times of Single Particles

B.1 General Characteristics of a Gamma Distribution

The gamma probability density function is described by the following function

$$f_t(t) = \frac{t^{\alpha-1}}{\Gamma(\alpha)\beta^{\alpha}} e^{\frac{-t}{\beta}},\ t>0 \qquad \text{(B.1)}$$

where t represents time and

$\alpha\beta$ = mean μ
$\alpha\beta^2$ = variance σ^2

The gamma cumulative distribution function $F_t(t)$ is

$$F_t(t) = \int_0^t f_t(t)\,dt \qquad \text{(B.2)}$$

Figure B.1 gives an example of the gamma probability density function and the gamma cumulative distribution function when $\alpha = 4.8$ and $\beta = 0.5$. Thus the average (or mean) is 2.4 s and the variance is 1.2 s. From the plot of the gamma cumulative distribution function it can be seen that average of 2.4 s indeed coincides with a $F_t(t)$ of 0.5, which is a 50% probability.

The asymmetric trend of the curves and the fact that the distribution is zero for $t \leq 0$ agree with the expectations for the distribution of residence times of particles in the cutter head. If the functions shown in Figure B.1 are representative for the residence times of the particles it

would mean that in this specific case 50% of the injected particles are sucked up within 2.4 s. Moreover, within approximately 6 s all the injected particles are sucked up.

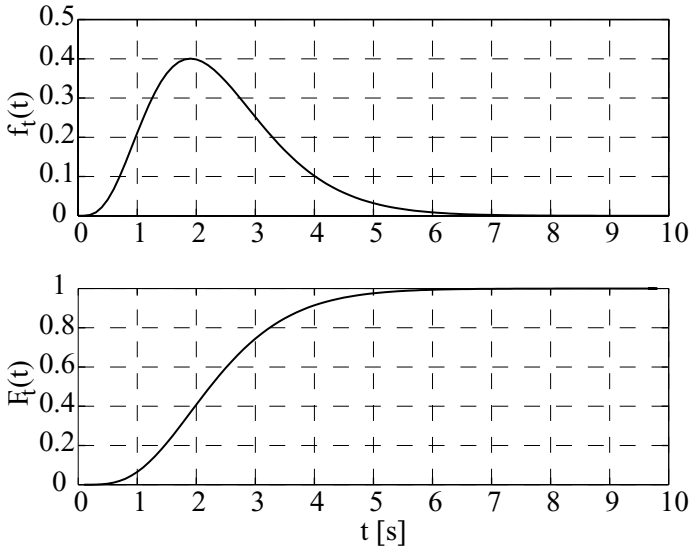

Figure B.1: Example of the gamma probability density function and the gamma cumulative distribution function

Method of maximum-likelihood

For each test 20 particle were injected. In other words each test has been repeated 20 times. Based on this sample an attempt is made to define the parameters that describe the above mentioned distribution functions, i.e. α and β. An infinite number of samples would be needed to exactly determine α and β. Instead, based on the probability distribution of the variables in the sample and the unknown parameter (α or β), an interval is created that, with a certain reliability, contains the unknown parameter (Lange, de 1989).

The maximum likelihood method is a method to find the values for the unknown parameters that would have most likely produced the data we in fact observed. To do this, estimators with a certain distribution, are used to represent the parameters. For example $\hat{a}$ and $\hat{b}$ could be the estimates for the parameters α and β. For large sample sizes, the maximum likelihood estimates will have an approximate normal distribution centered on the true parameter value. Assuming a normal distribution, a 95% confidence interval is created for $\hat{a}$ and $\hat{b}$. The true values of α and β are assumed to be the mean values of $\hat{a}$ and $\hat{b}$

B.2 Overview of the Averages and Standard Deviations of the Residence Times

In this paragraph the following variables are mentioned

n_c	rotational velocity of the cutter head	[RPM]
v_m	mixture velocity in the suction pipe	[m/s]
d_p	diameter of the particle	[m]
ρ_p	density of the particle	[kg/m^3]
μ_t	average residence time	[s]
σ_t	standard deviation of the residence times	[s]

The averages and standard deviations are derived from 20 samples.

Table B.1: Tests in the under-cut situation

Note that the gray shading in certain cells in the tables imply that these tests have not been performed.

ρ_p = 2600 kg/m^3; d_p = 6 mm

	v_m = 1.5 m/s		v_m = 2.0 m/s		v_m = 2.5 m/s		v_m = 3.0 m/s	
n_c	μ_t	σ_t	μ_t	σ_t	μ_t	σ_t	μ_t	σ_t
40					29.10	24.77	29.20	30.18
50			45.50	18.29	14.40	12.12	10.40	8.04
60	49.80	13.86	35.80	26.20	14.30	10.26	4.00	3.21
70	50.70	16.68	15.50	10.15	8.00	7.85	5.00	2.35
80	50.29	14.74	16.00	11.96	3.80	2.15	5.89	3.75
90	47.00	12.29	17.78	12.96	4.80	2.89	3.50	1.29

Note! For v_m = 1.5 m/s and 2.0 m/s the values are based on a limited amount of measurements and not reliable for the actual residence time.

ρ_p = 2600 kg/m^3; d_p = 10 mm

	v_m = 1.5 m/s		v_m = 2.0 m/s		v_m = 2.5 m/s		v_m = 3.0 m/s	
n_c	μ_t	σ_t	μ_t	σ_t	μ_t	σ_t	μ_t	σ_t
40					32.30	28.42	10.80	10.65
50			29.90	19.36	9.00	7.06	6.50	5.11
60			16.00	12.49	17.50	16.86	5.90	5.96
70			13.44	8.35	6.50	4.44	4.90	3.52
80			18.13	7.27	9.60	8.42	3.56	2.65
90			20.50	16.94	6.88	5.00	4.30	2.74

ρ_p = 2200 kg/m^3; d_p = 6 mm

	v_m = 1.5 m/s		v_m = 2.0 m/s		v_m = 2.5 m/s		v_m = 3.0 m/s	
n_c	μ_t	σ_t	μ_t	σ_t	μ_t	σ_t	μ_t	σ_t
30	25.20	23.17	6.40	4.93	4.20	3.98	2.50	1.70
40	35.50	38.85	5.90	5.50	8.00	9.43	1.30	0.52
50	48.60	17.98	12.20	12.52	2.40	1.20	2.20	1.53
60	53.00	20.22	30.00	26.32	6.00	4.24	2.20	1.29
70	38.37	32.05	12.11	10.00	4.50	2.99	2.40	1.10
80	23.67	13.75	8.60	7.44	3.20	1.32	2.67	1.02
90	17.14	16.67	5.33	3.02	4.22	2.83	2.60	1.27

Note! For v_m = 1.5 m/s the values are based on a limited amount of measurements and not reliable for the actual residence time.

ρ_p = 2200 kg/m^3; d_p = 10 mm

	v_m = 1.5 m/s		v_m = 2.0 m/s		v_m = 2.5 m/s		v_m = 3.0 m/s	
n_c	μ_t	σ_t	μ_t	σ_t	μ_t	σ_t	μ_t	σ_t
40			2.40	1.10	1.80	0.76	1.30	0.52
50	25.60	19.61	2.50	1.38	2.10	1.34	1.30	0.52
60	35.44	28.41	4.30	2.38	2.50	1.20	1.50	0.74
70	23.50	18.39	6.70	5.31	3.40	2.21	2.00	1.05
80	24.57	14.77	15.90	13.78	3.50	2.41	1.90	1.00
90	24.00	22.49	8.25	5.83	5.00	1.78	1.78	0.65

Note! For v_m = 1.5 m/s the values are based on a limited amount of measurements and not reliable for the actual residence time.

ρ_p = 1400 kg/m^3; d_p = 6 mm

	v_m = 1.5 m/s		v_m = 2.0 m/s		v_m = 2.5 m/s		v_m = 3.0 m/s	
n_c	μ_t	σ_t	μ_t	σ_t	μ_t	σ_t	μ_t	σ_t
30	3.30	2.65	2.10	1.27	1.50	0.51	1.90	1.52
40	3.80	1.73	1.20	0.35	1.20	0.35	1.50	0.62
50	3.70	1.86	2.00	1.05	1.50	0.51	1.60	0.64
60	3.40	1.92	2.90	1.82	2.40	1.42	1.80	0.63
70	4.50	2.71	2.10	0.95	1.90	0.85	2.40	1.39
80	5.44	4.70						
90	3.57	1.64	2.78	1.29	1.90	0.58	2.30	0.95

ρ_p = 1400 kg/m^3; d_p = 10 mm

	v_m = 1.5 m/s		v_m = 2.0 m/s		v_m = 2.5 m/s		v_m = 3.0 m/s	
n_c	μ_t	σ_t	μ_t	σ_t	μ_t	σ_t	μ_t	σ_t
30	1.70	0.80	1.50	0.62	1.10	0.25	1.40	0.70

40	3.10	2.24	1.80	1.11	1.30	0.43	1.10	0.25
50	4.30	2.26	2.50	1.62	1.40	0.66	1.10	0.25
60	3.60	1.89	1.70	0.65	1.60	0.64	1.30	0.43
70	6.20	4.63	1.90	0.58	1.60	0.64	1.40	0.48
80	5.20	3.77						
90	4.22	3.05	3.22	1.86	1.60	0.64	1.67	0.66

Table B.2: Tests in the over-cut situation

ρ_p = 2600 kg/m^3; d_p = 6 mm

	v_m = 1.5 m/s		v_m = 2.0 m/s		v_m = 2.5 m/s		v_m = 3.0 m/s	
n_c	μ_t	σ_t	μ_t	σ_t	μ_t	σ_t	μ_t	σ_t
50			16.20	14.97	9.80	6.37	12.00	11.52
60	35.71	15.79	18.90	17.45	4.50	2.90	3.10	1.95
70	19.63	22.31	10.14	8.78	6.60	4.97	3.30	1.72
80	20.00	15.52	8.14	5.17	6.00	5.09	3.10	2.48
90	31.90	24.96	7.75	2.01	7.40	6.15	2.40	1.41

Note! For v_m = 1.5 m/s the values are based on a limited amount of measurements and not reliable for the actual residence time.

ρ_p = 2600 kg/m^3; d_p = 10 mm

	v_m = 1.5 m/s		v_m = 2.0 m/s		v_m = 2.5 m/s		v_m = 3.0 m/s	
n_c	μ_t	σ_t	μ_t	σ_t	μ_t	σ_t	μ_t	σ_t
50			29.10	20.21	12.20	10.51	9.10	3.29
60	42.20	18.60	27.50	22.22	10.00	7.89	3.50	1.31
70	30.60	12.02	15.70	8.03	10.56	6.97	4.20	2.25
80	44.90	21.87	21.20	17.03	8.88	6.30	6.00	2.58
90	44.78	19.87	23.30	18.42	9.80	4.88	4.80	2.00

Note! For v_m = 1.5 m/s the values are based on a limited amount of measurements and not reliable for the actual residence time.

ρ_p = 2200 kg/m^3; d_p = 6 mm

	v_m = 1.5 m/s		v_m = 2.0 m/s		v_m = 2.5 m/s		v_m = 3.0 m/s	
n_c	μ_t	σ_t	μ_t	σ_t	μ_t	σ_t	μ_t	σ_t
40	44.30	23.06	22.70	18.41	20.70	13.24	9.50	6.91
50	22.56	16.08	10.50	6.26	6.20	4.31	4.70	2.24
60	16.63	9.07	7.00	3.38	2.70	1.50	2.50	1.49
70	12.60	13.75	8.90	4.69	2.60	1.24	2.80	1.08
90	17.56	15.38	4.40	2.84	2.10	0.95	2.20	1.10

Note! For v_m = 1.5 m/s the values are based on a limited amount of measurements and not reliable for the actual residence time.

ρ_p = 2200 kg/m^3; d_p = 10 mm

	v_m = 1.5 m/s		v_m = 2.0 m/s		v_m = 2.5 m/s		v_m = 3.0 m/s	
n_c	μ_t	σ_t	μ_t	σ_t	μ_t	σ_t	μ_t	σ_t
40	34.60	23.57	21.56	18.27	15.20	13.92	7.60	4.85
50	38.56	20.32	10.40	7.30	4.70	1.48	4.20	1.82
60	24.50	20.03	12.11	9.53				
70	23.00	19.67	10.40	6.32	4.60	1.61	3.10	1.19
80	18.67	16.10						
90	23.00	20.28	8.89	6.30	4.00	2.72	3.40	1.68

Note! For v_m = 1.5 m/s the values are based on a limited amount of measurements and not reliable for the actual residence time.

ρ_p = 1400 kg/m^3; d_p = 6 mm

	v_m = 1.5 m/s		v_m = 2.0 m/s		v_m = 2.5 m/s		v_m = 3.0 m/s	
n_c	μ_t	σ_t	μ_t	σ_t	μ_t	σ_t	μ_t	σ_t
20	34.00	25.28	33.40	33.52	5.60	4.14	2.70	0.76
30	7.80	6.06	4.30	2.28	8.90	11.13	10.30	13.16
40	8.00	6.12	2.10	0.82	2.50	1.04	1.70	0.51
50	7.60	4.71	2.30	1.01	1.90	0.58	1.30	0.43
60	5.11	2.35	2.00	0.87	2.80	1.24	1.40	0.48
70	3.90	2.10	2.60	1.46	1.90	0.58	1.70	0.80
90	2.33	1.75	1.90	0.73	2.00	0.87	1.80	0.63

ρ_p = 1400 kg/m^3; d_p = 10 mm

	v_m = 1.5 m/s		v_m = 2.0 m/s		v_m = 2.5 m/s		v_m = 3.0 m/s	
n_c	μ_t	σ_t	μ_t	σ_t	μ_t	σ_t	μ_t	σ_t
20	24.40	24.49	15.50	14.92	4.40	2.42	1.90	0.73
30	5.90	4.45	3.20	1.43	2.60	1.01	2.20	0.89
40	6.30	3.19	7.90	10.22	2.40	0.83	1.90	0.90
50	6.67	3.79	2.60	0.97	2.10	0.75	1.40	0.48
60	7.40	6.77						
70	3.33	2.13	3.90	2.01	2.40	1.32	1.50	0.51
90	4.00	2.06	1.78	0.65	3.70	2.23	1.20	0.35

Appendix C
Test Matrices for the Cutting Tests in Cemented Banks of Gravel

The test matrix of all performed tests in the cemented banks of gravel are given in the table below. The actual values of the parameters during the tests could vary slightly from these values.

Table C.1: Overview of all the cutting tests performed

Under cut					**Over cut**			
v_m	n_c	v_h	ξ		v_m	n_c	v_h	ξ
2.0	60	0.1	0.31		3.0	70	0.1	0.40
2.0	80	0.1	0.23		3.0	90	0.1	0.31
2.0	100	0.1	0.19					
					3.5	70	0.1	0.47
2.5	60	0.1	0.39		3.5	90	0.1	0.36
2.5	70	0.1	0.33					
2.5	80	0.1	0.29		4.5	91	0.1	0.46
2.5	90	0.1	0.26		4.5	110	0.1	0.38
2.5	120	0.1	0.20					
3.0	60	0.1	0.47					
3.0	70	0.1	0.40					
3.0	80	0.1	0.35					
3.0	90	0.1	0.31					
3.0	120	0.1	0.23					
3.5	70	0.1	0.47					

3.5	80	0.1	0.41	
3.5	90	0.1	0.36	
3.5	115	0.1	0.29	
5.0	60	0.1	0.78	
5.0	80	0.1	0.59	
5.0	100	0.1	0.47	
5.0	120	0.1	0.39	

in which ξ denotes the flow number

Additional tests

Table C.2: Tests performed with average particle diameter of 15 mm

v_m	n_c	v_h	ξ
3.0	60	0.1	0.47
3.0	90	0.1	0.31
3.0	120	0.1	0.23
4.0	100	0.1	0.38

Table C.3: Tests performed with cutter axis inclination angle of 25°

v_m	n_c	v_h	ξ
3.0	70	0.1	0.40
3.0	90	0.1	0.31
3.0	120	0.1	0.23

Appendix D
Average Volumetric and Transport Concentration Resulting from the Cutting Tests

A radioactive density meter with a systematic error of ± 2% was used for measuring the density of the mixture in the suction pipe. The integration time of the density meter was 1 s. The measurements showed that because of the short integration time, the measured density fluctuated heavily. The amplitude of the fluctuations was approximately 8 kg/m^3. This means that the random error of the measured density (noise) is ± 0.8%.

For interpretation of the test results and in order to get an impression of the production percentage, it is more convenient to plot the volumetric concentration than the density of the mixture. The volumetric concentration is defined as

$$c_v = \frac{\rho_m - \rho_w}{\rho_p - \rho_w} \tag{D.1}$$

in which ρ_m is the measured density of the mixture, ρ_w is the density of water and ρ_p is the density of the gravel particles. The volumetric concentration of the gravel bank is 0.64 which agrees with the maximum value for a dense packing of particles. The average volumetric concentrations resulting from the under-cut situation are plotted in Figure D.1.

The left plot in Figure D.1 shows the calculated average volumetric concentrations for the under-cut situation, where the volumetric concentration is averaged over the entire cutting phase. The volumetric concentrations are very low, especially for the low mixture velocities. As the density meter only measures within a certain cone in the suction pipe (not the entire cross-section) and the concentration of particles is very low, it is arguable whether the measured densities are very accurate. Still, the average volumetric concentration shows the same trend as the production curves. At each mixture velocity the volumetric concentration

initially increases with increasing rotational velocity. After a certain optimum has been reached the volumetric concentration decreases again.

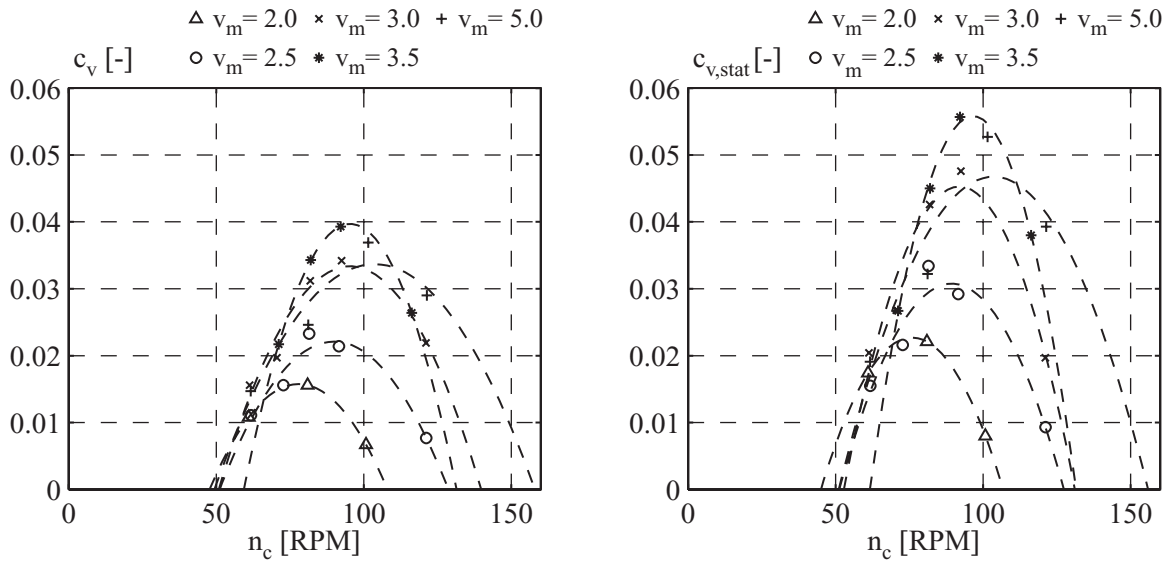

Figure D.1: Average volumetric concentration during the entire cutting phase and the average volumetric concentration in stationary domain vs. rotational velocity of the cutter head

For the mixture velocity of 5 m/s the maximum attainable volumetric concentration is lower than for the mixture velocity of 3.5 m/s. This means that beyond mixture velocities of about 3.5 m/s, the increase in mixture velocity does not result in a proportional increase in sucked up particles. This was also shown in Figure 6.6 where the maximum attainable production started to deviate from the dashed line for mixture velocities beyond 3.5 m/s.

In Chapter 6, the plot for the measured volumetric concentrations showed a reasonable time span in which its value was more or less stationary. At least it seemed to fluctuate around a constant value. Still, the stages in which the volumetric concentration increases (cutter head fills up with particles) and decreases (cutter head is emptied) cover a relatively large part of the total measurement. In practice these stages would be much shorter as the swing of the cutter dredge is much larger in practice compared to the length of the bank on model scale. Therefore, the time averaged value of the volumetric concentration in the stationary domain is plotted versus the rotational velocity at different mixture velocities (see right plot in Figure D.1). The average volumetric concentration in the stationary domain is considerably larger than the volumetric concentration averaged over the entire cutting phase. The difference between both volumetric concentrations varied from 25% to 30%. This means that the stages of increasing c_v and declining c_v have a considerable influence on the average value and can not be neglected in the entire measurement. For comparison with the situation in practice the average volumetric concentration in the stationary situation should be used.

As the diameter of the gravel particles is relatively large, there will be a significant difference in velocity between the water and the particles (slip velocity) in the suction pipe. Therefore the volumetric concentration can not directly be used to determine the production. Instead the delivered concentration (or transport concentration) should be used. From the weighed productions the average transport concentration is derived as follows.

$$c_t = \frac{\text{Production}}{\rho_p \frac{\pi}{4} D_{sp}^2 \overline{v}_m t_s} \tag{D.2}$$

where ρ_p is the density of gravel, D_{sp} is the diameter of the suction pipe, t_s is the time during which the concentration is transported and $\overline{v}_m$ is the average mixture velocity during t_s. Figure D.2 shows the average transport concentrations as a function of the rotational velocity of the cutter head for the different mixture velocities.

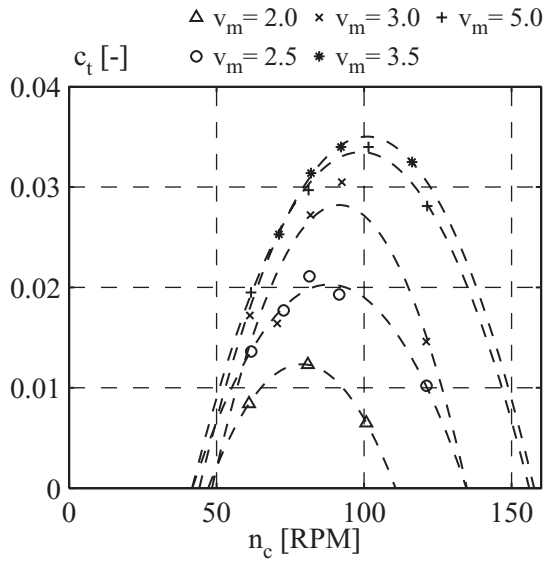

Figure D.2: Average transport concentration vs. rotational velocity of the cutter head

The average transport concentration is lower than the volumetric concentration and it also shows a (slight) decrease for mixture velocities larger than 3.5 m/s. The transport concentration is averaged over the entire measurement. In the stationary domain the average transport concentration will be larger (in analogy with the average volumetric concentration).

The volumetric concentrations for the over-cut situation are not plotted as the accuracy of these measurements was very low. Often it was not clear when the increase in concentration started as the average concentration was of the same order as the density fluctuations (noise).

Appendix E
Simulation Model for Particle Trajectories Along a Cutter Blade

E.1 Equation of motion for a single particle along a cutter blade

The cutter coordinate system and the blade coordinate system are shown in Figure E.1. In the blade coordinate system Y_{blade} is defined as parallel to the normal vector n. This normal vector is normal to the blade's surface in the contact point of particle and blade. It is positive when directed inwards.

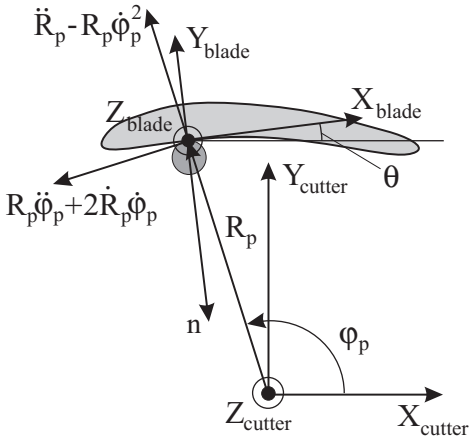

Figure E.1: Definition of the blade and cutter coordinate system and the accelerations of the particle

The position of the particle is determined by the cylindrical rotating coordinate system ($R_{p,cutter}$; $\varphi_{p,cutter}$; $Z_{p,cutter}$), where the $Z_{p,cutter}$ axis coincides with the Z_{cutter} axis. Furthermore, the transformation from the cylindrical coordinate system to the Cartesian coordinate system is obtained by:

$$\begin{aligned} X_{p,cutter} &= R_{p,cutter}\cos\varphi_{p,cutter} \\ Y_{p,cutter} &= R_{p,cutter}\sin\varphi_{p,cutter} \\ Z_{p,cutter} &= Z_{p,cutter} \end{aligned} \tag{E.1}$$

The acceleration terms for the particle at the position determined by R_p; φ_p and Z_p (subscript 'cutter' will be omitted for convenience sake) are

$$\begin{aligned} a_{Rp} &= \ddot{R}_p - R_p\dot{\varphi}_p^2 \\ a_{\varphi p} &= R_p\ddot{\varphi}_p + 2\dot{R}_p\dot{\varphi}_p \\ a_{Zp} &= \ddot{Z}_p \end{aligned} \tag{E.2}$$

As the particle can not move perpendicular to the blade's surface, the motion of the particle in this direction is restricted. For this it is convenient to write the accelerations in the blade coordinate system. The transformation from the blade coordinate system to the cutter coordinate system is achieved by two rotations of the coordinate system. First a rotation over an angle θ from the cutter coordinate system to a (temporary) blade coordinate system ($X_{blade,1}$; Y_{blade1}; $Z_{blade,1}$) as defined as in the left plot of Figure E.2.

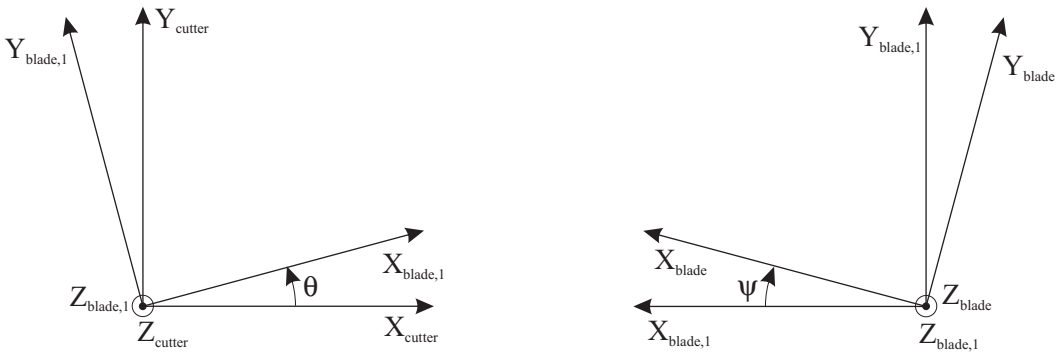

Figure E.2: Transformations from the cutter coordinate system to the blade coordinate system

Secondly, a transformation from the coordinate system $X_{blade,1}$; Y_{blade1}; $Z_{blade,1}$ to the blade coordinate system as defined in the right plot of Figure E.2.

In matrix notation these two transformations are achieved by:

$$\begin{bmatrix} X_{cutter} \\ Y_{cutter} \\ Z_{cutter} \end{bmatrix} = \begin{bmatrix} \cos\theta & -\sin\theta & 0 \\ \sin\theta & \cos\theta & 0 \\ 0 & 0 & 1 \end{bmatrix} \begin{bmatrix} X_{blade,1} \\ Y_{blade,1} \\ Z_{blade,1} \end{bmatrix} \tag{E.3}$$

$$\begin{bmatrix} X_{blade,1} \\ Y_{blade,1} \\ Z_{blade,1} \end{bmatrix} = \begin{bmatrix} 1 & 0 & 0 \\ 0 & \cos\psi & -\sin\psi \\ 0 & \sin\psi & \cos\psi \end{bmatrix} \begin{bmatrix} X_{blade} \\ Y_{blade} \\ Z_{blade} \end{bmatrix}$$

and thus

$$\begin{bmatrix} X_{cutter} \\ Y_{cutter} \\ Z_{cutter} \end{bmatrix} = \begin{bmatrix} \cos\theta & -\sin\theta\cos\psi & \sin\theta\sin\psi \\ \sin\theta & \cos\theta\cos\psi & -\cos\theta\sin\psi \\ 0 & \sin\psi & \cos\psi \end{bmatrix} \begin{bmatrix} X_{blade} \\ Y_{blade} \\ Z_{blade} \end{bmatrix} \tag{E.4}$$

For convenience sake the transformation is written as

$$\begin{bmatrix} X_{cutter} \\ Y_{cutter} \\ Z_{cutter} \end{bmatrix} = \begin{bmatrix} A_{11} & A_{12} & A_{13} \\ A_{21} & A_{22} & A_{23} \\ A_{31} & A_{32} & A_{33} \end{bmatrix} \begin{bmatrix} X_{blade} \\ Y_{blade} \\ Z_{blade} \end{bmatrix} = A \begin{bmatrix} X_{blade} \\ Y_{blade} \\ Z_{blade} \end{bmatrix} \tag{E.5}$$

Then, the transformation from the cutter coordinate system to the blade coordinate system is given by

$$\begin{bmatrix} X_{blade} \\ Y_{blade} \\ Z_{blade} \end{bmatrix} = A^{T} \begin{bmatrix} X_{cutter} \\ Y_{cutter} \\ Z_{cutter} \end{bmatrix} \tag{E.6}$$

in which A^T represents the transpose of the matrix A. Thus the acceleration terms for the particle written in the coordinate system for the blade become

$$\begin{aligned} a_{p,Xblade} &= A_{11}\left(a_{Rp}\cos\varphi_p - a_{\varphi p}\sin\varphi_p\right) + A_{21}\left(a_{Rp}\sin\varphi_p + a_{\varphi p}\cos\varphi_p\right) + A_{31}\ddot{Z}_p \\ a_{p,Yblade} &= A_{12}\left(a_{Rp}\cos\varphi_p - a_{\varphi p}\sin\varphi_p\right) + A_{22}\left(a_{Rp}\sin\varphi_p + a_{\varphi p}\cos\varphi_p\right) + A_{32}\ddot{Z}_p \\ a_{p,Yblade} &= A_{13}\left(a_{Rp}\cos\varphi_p - a_{\varphi p}\sin\varphi_p\right) + A_{23}\left(a_{Rp}\sin\varphi_p + a_{\varphi p}\cos\varphi_p\right) + A_{33}\ddot{Z}_p \end{aligned} \tag{E.7}$$

Due to the restriction that the particle can not move perpendicular to the blade's surface, the relative acceleration of the particle in direction of Y_{blade} equals zero. Or

$$\left(\ddot{R}_p\,\bar{e}_{Rp} + R_p\ddot{\varphi}_p\,\bar{e}_{\varphi p} + \ddot{Z}_p\,\bar{e}_{Zp}\right)\cdot\bar{e}_{Yblade} = 0 \tag{E.8}$$

Using the expression in Equation (E.1) and using the transformation matrix A in Equation (E.5) the condition above yields that

$$\left(A_{12}\cos\varphi_p + A_{22}\sin\varphi_p\right)\ddot{R}_p + \left(A_{22}\cos\varphi_p - A_{12}\sin\varphi_p\right)R_p\ddot{\varphi}_p + A_{32}\ddot{Z}_p = 0 \tag{E.9}$$

The cutter axis inclination angle λ is defined as in the following figure. Furthermore, the figure shows the orientation of the global and the cutter coordinate system.

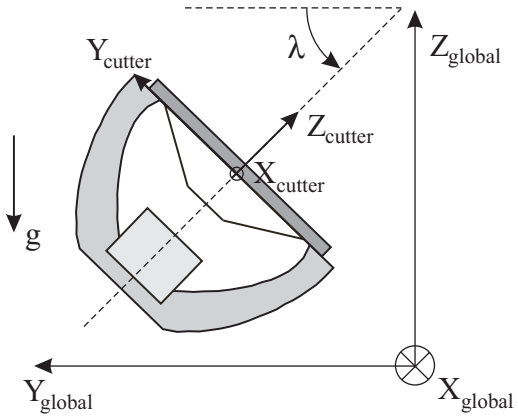

Figure E.1: Definition of the global coordinate system and the cutter axis inclination angle

The forces acting on the particle that are considered here are: gravitational force, normal force, friction force, drag force, pressure gradient force and the added mass force. The derivation of these forces is given in Chapter 8.

Gravitational force

The gravitational force F_g is

$$\overline{F}_g = m_p \overline{g} = -m_p g \left(\cos\lambda \overline{e}_{Ycutter} + \sin\lambda \overline{e}_{Zcutter} \right) \tag{E.10}$$

in which m_p is the mass of the particle and g is the acceleration of gravity.

Normal force

The normal force F_n acting on the particle is defined as

$$\overline{F}_n = -F_n \overline{e}_{Yblade} \tag{E.11}$$

thus positive when directed inwards. The normal force is a reaction force that results from the contact between particle and blade. The magnitude of the normal force is not known beforehand, but will be derived by solving the system of equations (E.17). The condition for the motion of the particle along the blade's surface gives an additional equation because of which the acceleration of the particle and the normal force can be derived.

Friction force

The friction force F_f is also a reaction force depending on the normal force and a friction coefficient

$$\bar{F}_f = -\mu F_n \frac{v_{p,Xblade,rel}\bar{e}_{Xblade} + v_{p,Zblade,rel}\bar{e}_{Zblade}}{\left|\bar{v}_{p,blade,rel}\right|} \tag{E.12}$$

in which μ is the mechanical friction coefficient between the particle and the blade. The relative velocity of the particle in the blade coordinate system is:

$$\bar{v}_{p,blade,rel} = v_{p,Xblade,rel}\bar{e}_{Xblade} + v_{p,Zblade,rel}\bar{e}_{Zblade} \tag{E.13}$$

Drag force

The drag force F_D on a particle is:

$$\bar{F}_D = \frac{\pi}{8}\rho_w d_p^2 C_d \left(\bar{v}_f - \bar{v}_p\right)\left|\bar{v}_f - \bar{v}_p\right| \tag{E.14}$$

in which ρ_f is the density of the fluid (water), d_p is the particle diameter, C_d is the drag coefficient.

Pressure gradient force

The force on a particle due to the pressure gradient F_{PG} is:

$$\bar{F}_{PG} = \rho_f V_p \left(\frac{D\bar{v}_f}{Dt} - \bar{g}\right) \tag{E.15}$$

in which V_p is the volume of the particle and

$$\frac{D}{Dt} = \frac{\partial}{\partial t} + \bar{v}_f \cdot \nabla$$

Note that the buoyancy effect (Archimedes) is taken into account in this force.

Added mass force

The added mass force F_{AM} is defined as:

$$\bar{F}_{AM} = \rho_f V_p C_{AM} \left(\frac{D\bar{v}_f}{Dt} - \frac{d\bar{v}_p}{dt}\right) \tag{E.16}$$

in which C_{AM} is the added mass coefficient and

$$\frac{d}{dt} = \frac{\partial}{\partial t} + \bar{v}_p \cdot \nabla$$

The equation of motion for the particle, written in the blade coordinate system, becomes

$$m_p a_{Xblade} = -m_p g\left(A_{21}\cos\lambda + A_{31}\sin\lambda\right) - \mu F_n \frac{v_{p,Xblade,rel}}{\left|\overline{v}_{p,rel}\right|} + \frac{\pi}{8}\rho_f d_p^2 C_d \left(v_{f,Xblade} - v_{p,Xblade}\right)\left|\overline{v}_f - \overline{v}_p\right|$$
$$+\rho_f V_p\left(\frac{Dv_{f,Xblade}}{Dt} + g\left(A_{21}\cos\lambda + A_{31}\sin\lambda\right)\right) + \rho_f V_p C_{AM}\left(\frac{Dv_{f,Xblade}}{Dt} - \frac{dv_{p,Xblade}}{dt}\right)$$

$$m_p a_{Yblade} = -m_p g\left(A_{22}\cos\lambda + A_{32}\sin\lambda\right) - F_n + \rho_f V_p\left(\frac{Dv_{f,Yblade}}{Dt} + g\left(A_{22}\cos\lambda + A_{32}\sin\lambda\right)\right)$$
$$+\rho_f V_p C_{AM}\left(\frac{Dv_{f,Yblade}}{Dt}\right)$$

$$m_p a_{Zblade} = -m_p g\left(A_{23}\cos\lambda + A_{33}\sin\lambda\right) - \mu F_n \frac{v_{p,Zblade,rel}}{\left|\overline{v}_{p,rel}\right|} + \frac{\pi}{8}\rho_f d_p^2 C_d \left(v_{f,Zblade} - v_{p,Zblade}\right)\left|\overline{v}_f - \overline{v}_p\right|$$
$$+\rho_f V_p\left(\frac{Dv_{f,Zblade}}{Dt} + g\left(A_{23}\cos\lambda + A_{33}\sin\lambda\right)\right) + \rho_f V_p C_{AM}\left(\frac{Dv_{f,Zblade}}{Dt} - \frac{dv_{p,Zblade}}{dt}\right)$$

Substituting the acceleration terms given in Equation (E.7) in the equation above yields the following the equation of motion for the particle.

$$\left(1+\frac{\rho_f}{\rho_p}C_{AM}\right)\begin{bmatrix}\left(A_{11}\cos\varphi_p + A_{21}\sin\varphi_p\right) & \left(A_{21}\cos\varphi_p - A_{11}\sin\varphi_p\right) & A_{31}\\ \left(A_{12}\cos\varphi_p + A_{22}\sin\varphi_p\right) & \left(A_{22}\cos\varphi_p - A_{12}\sin\varphi_p\right) & A_{32}\\ \left(A_{13}\cos\varphi_p + A_{23}\sin\varphi_p\right) & \left(A_{23}\cos\varphi_p - A_{13}\sin\varphi_p\right) & A_{33}\end{bmatrix}\begin{bmatrix}\ddot{R}_p\\ R_p\ddot{\varphi}_p\\ \ddot{Z}_p\end{bmatrix} =$$

$$+g\left(\frac{\rho_f}{\rho_p}-1\right)\begin{bmatrix}\left(A_{21}\cos\lambda + A_{31}\sin\lambda\right)\\ \left(A_{22}\cos\lambda + A_{32}\sin\lambda\right)\\ \left(A_{23}\cos\lambda + A_{33}\sin\lambda\right)\end{bmatrix} - F_n\begin{bmatrix}\mu\frac{v_{p,Xblade,rel}}{\left|\overline{v}_{p,rel}\right|}\\ 1\\ \mu\frac{v_{p,Zblade,rel}}{\left|\overline{v}_{p,rel}\right|}\end{bmatrix} +$$

$$+\frac{3}{4}\frac{\rho_f}{\rho_p}\frac{C_d}{d_p}\left|\overline{v}_w - \overline{v}_p\right|\begin{bmatrix}\left(v_f - v_p\right)_{Xblade,abs}\\ 0\\ \left(v_f - v_p\right)_{Zblade,abs}\end{bmatrix} + \frac{\rho_f}{\rho_p}\left(1+C_{AM}\right)\begin{bmatrix}\frac{Dv_{f,Xblade}}{Dt}\\ \frac{Dv_{f,Yblade}}{Dt}\\ \frac{Dv_{f,Zblade}}{Dt}\end{bmatrix} +$$

$$+\frac{\rho_f}{\rho_p}(1+C_{AM})\begin{bmatrix}(A_{11}\cos\varphi_p+A_{21}\sin\varphi_p) & (A_{21}\cos\varphi_p-A_{11}\sin\varphi_p) & 0\\ (A_{12}\cos\varphi_p+A_{22}\sin\varphi_p) & (A_{22}\cos\varphi_p-A_{12}\sin\varphi_p) & 0\\ (A_{13}\cos\varphi_p+A_{23}\sin\varphi_p) & (A_{23}\cos\varphi_p-A_{13}\sin\varphi_p) & 0\end{bmatrix}\begin{bmatrix}R_p\dot{\varphi}_p^2\\ -2\dot{R}_p\dot{\varphi}\\ 0\end{bmatrix}$$

The unknown variables that have to be determined are the normal force F_n and the relative accelerations of the particle: $\ddot{R}_p$, $\ddot{\varphi}_p$ and $\ddot{Z}_p$. Adding the restriction given by Equation (E.9) in the equation of motion and writing the accelerations and F_n in an explicit form yields the following equation that has to be solved.

$$\left(1+\frac{\rho_f}{\rho_p}C_{AM}\right)\begin{bmatrix}Const_1 & Const_2 & A_{31} & \mu\frac{v_{p,Xblade,rel}}{|\bar{v}_{p,rel}|}\frac{\rho_p}{(\rho_p+\rho_f C_{AM})}\\ Const_3 & Const_4 & A_{32} & \frac{\rho_p}{(\rho_p+\rho_f C_{AM})}\\ Const_5 & Const_6 & A_{33} & \mu\frac{v_{p,Zblade,rel}}{|\bar{v}_{p,rel}|}\frac{\rho_p}{(\rho_p+\rho_f C_{AM})}\\ Const_3 & Const_4 & A_{32} & 0\end{bmatrix}\begin{bmatrix}\ddot{R}_p\\ R_p\ddot{\varphi}_p\\ \ddot{Z}_p\\ \frac{F_n}{m_p}\end{bmatrix}=g\begin{bmatrix}Const_7\\ Const_8\\ Const_9\\ 0\end{bmatrix}+$$

$$+Const_{10}\left|\bar{v}_f-\bar{v}_p\right|\begin{bmatrix}(v_f-v_p)_{Xblade,abs}\\ 0\\ (v_f-v_p)_{Zblade,abs}\\ 0\end{bmatrix}+\frac{\rho_f}{\rho_p}(1+C_{AM})\begin{bmatrix}\frac{Dv_{f,Xblade}}{Dt}\\ \frac{Dv_{f,Yblade}}{Dt}\\ \frac{Dv_{f,Zblade}}{Dt}\\ 0\end{bmatrix}+$$

$$+\left(1+\frac{\rho_f}{\rho_p}C_{AM}\right)\begin{bmatrix}R_p\dot{\varphi}_p^2Const_1-2\dot{R}_p\dot{\varphi}_pConst_2\\ R_p\dot{\varphi}_p^2Const_3-2\dot{R}_p\dot{\varphi}_pConst_4\\ R_p\dot{\varphi}_p^2Const_5-2\dot{R}_p\dot{\varphi}_pConst_6\\ 0\end{bmatrix} \qquad \text{(E.17)}$$

with

$$Const_1=(A_{11}\cos\varphi_p+A_{21}\sin\varphi_p) \qquad Const_2=(A_{21}\cos\varphi_p-A_{11}\sin\varphi_p)$$
$$Const_3=(A_{12}\cos\varphi_p+A_{22}\sin\varphi_p) \qquad Const_4=(A_{22}\cos\varphi_p-A_{12}\sin\varphi_p)$$
$$Const_5=(A_{13}\cos\varphi_p+A_{23}\sin\varphi_p) \qquad Const_6=(A_{23}\cos\varphi_p-A_{13}\sin\varphi_p)$$

$$Const_7 = \left(A_{21}\cos\lambda + A_{31}\sin\lambda\right)\left(\frac{1-S_s}{S_s}\right) \quad Const_8 = \left(A_{22}\cos\lambda + A_{32}\sin\lambda\right)\left(\frac{1-S_s}{S_s}\right)$$

$$Const_9 = \left(A_{23}\cos\lambda + A_{33}\sin\lambda\right)\left(\frac{1-S_s}{S_s}\right) \quad Const_{10} = \frac{3}{4}\frac{C_d}{d_p S_s}$$

and S_s is the specific density ρ_p/ρ_f.

E.2 Flow chart for the simulation model

The flow chart for the simulation model to calculate the trajectory of a particle along the cutter blade is given in Figure E.2.

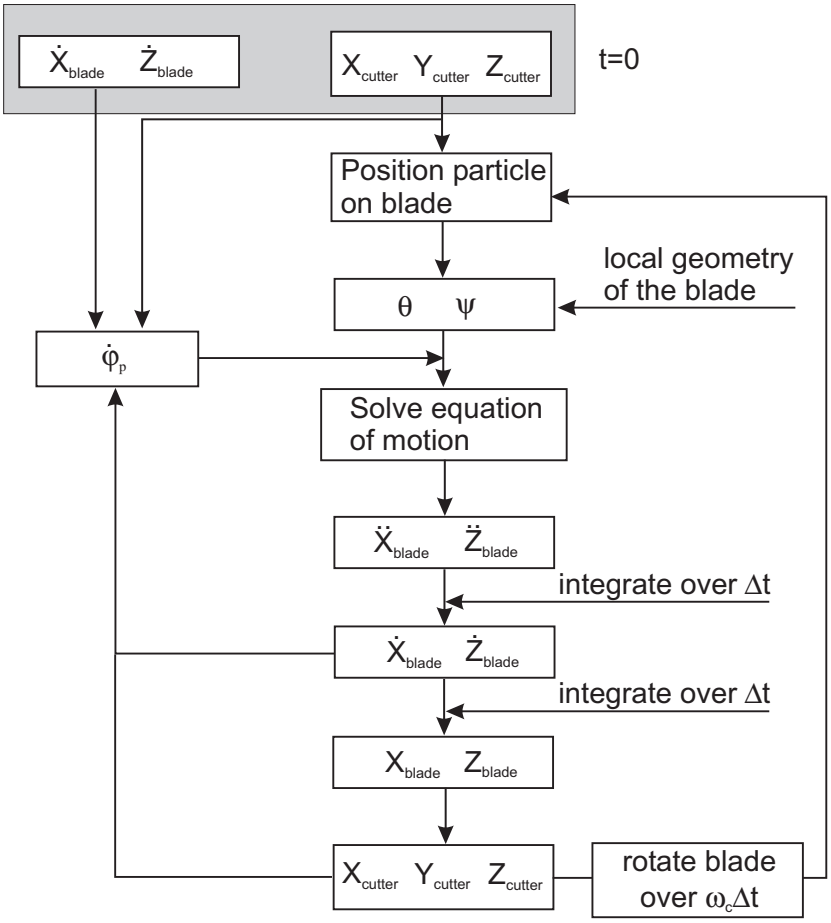

Figure E.2: Flow chart for the simulation model to calculate the trajectory of a particle along the cutter blade

For t = 0 s (initial condition), the position of the particle and the initial velocity of the particle need to be given. Specifying the initial position of the blade yields the relative position of the particle on the blade. The geometry of the blade in the specific point, or actually the plane

along which the particle can move, is given by θ and ψ. Given the angular velocity of the particle $\dot{\varphi}_p$, following from the initial position and velocity of the particle, the equation of motion can be solved. The equation of motion determines the acceleration of the particle along the local surface of the blade (and the normal force). By integrating the accelerations over the time step Δt, the change in velocity of the particle is obtained. Here, a forward Euler method is used for the integration. Integrating again over Δt gives the displacement of the particle.

With the new position and velocity of the particle and the rotation of the blade over an angle $\omega_c \Delta t$ about the cutter axis, the process is repeated for the next time step. This routine is stopped if the normal force becomes negative (particle is no longer in contact with the blade) or if the particle gets to close to the edge of the blade.

E.3 Estimation of the error made in the simulations

In general the Euler method is not very accurate compared with more advanced integration methods like e.g. the Runge-Kutta method. The local error for the Euler method is $O(\Delta t^2)$ while for a *n*th order Runge-Kutta method it is $O(\Delta t^{n+1})$. However, in this case solving the differential equations is not the decisive factor. A problem that arises when determining the trajectory of a particle along the rotating surface is illustrated in Figure E.3. The figure shows the particle on the blade at a certain point in time t and with a certain velocity.

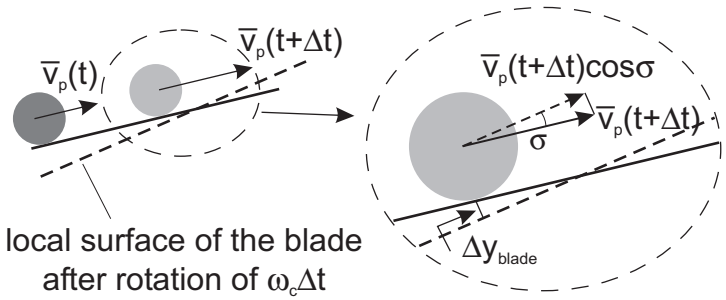

Figure E.3: Adjustment of the position of the particle and direction of the particle velocity

Solving the equation of motion over time step Δt gives the new position of the particle and the new velocity. However, this velocity is parallel to the blade's local surface at the previous point of time t. Due to the rotation of the blade by $\omega_c \Delta t$ and the new position of the particle the orientation of the local surface has changed (illustrated in the figure by the dashed line). Therefore the particle might not be in contact with the blade anymore and its velocity vector is not parallel to the blade's surface. In the simulation model this is solved by moving the particle perpendicular to the (new) blade's surface by a distance Δy_{blade} so that the particle is

located on the blade again. Furthermore, the component of the velocity vector parallel to the blade's surface at time t+Δt is taken as the new velocity vector (see Figure E.3). In other words the component of the velocity vector perpendicular to the blade's surface (i.e. in direction of Y_{blade}) is simply set to zero. The error made will have order of magnitude

$$\bar{v}_p\left(t+\Delta t\right)\sin\sigma$$

In the simulations the time step Δt is 5×10^{-5} s. Assuming that σ has the same order of magnitude as the incremental rotation of the blade this yields, for a rotational velocity of 120 RPM, $\sigma \approx 6.3\times10^{-4}$ rad (≈ 0.036º). As for small angles $\sin\sigma \approx \sigma$ and the velocity vector has order of magnitude 1 m/s, the error made will also have order of magnitude 1×10^{-4} m/s. In addition, assuming that the replacement of the particle has the same order of magnitude as the incremental displacement of the blade in time step Δt, the error made by repositioning the particle is: $6.3\times10^{-4}R_c$. With a radius of the cutter head R_c of 0.2 m, the error has order of magnitude 1×10^{-4} m.

The error was checked by performing simulations with a rotational velocity of 120 RPM and time steps of 5×10^{-5} s and 1×10^{-6} s (thus a factor 50 smaller). Comparing the results of the simulations it appeared that, in general, the order of magnitude of the local differences between the two solutions was 1×10^{-4}. At the points where the particle was repositioned on the blades the difference in solutions sometimes showed enormous spikes, resulting in differences with order of magnitude 1×10^{-3} or 1×10^{-2}. The spikes were caused by the discrete build up of the blade's surface. Figure E.4 shows the surface of the blade and the node points (black dots) that form the actual data points. The entire blade in build up by 30×28 node points only. Although the surface of the blade does not show meaningful bumps, it is not smooth. The right plot in Figure E.4 shows what happens when the particle moves from one square to another and the transition is not smooth.

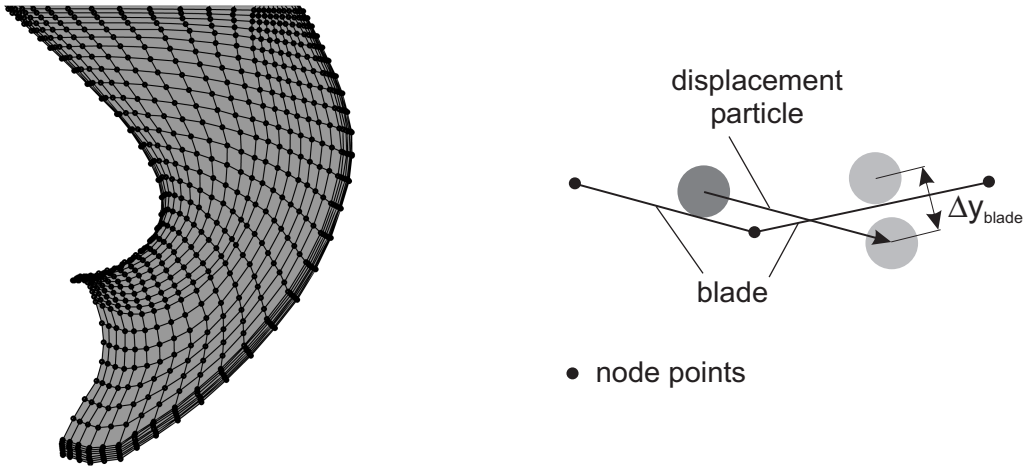

Figure E.4: Discrete build up of the blade's surface and consequences for repositioning the particle

The distance over which the particle has to be moved in order to position it back on the blade's surface again (Δy_{blade}) is relatively large. These irregular transitions from one square to another produce the spikes in the simulations.

Considering the above mentioned, it is fair to assume that the error made in the simulations roughly has order of magnitude 1×10^{-3} with a time step of 5×10^{-5} s. This is small enough given the aim of the simulations. Moreover, using a Runge-Kutta method to solve the differential equations will not have significant advantages as the maximum time step is still restricted. The increase in accuracy that would be gained if using a Runge-Kutta method is of minor importance as the accuracy of the Euler method is already sufficient (when using a time step of 5×10^{-5} s). A Runge-Kutta method could be an alternative if the Euler method would show stability problems.

Appendix F
Simulated Particle Trajectories Using a CFD Model for the Flow

As was mentioned in paragraph 5.5 a parallel research program has been set up in order to determine the flow inside the cutter head (Steinbusch et al., 1999; Dekker et al., 1999; Dekker et al., 2001). This research has been set up in cooperation with the section Engineering Fluid Dynamics of the Department of Mechanical Engineering of the University of Twente. To determine the particle trajectories along the cutter blade, the velocities and pressures resulting from this CFD model have been used.

For comparison the simulations described in paragraph 8.4.4 have been repeated. Thus the initial velocity of the particle equaled the velocity of the blade, n_c = 90 RPM and v_m = 3 m/s.

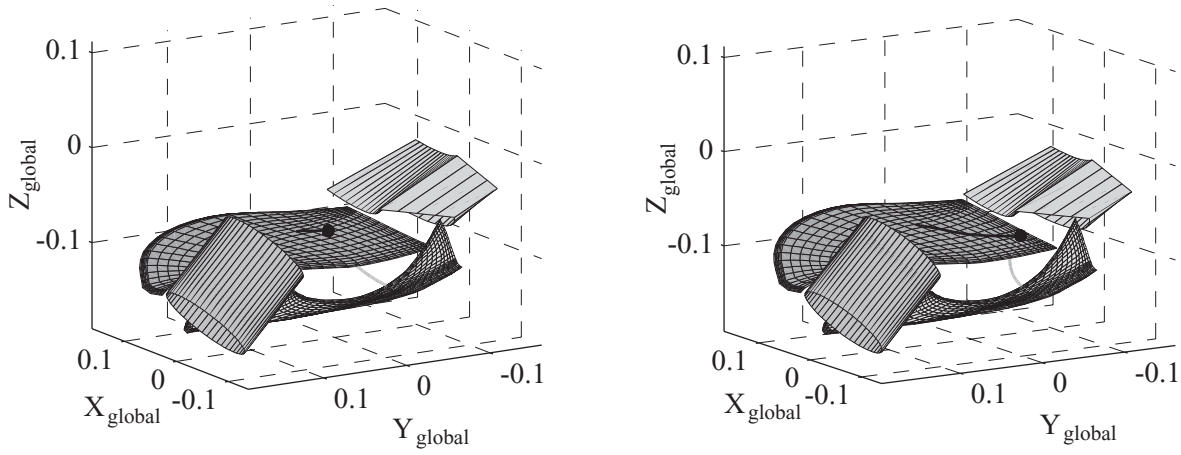

Figure F.1: The trajectories of a particle with C_d coefficients of 0.2 (left) and 1 (right) respectively, while n_c = 90 RPM and v_m = 3 m/s

The simulations have been performed with C_d values of 0.2 and 1 with an initial position of the blade right underneath the suction mouth. The trajectories of the particles are shown in Figure F.1. The Figure shows the initial position of the blade, the position of the blade at the end of the simulation, the hub and the suction mouth as it was implemented in the CFD model. The main difference with the previously used flow model is that the particle immediately moves towards the suction mouth. Both simulations stopped because the normal force acting on the particle became zero, which means that the particle is no longer in contact with the blade. For the simulations with C_d = 1 this implies that the particle is sucked up, considering the distance between the particle and the suction mouth. For the situation with C_d = 0.2 it is not clear whether the particle will be sucked up.

The trajectories of the particles can be explained by the strong flow towards the suction mouth. As the presence of the blades is taken into account, the surface through which water flows into the cutter head is smaller in comparison with the model that was used in Chapter 8. Therefore the water velocities will be larger in this case compared with the model from Chapter 8. In Figure F.2 the body acceleration of the particle in three directions is shown for both simulations, including the centrifugal and Coriolis acceleration.

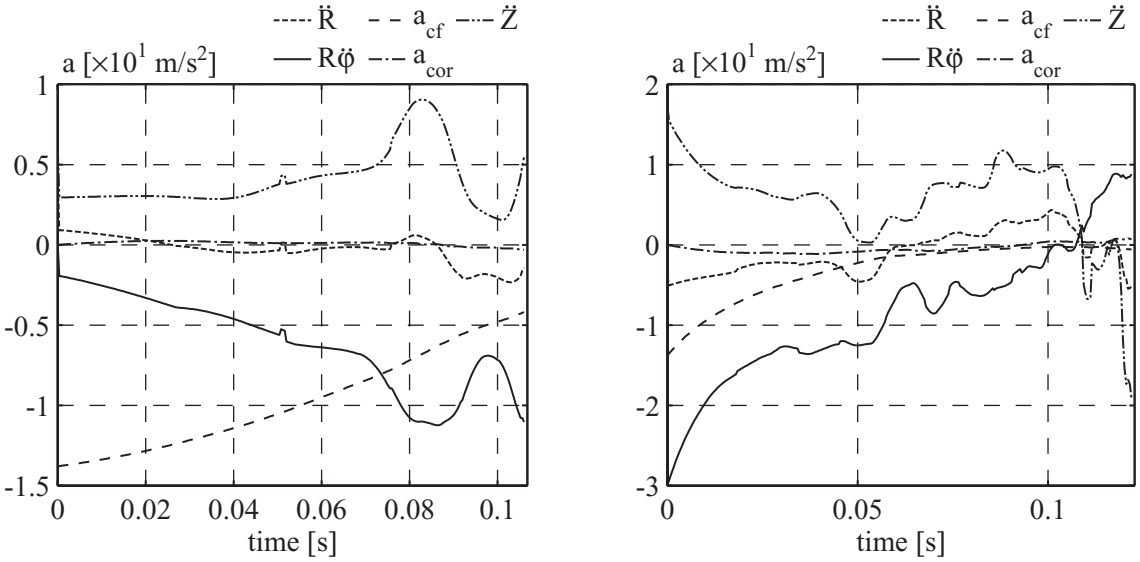

Figure F.2: The acceleration components of a particle with C_d coefficients of 0.2 and 1 while n_c = 90 RPM and v_m = 3 m/s

The relatively large value for the axial acceleration (thus towards the suction mouth) in both simulations is a result of the suction flow. In addition, the velocity difference between the blade and the water is significant: not only in axial direction but also in tangential direction. As the initial velocity of the particle equaled the blade velocity, the drag force acting on the particle will be large. This results in the large negative value for the tangential acceleration of

the particle (actually a deceleration). As the angular velocity of the particle decreases the centrifugal acceleration a_{cf} decreases as well (in an absolute sense). Considering the relatively low value for the centrifugal acceleration compared with the gravitational acceleration, it is not responsible for the axial transport of particles along the blade as described in Chapter 8.

More information on the influence of the flow is obtained by plotting the external forces acting on the particle.

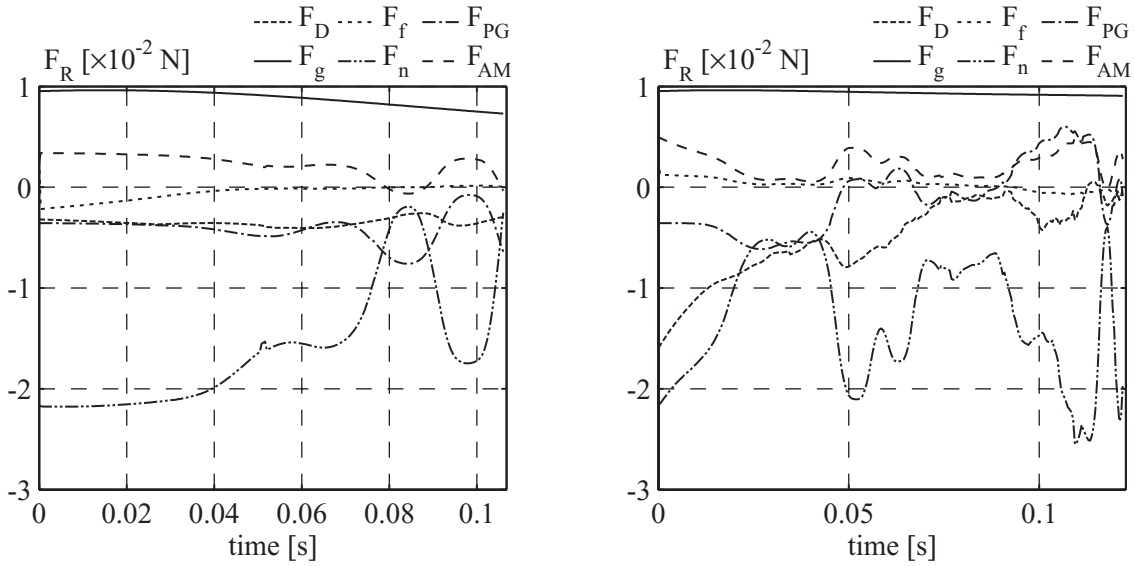

Figure F.3: The radial components of the forces on the particle with C_d coefficients of 0.2 (left) and 1 (right) while n_c = 90 RPM and v_m = 3 m/s

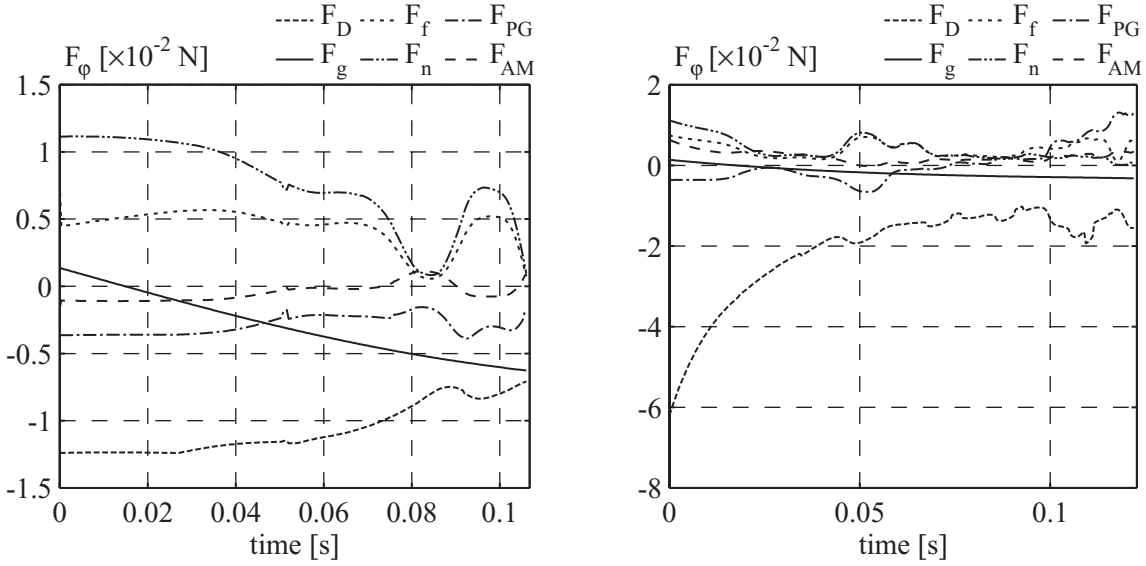

Figure F.4: The tangential components of the forces on the particle with C_d coefficients of 0.2 (left) and 1 (right) while n_c = 90 RPM and v_m = 3 m/s

In Figures F.3 to F.5 the radial, tangential and axial forces acting on the particle are plotted. The figure for the tangential forces, Figure F.4, indeed shows that the drag force is significant and decelerating the particle in tangential direction. The oscillations in the forces are again caused by the unevenness of the blade and the repositioning of the particle on the blade. Furthermore, examining the calculated flow it appeared that there could be significant jumps in the fluid velocities and pressures between adjacent node points.

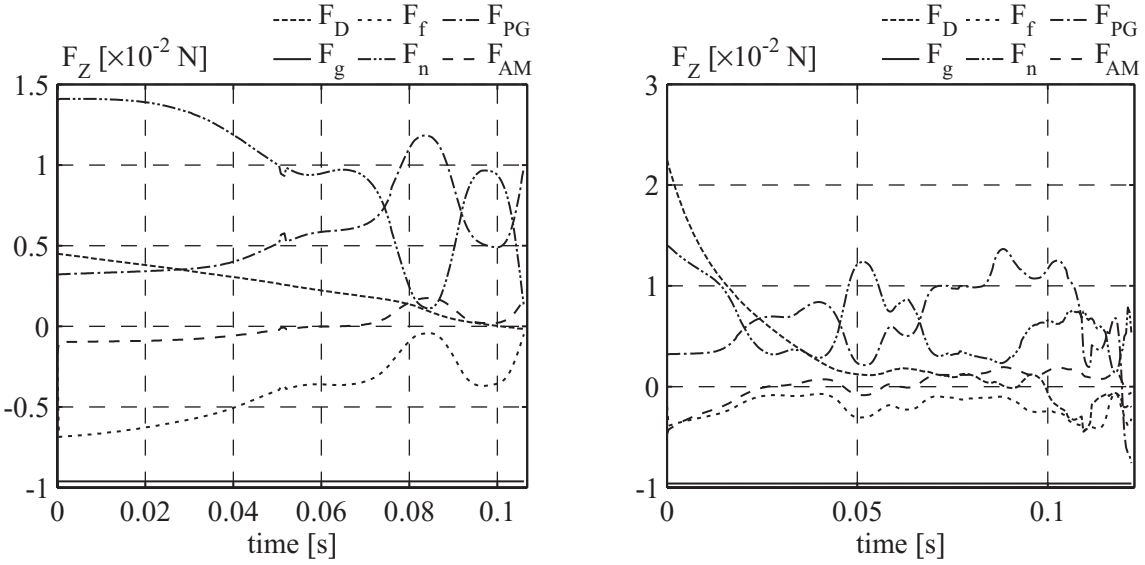

Figure F.5: The axial components of the forces on the particle with C_d coefficients of 0.2 (left) and 1 (right) while n_c = 90 RPM and v_m = 3 m/s

From the forces in axial direction it is clear that the drag force has a more or less adjusting role. When the particle velocity is adjusted to the fluid velocity, the drag force is significantly lower than the pressure gradient force in axial direction.

Examining the water velocities along the blade for all the simulations performed it appeared that the tangential velocity difference between the blade and the water was always large. The blade always rotated faster than the water, both near the hub as well as near the cutter ring (Dekker et al., 2002). The only place water could rotate faster than the blade was at the node point near the leading edge of the blade. As the velocity difference was generally large, the particles always moved from the leading edge of the blade towards the trailing edge even for the large rotational velocities. This is shown in Figure F.6 where the particle trajectories are plotted for the cases where n_c = 40 RPM and 120 RPM. In the first simulation the drag coefficient was 1 while in the second simulation it was 0.2.

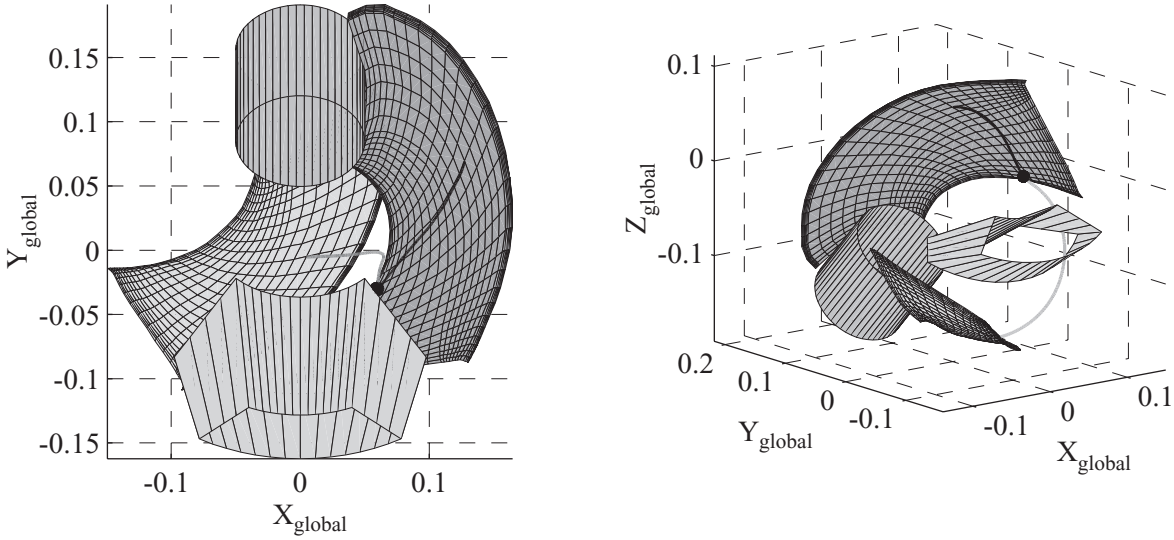

Figure F.6: The trajectory of a particle with n_c = 40 RPM, v_m = 3 m/s and C_d = 1 (left plot) and trajectory of a particle with n_c = 120 RPM, v_m = 3 m/s and C_d = 0.2 (right plot)

Relative to the blade, the particle trajectories are very much alike. The trajectories also resemble the simulations with a large slip factor performed in paragraph 8.4.4.

From several simulations that have been performed it was concluded that particles were easier sucked up for the lower rotational velocities (Burger and Talmon, 2002). The higher the rotational velocity, the less the particle seemed to move towards the suction pipe. None of the particles was thrown out of the cutter head, not even for the higher rotational velocities. This is in contradiction with the test results as found in Chapter 6. On the other hand, it confirms the findings of Chapter 8 that particles will only leave the blade at the leading edge if the slip factor between the blade and water is small. For positions of the blade in the vicinity of the suction mouth, the slip factor between the blade and water resulting from the CFD calculations often had a large value of approximately 0.5 (blade rotates much faster than the water).

Based on the large slip factor resulting from the CFD computations it is doubtful whether the pumping effect of the cutter head is taken into account and an outward flow exists for large rotational velocities. One cause for the absence of the pump effect is the applied Kutta-Joukowski condition (Batchelor, 1967). This condition requires that the flow leaves smoothly from the trailing edges. In reality this will not be the case and separation of the boundary layer will take place, especially for high rotational velocities of the cutter head. It is thus concluded that for determining the particle trajectories the simulation model will not suffice, although velocity measurements inside the cutter head have shown that the basic trends in the water velocities are simulated reasonably (Dekker et al., 2001).

The possibilities of improving the present CFD model are limited and it is recommended that an alternative CFD model is set up or commercial CFD software is used. An alternative approach would be the use of Reynolds-averaged Navier-Stokes equations instead of the potential flow model. The necessary turbulence closure relation will decrease the computational efficiency but it enables the use of empirical data. However, considering the complexity of the flow inside the cutter head, the capabilities of a RANS model should not be overestimated. On the other hand, simulating the turbulence is not the main purpose as it will have an insignificant influence on the trajectories of the large particles. The basic aim is to model the pump effect of the cutter head.

For low rotational velocities of the cutter head the CFD model will probably produce better results than for high rotational velocities as the pump effect of the cutter head is negligible. In that case an inward flow exists along the entire contour of the cutter head and the flow inside the cutter head is most of all a geometrical problem where continuity is the most important factor. However, for rotational velocities of the cutter head that are too low (lower than 20 RPM on prototype scale) the solution is less interesting for practical purposes. Further investigation of the CFD model is needed to determine if and up to what values for the rotational velocity acceptable solutions are obtained.

List of Symbols

Symbol	*Unit*	*Description*
A_{cut}	m^2	cut off area
A_{ij}	-	constants in the equation of motion
C	-	coefficient
D_c	m	outer ring diameter cutter head
Eu	-	Euler number
F	N	force
Fr	-	Froude number
F_t	-	cumulative distribution
L	m	characteristic length scale
N_{Bag}	-	Bagnold number
N_{Sav}	-	Savage number
P	-	production percentage
P_f	N/m^2	characteristic fluid pressure scale
Q	m^3/s	flow
R	m	radius
Re	-	Reynolds number
S	-	spillage percentage
S_s	-	specific density
St	-	Strouhal number
T	s	characteristic time scale
T_c	Nm	torque on cutter head drive shaft
U	m/s	characteristic velocity scale
V	m^3	volume
$V_{p,c}$	m^3	total volume of particles inside the cutter head

a	m/s^2	acceleration
c	-	concentration
d, D	m	diameter
$\bar{e}$	-	unity vector
f_t	-	probability density function
g	m/s^2	acceleration of gravity
h	m	cut thickness
l	m	mixing length
m	kg	mass
n_c	1/s; RPM	rotational velocity of the cutter head
p	N/m^2	fluid pressure
q	-	number of blades on cutter head
t	s	time
v	m/s	velocity

Greek Symbols	*Unit*	*Description*
Ω	rad/s	vorticity
α_{cut}	rad	angle between tip of a tooth and the vertical axis
γ	rad	helix angle
θ	rad	angle to describe the local geometry of the blade
λ	rad	cutter axis inclination angle
λ_c	-	linear concentration
μ	-	friction coefficient between particle and blade
μ_f	Ns/m^2	dynamic viscosity
μ_t	s	average residence time of a particle
ν	m^2/s	kinematic viscosity
ξ	-	flow number
ρ	kg/m^3	density
σ_t	s	standard deviation of the residence time
τ	N/m^2	viscous stress
φ	rad	rotation angle in the cutter head coordinate system
φ_i	rad	angle of internal friction
ψ	rad	angle to describe the local geometry of the blade
ω	rad/s	angular velocity

Operators	*Unit*	*Description*
$\dot{}$	1/s	first derivative in time: $\frac{\partial}{\partial t}$

$\ddot{}$	$1/s^2$	second derivative in time: $\frac{\partial^2}{\partial t^2}$
∇	1/m	gradient: $\left(\frac{\partial}{\partial X_i}, \frac{\partial}{\partial Y_i}, \frac{\partial}{\partial Z_i}\right)$
$\frac{D}{Dt}; \frac{d}{dt}$	1/s	material derivative: $\frac{\partial}{\partial t} + \bar{v} \cdot \nabla$

Indices

0	offset
AM	added mass
L	lift
PG	pressure gradient
abs	absolute
b	bank
buo	buoyancy
c	cutter head
cf	centrifugal
cor	Coriolis
d, D	drag
df	driving force
e	eddy
f	fluid, friction
g	gravitational, gravel grain
h	haul
m	mixture
max	maximum
min	minimum
n	normal
p	particle
r	residence, rock
rel	relative
res	resultant
s	slip, suction
sp	suction pipe
stat	stationary
t	transport
tot	total
ts	terminal settling

v	volumetric
w	water
R, φ, Z	radial, tangential, axial

Coordinate systems

$X_{blade}Y_{blade}Z_{blade}$	blade coordinate system
$X_{cutter}Y_{cutter}Z_{cutter}$	cutter head coordinate system
$X_{glob}Y_{glob}Z_{glob}$	global coordinate system (earth coordinate system)
$X_{sp}Y_{sp}Z_{sp}$	suction pipe coordinate system
RφZ	cylindrical coordinate system

Glossary

Word	*Synonyms*	*Description*	*page*
adapter		connection between the cutting teeth and the blade	3
angular velocity		the number of oscillations per unit of time [rad/s]	8
back plate		plate to seal off the cutter head near the cutter ring	3
bank	breach	soil formation round the cut of the cutter head	3
blade	arm	part of the cutter head on which the adapters are welded, provides the strength of the cutter head	3
cutter head	cutter	device responsible for the actual excavation of the formation	2
cutter ring	back ring	part of the cutter head to which the blades are connected provides strength of the cutter head	3
haul velocity	swing velocity, haulage velocity	translational velocity with which the cutter head moves through the bank	7
hub	cutter hub	part of the cutter head connecting the cutter head with the cutter head drive shaft	3
ladder		- hoistable frame at the end of which the cutter head is mounted - supports the cutter drive, cutter drive shaft and the submerged pump	2

Word	*Synonyms*	*Description*	*page*
		- provides the weight on the cutter head	
mixture velocity		the velocity of the mixture in the suction pipe	7
nominal value		value at which a device is designed to operate	6
operational parameters		parameters that can be varied during the dredging operation to influence the dredging process	7
over-depth		the extra depth that needs to be dredged to take account of the spillage layer	5
production percentage		ratio of the amount of sediment sucked up and the total amount of sediment cut [%]	15
production rate		the amount of sediment sucked up per unit of time [m^3/s]	16
rotational velocity	cutter head speed	amount of revolutions of the cutter head per minute [RPM]	7
spillage	sediment loss	sediment that is cut during the dredging process, but is not sucked up	1
spud poles	working spud	pole about which the cutter suction dredge swings	4
	auxiliary spud	pole used for stepping forward of the cutter dredge	
suction mouth	suction inlet	front part (orifice) of the suction pipe that coincides with the back plate	3
suction pipe	suction tube, inlet pipe	pipe through which the mixture is transported	3

References

Bagnold, R.A. (1954). Experiments on a Gravity-Free Dispersion of Large Solid Spheres in a Newtonian Fluid under Shear: Royal Society of London Proceedings, ser. A, Vol. 225, pp. 49–63.

Bagnold, R.A. (1956). The Flow of Cohesionless Grains in Fluids: Royal Society of London Philosophical Transactions, ser. A, Vol. 249, pp. 235–297.

Buckingham, E. (1914). On Physically Similar Systems; Illustrations of the Use of Dimensional Equations. Phys. Rev. Vol. 4, no. 4, 1914, pp. 345-376.

Burger, M. den, (1998). Meting Verblijftijden Deeltjes in Snijkop (Measurements of Particle Residence Times in a Cutter Head). Section of Dredging Technology, Report nr. 99.3.GV.5127, Delft University of Technology, Delft, The Netherlands. (in Dutch).

Burger, M. den, Vlasblom W.J. and Talmon A.M. (1999). Influence of Operational Parameters on Dredge Cutter Head Spillage. Proceedings Ceda Dredging Days 1999, Amsterdam, The Netherlands.

Burger, M. den and Talmon A.M. 2001. Mechanical Transportation of Particles Induced by Cutter Blade Geometry. Proceedings Ceda Dredging Days 2001, Amsterdam, The Netherlands.

Burger, M. den and Talmon, A.M. (2002). Particle Trajectories Along a Cutter Head Blade, Using the Results of a CFD Model for the Flow. Dredging ’02, Orlando Florida, USA.

Cantwell, B. and Coles, D. (1983). An Experimental Study of Entrainment and Transport in the Turbulent Near Wake of a Circular Cylinder. Journal of Fluid Mech., Vol. 136, pp. 321-374.

Dandy, D.S. and Dwyer, H.A. (1990). A Sphere in Shear Flow at Finite Reynolds number: Effect of Shear on Particle Lift, Drag and Heat Transfer. Journal of Fluid Mech., Vol. 216, pp. 381-410.

Deketh, H.J.R. (1995). Wear of Rock Cutting Tools. Laboratory Experiments on the Abrasivity of Rock. Balkema Rotterdam, The Netherlands.

Dekker, M.A., Verdoodt, L.L.J. and den Burger, M. (1999). Validation of a Flow Generated by a Cutter Head. Proceedings Ceda Dredging Days 1999, Amsterdam, The Netherlands, pp. 217-226.

Dekker, M.A. (2001). Analyse van Stromingsmetingen Binnen en Buiten een Snijkop (Analysis of Flow Measurements Inside and Outside a Cutter Head). Opdrachtnummer 2001.BT.5529, Laboratory of Soil Transportation, Delft University of Technology, Delft, The Netherlands. (in Dutch).

Dekker, M.A., Vlasblom, W.J. and den Burger, M. (2001). Measurements of the Flow Generated by a Cutter Head. Proceedings of WODCON XVI 2001, Kuala Lumpur, Malaysia.

Dekker, M.A., Kruyt, N.P., den Burger, M. and Vlasblom, W.J. (2002). Experimental and Numerical Investigation of Cutter Head Dredging Flows. Journal of Waterway, Port, Coastal, and Ocean Engineering *(accepted for publication).*

Fuchs, N.A. (1964). The Mechanics of Aerosols. Pergamon Press, London, UK.

Hetsroni, G. 1989 Particles-turbulence interaction Int. Journal of Multiphase Flow, Vol. 15, Issue 5, pp. 735-746.

Hinds, W.C. (1982). Aerosol Technology; Properties, Behaviour, and Measurement of Airborne Particles. John Wiley & Sons, New York.

Jan, C.D. and Chen, J.C. (1997). Movement of a Sphere Rolling Down an Inclined Plane. Journal of Hydraulic Research, Vol. 35, pp. 689-706.

Joanknecht, L.W.F. (1976). A review of Dredge Cutter Head Modeling & Performance. Proceedings WODCON VII, San Francisco, California, USA, pp. 995-1016.

Kruyt, N.P., Esch, B.P.M. van, and Jonker, J.B. (1999). A Superelement-based Method for Computing Unsteady Three-dimensional Potential Flows in Hydraulic Turbomachines. Communications in Numerical Methods in Engineering 15, 381-397.

Kruyt, N.P. (2002). Lecture Notes Turbomachines II, Turbomachinery Laboratory, Department of Mechanical Engineering, University of Twente, The Netherlands.

Kurose, R. and Komori, S. (1999). Drag and Lift Forces on a Rotating Sphere in a Linear Shear Flow. Journal of Fluid Mechanics, Vol. 384, pp. 183-206.

Kurose, R., Misumi, R. and Komori, S. (2001). Drag and Lift Forces Acting on a Spherical Bubble in a Linear Shear Flow. Int. Journal of Multiphase Flow, Vol. 27, Issue 7, pp. 1247-1258.

Lange, S.J. de, (1989). Inleiding Kansrekening en Statistiek. Delftse Uitgevers Maatschappij b.v., The Netherlands. (in Dutch).

Mei, R. (1992). An Approximate Expression for the Shear Lift Force on a Spherical Particle at Finite Reynolds Number. Int. Journal of Multiphase Flow, Vol. 18, pp. 145-147.

Miltenburg, C.J.M. (1983). Stroming en Mengselvorming in Grote Snijkoppen (Flow and Mixture Forming in Large Cutterheads). laboratoriumopdracht La0/82/101, Laboratory of Soil Transportation, Delft University of Technology, Delft, The Netherlands. (in Dutch).

Mol, A. (1977a). Stroombeeld rond en in Cutter deel II: Vrij in Water Draaiend; Injekties met Kleurstof (Flow around and in a Cutter Head part II: Freely Rotating in Water; Injections with Dye). WL|Delft Hydraulics BAGT 236, The Netherlands. (in Dutch).

Mol, A. (1977b). Stroombeeld rond en in Cutter deel III: Stroombeeld in Cutter bij Kunstmatige Taluds; Injekties met Stukjes Plastic (Flow around and in a Cutter Head part III: Flow Field inside the Cutter Head placed in an Artificial Bank; Injections with Plastic Particles). WL|Delft Hydraulics BAGT 237, The Netherlands. (in Dutch).

Mol, A. (1977c). Cutterproeven op Sand; 19 (Cutting tests in sand). WL|Delft Hydraulics BAGT 255, The Netherlands. (in Dutch).

Moret, G.E. (1977a). Stroombeeld rond en in Cutter deel I: Stroombeeld rondom Cutter bij Kunstmatige Taluds; Injekties met Kleurstof (Flow around and in a Cutter Head part II:

Flow around Cutter Head placed in an Artificial Bank; Injections with Dye). WL|Delft Hydraulics BAGT 235, The Netherlands. (in Dutch).

Moret, G.E. (1977b). Stroombeeld rond en in Cutter deel IV: Stroombeeld bij Kunstmatige Taluds; Injekties met Grof Zand, Fijn Grind en Kunstmatige Kleibrokken (Flow around and in a Cutter Head part IV: Flow around a Cutter Head placed in an Artificial Bank; Injections with Coarse Sand, Fine Gravel and Artificial Pieces of Clay). WL|Delft Hydraulics BAGT 238, The Netherlands. (in Dutch).

Newmark, N.M. (1959). A method of computation for structural dynamics. Proc. A.S.C.E., 8, pp. 67-94.

Odar, F. and Hamilton, W.S. (1964). Forces on a Sphere Accelerating in a Viscous Fluid. Journal of Fluid Mechanics, Vol. 18, pp. 302-314.

Press, W.H. et al., (1999). Numerical recipes in Fortran 77: The Art of Scientific Computing. Cambridge University Press, Cambridge, UK.

Rijn, L.C. van, (1984). Sediment Transport, Part II, Suspended Load Transport. Journal of Hydr.Eng. ASCE, Vol. 110, no.11.

Roxborough, F.F. and Phillips, H.R. (1974). Experimental studies on the excavation of rock using picks. Proceedings of the Congress of the International Society for Rock Mechanics. 3, Vol. 2, Part B, Advances in rock mechanics; reports of current research, pp. 1407-1412.

Saffman, P.G. (1965). The Lift on a Small Sphere in a Slow Shear Flow. Journal of Fluid Mechanics, Vol. 22, Part 2, pp. 385-400.

Savage, S.B. (1984). The Mechanics of Rapid Granular Flows: Advances in Applied Mechanics, Vol. 24, pp. 289–366.

Savage, S.B. and Hutter, K. (1989). The Motion of a Finite Mass of Granular Material Down a Rough Incline: Journal of Fluid Mechanics, Vol. 199, pp. 177–215.

Slotta, L.S. (1968). Flow Visualization Techniques used in Dredge Cutter Head Evaluation. Proceedings of WODCON II 1968, Rotterdam, The Netherlands, pp. 56-77.

Slotta, L.S., Joanknecht, L.W.F. and Emrich E. (1977). Evaluation of Dredge Cutter head production as Affected by Cutter Height. Draft Report for ESCO Corporation from Department of Mechanical Engineering, Laboratory of Soil Transportation, Delft University of Technology, Delft, The Netherlands, January, 1977.

Steinbusch, P.J., Vlasblom, W.J., den Burger, M. and Kruyt, N.P. (1999). Numerical Simulation of the Flow Generated by Cutter Heads. Slurry Handling and Pipeline Transport, 14th International Conference, Hydrotransport 14, Maastricht, The Netherlands.

Turton, R. and Levenspiel, O. (1986). A Short Note on Drag Correlation for Spheres. Powder Technol., Vol. 47, pp. 83-86.

Verhoef, P.N.W. (1997). Wear of Rock Cutting Tools: Implications for the site investigation of rock dredging projects. Balkema Rotterdam, The Netherlands.

White, F.M. (1994). Fluid Mechanics, 3rd ed., McGraw-Hill, New York.

Acknowledgements

First of all I would like to thank prof. ir. W.J. Vlasblom for his advice and support throughout this research and for giving me the opportunity to carry out this research. Many thanks to dr. ir. A.M. Talmon for his guidance, support and encouragements that have been essential for the completion of this thesis.
This research was supported by the Vereniging van waterbouwers in Bagger-, Kust- en Oeverwerken (VBKO) and the Dutch ministry of economic affairs (SENTER).

Special thanks to all the colleagues at the section of Dredging Technology and the section of Transport Technology for a pleasant cooperation. In particular I would like to express my gratitude to ir. Joost Joustra, dr. ir. Cees van Rhee and ir. Dingena Schott for the many helpful discussions and an enjoyable working environment. I would like to thank ing. Arie Zwartbol, for the many hours he spent in preparing the laboratory tests and assistance during the tests. In addition, I would like to thank Arie Klein and Clemens van der Snoek for their contribution to the laboratory tests.
The tests could not have been performed without the aid of the following (former) students: Paul Krikke, Renske van Kinderen, Hermen Bijleveldt, Meindert Zwanenburg, Mischa Lauret and Guus Siteur.

Special gratitude to Peter Jan Steinbusch and Michel Dekker for their contribution to this research project by setting up the flow model. For performing the laboratory tests or processing the data I would like to thank Luk Verdoodt, Arie Eskes, Gerard Velthoen and Michael Vredevoort.

Last but not least, I want to thank my family and friends for their continuous support and encouragements.

Biography

Marco den Burger was born on the 26th of January 1971 in Rotterdam, the Netherlands. After finishing high school at the Hugo de Groot (OSG) in Rotterdam in 1989, he studied Mechanical Engineering at the Delft University of Technology. He graduated in 1995 at the section of Dredging Technology on a kinematic model for roller cone bits. This final thesis was performed at Shell (SIEP) in Rijswijk, the Netherlands. After graduating he became a doctoral student at the section of Dredging Technology where he has been working on this PhD thesis.